STUDY OF COSMIC RAY VARIATIONS

THESIS PRESENTED

BY

SANT PRASAD AGRAWAL

FOR THE DEGREE OF

DOCTOR OF PHILOSOPHY

OF THE

GUJARAT UNIVERSITY

JANUARY 1973

PHYSICAL RESEARCH LABORATORY
AHMEDABAD-9

STATEMENT

This thesis presents results on cosmic ray time variations
obtained from detailed analysis of ground based cosmic ray data.
It has been evident for some time that even though the cosmic ray
current outside the solar system is largely isotropic, the inter-
planetary magnetic fields modulate these particles within the
solar system to a considerable extent. Like Seismic waves, the
cosmic ray particles can therefore be used to continuously
'sound' the interplanetary medium. Together with 'in situ' space
observations, the ground observations provide an essential tool
for understanding the electromagnetic state of the entire inter-
planetary medium.

Even though, considerable amount of studies of both long
term and short term (including anisotropic variations) variations
have been conducted in the past, the low counting rate and the
consequent poor statistics have prevented a better understanding,
particularly of anisotropic variations of small amplitude ($< 1\%$),
such as diurnal and semi-diurnal variations. With the availability,
since IQSY, of a large number of high counting rate super neutron
monitors and large area scintillation telescopes, this lacuna
has been overcome to a considerable extent. Each ground based
monitor which looks into only a small region of the sky at any
given time, scans the entire sky during the course of a day as
the earth spins on its axis. With a geographically well distri-
buted set of high counting rate super neutron monitoring stations,
it is now possible to keep a continuous watch of the interplane-
tary medium, both in time and space, by studying the observed

cosmic ray intensity variations at earth. Inspite of large number of 'in situ' direct space observations now available, the cosmic ray observations are still very important since the former represents only the conditions at a given point, unlike cosmic ray observations which are affected by magnetic fields in the entire interplanetary medium. However, such space observations do form rigid boundary conditions within which the cosmic ray time variation results have to be interpreted.

Even though a number of super neutron monitors are in existence in longitudinal zones corresponding to Canada, U.S.A., and Europe, the Asian zone has been particularly conspicuous due to the absence of reliable monitoring stations till 1963. Having realised the importance of establishing high counting rate super neutron monitor, the author took a leading part in setting up an 18-NM-64 super neutron monitor at Ahmedabad (23.01 N, 72.61 E), in accordance with the standard design recommended for IQSY monitors, and by using the old copper counters kindly made available by Dr. Carmichael of Canada. The data from Ahmedabad, which is an equatorial monitoring station with a cut-off-rigidity $\sim$ 16 GV, provides an additional advantage in the determination of the rigidity spectral characteristics of the time variation of cosmic rays. The author was intimately involved in the fabrication and assembly of the neutron monitor pile, in the complete check out of its data recording system, and in the various detailed tests performed, before starting the actual data recording in July 1968. The stability of the detector

system was further ensured by periodic tests involving detailed pulse height analysis of each counter. The pressure corrected data from Ahmedabad is also being made available, on a routine basis, to the world data centres.

With the availability of data from Ahmedabad neutron monitor, it has been possible to further extend the mean rigidity of response by recording the multiplicity of the event and its time variation. The multiplicity of an event is usually referred to the phenomena where, following a cosmic ray interaction in the monitor several associated evaporation neutrons may be detected. The study of various multiplicities have indicated, that high energy event is usually associated with higher multiplicity, even though such studies can be carried out only on a time averaged basis due to the lower counting rates. The author has been involved in the design and fabrication of three multiplicity meters of conventional type which are in operation since 1969. The preliminary results obtained from these recordings on the attenuation coefficient and the multiplicity spectra were reported at Budapest (Agrawal et al, 1970), a reprint of which is attached as an appendix.

The present thesis deals with the complete analysis of the data obtained by the author from Ahmedabad neutron monitor during 1968-1971. Along with the data from world wide network of neutron monitors and Deep River meson monitor, the author has studied the characteristics of diurnal and semi-diurnal aniso-tropies in a very great detail. Realising that the semi-diurnal

anisotropy can be contaminated by pressure effects, the author
has performed rigorous analysis to determine the exact pressure
coefficient applicable to Ahmedabad neutron monitor data. These
results are shown to be consistent with the results from latitude
survey and those obtained from multiple station regression analysis
conducted by other investigators. Similarly, the applicable tem-
perature coefficients for Deep River mesons have been derived
and the meson data corrected with these temperature coefficients
have been used to deduce some of the characteristics of diurnal
and semi-diurnal anisotropies.

The variational coefficients, which provide the means of
transforming the observed phase and amplitude at any given station
to the interplanetary space, are available only for values of β
ranging from 0.6 to -1.5 in literature (McCracken et al, 1965).
Since the semi-diurnal component of cosmic radiation has been
shown to have a positive spectral exponent, the author has
extended the variational coefficients calculations for values
of β going upto + 2.0 and for different values of R_{max}, to derive
the exact exponent.

The thesis is divided into five chapters. The first
chapter briefly reviews the subject of time variation of cosmic
ray intensity, in particular, the present understanding of the
daily variation. The experimental set up of the super neutron
monitor at Ahmedabad, the type of tests carried out to ensure
the reliability of the data, and a brief account of the associated
data recording system are described in second chapter. The

third chapter gives an account of the analytical methods employed for processing the data from various neutron and meson monitors including Ahmedabad. The evaluation of appropriate attenuation coefficient for Ahmedabad neutron data is also included in this chapter. The detailed characteristics of the diurnal and semi-diurnal variation of cosmic ray intensity derived from data from a number of monitors and their theoretical interpretations are described in the last two chapters.

Some of the important results that have emerged from the present study are listed below:-

(1) The attenuation coefficient (α) applicable to Ahmedabad neutron monitor intensity is found to be $= 0.84 \pm 0.02\%$ / mm Hg, and is time invariant during the period 1968-1971.

(2) The step like excursions in the modulation function of the long term variation of the cosmic ray intensity during 1968-1971 are predominantly seen at higher energies, thus independently confirming the earlier observations.

(3) A significant phase shift to earlier hours in the time of maximum of diurnal variation of cosmic ray intensity in the year 1971 is noticeable at a number of stations. The phase shift is found to be larger at equatorial stations as compared to other stations.

(4) The yearly average diurnal anisotropy is rigidity independent ($\beta \approx 0$) with a time of maximum corresponding to 18 hour in space and is time invariant during the period 1958-1970. The amplitude, which is $\sim 0.4\%$ in space, varies as cosine of

declination. The yearly average diurnal anisotropy is consistent
with the particles undergoing corotation with the interplanetary
field.

(5)   The yearly average amplitude shows small but significant
changes with solar cycle due to the variation of upper cut-off-
rigidity (R_{max}), beyond which cosmic ray particles do not
corotate. R_{max} shows a minimum of about ∼35 GV during the
quiet solar year of 1965 and a maximum of about ∼ 100 GV during
1968-1969.

(6)   The diurnal anisotropy on a day to day basis, shows large
variability both in time of maximum and in amplitude. Comparing
with the low energy cosmic ray flare observations, a new concept
of the diurnal anisotropy is proposed to explain both the average
characteristics and day to day variability of the diurnal aniso-
tropy. According to this concept, the diurnal variation during
both quiet and disturbed periods can be understood in terms of
convection and field aligned diffusion. On an average basis,
the net radial convection current is zero i.e. the convection
and diffusion vector balance each other resulting in corotational
anisotropy. On a day to day basis, the two vectors need not
necessarily balance each other resulting in varying amplitudes
and times of maxima for the observed diurnal anisotropy.

Resolving the diurnal vector into these two components,
it is shown that both, on an yearly average basis and on a
27 day average basis, the diffusion vector is aligned along the
direction of the interplanetary magnetic field vector to

within $3 \pm 2^\circ$, indicating that the ratio of the perpendicular diffusion coefficient to parallel diffusion coefficient is $\lesssim 0.05$. Considering specific examples of days on which the diurnal variation has very large amplitudes, it is shown that this concept holds good even on a day to day basis. The spectral characteristics and observed time of maximum during such periods of enhanced diurnal variation activity are also found to be consistent with their being caused by a superposition of convective flow on enhanced field aligned diffusive flow.

(7) From the observed quiet day diffusion vector, which has an amplitude of $0.53 \pm 0.01\%$ on an average basis, the positive radial density gradient of cosmic ray intensity has been derived and is shown to be $\sim 4.5\%/$AU. During periods of enhanced diurnal activity, when the average diffusion vector has an amplitude $\sim 1.2 \pm 0.1\%$, the density gradient increases to $\sim 10\%/$AU. These values are consistent with our present understanding of the cosmic ray phenomena.

(8) The enhanced diurnal amplitude days are often found to occur on trains of consecutive days. During the early part of the enhanced diurnal wave train, the abnormal variation is found to be caused by a depletion (sink) of cosmic ray particle population from the garden-hose direction. At late times ($T \gtrsim 4$ days), the enhanced variation is found to be due to an excess of cosmic ray intensity from the anti-garden-hose direction, which is attributed to the development of a source along this direction due to earlier enhanced convection. The change over from sink
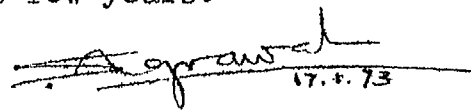
to source requires about 4-5 days, which represents a relaxation time of the modulation region having a dimension of $\sim$2-3 AU.

(9)   The properties of the average semi-diurnal anisotropy of cosmic radiation in the rigidity range 1 to 200 GV is found to be rigidity dependent with a spectral exponent of +1.   The amplitude varies as $Cos^2\lambda$, where λ is the declination.   The time of maximum of average semi-diurnal anisotropy is found to be along a direction essentially perpendicular to interplanetary magnetic field direction.   Both, the amplitude and phase of the anisotropy, are time invariant during the period 1958-1970.

(10)   From an analysis of data during 1968, the semi-diurnal anisotropy is shown to be aligned perpendicular to field direction even on a day to day basis.

The new concept of diurnal anisotropy of cosmic ray intensity proposed here is extremely interesting, since the same physical concept has been invoked to explain the anisotropy observations during different phases of a flare event.   Detailed analysis on a day to day basis, and identification of days on which transverse currents could become important constituting additional term to the daily variation will greatly aid in our understanding of the cosmic ray modulation phenomena.   With the availability of field and plasma parameters on a day to day basis, this should be possible in the next few years.

(U.R. RAO)   (S.P. AGRAWAL)

Date: 17-1-1973

LIST OF PUBLICATIONS

1. Variation of the limiting energy of corotating cosmic rays with solar cycle

   by Agrawal, S.P. and Rao, U.R.
   Proc. 11th Symposium Cosmic Rays, Astrophysics, Geophysics and Elementary Particle Physics (1969)
   2, 332-338.

2. Multiplicity measurements at Ahmedabad

   by Agrawal, S.P., Ray, S.K. and Rao, U.R.
   Acta Physica Hungaricae (1970)
   29, Suppl.2, 597-600.

3. Semi-diurnal anisotropy of cosmic radiation in the energy range 1-200 GeV

   by Rao, U.R. and Agrawal, S.P.
   Acta Physica Hungaricae (1970)
   29, Suppl.2, 77-82.

4. Semi-diurnal anisotropy of cosmic radiation in the energy range 1-200 GeV

   by Rao, U.R. and Agrawal, S.P.
   J. Geophys. Res., Space Phys. (1970)
   75, 2391-2401.

5. Comparison of long term variation of diurnal anisotropy derived between meson and neutron monitors during the period 1965-1969

   by Agrawal, S.P., Ananth, A.G. and Rao, U.R.
   Proc. 12th Int. Conf. Cosmic Rays, Hobart (1971)
   2, 646-650.

6. Diurnal variation of cosmic radiation in the energy range 1-100 GeV, on a day to day basis

   by Ananth, A.G., Agrawal, S.P. and Rao, U.R.
   Proc. 12th Int. Conf. Cosmic Rays, Hobart (1971)
   2, 651-656.

7. Effect of non-uniform solar wind velocity on interplanetary
    medium and on cosmic radiation

    by Ananth, A.G. and <u>Agrawal, S.P.</u>
    Ind. J. Pure & Applied Phys. (1971)
    <u>9</u>, 498-500.

8. Characteristics of cosmic ray diurnal variation from Deep
    River neutron and meson data and temperature effects

    by <u>Agrawal, S.P.</u>, Ananth, A.G. and Rao, U.R.
    Can. J. Phys. (1972)
    <u>50</u>, 1323-1331.

9. Characteristics of quiet as well as enhanced diurnal
    anisotropy of cosmic radiation

    by Rao, U.R., Ananth, A.G. and <u>Agrawal, S.P.</u>
    Planet. Space Sci. (1972)
    <u>20</u>, 1799-1316.

The cooperation of the computing centre under Mr. S.R. Thakoré, especially of Mr. I.V. Vayeda for his help in the preparation of various computer programmes and of Dr. Dinesh Patel, is gratefully acknowledged. The author is thankful to Miss Hansa, Messrs. N.R. Shah and V.R. Choksi for providing able computational assistance. The author is grateful to Mr.R. Mahadevan and to many others for their constant help. Messrs. K. Unnikrishnan and C.V. Ashokan receive special thanks for the painstaking and excellent job of typing the thesis and Mr. M.N. Narayanan for providing the draft.

The financial support received from the Department of Atomic Energy, Government of India, and from Day Fund Grant Nos. NAS-1492 and 17 from the National Academy of Sciences, U.S.A. are gratefully acknowledged. The grant of long study leave to the author by the Government of Madhya Pradesh is also acknowledged.

Finally, I am deeply indebted to my mother for her moral support and encouragement. Last, but not the least, I greatly appreciate the understanding and cooperation shown by my wife throughout the work.

17-1-1973   (S.P. AGRAWAL)

C O N T E N T S

...

C H A P T E R - I

INTRODUCTION

1.1 General survey of cosmic ray variations

Galactic cosmic radiation, even though largely isotropic outside our own solar system, undergoes significant modulation within the solar system. The sun with its continuously blowing solar wind and carrying with it frozen in magnetic fields can essentially affect cosmic ray particles even upto energies of $\sim$ 500 GeV resulting in time variations ranging in periodicities from a few minutes to eleven years, or more. Besides the isotropic time variation, the presence of non-uniform and changing small scale irregularities in the interplanetary magnetic field also produces considerable space and time variations. Before the availability of space-probes, the cosmic ray space and time variations were studied primarily through ground based monitors.

The sun is also found to locally produce cosmic rays during solar flares, normally with energies $\lesssim$ 100 MeV, but occasionally extending even to energies $\gtrsim$ 1 GeV, producing a detectable enhancement in the count rate registered by the ground based detectors. The spiral nature of the interplanetary magnetic field and its associated small scale structure was first inferred from these indirect ground based observations of solar flare increases (McCracken, 1962) which have since been confirmed by 'in situ' measurements from several space-crafts. In recent years low energy solar cosmic rays monitored by various space-crafts, almost continuously, have been used very effect-

ively to understand the interplanetary medium through which these particles travel. A comprehensive survey of the solar cosmic ray phenomena has been published very recently by McCracken and Rao (1970).

Even though a large number of space-probe observations have now become available, yielding almost continuous information on particles and fields in the interplanetary space, the observations are mainly limited to low energies ($\lesssim 100$ MeV) and are also confined to near earth region practically in the plane of ecliptic. Therefore inspite of the availability of a large body of measurements, the ground based continuous monitoring systems are essential not only for investigating the variation of high energy particles ($\gtrsim 1$ GeV) but also to provide, a continuous index of cosmic radiation and thus a quantitative measure of the characteristics of the electromagnetic state of the interplanetary space. Further, at very high energies, it is also possible to relate specific variations with the electromagnetic conditions of 'inaccessible' regions away from the plane of ecliptic and at large distances away from the orbit of the earth. Thus the study of time variation of cosmic rays forms an essential complementary study to the 'in situ' measurements for providing a complete understanding of the interplanetary processes. The various aspects of cosmic ray time variation have been recently reviewed in a very comprehensive manner by Lockwood (1971), Pomerantz and Duggal (1971), and Rao (1972).

1.2 Time variation of galactic cosmic ray intensity

The continuous and systematic registration of the cosmic ray flux by ground based monitors, commenced as early as 1936 with the establishment of a network of ionization chambers by the Carnegie Institute of Washington. However, the major advance in our understanding of the interplanetary medium from the study of cosmic ray time variations, became possible only after the establishment of world-wide set up of neutron and meson monitors during I.G.Y. The encouraging results obtained from the analysis of the data collected during I.G.Y. period and earlier, prompted the establishment of very high count rate super neutron monitors and large area scintillation telescopes during I.Q.S.Y. period. The data now obtained from these high counting rate monitors (since I.Q.S.Y.) have sufficient statistical accuracy, so as to permit the study of time variations even on a day to day basis.

Since the observed cosmic ray variations on ground pertain to the variation of secondary particles, it is necessary to relate these to primary variations. Essentially there are two important effects which must be considered prior to their being related to primary variations. The first relates to the understanding of the generic relationship between the primaries and the secondaries they produce through their interactions in the earth's atmosphere. The second relates to the motion of the primary particles in the earth's magnetic field.

Number of theoretical attempts (Dorman, 1957 and reference

therein; Wainio et al, 1968; Debrunner and Flückiger, 1971) have been made to relate the secondary cosmic ray production to primary intensity at the top of the atmosphere. However, in practice, it has been found easier to derive the multiplicity or yield function from observed latitude effects. Since a detailed treatment of the derivation of multiplicity function is not only beyond the scope of this thesis, but is also available in literature, we will only define the term explicitly and will not attempt a detailed discussion of the subject.

A number of authors (Neher, 1952; Treiman, 1952; Simpson et al, 1953; Dorman, 1957; Webber and Quenby, 1959; Lockwood and Webber, 1967) have obtained the appropriate multiplicity function applicable to cosmic ray variation studies. Following Dorman (1957) we can express the observed variation at earth ($\partial N_\lambda^i / N_\lambda^i$) as

$$\frac{\partial N_\lambda^i}{N_\lambda^i} = -\delta E_\lambda^c \cdot W_\lambda^i (E_\lambda^c, h) + \int_{E^c}^{\infty} \frac{\delta m^i (E,h)}{m^i (E,h)} \cdot W_\lambda^i (E,h) \, dE$$

$$+ \int_{E^c}^{\infty} \frac{\delta D(E)}{D(E)} \cdot W_\lambda^i (E, h) \, dE \qquad \ldots 1.1$$

where N_λ^i is the observed intensity of the secondary component i at latitude λ and at atmospheric depth h. E_λ^c is the cut-off-energy at latitude λ. D (E) is the differential energy spectrum given as $AE^{-\gamma}$ where A is a constant and $\gamma \approx 2.6$. $m^i (E, h)$ is the multiplicity and $W_\lambda^i (E, h)$ is coupling constant or the differential response function which is easily obtained from the

available latitude surveys. The first term on the right hand side of equation 1.1, represents the variation due to the changes in the cut-off-energy, which is usually very small and therefore negligible except for days associated with magnetic storms. The second term is due to the changes in the terrestrial atmospheric (meteorological effects) parameters such as pressure and temperature which can be corrected for. The third term includes the variation due to changes in the primary energy spectrum, and is of interest in the studies of time variation of cosmic rays. However, the equation does not include the effects of the asymmetric magnetosphere, which can be significant in the studies of the daily variation at energies $\lesssim 1$ GeV, though negligible at higher energies.

The geomagnetic field acts as a spectrum analyser allowing charged particles of energy greater than a minimum energy (E_λ^C) at any point to enter the earth, the cut-off-energy (E_λ^C) being maximum at the equator and minimum near the pole. The trajectory of the particles, even at energies much higher than E_λ^C, are strongly influenced by the earth's magnetic field. By tracing the actual trajectories of the particles in a realistic simulation of the geomagnetic field, Rao et al (1963) have demonstrated that even though any given neutron monitor has a large opening angle at the ground, it essentially scans only a very narrow region in the celestial sky. They have defined the 'Asymptotic cone of acceptance' of any given detector as the cone in the

celestial sphere from which cosmic ray particles significantly contribute to the counting rate of the detector. The asymptotic cone of acceptance of the detector corotates with the earth, as the earth spins on its axis, thus scanning a narrow belt in the celestial sky in a period of one day.

The observed cosmic ray intensity variations include essentially both isotropic time variations, such as the eleven year solar cycle variations, Forbush decreases, 27-day variations and anisotropic (spatial) variations such as solar diurnal and semi-diurnal variations. As will be demonstrated in the third chapter it is possible to separate out the space variation from the time variation by studying data from a number of neutron or meson monitors which are situated at different longitudes.

To be able to theoretically interpret the modulation of the galactic cosmic ray intensity, it is necessary to understand the motion of cosmic ray particles in the irregular interplanetary magnetic fields carried by the continuously blowing solar wind. Parker (1958 a) noted that the interplanetary magnetic field frozen into the solar wind will tend to convect the particles radially outward at the solar wind velocity. This will eventually set up an outward radial density gradient of cosmic rays that causes particles to diffuse inward. In a steady state condition assuming spherical symmetry, the model qualitatively explains the eleven year solar cycle variation.

Similarly, all other variations both isotropic and anisotropic listed earlier, are explainable in terms of varying solar wind and interplanetary magnetic field parameters. Till the availability of space observations, the properties of the interplanetary space were largely inferred from indirect cosmic ray observations. Since now a large amount of direct space observations of fields, plasmas and particles in interplanetary space are available, it is now possible to have a detailed comparison between the theory and observations. Therefore, in the following we will briefly enumerate the average gross features as well as day to day variations of the interplanetary medium (Solar wind and Interplanetary magnetic field), and then discuss the cosmic ray time variation observations and their theoretical interpretation in the light of these measurements. It should be emphasized that even though the direct space-probe observations constitute boundary lines, the cosmic ray observations, being dependent on the electromagnetic state of the entire interplanetary medium (unlike the 'in situ' measurements), provide a very important tool for the understanding of the entire interplanetary medium.

1.3 Interplanetary medium

A clear understanding of the motion of the cosmic ray particles in the disordered interplanetary magnetic field (I.M.F.) is very essential for the study of the modulation of cosmic rays. The magnetic irregularities which act as effective

scatterers are carried away from the sun by radially moving
solar plasma with supersonic velocities ~ 300 to 1000 km per
second. The cosmic ray particles essentially random walk through
the I.M.F. and their statistical motion can be understood, in
practice, only if the diffusion coefficient is well known. Since
the diffusion coefficient is dependent on the power spectrum of
the I.M.F. irregularities moving with the solar wind, an under-
standing of both the solar wind and I.M.F. is most essential.

1.31 Solar wind

Even though the emission of solar plasma was inferred long
ago to explain the geomagnetic disturbance and Aurorae, the first
evidence for the continuous emission of the supersonic solar wind
was pointed out by Biermann (1951, 1957) in his explanation of
the observed acceleration of the type I comet tails. Subsequent-
ly, Parker (1958 b) developed the theory of continuous hydrodyna-
mical expansion of the solar corona and showed that the inner
corona with observed temperatures of ~ 10^6 K is too hot to be
held static by the sun's gravitational field. The gross proper-
ties of the radially blowing supersonic solar wind, predicted
by the theory have been verified, since then, by a number of
direct space-craft measurements. A number of excellent reviews
dealing with both the observational data and the theoretical
aspects (Dessler, 1967; Axford, 1968; Hundhausen, 1968, 1970;
Parker, 1969; and Burlaga, 1971) are available in literature.
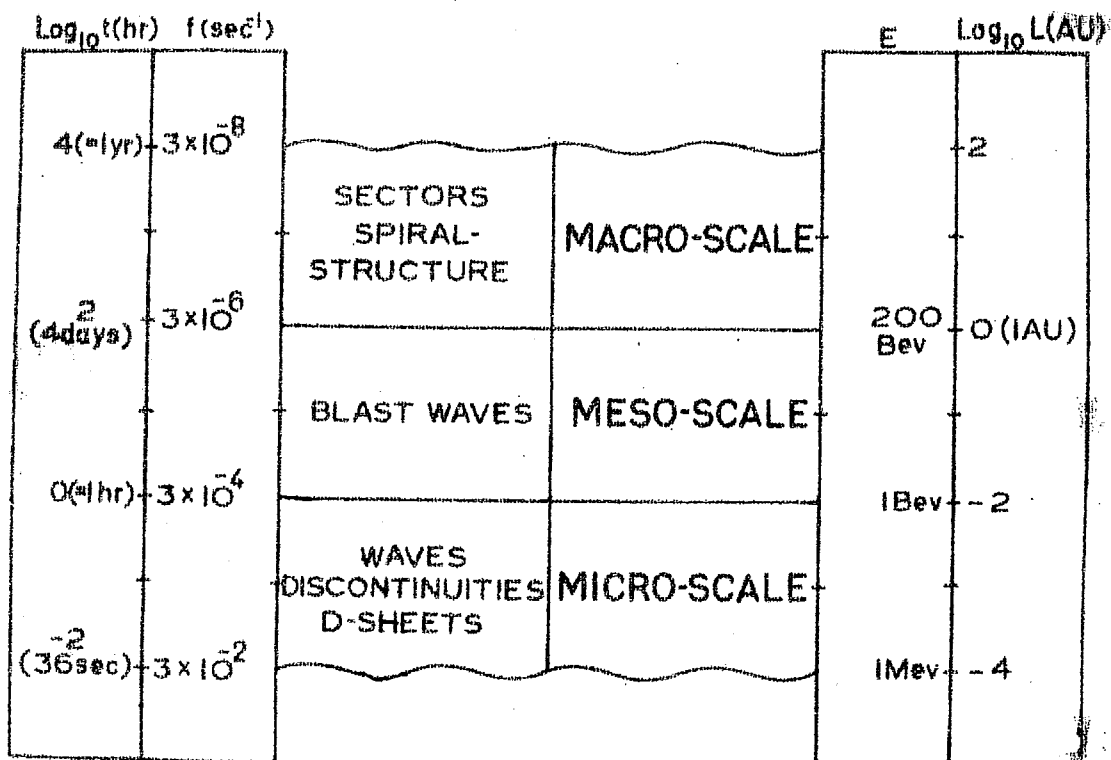
Fig. 1.1 - Different scales are defined in terms of chara-
cteristic times, frequencies and lengths. Some characteristic
features seen on different scales are shown. E is the energy of
proton whose gyroradius is the scale length in a 5 γ field (after
Burlaga, 1971).

For a clear understanding of the observed properties of

the solar wind plasma particles, an idea of scale length (time)

was introduced by Burlaga and Ness (1968) to classify and inter-

pret the data. Instead of using the scale length, they have

suggested that the length be converted to time by dividing it by

the appropriate solar wind bulk speed. Figure 1.1, which represents

the different scale lengths, clearly shows that for particle energy

$\gtrsim 2$ GeV (I.M.F. = 5γ), only the Marco and Mesoscale properties of

TABLE 1.1 - Observed properties of the typical quiet day solar
wind and its variability at 1 AU

Characteristics	Average (quiet periods)	Variability
Flow speed	320 km S^{-1}	$275-800$ Km S^{-1}
Flow direction	1.6°E of sun	-8°E to $+8^\circ$W
Proton and Electron density	8 cm^{-3}	1 to 50 cm^{-3}
Proton temperature	4×10^4K	3×10^4 to 5×10^5K
Electron temperature	$1-1.5 \times 10^5$K	1 to 2×10^5K
Proportion of He (α) (n_α / n_p)	0.05	0.01 to 0.20
Magnetic field	5Υ	2 to 12Υ

the solar wind are important, where as Microscales are most
relevant for low energy particles ($\lesssim 1$ GeV). The gross behavi-
our of the solar wind at the earth's orbit in the Mesoscale
dimensions and its variability within it is given in Table 1.1.
The bulk speed of the solar wind seldom decreases below 300 km
per second, typical quiet period wind speeds ranging between
300 to 350 km per second. The corresponding proton temperature
is $\sim 3 \times 10^4$K, which indicates a supersonic flow with Mach
number ~ 10.

The solar wind velocity exhibits strong time variations
due to the emission of plasma from different regions of the
solar disc with differing characteristics. Many investigators

have demonstrated an excellent correlation between $\leq Kp$ indices of geomagnetic field disturbance and the solar wind velocity on a time scale $\lesssim 1$ year (Snyder et al., 1963; Pai et al., 1967; Bame et al., 1967). A pronounced 27-day recurrence tendency both in high $\geq K_p$ and enhanced solar wind velocity has also been noted, which are probably related to M-region storms (Snyder et al., 1963). However, on a long term basis, contrary to theoretical expectations, the solar wind as well as I.M.F. parameters seem to be practically invariant with the solar cycle (Gosling et al., 1971; Mathews et al., 1971; Hedgecock et al., 1972), except probably in the case of the field component in a direction perpendicular to the ecliptic (B_z) plane (Quenby and sear, 1971).

1.32 Interplanetary magnetic field (I.M.F.)

The interplanetary magnetic field, being embedded in a highly conducting plasma, behaves as if it is 'frozen in' with the moving plasma (Alfven, 1950), and therefore is stretched out in the form of an Archimedes spiral by the supersonic solar wind, as the sun rotates (Parker, 1958 a, b; Ahluwalia & Dessler, 1962). The angle χ between the normal to the spiral field line and the radial direction (Figure 1.2) is given by

$$\text{Tan} \chi = \frac{V}{\Omega r} \qquad \ldots \ldots 1.2$$

where V is the solar wind velocity, Ω is the angular velocity of the sun and r is the heliocentric distance. χ is $\approx 45^\circ$ at the orbit of earth ($r = R_e = 1$ AU) for $V \approx 400$ km per second.
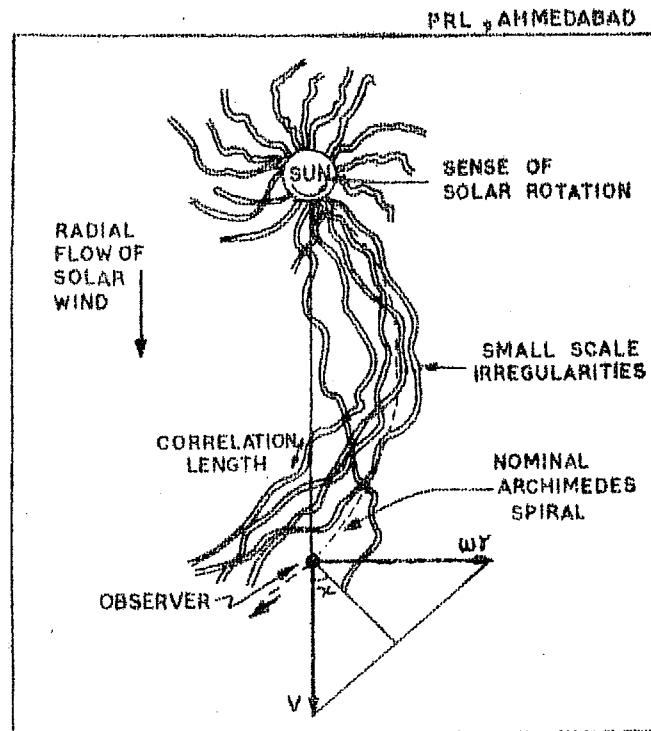
Fig. 1.2 - Interplanetary magnetic field configuration illustrating the random walk of field lines as a result of large scale inhomogeneities in the solar wind. The perfect Archimedes field line due to uniform radial expansion of solar wind is represented by dotted line.

Direct observations of the I.M.F. from a number of space-craft platforms have now conclusively proved,that the large scale structure of the field is in very good agreement with the predicted Archimedean spiral configuration and is distributed in the form of a well defined sector structure with I.M.F. being alternatively positive (away from the sun) and negative (towards the sun). The sector pattern has been found to exist throughout the solar cycle (Wilcox and Ness, 1965; Wilcox and Colburn, 1972). From a corre-lation study of the polarity of the mean photospheric field and the I.M.F. near earth, a lag of 4-5 days was obtained for the best correlation, which is consistent with the transit time of the solar

wind, thereby establishing the solar origin of I.M.F. (Severney et al, 1970). It is interesting to note that even though, the average I.M.F. magnitude and direction have not changed significantly over the period 1965-1969, the frequency of the number of days with higher field amplitudes does show an increase with solar activity.

The ideal spiral nature of the large scale I.M.F. when observed with time scales of $\sim$1 day or less (microscale) is altered considerably due to the presence of a continuous distribution of small scale irregularities. Due to the Alfven velocity being quite small, the field fluctuations are also frozen into the solar plasma, and the observed time dependence at a given position can be easily transformed into spatial variations. The origin of these irregularities have been attributed to (Michel, 1967; Jokipii and Parker, 1969) the motion of the prominent photospheric features such as granulations ($\sim 10^3$ km diameter) and super-granulations ($\sim 2 \times 10^4$ km diameter). In addition the turbulent motion of the solar plasma makes the field line stochastic (executing a random motion) even if they were symmetrical to start with. A large part of the random walk is due to the horizontal displacement of the feet of the lines of force resulting from the motion of granules and supergranules. The maximum displacement at the orbit of the earth is O (0.1 AU) from the mean Archimedean spiral direction (Jokipii and Parker, 1968). The presently available information on the large scale

I.M.F. has been recently reviewed by Schatten (1971).

From the observed variation of the I.M.F., the frequency power spectrum $P_{xx}(f)$, which is simply the Fourier transform of the autocovariance function, can be computed very easily. The scattering due to irregularities is maximum for particles whose cyclotron or gyroradius is of the same order as the scale size of the irregularities. In other words the scattering for particles of rigidity R GV depends mainly on the power $P_{xx}(f)$ in the transverse component of the field in the vicinity of 'resonant frequency' f given by

$$f(R) = 10^{-4} \cdot R^{-1} \cdot Hz \qquad \qquad .. \; 1.3$$

$P_{xx}(f)$ can be approximated by a power law in frequency

$$P_{xx}(f) \propto f^{-\alpha} \qquad \qquad .. \; 1.4$$

Both $P_{xx}(f)$ and α have been found to vary considerably both on a day to day basis and also on long term basis (Coleman Jr., 1966; Jokipii and Coleman, 1968; Siscoe et al., 1968; Sari and Ness, 1969). Knowing α, both the parallel ($K_{\parallel}$) and perpendicular ($K_{\perp}$) components of the diffusion coefficient K, can be computed from the relations

$$K_{\parallel} = \begin{cases} A \, \beta \, R^{2-\alpha} & \text{for } R_u > R > R_L \\ 1/3 \; cD\beta & \text{for } R < R_L \end{cases} \qquad .. \; 1.5$$

Where A is a constant, R_u is the rigidity at which the cyclotron radius r_c of the particles becomes comparable to scattering mean-free-path $\lambda = 3 \, K_{\parallel}/c\beta$. R_L is the particle rigidity for which mean-free-path λ becomes smaller and approaches D, the

correlation length of the I.M.F., which is typically $\sim 2 \times 10^{11}$ cm.

and $\quad K_{\perp} = K_{\perp}^{m} + (\dfrac{r_c^2}{\lambda^2}) \cdot K_{\parallel}$ .. 1.6

The first term $K_{\perp}^{m}$ represents diffusion due to the random walk of field lines, while the contribution from the resonant scattering due to field fluctuations is contained in the second term. At lower energies ~ 10 MeV, $K_{\perp}^{m} \approx K_{\parallel}$ leading to an isotropic diffusion.

Inspite of the reasonably satisfactory theoretical treatment relating the observed field fluctuation to the motion of the cosmic ray particles (Jokipii, 1971), the practical usage is very limited due to the scanty and unreliable information of the spectral density at frequency $\lesssim 5 \times 10^{-5}$. Hz (resonant particle rigidity $\gtrsim 2$ GV). Therefore, the presently available magnetic field derived power spectrum is not very useful to draw any significant conclusion regarding the propagation of high rigidity particles, to which the ground based instruments are sensitive. Even at higher frequencies, corresponding to low rigidity cosmic rays, the presently known properties of the I.M.F. can only serve as boundary conditions, and a complete understanding of the modulation phenomena has to await, till the simultaneous measurement of plasmas and fields at different heliolatitudes and heliodistances become available.

1.4 Modulation of galactic cosmic rays

Various theoretical models have been proposed to account

for the experimental observations of cosmic ray modulation, the radial density gradient, the anisotropies and their interconnection, in terms of either the electric fields in the interplanetary space or the interplanetary magnetic field structure, including solar wind. All the models and processes that have been advanced to explain the galactic cosmic ray modulation, fall mainly in two classes (1) Electric field model and (2) Diffusion - convection model. However, since the diffusion-convection model incorporating the energy loss term, leads to the most satisfactory explanation of the observed long term variation, the radial density gradient and anisotropies (Gleeson, 1971 a), in the following, we briefly discuss this model and its predictions for the radial density gradient.

1.41 Diffusion - convection model, isotropic diffusion

The establishment of a positive radial density gradient of cosmic rays in the solar system due to supersonic solar wind implies the presence of an outward convection (UV) and an inward diffusion ($- K \frac{\partial U}{\partial r}$) which in the steady-state condition must balance each other (Parker, 1958 b, 1963), Therefore

$$UV = - K \frac{\partial U}{\partial r} \qquad \qquad .. \ 1.7$$

For a spherically symmetric system equation 1.7 yields

$$U (r, E) = U_{\infty} (E) \ \exp (\int_{r}^{D} -\frac{V}{K} \ dr) \qquad .. \ 1.7a$$

where U (r, E) and U$_{\infty}$ (E) are the flux of particles of kinetic energy E at a distance r from the sun and at an outer boundary

r = D respectively and K is the isotropic diffusion coefficient. The simple convection-diffusion model has now been greatly improved by a number of workers (Gleeson and Axford, 1967; Jokipii and Parker; 1967, 1970), taking into account

(1)   Adiabatic energy changes due to non-zero divergence of solar wind velocity (Parker, 1965; Gleeson and Axford, 1967; Singer et al., 1962).

(2)   Anisotropic diffusion due to average (non-fluctuating) I.M.F. (Parker, 1965; Axford, 1965 b) and

(3)   Relationship between diffusion tensor and the magnetic field power spectrum (Jokipii, 1966, 1967; Hasselmann and Wibberentz, 1968; Roelof, 1968).

The detailed discussion of the theoretical formulation of the transport of cosmic rays has been published recently by Jokipii (1971).   The differential number density U (r, E, t) and differential current density S (r, E, t) in an isotropic velocity distribution at kinetic energy E and heliocentric distance r from the sun, is given by the equation of transport and streaming (Parker, 1965; Gleeson and Axford, 1967; Fisk and Axford, 1969, 1970; Gleeson, 1971 a, b)

$$\frac{\partial U}{\partial t} + \frac{1}{r^2} \frac{\partial}{\partial r} (r^2 VU - r^2 K \frac{\partial U}{\partial r}) - \frac{1}{3r^2} \frac{\partial}{\partial r} (r^2 V) \frac{\partial}{\partial E} (\propto EU) = 0 \quad .. \quad 1.8$$

$$S (r, E, t) = CVU - K \frac{\partial U}{\partial r} \quad\quad .. \quad 1.9$$

where the Comton-Getting factor (C) is given by

$$C (r, E, t) = 1 - \frac{1}{3U} \frac{\partial}{\partial E} (\propto EU) \quad\quad .. \quad 1.10$$

and $\alpha(E) = -\dfrac{E + 2 E_0}{E + E_0}$ .. 1.11

$V(r, t)$ is the solar wind speed, $K(r, E, t)$ is the diffusion coefficient and E is the kinetic energy of the particle with rest mass E_0.

After having solved equation 1.8 for U by specifying the galactic spectrum and the diffusion coefficient within the cavity, the result for U, can be substituted in 1.9 to determine the flow or anisotropy of the particles. Though there is no exact general analytical solution of the equation of transport (1.8)as yet, the numerical solution now available are being used very extensively to explore the physics of the modulation of cosmic rays. Analytical solution with certain useful approximations can, however, be obtained which are briefly discussed below.

(a)   At high energies (> 200 MeV) the term $| S/UV | \ll 1$, and hence instead of using equation 1.8, one can drop the term S in equation 1.9 and write a much simpler equation, generally known as force field equation

$$CVU - K \dfrac{\partial U}{\partial r} = 0 \qquad \qquad .. \; 1.12$$

If K, the diffusion coefficient is assumed to be a separable function of distance (r) and rigidity (R) and is of the form

$$K = K_1 (r, t). K_2 (R, t).\beta \qquad \qquad .. \; 1.13$$

where $\beta = v/c$ and v the particle velocity, equation 1.12 can be integrated to obtain the force field solution (Gleeson and

Axford, 1968 b). At kinetic energies $\gtrsim$ 2 GeV/nucleon the spectral slope of the intensity of cosmic rays is fairly constant (C = 1.5) and therefore the equation 1.12 with C = 1.5, yields the modified convection-diffusion equation.

The radial density gradient of the cosmic rays is given by (from equation 1.12)

$$G = \frac{1}{U} \frac{\partial U}{\partial r} = \frac{V}{K} \cdot C(r, E) \qquad \qquad .. \; 1.14$$

For $K = 9.3 \times 10^{21}$ cm^2 s^{-1} at 5 GeV, it works out to be $\approx +$ 9%/AU which compares well with the experimental observations (O'Gallagher, 1967). The results on the radial density gradient have been summarised by Rao (1972) and O'Gallagher (1972), very recently and these along with our own results obtained from the anisotropy measurements will be discussed in chapter IV. We also note that equation 1.14 predicts the rigidity dependence of the radial density gradient, to be dependent on the rigidity dependence of the diffusion coefficient K.

The radial anisotropy ξ is given as (Fisk and Axford, 1970)

$$\xi = -+\alpha \left(\frac{V}{2v} \right) \cdot \left(-\frac{r}{U} \frac{\partial U}{\partial r} \right) \qquad \qquad .. \; 1.15$$

for the cosmic ray spectrum of the form $E^{-\gamma}$. The radial anisotropy at high energies ($\gtrsim$ 2 GeV) is $\lesssim$ 0.02% and is consistent with the observations (McCracken and Rao, 1965; Rao, 1972).

1.42 Diffusion - convection model, anisotropic diffusion

The diffusion of cosmic rays into the solar system is in

general, highly anisotropic with $K_{\parallel} > K_{\perp}$, where $K_{\parallel}$ and $K_{\perp}$ are the diffusion coefficients parallel and perpendicular to field lines (Axford, 1965 b). For an idealized spiral I.M.F., the cosmic ray density U at a radial distance r and colatitude θ is given by (Parker, 1965)

$$U(r, \theta) = U_{\infty} \exp \left\{ -\frac{V(D-r)}{K_{\parallel}} \left[1 + \frac{\Omega^2 \sin^2 \theta}{3V^2} (D^2 + D\,r + r^2) \right] \right\} \quad \text{.. 1.16}$$

where Ω is the angular velocity of the sun. Since the term in the square bracket of equation 1.16 is greater than 1, the density reduction will be larger than that expected for the case of the isotropic diffusion.

The radial gradient, at the orbit of earth ($\Omega r = V, \theta = 90^{\circ}$) for the anisotropic diffusion case is approximately given by

$$G = \frac{1}{U} \frac{\partial U}{\partial r} \approx -\frac{2V}{K_{\parallel}} \quad \text{.. 1.17}$$

1.43 Long term modulation

Since the discovery of the inverse relationship between the sun-spot activity and the cosmic ray intensity (Forbush, 1958) much has been learnt concerning the eleven year modulation of the cosmic ray intensity. A large amount of data concerning the rigidity dependence of the long term variation and its functional relationship with other solar and terrestrial parameters are now available to facilitate strict comparison with the theoretical predictions. The data indicate that the modulation is

maximum at low energies and even during solar activity minimum there exists a residual modulation of cosmic ray intensity.

The lag between the peak cosmic ray intensity and the minimum in the solar activity can be utilised to estimate the size of the modulating region. Using sun-spot number as the parameter to define solar activity, a lag of 9-12 months was found (Forbush, 1958) which corresponds to $D \approx 100$ AU, a value which is an order of magnitude greater than that obtained from many other evidences. Moreover the value is found to be different for different periods of the solar cycle. Quenby (1965) has, however, pointed out that consideration of sunspot number close to the solar equator ($\lambda \pm 10^{o}$) substantially reduces the time lag. Subsequent studies have shown that coronal green line intensity ($\lambda 5303$) from the equatorial region of the sun ($\pm 10^{o}$) is a better index of the solar activity (Simpson and Wang, 1967; Hatton et al., 1968; Pathak and Sarabhai, 1970). Comparison with both ΣK_p and $\lambda 5303$ intensity shows that the time lag between the solar activity and cosmic ray intensity is of the order of 1 month which corresponds to $D \approx 7$ AU. The size of the modulating region inferred from the radial density gradient measurements obtained both from spacecraft and ground based data are in fair agreement with the above value (Rao, 1972).

Using the spectrum measurements of protons, helium, and electrons it has been found that the diffusion-convection theory with the energy loss term included, is successful in explaining

the experimental observations for particles of energy $\gtrsim$ 100 MeV.
The theory has also been successful in predicting the radial
density gradient which depends upon the residual modulation of
the cosmic ray intensity, the larger the modulation the larger
being the density gradient, provided D remains constant. Compre-
hensive reviews are available in literature (Webber, 1967;
Gleeson, 1971a; Rao, 1972) explaining the latest observations on
long term modulation and their theoretical interpretation. Since
the subject of the long term modulation does not directly form a
part of this thesis, we have made only a brief reference to this
aspect of cosmic ray modulation.

1.5 Spatial anisotropies and the daily variation

The spatial anisotropies in the interplanetary space are
registered by ground based detectors once each day as their
'asymptotic cone of acceptance' sweeps through the directions
containing the spatial anisotropy. Practically all the study of
the daily variation of cosmic ray intensity has been conducted
from ground based observations using neutron and meson monitors,
even though of late the data from the underground detectors
have also provided some information on the daily variation at
very high energies. It must be remembered, however, that all
these monitors respond to a wide range of energies. At ground
these monitors respond from an energy of $\sim$ 1.5 GeV (limited by
the atmosphere) to a few hundred GeV.

Most important amongst the spatial anisotropies are

the diurnal and semi-diurnal anisotropies, the existence of both of which has now been established beyond any doubt. The diurnal and semi-diurnal anisotropies and their characteristics have been intensively studied for the last few years and in what follows, we shall discuss their theoretical formulation and the experimentally observed characteristics.

1.51 Diurnal anisotropy (corotational concept)

Based on the concept of the solar wind and smooth spiral field (Parker, 1960), Ahluwalia and Dessler (1962) proposed a simple model to explain the average behaviour of the diurnal anisotropy, according to which the cosmic ray particles drift due to the electric field $\underset{\sim}{E}$ ($\underset{\sim}{E} = \underset{\sim}{V} \times \underset{\sim}{B}$). From an elaboration of the model they predicted that

1) The source of the diurnal variation which is in the ecliptic plane is energy independent ($\beta = 0$),

2) all particles whose rigidity is below an upper cut-off-rigidity ($R_{max} \approx 100$ GV) undergo diurnal variation,

3) the direction of the anisotropy is perpendicular to the I.M.F. direction, and

4) the amplitude of the anisotropy is proportional to the solar wind velocity.

Whereas the first two predictions were in agreement with the observed characteristics of the average diurnal variation, the observed direction and the amplitude of anisotropy (Bercovitch, 1963; Rao et al., 1963; Snyder et al., 1963) did not agree with

predictions. In addition Stern (1964) raised a fundamental objection that assuming conservative fields and the application of Liouvelli's theorem, the cosmic ray intensity should be isotropic at all accessible regions of the interplanetary medium, if it were so outside the solar modulating boundary. This follows from the fact that the electric field $\underset{\sim}{E}$, also sets up a density gradient normal to the sun's equatorial plane and is of the right magnitude to cancel the diurnal variation completely.

In order to overcome this difficulty Parker (1964) and Axford (1965a) pointed out that, in reality, the fields are not conservative ($\frac{\partial \underset{\sim}{B}}{\partial t} \neq 0$), due to the presence of large number of small scale irregularities moving out with the solar wind. The scattering of particles by these irregularities wipes out a major portion of the perpendicular density gradient established by the electric field $\underset{\sim}{E}$. The two models are essentially similar, except in minor details and therefore lead to the same result. Parker (1964) considered the presence of magnetic field irregularities beyond the orbit of earth, while Axford (1965a) assumed the exis-tence of scattering centres throughout the interplanetary medium. With the three basic assumptions namely

1) no diffusion perpendicular to the magnetic field,

2) the gradient perpendicular to the ecliptic is zero, and

3) no radial streaming i.e. sun is neither a source nor a sink of cosmic rays, both the models predict that the average diurnal variation is caused by azimuthal streaming i.e. the

cosmic ray particles undergo rigid bulk corotation with the I.M.F. The average diurnal or corotational anisotropy (ξ) is then given by (Compton and Getting, 1935),

$$\xi = \frac{3C}{V} \cdot V_{co}$$
$$\text{and} \quad C = (2 + \alpha\gamma)/3 \qquad \qquad \text{.. } 1.18$$

where $V_{co} = \Omega r$, is the corotational streaming velocity, and is equal to $V \tan \psi$ ($\psi = 90 - \chi$, Figure 1.2). For particles of energy $\gtrsim$ 2 GeV ($v \approx c$, velocity of light) and at the orbit of earth (r = 1 AU) where $V_{co} \approx$ 400 km per sec, $\xi \approx$ 0.6%. It is immediately seen that the theory predicts an energy independent anisotropy (at relativistic energies) with a time of maximum at 1800 hours ($90°$E of Sun) and an amplitude ξ = 0.6% (Figure 1.3). Comparing with the observations, the theoretical predictions are in reasonably good agreement with observed average diurnal variation (McCracken and Rao, 1965; Rao, 1972) except for the predicted amplitude being almost 50% larger than the observed amplitude.

The reduction in the observed diurnal amplitude has been attributed to the transverse diffusion ($K_\perp$). Parker (1967) considers two different situations which can lead to a decrease in the corotational amplitude.

(a) ϵ very small beyond the orbit of earth

If the ratio $\epsilon = K_\perp / K_{\parallel}$ is too small, beyond the orbit of earth, it is evident that the cosmic ray particles may reach the earth without much relief to the pressure gradient leading to a diurnal amplitude much smaller than is expected. On the
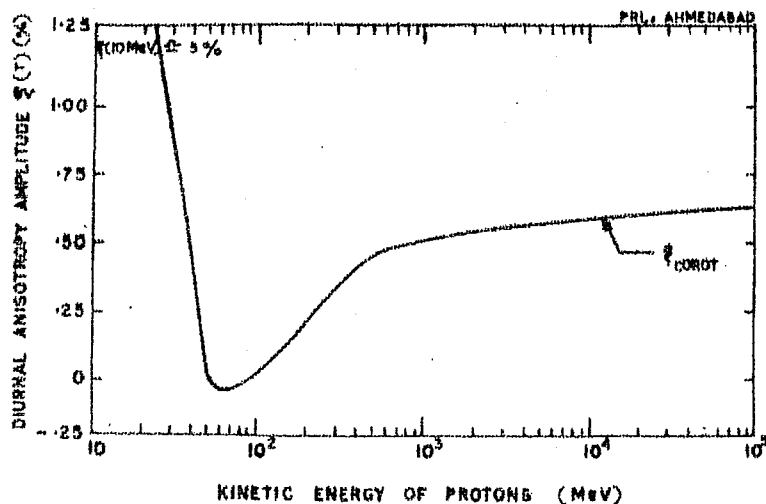
Fig. 1.3 - Theoretically expected (maximum) amplitudes of corotational anisotropy plotted as a function of particle kinetic energy.

other hand, if it is too large, the amplitude would approach the theoretical limit of $\approx$ 0.6%. A typical value of $\epsilon = K_\perp/K_\parallel \approx O(10^{-2})$, beyond the orbit of the earth is about the right order of magnitude to account for the reduction in the amplitude of diurnal variation.

(b) ϵ large near the orbit of earth

If the diffusion across the lines of force ($K_\perp$) and beyond the orbit of earth, has completely removed the gradient perpendicular to the ecliptic caused by the electric field as discussed in (a) above, one expects to observe the theoretical upper limit of the corotational amplitude. However, this upper limit can be expected only when $\epsilon \ll 1$, at the earth's orbit. The expected corotational anisotropy which also includes the effect of finite ϵ (near the orbit of earth) is given by (Krymskiy, 1964; Parker, 1967; Forman and Gleeson, 1970).

$$\xi = \frac{3CV}{v} \left[\frac{(1 - \epsilon) \tan \psi}{1 + \epsilon \tan^2 \psi} \right] \qquad \qquad .. \quad 1.19$$

which in the two extreme cases either yields the limiting anisotropy or zero anisotropy

(1) If $\epsilon = 0$ i.e. $K_\perp$ is negligible equation 1.19 reduces to 1.18

(2) If $\epsilon = 1$ i.e. $K_\perp = K_\parallel$, the corotational anisotropy ξ vanishes.

In other words, the observed reduction in the amplitude of the anisotropy at relativistic energies can be understood in terms of finite $K_\perp$, with $\epsilon \approx 0.15$ at the orbit of earth. The observed isotropy of ~ 10 MeV protons (Rao et al., 1967) can be explained if $K_\perp \approx K_\parallel$ ($\epsilon \approx 1$) at low energies due to the meandering of field lines (Jokipii and Parker, 1969).

Recently, Subramanian (1971a) has made a careful analysis of the extra-atmospheric factors affecting the anisotropy observed by the neutron monitors, and has concluded that if due allowance is made to the four minor cumulative effects which includes the use of variable γ (the exponent of the energy spectrum of the primary radiation) ranging from 1.5 to 2.5 corresponding to rigidity range 2 to 15 GV, and the normalization of the variational coefficient at much higher rigidity than 500 GV, then the observed amplitude is in good agreement with the theoretically expected amplitude indicating that the transverse diffusion near earth ($K_\perp$) is negligible at relativistic energies. Such a conclusion is essentially in agreement with those obtained by McCracken

et al. (1968, 1971) from the low energy flare particle obser-
vations.

Even though the explanation of the average diurnal varia-
tion in terms of corotation has been satisfactory, considerable
deviations from the average picture in both amplitude and phase
exists on a day to day basis. A significant fraction of the
days in each year have either amplitudes much higher ($> 0.6\%$)
than predicted by the theory or with phase significantly different
from the 18 hour (corotational) direction (see Figure 1.5, pre-
sented later in Sec. 1.54), both of which cannot be explained
with the above simple theory, suggesting that the basic assumpt-
ions inherent in the model can only provide an explanation for
the gross average behaviour of the diurnal variation. The short
term and day to day variations of diurnal anisotropy have to be
understood in terms of changing electromagnetic parameters of
the interplanetary medium.

1.52 Diurnal anisotropy (general concept)

Gleeson (1969), starting with the relativistic Boltzmann
equation, has obtained a most general expression for the diffe-
rential current density for a spherically symmetric system
where the magnetic field $\underline{B}$ is general and there is also an
electric field $\underline{E}$.

$$\underline{S} = U\underline{V} = \Psi_{\parallel} + \frac{1}{1 + \eta^2}\Psi_{\perp} + \frac{\eta}{1 + \eta^2}\ (\Psi_{\perp} \times \frac{\underline{B}}{B}) \quad .. \quad 1.20$$

where $\Psi = C\ (r, E)\ U\underline{V} - K\ (\frac{\partial}{\partial r}\frac{U}{})\ + C\ (r, E)\ \frac{\eta U}{B}\cdot\underline{E} \quad .. \quad 1.20a$

$\eta = \omega\tau$, $\omega = \frac{eB}{m}$ is the proton gyroradius, τ is the average time between collisions, $K = \frac{v^2\tau}{3}$ is the isotropic diffusion coefficient which in the presence of magnetic field $\underset{\sim}{B}$ has components $K_{\shortparallel} = K$ and $K_{\perp} = K/(1 + \eta^2)$ and $C(r, E)$ is given by equation 1.10.

Since in the interplanetary medium electric field $\underset{\sim}{E} = -\underset{\sim}{V} \times \underset{\sim}{B}$, the above equation (1.20) can be easily written in terms of either $\underset{\sim}{E}$ or $\underset{\sim}{B}$ (Forman and Gleeson, 1970, unpublished). In terms of electric field

$$\underset{\sim}{S} = CU\underset{\sim}{V}_{\shortparallel} - K \left(\frac{\partial U}{\partial \underset{\sim}{r}}\right)_{\shortparallel} - \frac{K}{1+\eta^2} \left(\frac{\partial U}{\partial \underset{\sim}{r}}\right)_{\perp} + \frac{\eta K}{1+\eta^2} \frac{\partial U}{\partial \underset{\sim}{r}} \times \frac{\underset{\sim}{B}}{B} + CU \frac{\underset{\sim}{E} \times \underset{\sim}{B}}{B^2} \qquad 1.21$$

while in terms of solar wind velocity

$$\underset{\sim}{S} = CU\underset{\sim}{V} - K \left(\frac{\partial U}{\partial \underset{\sim}{r}}\right)_{\shortparallel} - \frac{K}{1+\eta^2} \left(\frac{\partial U}{\partial \underset{\sim}{r}}\right)_{\perp} + \frac{\eta K}{1+\eta^2}\frac{\partial U}{\partial \underset{\sim}{r}} \times \frac{\underset{\sim}{B}}{B} \qquad .. \quad 1.22$$

In equation 1.21, $\underset{\sim}{E} \times \underset{\sim}{B}$ drift is displayed explicitly and the convection term $CU\underset{\sim}{V}_{\shortparallel}$ is along the magnetic field, while equation 1.22 combines these two terms to yield a single convective term $CU\underset{\sim}{V}$. The other two terms represent the diffusive and gradient drift effects. The two equations are vectorially represented in Figure 1.4 a, b.

Forman and Gleeson (1970) have further added a term $K_{1}'(B, t, r)$ to the normal anisotropic diffusion effect $(K_{\shortparallel}/1+\eta^2)$ in equation 1.22 to include the effect of random walk of field lines (Jokipii and Parker, 1969) and obtained the modified streaming equation

$$\underset{\sim}{S} = S_c - K_{\shortparallel}\left(\frac{\partial U}{\partial \underset{\sim}{r}}\right)_{\shortparallel} - K_{\perp}\left(\frac{\partial U}{\partial \underset{\sim}{r}}\right)_{\perp} - \frac{v^2}{3\omega} \cdot \frac{\eta^2}{1+\eta^2} \left(\frac{\partial U}{\partial \underset{\sim}{r}}\right) \times \frac{\underset{\sim}{B}}{B} \qquad .. \quad 1.23$$

$$S_c = CU\underset{\sim}{V} \qquad\qquad .. \quad 1.23a$$
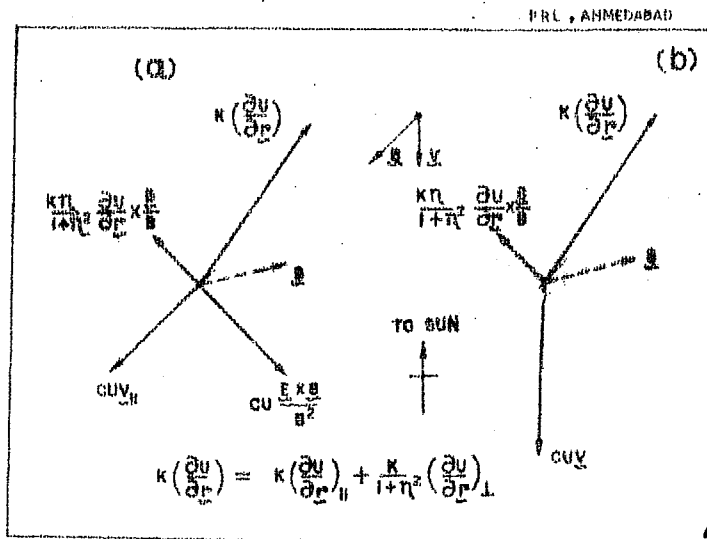
Fig. 1.4 - Showing the two representations of the components of the differential current density. In (a) the electric field is emphasised, in (b) the convective component CU$\underline{V}$. The sum is shown as the dotted vector $\underline{S}$.

$$K_\perp = K'_\perp (\underline{B}, t, r) + K_{\#}/(1 + \eta^2) \qquad \qquad .. \ 1.24$$

$$\text{and} \quad \underline{\underline{K}} \left(\frac{\partial U}{\partial r}\right) = K_{\#} \left(\frac{\partial U}{\partial r}\right)_{\|} + K_\perp \left(\frac{\partial U}{\partial r}\right)_\perp \qquad \qquad .. \ 1.24a$$

The diffusion tensor $\underline{\underline{K}}$ now includes the contribution due to the random motion of the field lines. The gradient contribution (the last term on the right hand side of equation 1.23) contains the normal scattering, expected in the presence of uniform magnetic field. $K'_\perp$ will come from the zero frequency spectrum, while $K_{\#}$ is obtainable from the high (resonant) frequency spectrum. Equation 1.23 contains two characteristic times, $\mathcal{T}$ and L/V corresponding to the two processes, scattering and random walk of field lines. The observation time t_o should be much greater than either of the characteristic times $\mathcal{T}$ or L/V for the process to be operative. Typically $\mathcal{T} \approx 20$ sec., and L, the correlation length of the magnetic field is $\approx 2 \times 10^{11}$ cm, hence L/V ≈ 80 min.

Therefore the scattering type diffusion coefficient is appropria-
te for solar burst events of short time duration (Rao et al.,
1967) where $\tau \ll t_o \ll L/V$, while the complete diffusion coeffici-
ent is more appropriate for long term average such as envolved
in the diurnal variation of galactic cosmic rays.

The azimuthal streaming $\underset{\sim}{S}_\phi$ in the limiting case of rigid
corotation can be obtained simply by neglecting the third and
fourth term of equation 1.23 with the assumption that
(a) $(\frac{\partial U}{\partial r})_\perp$ is zero (b) $K_\perp$ is negligible, and with an addi-
tional constraint of no radial streaming i.e. $\underset{\sim}{S}_r = 0$. These
conditions lead to an azimuthal anisotropy of bulk motion predi-
cted by Parker and Axford and discussed earlier (equation 1.18).

A decrease in the amplitude of the azimuthal anisotropy is
expected if either or both of the conditions (a) and (b) are not
valid (provided $\underset{\sim}{S}_r = 0$). In the first case (a) the reduction
will be due to the density gradients perpendicular to ecliptic
plane. The required gradients which fits the observations are
quite large and have not been observed. In the second case (b)
the reduction will be due to the contribution of finite $K_\perp$, the
amplitude, however, being governed by equation 1.19.

It is thus apparent from above, that the azimuthal or
corotational anisotropy is a direct consequence of the condition
of no radial streaming ($\underset{\sim}{S}_r = 0$), with its amplitude being dicta-
ted by the relative importance of the three terms other than
the convection term (equation 1.23).

The average diurnal variation observed by neutron monitors ($E \gtrsim 2$ GeV) in fact, do indicate that the contribution from $K_\perp$ and $(\frac{\partial U}{\partial r})_\perp$ are essentially zero (Subramanian, 1971a; Rao, 1972) and radial streaming is very small consistent with the theoretical predictions (Gleeson and Axford, 1968 a, b; Fisc and Axford, 1969).

From a detailed study of the solar flare cosmic ray events, McCracken et al (1968, 1971) and Rao et al (1971) have shown that late in the decay, convection is the most dominant mechanism in the interplanetary medium and $K_\perp$ is negligible. Very late in the decay ($\gtrsim 4$-5 days) they observed an easterly anisotropy which was attributed to a balance between the outward convection and inward field aligned diffusion due to the density gradients. These observational results have been explained recently by Ng and Gleeson (1971). Thus it is evident that the convection is the dominant mechanism operating both at low as well as at high energies. Based on the above concept which has been quite successful at low energies, the role of convection and diffusion has been extended to high energies to explain the day to day variations observed in the diurnal variation. The detailed mechanism with the supporting evidence will be presented in Chapter IV.

1.53   Characteristics of the diurnal variation

From an extensive analysis of the neutron monitor observations during 1954-1965 (Rao et al., 1963; McCracken and Rao, 1965), the average diurnal variation of cosmic ray intensity

can be adequately expressed by

$$\frac{\partial J(R)}{J(R)} = AR^{\beta} \cdot \cos(\psi - \psi_0) \cdot \cos\Lambda \quad \text{for } R < R_{max})$$
$$= 0 \quad \cdots \quad \text{for } R > R_{max}) \quad 1.25$$

where A is a constant equal to $(0.38 \pm 0.02) \times 10^{-2}$, $\beta = 0$,

$\psi_0 = 89 \pm 1.6^{\circ}$ measured anti-clockwise from the noon meridian.

Λ is the declination and R_{max} is usually of the order of 100 GV.

In other words, the average diurnal anisotropy of cosmic radiation is

(a)   rigidity independent in the rigidity range 1-100 GV;

(b)   varies as cosine of the declination;

(c)   has a time invariant amplitude in space of

       $\approx 0.38 \pm 0.02\%$ and

(d)   has a maximum flux incident from $89 \pm 1.6^{\circ}$ East of

       the earth-sun line.

Results obtained by other investigators, are essentially in

agreement with these findings (Bercovitch, 1963; Pomerantz et

al., 1962; Kane, 1964; Faller and Marsden, 1965; Willets et al.,

1970). The yearly mean diurnal amplitude and phase are found to

be practically constant over the solar cycle, except for the

small though significant decrease in amplitude in the years of

the minimum solar activity (Duggal et al., 1967). The mean

amplitude of the diurnal variation of the nucleonic component

in 1965 for example was $\approx$ 20% less than in 1958. The decrease

in amplitude in 1965 is now understood as due to a significant

reduction of the upper cut-off-rigidity (R_{max}). It seems that

except for the systematic and significant variation of R_{max},

all other parameters defining the diurnal variation are almost constant throughout the solar cycle. The change of R_{max} has been investigated by a number of workers including the author, and the detailed results are presented in Chapter IV.

Even though the neutron monitor results have not indicated any long term changes in the diurnal variation, at least for the period 1957-1970, the analysis of the data from other detectors responding to higher energies such as meson monitors and underground detectors, have always shown significant variation from year to year. Forbush and Venkatesan (1960) carried out a rigorous statistical analysis which revealed that significant variations in both amplitude and time of maximum of diurnal variation occurred during the period 1937-1959. From an analysis of the ion-chamber data from Godhavan, Cheltenham, Christchurch and Huancayo of more than 30 years Forbush (1967, 1969) concluded that the average diurnal variation is composed of two distinct components W and V. The W component has its maximum (or minimum) in the direction 128° East of the earth-sun line, which is roughly the average I.M.F. direction, and varies sinusoidally about zero mean with a periodicity of 20 years. The second component V has its maximum along 90° East of the earth-sun line and is subjected to larger variations well correlated with the geomagnetic activity. The spectral nature of both the components seems to be alike namely they are both energy independent (Duggal et al., 1970 a, b). Jacklyn et al. (1970) using the surface meson as well as the underground observations, however, have not

confirmed any systematic change in the diurnal phase for the period 1953-1966, while the change in amplitude was attributed by them to a change in R_{max}.

1.54 Short term anisotropic variation

In the recent past, it has been widely recognised that the average behaviour of the daily variation of cosmic rays which in essence represents the average interplanetary conditions is well understood. However, in contrast to the average properties, relatively very little is understood about the short term variations of the diurnal and semi-diurnal anisotropies, inspite of the realisation that an understanding of the production mechanism of the cosmic ray anisotropy on individual days can be used as a probe to monitor the changing interplanetary conditions.

Several investigators (Rao and Sarabhai, 1961, 1964; Patel et al, 1968; Pomerantz and Duggal, 1971; Rao, 1972) have pointed out the existence of a considerable variation in both the diurnal as well as semi-diurnal vectors from one day to another. Figure 1.5 shows typical frequency distribution of the diurnal and semi-diurnal amplitude and phase for each day in the year 1968 to 1971, as observed at the Ahmedabad neutron monitoring station. The fluctuation in both diurnal and semi-diurnal component are seen to be far more than that can be anticipated statistically. Further it is also seen that the variability in the amplitude and time of maximum of the semi-diurnal component is much larger than that observed in the diurnal component.
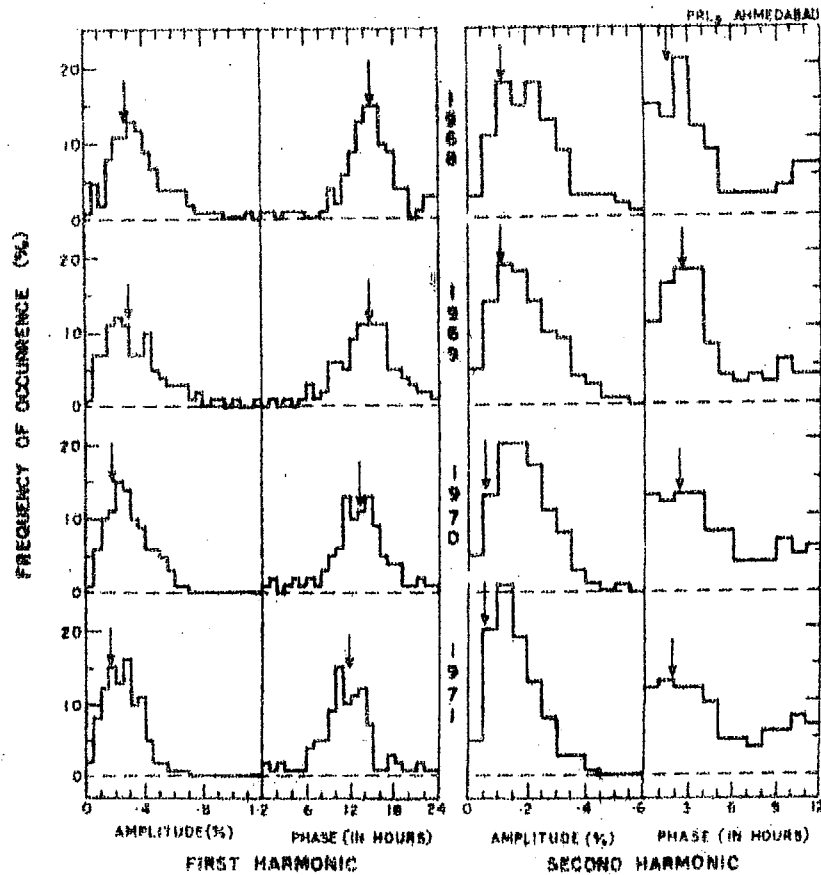
Fig. 1.5 - Histogram showing the frequency distribution of the amplitude and the time of maximum of the diurnal and semi-diurnal vari-ation as observed at Ahmedabad for the year 1968 to 1971. Arrows point to the vector average value for each year.

Applying the method of variational coefficient (Rao et al., 1963), Patel et al. (1968) have determined the energy spectrum of diurnal and semi-diurnal variation on a day to day basis for the period 1964-1965 and have found a large variability in the energy spectrum, though a significant part of the large variability can be due to the world wide intensity changes which occur at the same Universal Time (UT) at all the stations. However, during solar activity minimum, the number of days with significant contribution from the world wide variations are expected to be less. Therefore, even though the variability in the amplitude of the diurnal variation ($\leq 0.6\%$) can be understood in terms

of the partial cancellation of the perpendicular density gradients on a day to day basis, the large variability in the spectral characteristics and time of maximum cannot be understood by azimuthal streaming process alone. Sarabhai and Subramanian (1965), have qualitatively discussed this aspect and have pointed out that besides azimuthal streaming there are at least three more processes operative on a day to day basis.

1. Streaming in the longitudinal sector - Additional streaming due to the difference in the solar wind velocity and in the distribution of the small scale magnetic field inhomogeneities at different helio-longitudes (Parker, 1964).

2. Scattering at magnetic field irregularities - If a density gradient away from the plane of ecliptic exists, scattering at magnetic field irregularities can cause a short circuiting of these latitudinal gradients. This process will produce an aniso-tropy with a negative spectral exponent with a minimum along the magnetic field.

3. Latitudinal gradients of cosmic ray intensity, will produce a predominant semi-diurnal component with a positive exponent and time of maximum aligned perpendicular to the magnetic field. Besides if the intensity distribution away from the plane of ecliptic has a strong N-S asymmetry a significant first harmonic component will also be introduced in the daily variation.

It may, however, be noted that all the above processes are contained in the general equation of streaming (equation-

1.23) of Forman and Gleeson (1970) except for the prediction of semi-diurnal variation and that the equation 1.23 becomes invalid near the sector boundary crossing of the I.M.F. (Axford, 1965 a; Gleeson, 1969), where the condition $\omega T \gg 1$ is not satisfied.

Though the diurnal anisotropy during cosmic ray storms is usually altered, no systematic relationship with the intensity and nature of the storm has yet been established. There have been some reports that the amplitude of the diurnal variation increases and phase advances to earlier hours when such disturbances occur (Dorman, 1957; Tanskanen, 1968; Ostmann and Awadalla, 1970). However, this conclusion is not always true (Kane, 1962). An initial anisotropy in the onset of Forbush decrease aligned along a direction 30-50° West of the earth-sun line has been confirmed by many workers. The anisotropy sometimes develops even before the onset of the sudden commencement (Fenton et al., 1959; Ables et al, 1967; Mathews et al., 1963; Mercer and Wilson, 1968). The observed initial anisotropy has been explained (McCracken, 1962) as due to the sampling of the inner region of plasma cloud emitted from the sun containing the observed cosmic ray intensity which becomes accessible to detectors looking along this direction. Very recently Lindgren (1970) and Razdan and Bemalkhedkar (1971) have shown that the 27 day recurrent Forbush decreases in their recovery phase are usually associated with enhanced diurnal amplitudes with the direction of maxima in the 9-10 hour direction.

A recurrent tendency in the amplitude of the diurnal variation with periods of 27 days and well correlated with Σ Kp index, was reported by Kodama (1967) on the basis of power spectra and Chree analysis of Deep River neutron and meson data for 1962-1964, even though such an effect has not been confirmed universally (Kane, 1964).

Recently a number of investigators have detected a significant change in the diurnal amplitude and phase with the reversal of the average I.M.F. in alternate sectors. Based on the assumption of the existence of a north-south gradient in the cosmic ray density, density increasing southward i.e. below the equatorial plane of the sun (Barker and Hatton, 1970, 1971; Subramanian, 1971 b; Hashim and Bercovitch, 1972) the expected diurnal amplitude will be larger and phase shifted to earlier hours for positive I.M.F. direction (away from the sun) in comparison to days having negative polarity interplanetary magnetic field (towards the sun).

Using the available I.M.F. data and the observed daily variation, the above effect has essentially been confirmed by a number of workers (Mori, 1966; Ryder and Hatton, 1968; Patel et al., 1968; Hatton and Barker, 1971; Swinson, 1971; Hashim and Bercovitch, 1972). From these observations Hashim and Bercovitch (1972) have estimated the density gradient perpendicular to ecliptic plane, being 5.5 $R^{-0.6}$%/AU, which differ both in magnitude and rigidity dependence from the radial gradient.

The occurrence of trains of days with abnormally high amplitudes have been reported by a number of workers both during disturbed and quiet periods. Mathews et al.(1969) and Hashim and Thambyahpillai (1969) have independently concluded that during many days, exhibiting trains of large amplitude, the anisotropy was predominantly caused by a large decrease along the garden-hose direction. The possible existence of sinks in the garden-hose direction on such days was inferred much earlier by Rao and Sarabhai (1964), from the study of the distribution of time of maxima and minima of the daily variation. The large amplitude wave train occurring in July 1961 has revealed a systematic anti-clockwise shift of the diurnal anisotropy, the vector rotating completely around the clock in about 8 days (Duggal and Pomerantz, 1962). Smaller phase changes upto $\sim$ 10-12 hour during the entire event are more common. However, a good number of events, occurring during quiet period, have shown a significant change of diurnal phase towards later hours (21 hour direction). These events have been analysed in detail to find their characteristics in relation with the observed I.M.F. for the period 1966-1968, and the results have been used to advocate a simple model to explain the diurnal variation on a day to day basis (Chapter IV). Like-wise trains of days with negligibly small diurnal amplitudes are also found to occur, the analysis and results pertaining to them will also be discussed in Chapter IV.

1.55 Characteristics of the semi-diurnal variation

Analysis of the solar daily variation in terms of its Fourier components shows, on an average, a significant 12 hour

(semi-diurnal) wave in addition to the 24 hour component. The presence of such a component in the anisotropy of cosmic radiation has been suggested by a number of investigators (Rau, 1939; Elliot and Dolbear, 1950, 1951) long ago. However, the extra terrestrial nature of the semi-diurnal variation was not firmly established till recently (Elliot, 1952; Dorman, 1957; Katzman and Venkatesan, 1960), due to its possible atmospheric origin. From a comparison of the observed variation in the east and west pointing telescope inclined at the same angle to zenith, where the atmospheric contribution can be cancelled to a first approximation (Elliot and Rothwell, 1956), Rao and Sarabhai (1961) were able to provide a reasonable evidence for the existence of a significant semi-diurnal component. However, due to the presence of large amplitude of semi-diurnal pressure wave, which can introduce a pressure induced variation, the poor statistical accuracy due to the low counting rate of the monitors, and the large variability of the observed semi-diurnal variation on a day to day basis (Ahluwalia, 1962; Rao and Sarabhai, 1961), the existence of semi-diurnal variation of cosmic rays could not be firmly established.

The first conclusive experimental evidence for the presence of a significant semi-diurnal anisotropy of cosmic rays, with its maximum aligned in a direction perpendicular to the direction of the I.M.F. was obtained by Ables et al.(1965). The authors used neutron monitor data including super neutron monitors, for improved statistics and power spectral analysis followed by

sophisticated numerical filter techniques for improved signal to noise ratio. Subsequent analysis by the author as well as by other investigators have not only confirmed the existence of the semi-diurnal anisotropy but have also provided its detailed characteristics, which on an average basis can be summarised as follows,

1) The average semi-diurnal amplitude in space for cosmic ray particles in the rigidity range 1-200 GV has a value = 0.11 ± 0.02% during the period 1958-1970, with its time of maximum along ∼ 0300 hours direction, essentially perpendicular to the direction of average I.M.F.

2) Both the phase and amplitude are time invariant within the statistical accuracy.

3) The anisotropy is rigidity dependent with a positive spectral exponent of ∼ + 1.0, as compared to $\beta = 0$ for the diurnal variation.

4) Unlike the diurnal variation for which the amplitude has a cos λ dependence, where λ is the mean asymptotic latitude of response, the semi-diurnal anisotropy has a $\cos^2 \lambda$ dependence. The details of the analysis and the results obtained by the author will be presented in Chapter V.

Both Subramanian and Sarabhai (1967) and Quenby and Lietti (1963) have suggested that the second harmonic component of the cosmic ray daily variation can be due to the particle density gradient in the plane perpendicular to the plane of ecliptic. If we assume an Archimedes spiral configuration for

the I.M.F., it is evident that the particles arriving along the sun's polar field lines suffer much less modulation as compared to those arriving in the ecliptic plane, thus giving rise to a cosmic ray density gradient, with the intensity increasing away from the plane of ecliptic. Viewing along the I.M.F. lines of force (i.e. along the garden-hose direction) a neutron monitor on earth measures cosmic ray flux characteristic of equatorial plane. Viewing in a direction perpendicular to the magnetic field, the detector samples particles arriving from higher helio-latitudes: the heliolatitude corresponding to the gyroradius of the particle under consideration. Thus the higher the energy the higher the heliolatitude of sampling by a monitor. Conse-quently, the positive gradient of cosmic ray density with the increase in heliolatitudes gives rise to a semi-diurnal maximum aligned in a direction perpendicular to the direction of I.M.F., because the earth, as it spins, measures cosmic ray intensity twice along and twice perpendicular to the field direction in the course of a day. Both the theories, predict that the semi-diurnal anisotropy as observed in space (1) has an exponent of $R^{+1.0}$, where R is rigidity; (2) varies as $Cos^2\lambda$ and (3) has a maximum flux in a direction perpendicular to the I.M.F. The positive spectral exponent predicted by the theory is consistent with the much larger semi-diurnal variation observed at equato-rial latitudes.

According to Quenby and Lietti (1968), the perpendicular gradient of the cosmic ray flux is a consequence of the random

scattering of particles by scattering centres superimposed on the quiet time Archimedean spiral. The galactic particles that arrive over the pole experience easy access, since they diffuse along almost straight field lines, where as those entering in the solar equatorial plane are constrained to follow many spiral loops. Consequently, the cosmic ray density should rise on each side of the solar equatorial plane. Subramanian and Sarabhai (1967), on the other hand infer the perpendicular cosmic ray density gradient from $\lambda 5303$ index measurements, based on their finding of the inverse relationship between $\lambda 5303$ green coronal line and the cosmic ray intensity. For a given cosmic ray density distribution, both the theories predict practically same results. Following Quenby and Lietti (1968), we can write, the cosmic ray density near the earth's orbit as

$$N_a = N_\infty \exp \left[\frac{- VD^3}{3\ K_\| \ a^2} \cdot \mathrm{Sin}^2\theta \right] \qquad \qquad ..\ 1.26$$

which for typical value of V = 400 km per sec, $\lambda = 10^{12}$ R cm and D = 40 AU reduces to

$$N_a = N_\infty \cdot \exp \left[\frac{-\ 2.4}{R}\ \mathrm{Sin}^2\theta \right] \qquad \qquad ..\ 1.27$$

The Taylor expansion of the above expression gives a peak to peak amplitude of the second harmonic, which for a detector that looks at an asymptotic latitude λ with respect to the solar equatorial plane and at an asymptotic longitude ψ measured from spiral field direction, is given by

$$r_2 = 0.005\ R(\ 1 - Cos^2\psi\ Cos^2\lambda\ )^{3/2} \left[\ 1 + \frac{\tan^2\lambda}{Sin^2\psi}\right]^{-1}$$

$$\text{for } R < R_{max}$$

and $\quad r_2 = 0 \qquad\qquad$ for $R > R_{max}$ $\qquad\qquad$ .. 1.28

where R is in GV and R_{max} is the maximum rigidity upto which the semi-diurnal anisotropy exists.

The essential requirement of both the models described above is the existence of cosmic ray density gradient perpendicular to the solar equatorial plane. The presence of such gradients, in principle, can be inferred from the observed long term changes in the cosmic ray intensity due to the earth's motion around the sun, which changes its position by $\pm 7.25^{\circ}$ with respect to sun's equatorial plane in the course of one year. However the results obtained from the neutron monitor observations, though not conclusive (Kane, 1968; Barker and Hatton, 1970; Subramanian, 1971 b), have not generally supported the existence of required gradients.

It has been felt for a long time, that the semi-diurnal anisotropy would result merely from the 'pitch angle distribution' of the particles in the I.M.F. (Sarabhai et al., 1965). Nagashima et al. (1972 a, b) have recently developed an analytical method to determine 3-dimensional cosmic ray anisotropy vectors in interplanetary space and have shown that the observations are in favour of the pitch angle distribution model for the production of the semi-diurnal anisotropy. More recently Barnden (1972) has introduced the 'origin of scatter' technique,

a theoretical method to calculate the count rate variation in an earth based detector. He finds that the presently accepted values of the radial gradients of the cosmic ray density are sufficient to produce the observed semi-diurnal anisotropy. In other words, the pitch angle distribution of the cosmic ray particles manifests itself as semi-diurnal anisotropy. Whereas the presently available experimental observations are not yet capable of deciding between the two theories, the new concept provides a fresh insight to the understanding of the cosmic ray modulation phenomena.

C H A P T E R - II

EXPERIMENTAL TECHNIQUE - SUPER NEUTRON MONITOR

2.1   Introduction

A primary cosmic ray interacting with the nucleii at the
top of the atmosphere results in a cascade of secondary particles,
including the evaporation neutrons. The evaporation neutrons
which are proportional to the nucleonic component intensity show
much larger variation with the latitude as compared to other
secondaries such as muons, indicating their association with lower
energy part of the spectrum of the primary cosmic radiation
(Simpson, 1948, 1949). Though a simple neutron detector such as
BF_3 filled proportional counter can be easily used to detect the
atmospheric evaporation neutrons, Simpson et al (1953) pointed
out that such a detector is unsuitable for continuous monitoring
of cosmic ray intensity due to (a) a slow neutron detector using
a bare BF_3 counter with the atmosphere as moderator will be great-
ly affected by large changes in the climatic conditions of the
atmosphere and (b) the fast neutron detector using a BF_3 counter
surrounded by a local moderating medium will readily respond to
changes of ambient neutron production near the detector resulting
from movement of heavy materials. The use of lead, as a target
of high atomic mass (A), for the local production of evaporation
neutrons (production rate is $\propto A^{+0.4}$) has not only removed the
above shortcomings but also increased the count rate of the
detector, thus improving the statistical accuracy.

The first neutron monitors, which consisted of BF_3 proportional counters surrounded by paraffin moderator, lead producer and a shield of hydrogenous material, were installed by Simpson at Chicago, Climax, Huancayo and Scarmento peak around 1952. Later a standard design was recommended by Simpson (1957) and a network of about 50 standard neutron monitors was established during IGY. While a large amount of valuable information was obtained from the data from these monitors, by the end of 1958 it had become clear that their counting rate were too low to permit unambiguous studies of many aspects of the cosmic ray time variations. This led to the super neutron monitors (NM-64) which employ large size BF_3 counters and which has now been adopted as the standard geometry (Carmichael, 1964). A full size NM-64 super neutron monitor consists of 18 counters in three independent units each containing six counters. The counting rate of an 18-NM-64 monitor is about a million per hour at a sea level station having cut-off-rigidity $\leqslant$ 2 GV.

Inspite of more than thirty NM-64 type monitors which were in operation during 1968, to provide a world-wide coverage both in latitude as well as in longitude, conspicuous gaps in coverage in the longitude range 25^OE to 130^OE, and almost complete absence of equatorial monitor are noticeable. The establishment of Ahmedabad super neutron monitor in the year 1968 with high counting rate, not only fills this wide gap but also records the cosmic ray intensity at a very high cut-off-rigidity. A list of all the cosmic ray neutron monitoring stations (both IGY and

TABLE 2.1 - List of all the cosmic ray neutron monitoring stations (cut-off-rigidity ≥ 8 GV), which either started functioning in the year 1968 or were functional before 1968.

S.No.	Name of the station	Latitude	Longitude	Altitude (Meters)	Cut-off-rigidity (GV)
(a) IGY Standard Monitor					
1.	Cordoba	-31.40	295.32	430	11.45
2.	Gulmerg	34.07	74.42	2740	11.91
3.	Haleakala	20.36	203.72	3050	13.30
4.	Huancayo	-12.03	284.67	3350	13.49
5.	Makerere (Kampala)	0.33	32.56	1195	14.98
6.	Mina Aguilar	-23.10	294.30	4000	12.51
7.	Mt. Norikura	36.12	137.56	2770	11.39
(b) Super Neutron Monitor (NM-64)					
1.	Ahmedabad	23.01	72.61	S.L.	15.94
2.	Buenos Aires	-34.58	301.50	S.L.	10.63
3.	Chacaltaya	-16.31	291.85	5220	13.10
4.	Kula (Hawaii)**	20.71	203.74	930	13.30
5.	Mexico City	19.33	260.82	2270	9.53
6.	Mt. Norikura	36.12	137.56	2770	11.39

** Temporary Station

NM-64) with cut-off-rigidity ≥ 8 GV, and which were operational during 1968, are given in Table 2.1. The table very clearly brings out the fact, that Ahmedabad has the highest cut-off-rigidity amongst all the stations. Besides, Ahmedabad is one

IQSY NEUTRON MONITORS

GEOGRAPHIC LATITUDE

GEOGRAPHIC LONGITUDE

IGY NEUTRON MONITORS

GEOGRAPHIC LATITUDE

GEOGRAPHIC LONGITUDE

MUON DETECTORS

GEOGRAPHIC LATITUDE

GEOGRAPHIC LONGITUDE
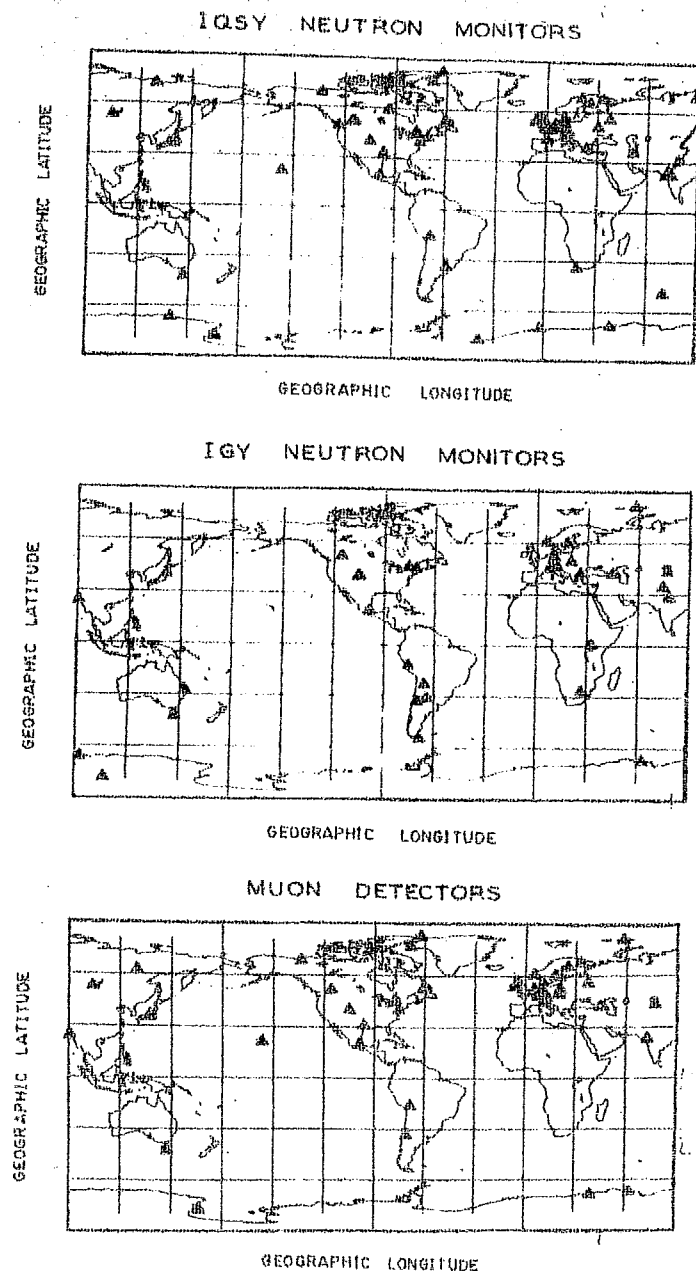
Fig. 2.1 - Showing the positioning of the presently running NM-64 (IQSY) type and IGY type neutron monitoring stations. The arrow indicates the location of Ahmedabad station. The position of the stations operating meson monitor telescopes are also included (after Shea, 1972).

of the very few sea-level stations for which the coupling coefficients are better known and therefore, the data from this monitoring station is of very great value in the interpretation of the time variation phenomena. The number of super neutron monitor stations have steadily increased, in the past three to four years, and the

few existing gaps can be partially filled using the data from the IGY type neutron monitor stations (Figure 2.1).

2.2   Description of the Super Neutron Monitor at Ahmedabad

The basic design of the super neutron monitor (18-NM-64) at Ahmedabad (India) closely follows the design recommended by Dr. Carmichael.   It consists of eighteen large BF_3 proportional counters sensitive to thermal neutrons, each counter being enclosed within a cylinder of paraffin moderator.   The counter assembly consisting of moderator and counter is surrounded by lead.   The 18-counters are arranged in three arrays of 6 counters each. Each array is completely shielded by paraffin reflector which prevents the escape of neutrons that would otherwise fail to be detected.   The shield also prevents the detection of low energy neutrons produced in the condensed material outside the monitor. Except for the use of the paraffin wax both as a reflector and moderator in place of polyethylene and the use of old copper counters (Fowler, 1963), the design of super neutron monitor at Ahmedabad is the same as that recommended for IQSY (Carmichael, 1964).   The copper counters used here were the ones used by Dr. Carmichael at Deep River from 1961-1964.   The background count rate due to residual alpha (α) contamination is ≈ 2 counts per minute as compared to 5 counts per minute for the stainless steel counter.

Figure 2.2 shows one of the three identical and independent sections of the neutron monitor assembly at Ahmedabad.

Fig. 2.2 Showing the photograph of the third tray of the 18–NM–64 detector assembly at Ahmedabad. The boxes projecting out of each of the proportional counters (extreme right), contain the pre-amplifier–discriminator assembly. The two boxes on the top of the monitor contain (1) the amplifier–mixer assembly (2) the high voltage (E.H.T.) distribution points.

The box projecting out of each of the counters, seen in the
figure, contains the pre-amplifier and discriminator assembly
attached to each counter. The entire monitor is housed in a
separate well shielded building whose temperature is maintained
at $70 \pm 1^{\circ}F$. The output of each of the discriminators is fed
to the amplifier-mixer box seen at the top of the assembly.

2.21 The principle of neutron counter

The proportional counters filled with Boron trifluoride
(BF_3) gas enriched with the isotope B^{10} are most suitable for
the detection of thermal neutrons. The large size counters used
in NM-64 monitor are filled with pure BF_3 gas (96% B^{10} isotope)
at a pressure of 20 cm Hg at $22^{\circ}C$ and are usually operated at
2800 V potential at which the gas multiplication is ~ 35. The
counters have a plateau in the proportional region (2800 V) for
over a range of ~ 400 V, with a slope less than 1% per 100 volts.
A neutron which is captured by a B^{10} nucleus induces the exother-
mic reaction

$$_5B^{10} + {_0n^1} \longrightarrow {_3Li^7} + {_2He^4} \qquad .. \ 2.1$$
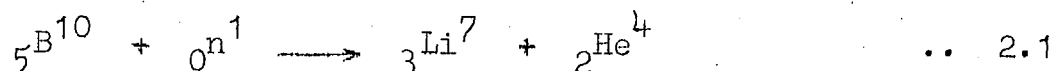
The cross-section of this reaction follows a 1/v dependence
(v is the velocity of the captured neutron) and is ≈ 3820 barns
at thermal energies (1/40 ev). In 94% of the reaction $_3Li^7$
nucleus is left in a 0.48 MeV excited state, 2.30 MeV being
shared by the $_3Li^7$ and $_2He^4$ nuclei. In the remaining 6% the
$_3Li^7$ nucleus is left in the ground state and $_3Li^7$ and $_2He^4$ nuclei
have a total kinetic energy of 2.78 MeV. The output pulse

height which is ≈ 1 millivolt depends strongly on the high
voltage applied to the counter. As the counter is operated in
the proportional region, it is easily possible to discriminate
these pulses against relatively small pulses produced by the
passage of muons, electrons, gamma rays, etc., through the
counter. Further, since only one nucleus is consumed in each
reaction, the BF_3 counters have a very long life.

2.22 Production of thermal neutrons

The capture cross-section of the BF_3 filled proportional
counter being maximum for thermal energy neutrons, the choice of
the geometry and quantity of the reflector, lead producer and
moderator must be optimised to obtain maximum efficiency
(Table 2.2). The entire assembly of lead cylinders containing
six neutron counters is encased in a simple rectangular box of
low density paraffin wax of 7.5 cm (3") thickness. The paraffin
wax acts as a reflector and establishes the full albedo of neutrons
from the lead producer inside the monitor. It also diminishes
the proportion of low energy neutrons arriving at the detector
from outside though the chosen thickness of 7.5 cm is not comple-
tely adequate to isolate the monitor from all the evaporation
neutrons produced outside. Typically the contribution of such
neutrons is ≈ 5%. However, since this contribution can change
with the change in the environment (Bercovitch, 1967) it is very
important to ensure that no unnecessary transient material is
kept near the monitor.

TABLE 2.2 - Dimensions and counting rate of I.G.Y. type stand-
ard neutron monitor and NM-64 type super neutron monitor

Specification	Standard IGY Monitor	NM-64 Monitor
Number of counters per tray	6	6
Number of trays in one unit	2	3
Counters		
Active length (cm)	86.4	191
Diameter (cm)	3.8	14.8
Pressure (cm Hg)	45	20
Inner moderator		
Average thickness (cm)	3.2	2.0
Producer		
Average depth (g cm^{-2})	153	156
Area per tray (m^2)	0.94	6.21
Length parallel to counters (cm)	102	207
Reflector		
Average thickness (cm)	28	7.5
Counting rate (typical)		
of a high latitude sea level station per tray per hour	~12000	~250000
per m^2 of producer	~12800	~40000

The local neutron producer is of lead of purity greater
than 99.9% in the form of cylinders of 25.4 cm internal diameter
and 35.6 cm outside diameter with an outer rectangular proje-
ction on two sides. Each cylinder is of overall length 207 cm

and is cast in the form of 18 lead rings each of length ∿11.5 cm.
Each ring weighs 89.3 ± 0.6 kg (∿ 200 pounds) making the total
mass of the entire lead cylinder equal to 1608 ± 10 kg.

The moderator tube in Ahmedabad NM-64 monitor consists of
2 cm thick paraffin wax contained in an alluminium cylinder with
outer diameter 25.4 cm thus fitting closely with the lead cylin-
der. However, the stainless steel counters, which are now
available commercially, are wrapped in a polyethylene tube,
which besides being an efficient moderator, also serves as a
protecting case for the delicate counter.

A cosmic ray particle interacting in the lead produces
several associated evaporation neutrons, the number of these
evaporation neutrons in general, being proportional to the energy
of the interacting particle. Typically a parent particle of
energy 200 to 300 MeV produces on an average of about ∿ 10 evapo-
ration neutrons. In the neutron monitor a spectrum of excitation
energy of the lead nuclei results because (a) the incident
nucleons have a range of energies (b) nucleons with a given
energy produces a range of excitation energies due to the statis-
tical nature of the intranuclear cascade. These evaporation
neutrons are quickly slowed down to thermal energies by collisions
with the modulating material and most of which are subsequently
captured by B^{10} atoms of the counter gas. A small portion may
be lost through capture by hydrogen atom in the moderator or
counter walls. The detection efficiency of the evaporation
neutrons in NM-64 monitor is about 6% (Hatton and Carmichael, 1964).

2.23 Data recording system

With the improvement in the counting rate of the monitor it was soon realised that for applying adequate correction for atmospheric variations, it is necessary to record the data at shorter intervals such as 4-5 minutes. The frequency of data sampling needs to be further increased during periods when cosmic ray enhancement due to solar flare occurs. To handle such a large amount of data, it is desirable to have a completely automatic data recording system of the type developed at M.I.T. (Richard et al, 1963).

The block diagram (Figure 2.3) summarizes the basic operation of the complete neutron monitor data system at Ahmedabad. The $\sim$1 mV pulses coming out of the counter are fed to a pre-amplifier followed by a three-stage amplifier and a simple tunnel diode discriminator, all contained in the front end box of the counter. .The discrimination threshold is so adjusted as to reject the small pulses produced by other secondary particles such as mesons electrons and γ-rays. The counting rate of each counter at Ahmedabad is approximately 10,000 per hour. The output of the discriminators, are suitably amplified and mixed together, the mixed output being counted in conventional decade scalers. The count from each of the three sections are accumulated for four minute intervals. At the end of each interval, the counts registered in the scalers are transferred to a temporary binary memory system and the decades are cleared immediately with dead time of 6 μs for further counting.
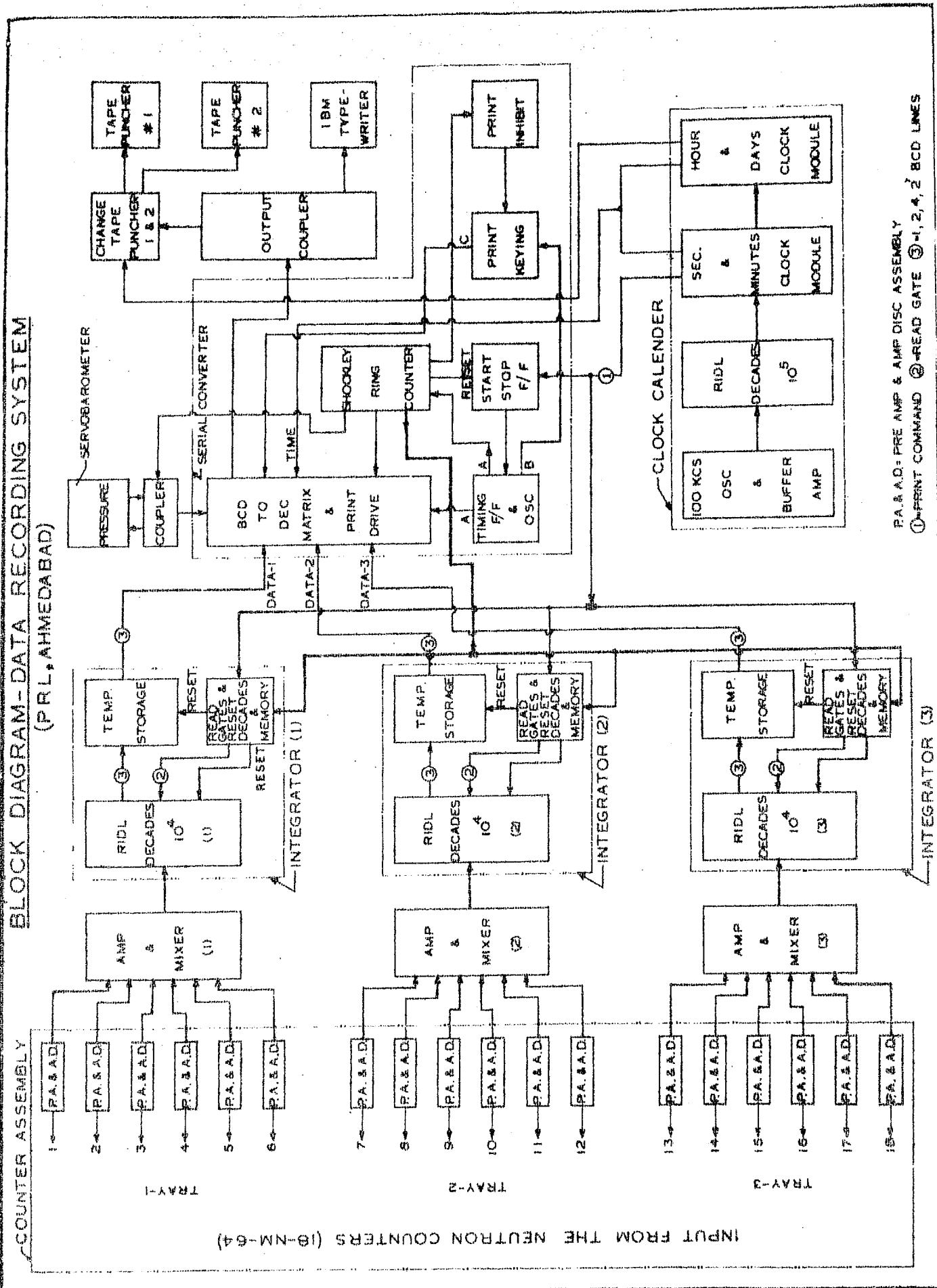
Fig. 2.3 - Block diagram of data recording system along with the Pre-amplifier, Discriminator and Amplifier-Mixer assembly.
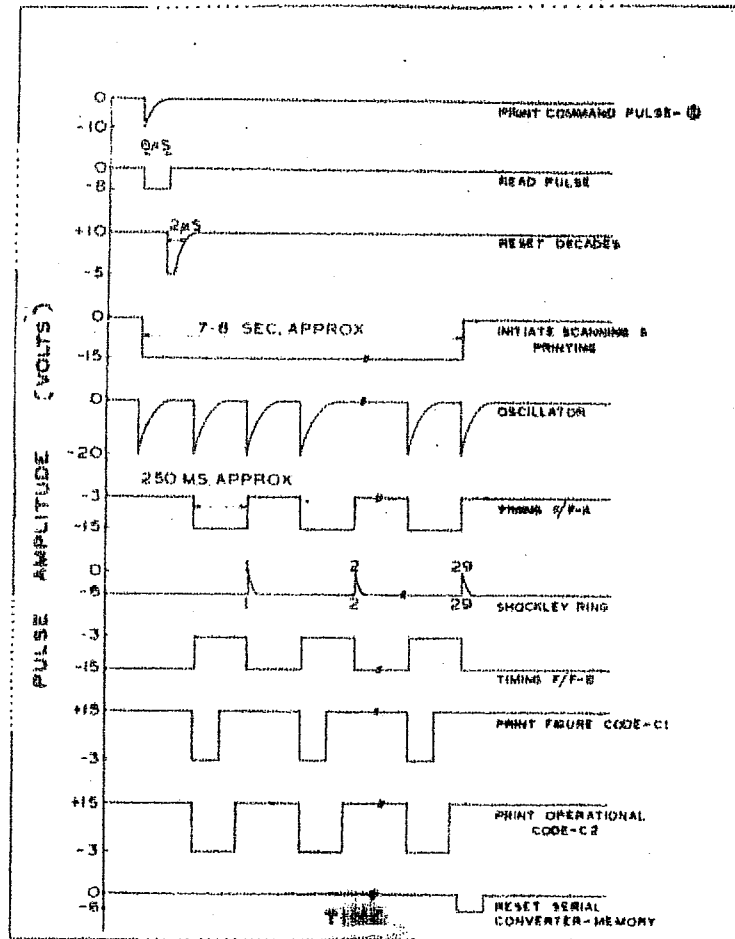
Fig. 2.4 - Time sequence involved in the operation of entire circuit in every 7-8 second printing (for each four minute data cycle).

The data from the memory is then serially transferred in BCD form on to a paper tape punch and in decimal form on to a typewriter. The pressure data from the digital servobarometer (indicating the pressure nearest to 0.1 mm) as well as the time information is also recorded for each interval. Figure 2.4 depicts the time sequence of various operations involved.
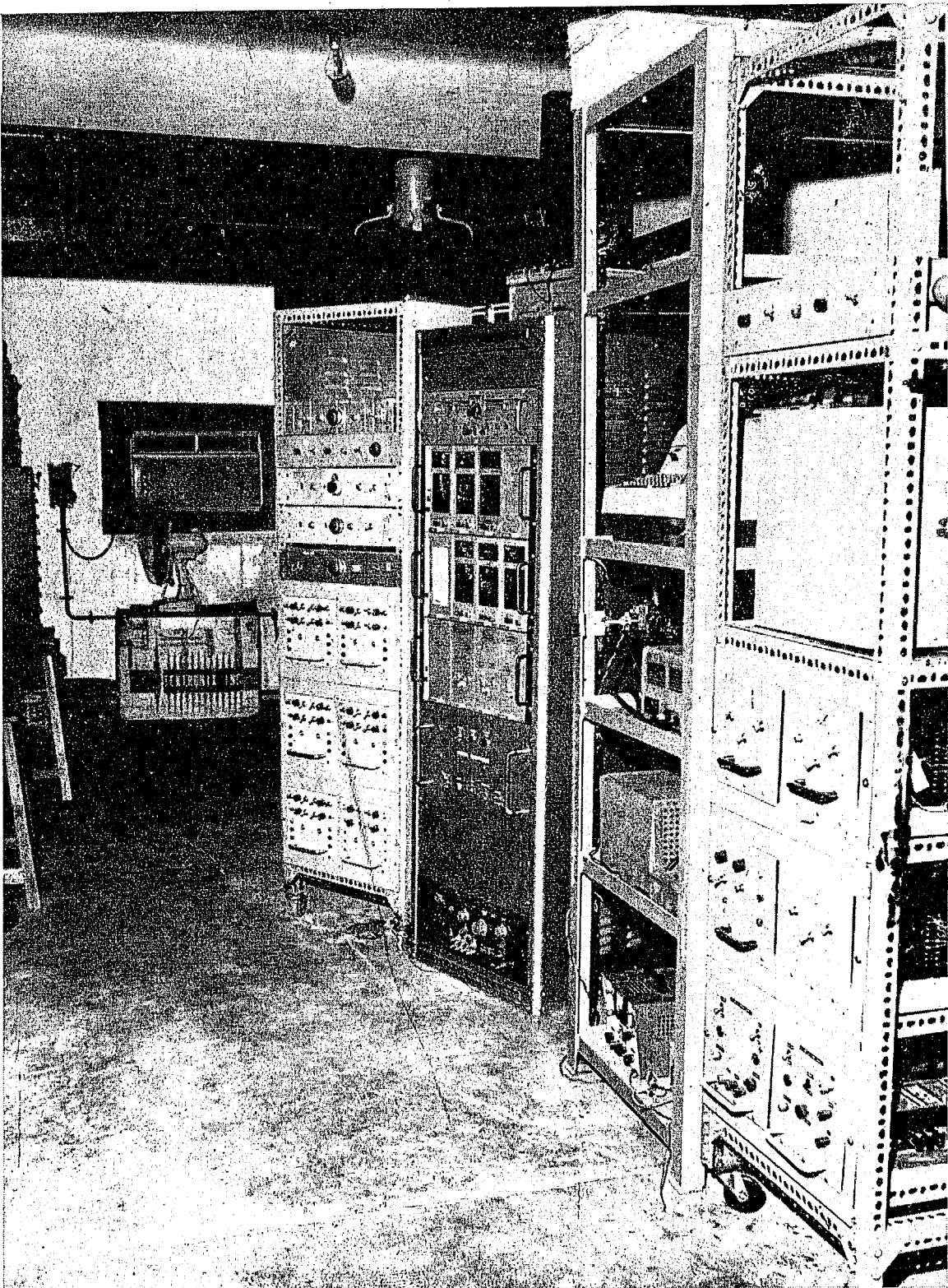
Fig. 2.5 Shows the complete data recording system housed in a separate room (in front
of the counter assembly room). The rack on the extreme left contains both low
voltage and high voltage units, while the next two racks contain complete data
processing and recording system. The rack on the extreme right contains the 3
multiplicity meters along with their associated power supply units and the auto-
matic camera system to photograph the mechanical counters registering the counts
from the multiplicity meters.
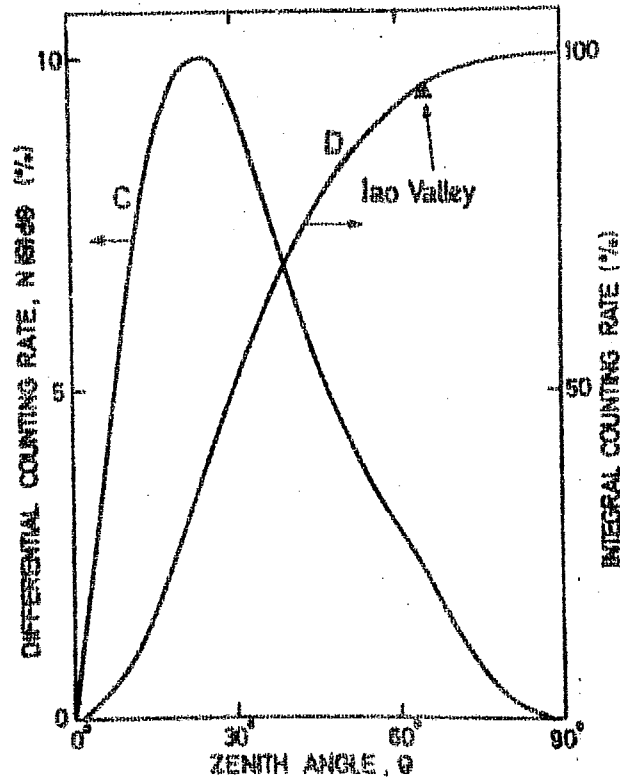
Fig. 2.6 - The differential (Curve C) and integral
(Curve D) counting rates of a neutron monitor as a function
of zenith angle as deduced by Phillips and Parsons (1962).
Also shown is a point determined from the mobile NM-64
monitor survey of Carmichael et al (1969) when the monitor
was situated in the Iao Valley, Hawaii (after Hatton, 1971).

2.3 Zenith angle dependence of neutron monitor

The relative contribution to the counting rate from

secondary nucleons incident from a zenith interval $d\theta$ at θ

is given by

$$N(\theta). d\theta \propto J(\theta). S(\theta). \sin\theta . d\theta \qquad ...2.2$$

where $J(\theta)$ is the zenith angle distribution of the nucleon-

ic component, and $S(\theta)$ is the sensitivity of the monitor to

this component as a function of zenith angle.

S (θ) is found to be approximately constant indicating that the neutron monitor behaves as an omnidirectional detector. The smaller area presented to the incident nucleons at large zenith angles is compensated by the greater probability of the nucleons interacting and the larger number of evaporation neutrons produced following these interactions.

The zenith angle distribution of the nucleonic component was determined by Phillips and Parsons (1962) using a mobile IGY monitor and is consistent with $J(\theta) \propto Cos^5\theta$ over the range 0 to 40° but for $\theta > 40^{\circ}$, the function falls off more slowly. These authors also determined the variation of the count rate with zenith angle (Figure 2.6) and found that the greatest contribution was from zenith angle $\sim 25^{\circ}$. Curve D in Figure 2.6 (which is the integral of equation 2.2) shows that a substantial percentage ($\sim 7\%$ for $\theta > 60^{\circ}$) of the count rate comes from large zenith angles. The results of Carmichael et al (1969) for Iao Valley, Hawaii, is also shown in the same figure, and is consistent with the earlier result obtained by Phillips and Parsons. Thus it is apparent that if a constant recording efficiency is to be maintained over periods of time of the order of a solar cycle, the erection and demolition of buildings adjacent to fixed monitors should be taken into account. These changes will not only affect the attenuation of the nucleonic beam from low zenith angles, but will also alter the low-energy environmental background which is quite important in the case of the NM-64 monitor.

TABLE 2.3 - The percentage contributions made by various secondary components to the counting rate of the IGY and NM-64 monitors

Component	Percentage contribution	
	IGY Monitor	NM-64 Monitor
Neutrons	83.6 ± 2.0	85.2 ± 2.0
Protons	7.4 ± 1.0	7.2 ± 1.0
Pions	1.2 ± 0.3	1.0 ± 0.3
Stopping muons	4.4 ± 0.8	3.6 ± 0.7
Interacting muons	2.4 ± 0.4	2.0 ± 0.4
Background	1.0	1.0

2.4 Total count rate and the production of neutrons in the neutron monitor

A number of authors have estimated the contributions to the counting rate made by various secondary components, using different methods, for both IGY and NM-64 monitors (Simpson et al, 1953; Hughes and Marsden 1966; Harman and Hatton, 1968). A summary of the relative contributions of different primary components by Hatton (1971) for Leeds IGY and NM-64 monitor, which is also applicable to any high latitude neutron monitor, is given in Table 2.3.

A slight increase in the neutron contribution in NM-64 monitor as compared to IGY monitor has been attributed to the smaller thickness of the reflector in the NM-64 monitor (3"). This increase occurs preferentially in the neutron contribution

due to the low energy neutrons (< 100 MeV) having a smaller
absorption mean free path in the paraffin wax, than the other
components. The reflector thickness is also able to modify the
median energy response of $\sim$ 160 MeV for IGY monitor to $\sim$ 130 MeV
for NM-64 monitor.

2.41   Neutron production by nucleons

Nucleon-nucleus interactions are usually described in
terms of a two stage process. In the first phase 'cascade phase'
knock on nucleons and created pions are emitted with a broad
energy spectrum extending upto energies comparable with the inci-
dent nucleon energy and with an angular distribution peaked in
the direction of motion of the incident nucleon. At the end of
the first phase the residual nucleon is left in an excited state
and further emission of particles, predominantly evaporation
neutrons, follows during the second phase, the de-excitation or
evaporation phase. The evaporation neutrons are characterized
by an isotropic angular distribution and an energy spectrum
peaked around a few MeV. Both theoretically (Shen, 1968) and
experimentally (Hughes et al, 1964) it is known that the average
number of evaporation neutrons produced, increases both with
the increase in the energy of the incident particle, and with
the increasse in the producer thickness. However, the use of
neutron monitor as an energy spectrometer is limited by the
stochastic nature of the processes leading to the production
of the evaporation neutrons which results in a broad, approxi-
mately exponential neutron production spectrum. A more

detailed discussion of the neutron production by various second-
ary components is, however, not attempted.

2.5   Stability of the neutron monitor

Even though long term monitoring of the stability of the
neutron monitor can be accomplished through inter-comparison of
the counting rate ratios of the three identical sections of the
monitor the pulse height calibration on a long term basis is
essential (McCracken et al, 1966 a) for keeping a completely
reliable check of the total system particularly because of the
monitors succeptibility to abrupt changes in efficiency. Such
abrupt changes can occur due to a number of factors such as

(a)   The deterioration or replacement of the counter

(b)   Change in the counter position relative to the producer

(c)   Variation in the applied voltage to the counter

(d)   Drift in the discriminator levels

(e)   Change in the amplifier dead time (pulse width).

2.51 Plateau and pulse height spectra

A typical plot of the counting rate of a neutron counter
against the applied high voltage (E.H.T.) shows, that with the
increase of E.H.T. the counter enters into the proportional
region where the pulses due to thermal neutrons are relatively
big as compared to the pulses from γ -rays and other charged
particles (noise pulses), and consequently can be easily discri-
minated against background noise. The proportional region in
NM-64 monitor usually extends from ~2700 volts to 3100-3200

PHL, AHMEDABAD
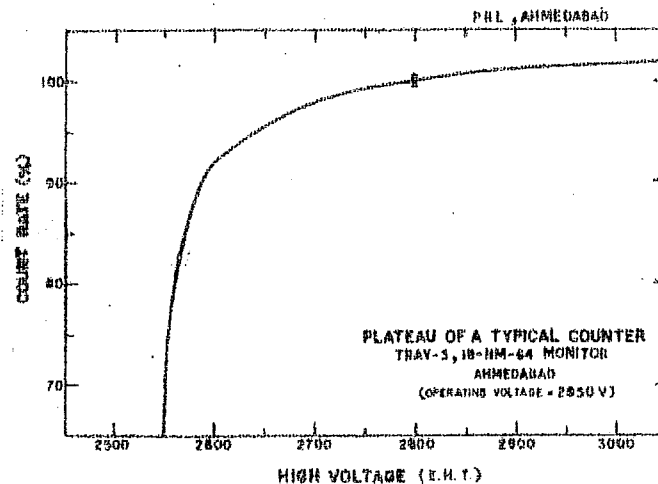
Fig.2.7 — The percent counting rate using the Pu-Be neutron source versus the applied voltage, for a typical 18-NM-64 counter. The error is typical and has been derived from the dispersion between various measurements at the same voltage. The operating voltage for tray-3 is 2850 volts.

volts with the plateau having a range of ≈400-500 volts with a slope of ≤1% per 100 volts. The plateau of a typical counter in tray 3 of Ahmedabad 18-NM-64 monitor obtained by using a 15 millicurie Pu-Be neutron source is shown in Figure 2.7. Since each tray of the neutron monitor containing six counters is operated on a single high voltage these counters are preselected making sure that they have essentially similar plateau characteristics. Having determined the plateau for each tray, optimum operating voltage for each tray is selected.

The pulse height distribution for a typical counter operating at different high voltages is shown in Figure 2.8 — 'a, b, c'. The peaks 'A' and 'B' which are found to shift to higher channels with the increase in E.H.T. correspond to 2.30 and 2.78 MeV alpha particles respectively, and the low
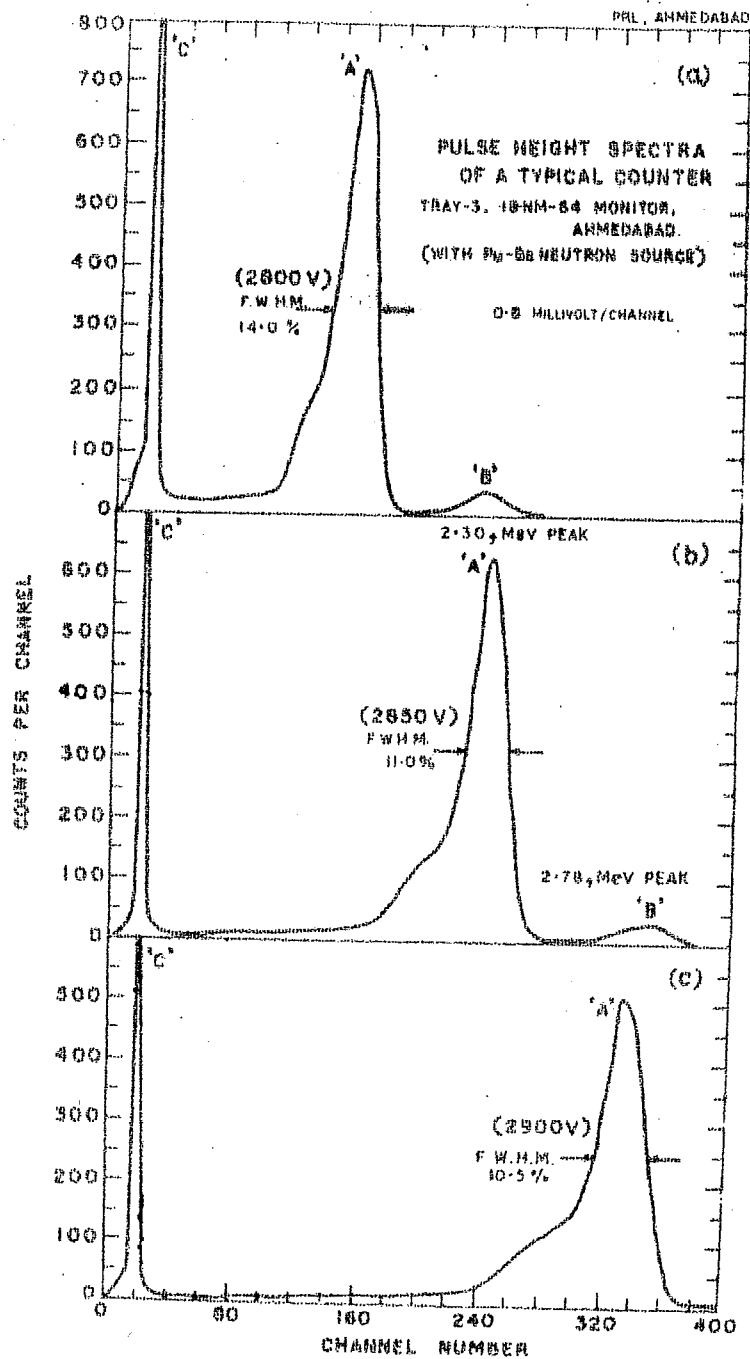
Fig. 2.8 - The pulse spectrum of a typical 18-NM-64
counter employed in Ahmedabad neutron monitor at three
different operating voltages. The pulse amplitude pertains
to the counter pulses just prior to discrimination in the
tunnel diode discriminator.

amplitude pulses named 'C' are the noise pulses. The resolution
of the counters measured by the full width at half maximum
(F.W.H.M.) is typically about 11% at the operating voltage and
varies from ~9% to ~20% for all the 18 counters used in Ahmeda-
bad monitor. The total count rate of the counter at the operating
voltage can be obtained by determining the area under the entire
pulse height distribution curve above the discriminator level
(Figure 2.8).

The property that the peak in the pulse height distribution
is dependent on the applied high voltage or in general the total
gain of the system can be profitably used (McCracken et al, 1966a)
to monitor the long term stability of the neutron monitors.
Besides as McCracken et al (1966a), have pointed out that by
regular examination of the pulse shape and height distribution
of the counters, a gradually deteriorating counter can be easily
detected well in advance of the time when they will actually fail
to pass the plateau test, thus providing an opportunity for
taking appropriate corrective measures. In practice it is found
that a change of about 5 volts in E.H.T. produces a shift of 10
channels in the peak pulse height and also an increase of ~0.06%
in the count rate of the section.

2.52 Simultaneous changes in all the three trays.

Even though efficiency changes in any one section at a
time can be easily detected and corrected for, simultaneous
changes in all the 3 trays, are difficult to detect by inter-
comparison.

By comparing the data from a number of stations which
have comparable response to primary variations, many authors
(Kane, 1960; Bercovitch and Robertson, 1965; McCracken et al,
1966a) in the past, have pointed out that the variance between
the pressure corrected data of two stations is usually a few
times greater than that given by the counting rate statistics.
Dyring and Sporre (1970) and Bachelet et al (1972a), after
examining data from a number of neutron monitors during 1957-
1965, have concluded that a number of factors can affect the
long term stability of the neutron monitor such as (1) change
of the pressure coefficient with the solar cycle (2) the season-
al temperature wave which mainly affects the high latitude
neutron monitors and (3) the changes in the efficiency of the
instrument, which includes both gradual as well as step like
changes, either due to change in the electrical characteristics
of the equipment or due to change in absorbing material overhead.
However, all these effects are minimal at low latitude station
such as Ahmedabad.

2.6   Data processing

Since the ratio between any two of the three independent
trays will not be affected by any variation outside the monitor,
the ratios can be utilised to determine the self consistency
of the data.   The cosmic ray particles both primaries and
secondaries having a random distribution in time will obey a
Poisson distribution.   The fractional statistical error asso-

COSMIC RAY & PRESSURE DATA

18-NM-64 MONITOR
AHMEDABAD

DAY-236, HOUR INTERVAL 10-11,   DATE:- 24·08·1970

1	2	3	4	5	6	7	1	2	3	4	5	6	7	1	2	3	4	5	6	7
4116	4077	4145	04	0	236	7384	3938	3980	4308	08	0	236	7384	4079	4190	4037	12	0	236	7384
4241	4124	4262	16	0	236	7383	4045	4062	426 11	20	0	236	7384	4034	4164	4221	24	0	236	7384
4010	4153	4102	28	0	236	7383	4046	4188	4050	32	0	236	7383	3914	4036	4204	36	0	236	7383
3991	4131	4156	40	0	236	7383	4175	4002	4339	44	0	236	7383	4033	4070	4044	48	0	236	7383
4100	3967	4214	52	0	236	7383	3972	4035	4315	56	0	236	7383	4152	4074	4100	00	1	236	7382

EACH LINE CONTAINS 3, 4 MINUTE COUNTS
1, 2, 3 - COSMIC RAY COUNTS TRAY 1, 2, 3
4, 5, 6 - CLOCK CALENDAR (4-MIN, 5-HR, 6-DAY)
7 - PRESSURE IN ·1 MM. Hg

Fig. 2.9 - Showing a typical sample of the data recording format in the 'IBM' typewriter at 4-minute interval for a period of one hour.

ciated with the 4-minute count rate N, of any tray can be written as

$$\sigma = M/(N)^{\frac{1}{2}} \qquad \qquad \ldots 2.3$$

where M is the multiplicity, which is $\sim$ 1.4 for Ahmedabad monitor. The error associated with the ratio's will be

$$\sigma_r = \sigma.(2)^{\frac{1}{2}} \qquad \qquad \ldots 2.4$$

From the error calculated for each individual tray rate, errors associated with the ratio of count rate between two trays for any given interval of time can be calculated. For 4-minute ratio's where the statistics is not very good, 4σ level has been laid down as the minimal acceptance criteria for accepting or rejecting an individual tray data. By summing
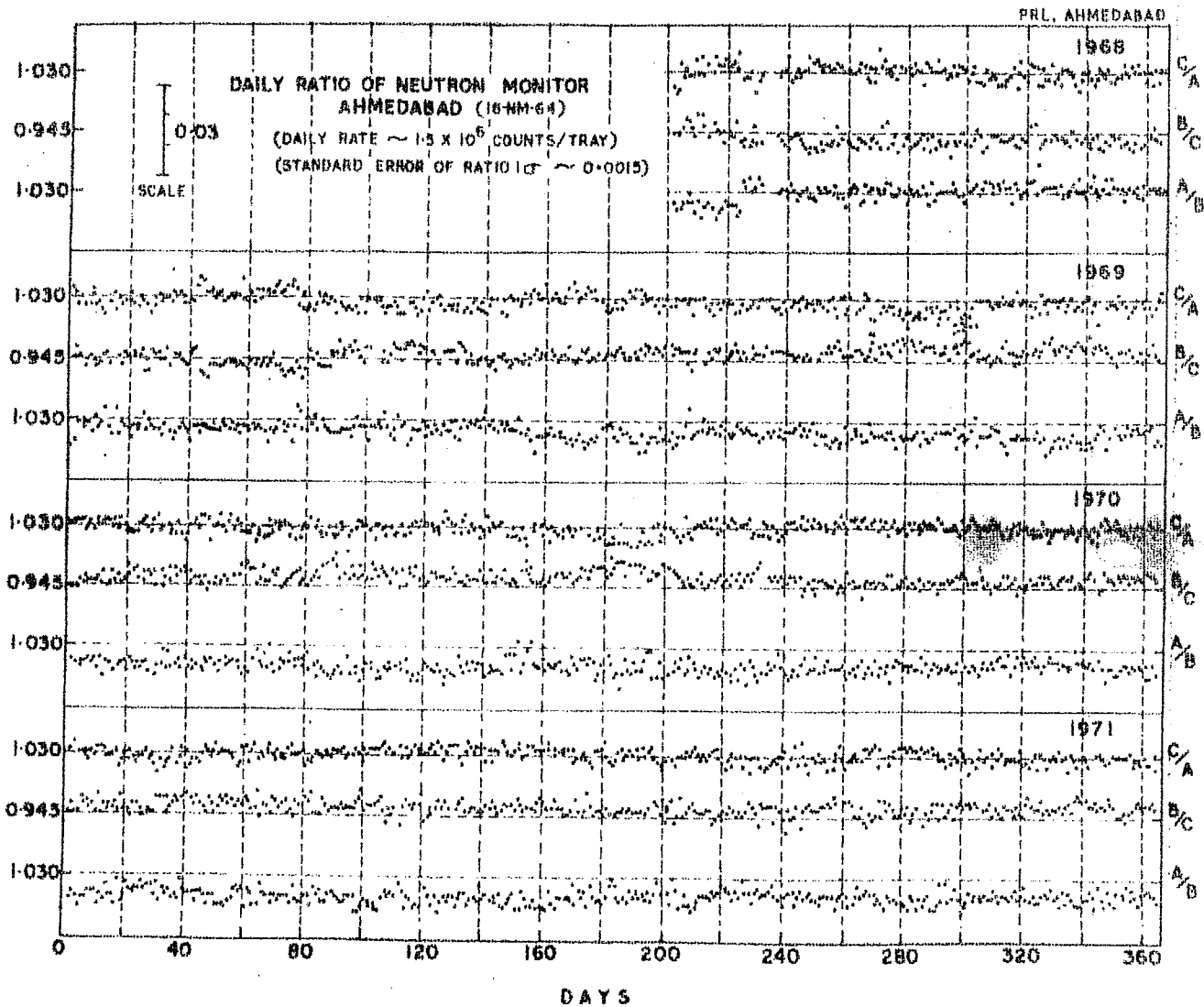
Fig. 2.10 - Individual daily ratio of three trays (A/B, B/C, C/A), for 18-NM-64 monitor Ahmedabad during 1968-1971. The quoted error has been obtained from the observed daily count rate/tray.

the accepted four minute data over appropriate time intervals, the total as well as individual tray cosmic ray neutron data for each hour is obtained. The hourly cosmic ray data is then corrected for pressure variations which is also obtained from the 4-minute recorded data (Figure 2.9). The pressure corrected hourly data, thus obtained from the basic data, is then used for all further analysis.

The daily total counts for each day is also computed separately for each of the three trays from which the daily ratio's (R_i) are calculated. The time series of these daily ratios are plotted for each day (Figure 2.10), for the entire period, 1968-1971, which testifies to the long term stability of the monitor.

C H A P T E R - III

METHOD OF ANALYSIS

3.1 Atmospheric effects

The particles that are registered by ground based instruments are largely secondary particles produced in the nuclear interactions of the primary cosmic ray particles with the earth's atmosphere, and as such are very sensitive to the meteorological variations. An accurate knowledge of the atmospheric transition effects of cosmic ray particles which includes (1) the cascade processes responsible for the production of secondary cosmic rays at different levels in the atmosphere and (2) the effects of the variation of the meteorological conditions such as pressure and temperature throughout the atmosphere, on the intensity fluctuations at different levels is therefore very essential, before one can relate the observed secondary variation to variation of primary intensity.

The effect of the changing meteorological conditions on cosmic ray variation has been studied quite extensively both theoretically and by employing well known correlation techniques between the observed cosmic ray intensity variations and the meteorological parameters. A very comprehensive review of the atmospheric effects has been given by Bercovitch (1967). Essentially two major corrections are to be applied to cosmic ray data. The first one to correct for pressure changes i.e.

the changes in the mass of the absorber overlying the monitor
and the second is related to the variation in the differential
density of the upper atmosphere or the change of the height of
the production layer, due to changes in the temperature. The
latter correction (temperature changes) is particularly import-
ant when the cascade processes producing the secondary component
i, involves particles with life-times that are comparable with
the time of flight from their point of origin to the detector.
The temperature correction is considerable for mesons, whereas
it is relatively negligible for the nucleonic component.

In general, the correction for variations in the atmosphe-
ric pressure can be applied with a good degree of precision
provided the attenuation coefficient (α) is accurately known.
The attenuation coefficient (α), appropriate to neutron monitor
is found to be a function of both altitude and latitude
(Bachelet et al, 1965, 1972 b; Carmichael et al, 1968) and at a
given location is also found to vary during a solar cycle being
maximum at minimum solar activity. The atmospheric effects
related to neutron monitor intensity has been very recently
reviewed by Hatton (1971).

3.11 Attenuation coefficient - Ahmedabad 18-NM-64 monitor

The common method of estimating the attenuation coeffi-
cient

$$\alpha = -\frac{1}{N} \cdot \frac{dN}{dP} \qquad\qquad .. 3.1$$

for the intensity N of a particular neutron monitor for any epoch is to make a linear regression of the logarithm of the intensity, $I = Ln(N)$, with the atmospheric pressure P. However, as is well known, a straight forward regression is likely to form a large autocorrelated residuals due to intensity variations independent of pressure, arising mainly from primary fluctuations and changes in monitor efficiency.

To overcome the disadvantages connected with large auto-correlated residuals, various methods have been suggested (a) dividing the data in short sub-periods to avoid days on which intensity is disturbed (b) introducing data from a second station having similar characteristics, to cancel out the primary fluctuations or (c) prefiltering the data. However, in methods (a) and (c), days with large changes in daily mean intensity and unaccompanied by an appreciable change in the daily mean pressure are usually rejected before performing such an analysis. Bachelet et al (1967, 1972 b) have used a combination of both techniques (b) and (c) i.e. reduction of primary variations with the help of a number of auxiliary stations, plus use of a varying filter, estimated from the correlation structure of the residuals. Carmichael and Bercovitch (1969) Kodama and Inoue (1970) and Carmichael and Peterson (1971), on the other hand, have derived the attenuation coefficient for various latitudes and altitudes from conducting the latitude survey with a mobile monitor.

Figure 3.1 shows the attenuation coefficient (α) for various sea level stations having different cut-off-rigidities, obtained by Bachelet et al (1972 b), for 1964-1965, along with the latitude survey results of Carmichael and Bercovitch (1969). The expected values for the years 1957-1958 and the latitude survey results of Kodama and Inoue (1970), for 1967 are also shown in the same figure. It is interesting to note that the agreement in values of attenuation coefficient for low latitude stations having a cut-off-rigidity $\gtrsim 8$ GV obtained by different authors are quite consistent with each other.

The attenuation coefficient (α) can be simply estimated by using straight forward regression analysis with data for short period intervals of three months each. For the period 1968-1971, this method yields a mean value of $\alpha = 0.83 \pm 0.02$. For a more rigorous evaluation of α for the Ahmedabad 18-NM-64 monitor, we have followed the successive differencing method of Lapointe and Rose (1962), which consists of performing the regression analysis between the successive differences of the logarithm of the daily mean intensity (I) and the daily mean pressure (P) i.e.

$$Ln (N_2) - Ln (N_1) = -\alpha (P_2 - P_1) \qquad .. \ 3.2$$

Inspite of the limitation of this method, it has been preferred in the absence of availability of any other neutron monitor having comparable cut-off-rigidity. After applying adequate
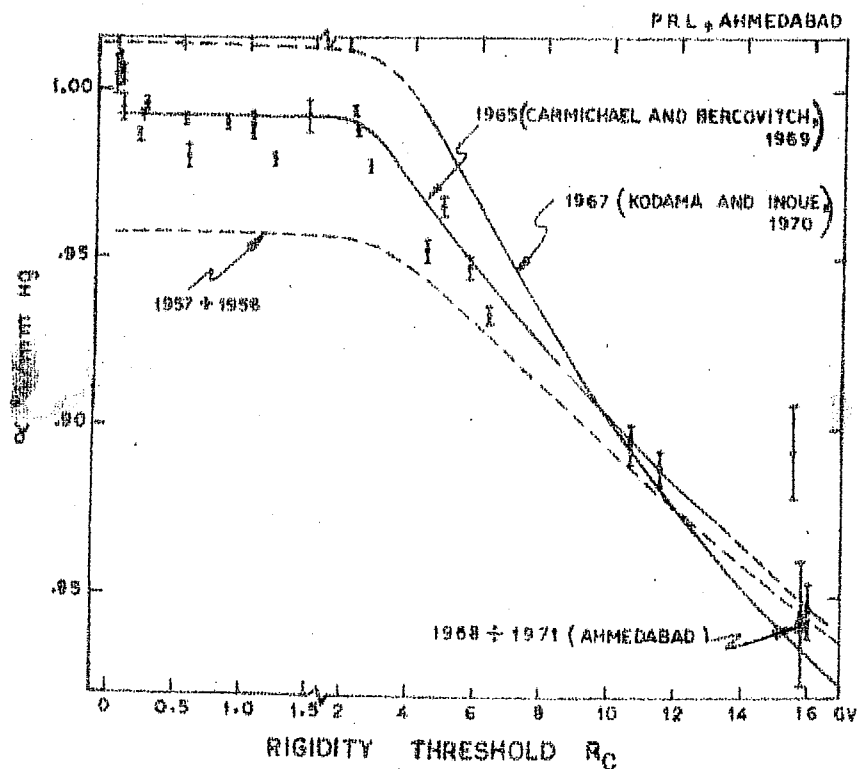
Fig. 3.1 - Showing the latitude dependence of the sea level attenuation coefficient (α), for different epochs of the solar cycle obtained from various latitude survey results. The station coefficients in 1964–1965 computed by Bachelet et al (1972'b) are also shown along with 1σ error. The result for Ahmedabad for the period 1968–1971 is represented by a triangle.

correction for changes in the efficiency of the monitor with time, the attenuation coefficient (α) for Ahmedabad (cut–off–rigidity $\sim$ 16 GV) has been derived for the entire data 1968–1971, using this method. The attenuation coefficient so derived for each year during 1968–1971 is given in Table 3.1. The results show a time invariance of α with a mean value = 0.84 $\pm$ 0.02% / mm Hg, in good agreement with the results of other investigators shown in Figure 3.1. This conclusion is

TABLE 3.1 - The attenuation coefficient for Ahmedabad 18-NM-64 monitor for the period 1968 to 1971, derived by successive differencing method.

Year	Correlation Coefficient	Attenuation coefficient %/mm Hg.
1968	0.95	0.81 ± 0.04
1969	0.97	0.87 ± 0.02
1970	0.98	0.88 ± 0.02
1971	0.98	0.80 ± 0.02

also consistent with the results reported by Forman (1968) and Bachelet et al (1972 b), that the solar cycle variation of α for stations having cut-off-rigidities $\gtrsim 16$ GV is negligible ($\leqslant 0.01\%$).

The day to day variation of pressure P at equatorial stations like Ahmedabad is very small of the order of 1 mm and seldom increases beyond 2.5 mm. However, the average amplitude of first (diurnal) and second (semi-diurnal) harmonic of the pressure wave are practically comparable being ~ 0.75 and ~ 0.90 mm Hg respectively. Since the second harmonic component of the cosmic ray daily variation (r_2^c) is usually small and is $< 0.1\%$, days with high second harmonic amplitude of pressure (r_2^p) can be very usefully utilised to confirm the correctness of the attenuation coefficient obtained earlier. For the period 1968-1971 we have therefore selected all days with $r_2^p \gtrsim 1.0$ mm and grouped them in intervals of 0.1 mm. For the same days and

for each group the corresponding uncorrected semi-diurnal component (r_2^U) has also been obtained. A regression analysis between the two sets of averages (r_2^U and r_2^p) yields the attenuation coefficient which is in very good agreement with the mean value of $\alpha = 0.84\%$ / mm Hg, obtained earlier, which gives added confidence in the pressure correction factor.

3.12 Pressure correction - Ahmedabad neutron monitor intensity

The observed neutron intensity **N** at pressure P reduced to a standard pressure P_0 using the relationship

$$N_0 = N \exp (\alpha \triangle p) \qquad\qquad .. 3.3$$

where $\triangle_p$ = P-P_0 and N_0 is the pressure corrected intensity (count rate), P_0 is normally taken as the yearly average pressure for the station, which for Ahmedabad is ~ 750.08 mm (1000 mb) and $\alpha = 0.84\%$/mm Hg.

The hourly pressure corrected count rate is obtained using the above equation and the 'uncorrected count rate' obtained in sec 2.6 from the 4-minute data of 3-independent trays, along with the corresponding pressure for the particular hour. The hourly pressure corrected data for neutrons reduced to a standard pressure (1000 mb) as described above forms the basic data for all further analysis.

3.2 Solar daily variation (anisotropies)

Even though the daily variation can be studied in

several different ways (Rao and Sarabhai, 1964; Kane, 1966) most of the information on the cosmic ray daily variation has been derived through a study of the diurnal (I Harmonic) and semi-diurnal (II Harmonic) components. The amplitude and phase of the harmonic components are generally derived by Fourier analysing the hourly intensity data (Chapman and Bartels, 1940), which implicitly assumes that the variation is constant for at least 24 hours. However an indirect check, of short period variation having duration of less than 24 hours, can be accomplished by comparing the amplitude and phase of the diurnal variation recorded by different stations having similar characteristics, but well distributed in longitude. A large discrepancy in either the amplitude or the time of maximum shows that either the anisotropy is changing within 24-hours or the universal time effects are predominant.

3.21 Harmonic Analysis

A time dependent harmonic function $F(t)$ with 24 - equidistant points in the interval $t = o$ to $t = 2\pi$ can be expressed in terms of Fourier's series.

$$F(t) = a_o + \sum_{n=1}^{24} (a_n \cos nt + b_n \sin nt) \qquad .. \ 3.4$$

where a_o is the mean value of $F(t)$ in the interval 0 to 2π and a_n, b_n are coefficients of the nth harmonic given by

$$a_0 = \frac{1}{24} \sum_{i=1}^{24} r_i$$

$$a_n = \frac{1}{12} \sum_{i=1}^{24} r_i \cdot \text{Cos } nt_i \qquad \quad \therefore 3.5$$

$$b_n = \frac{1}{12} \sum_{i=1}^{24} r_i \cdot \text{Sin } nt_i$$

where $r_n \cdot \text{Cos } (nt - \phi_n) = a_n \text{ Cos } nt + b_n \text{ Sinnt}$ .. 3.6

The amplitude r_n and phase ϕ_n of the nth harmonic is

$$r_n = (a_n^2 + b_n^2)^{\frac{1}{2}}$$

$$\text{and } \phi_n = \text{Arc Tan } (b_n/a_n) \qquad \quad .. 3.7$$

Since the daily variation of the cosmic ray intensity can be adequately represented by the first two harmonics, it is customary to reconstruct the daily variation curve using these two harmonics for further study.

$$V_i = a_1 \cdot \text{Cos} t_i + b_1 \cdot \text{Sin} t_i + a_2 \cdot \text{Cos} 2t_i + b_2 \cdot \text{Sin} 2t_i \text{ .. 3.8}$$

It is found that the distribution of both a_n and b_n are gaussian, provided that the hourly values also follow the same distribution. The standard error of the various harmonics of gaussian distribution is given by

$$\sigma_{a_n}^2 = \sigma_{b_n}^2 = \sigma_{r_n}^2 = \sigma_1^2/12 \qquad \quad .. 3.9$$

$$\text{and } \sigma_{\phi_n} = \sigma_{r_n}/r_n$$

where σ_1 is the standard error associated with the hourly values of the cosmic ray intensity.

3.22   24-hour moving average

The cosmic ray intensity recorded by the ground based instruments contain contribution from long term variation ($\geqslant$ 1 day) superposed on the daily variation which can influence the daily variation amplitude and phase unless corrected for. The method of 24-hour moving average has been found to be very satisfactory to remove the linear slope effects (constant gradients) of period $\geqslant$ 24 hour (Dorman, 1957). The method however fails when large and non-linear gradients of cosmic ray intensity are involved.

3.23   Graphical representation of daily variation

The amplitude and phase of both the harmonics can be represented graphically in a harmonic dial or clock diagram either as a (a) vector addition diagram with vectors starting at the end point of the previous vector, or as a (b) cloud of points having their origin at a fixed point. Both these representations are very commonly used in the study of the daily variation of cosmic rays. Figure 3.2 a, b, illustrates the two representations for the observed monthly mean diurnal and semi-diurnal vectors for the year 1971 for Ahmedabad 18-NM-64 monitor.

3.3   Asymptotic cone of acceptance of a detector and variational coefficients

The asymptotic direction of approach of any particle incident at a given point on the earths surface is defined as
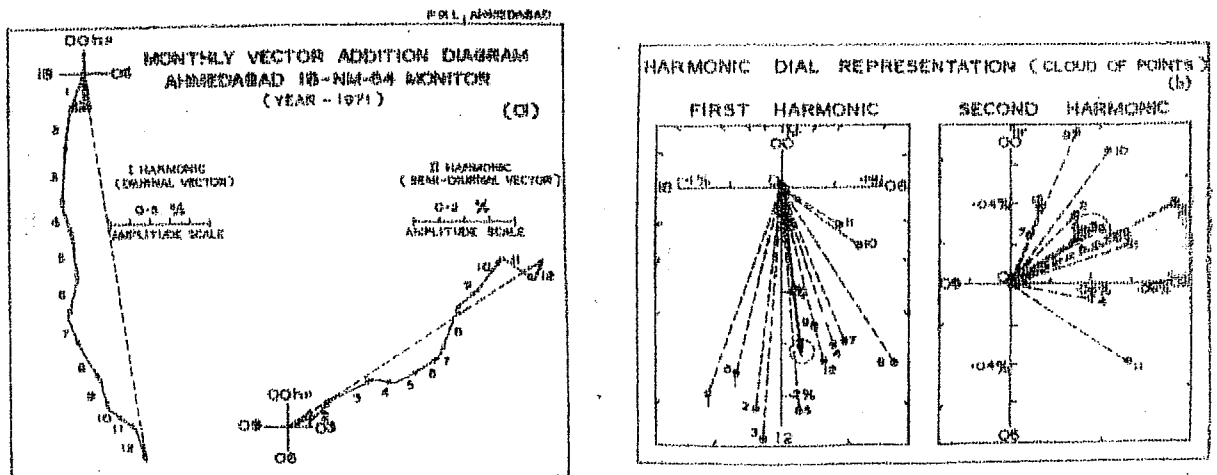
Fig. 3.2 - Graphical representation of monthly average diurnal and semi-diurnal variation (a) vector addition diagram and (b) the harmonic dial representation, for Ahmedabad 18-NM-64 data for the year 1971.
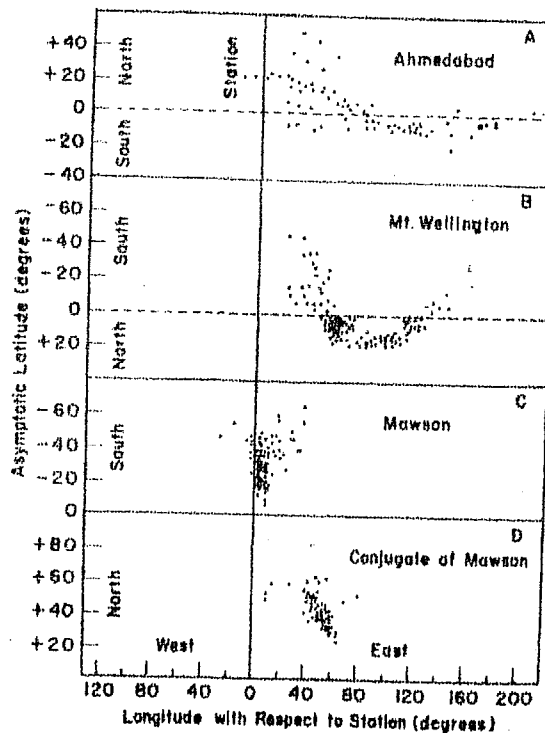

Fig. 3.3 - The asymptotic direction of approach for particles arriving at four different locations. Location D has the same geomagnetic latitude as Mawson (after Rao et al, 1963).

the direction prior to its entry into the geomagnetic field. The asymptotic direction of cosmic ray particles of different rigidities have been evaluated through numerical integration of the equation of motion of the particle in a six degree simulation of the geomagnetic field (McCracken et al, 1962). The asymptotic direction of approach for a number of neutron monitoring stations for different rigidities and incident directions have been published by McCracken et al (1965).

For any quantitative study of the time variation of cosmic radiation, a detailed knowledge of the dependence of the counting rate on the asymptotic direction is essential. Rao et al (1963) have shown that in such studies it is convenient to use the concept of the 'Asymptotic cone of acceptance of a detector' which has been defined as the solid angle containing the asymptotic directions of approach which make a significant contribution to the counting rate of the detector. Figure 3.3 shows the asymptotic directions of approach of particles of selected rigidities between 2 and 100 GV and directions of approach into the atmosphere with zenith angles 0, 16, 32 degrees in the north-south and east-west geomagnetic planes, for four locations including Ahmedabad. The figure clearly brings out that the geomagnetic field causes the phase, duration and amplitude of a time variation that is due to any anisotropy in the cosmic radiation to vary from station to station and, to a lesser extent, from detector to detector at any one station.

3.31 Variational coefficients

If the cosmic ray intensity from within the solid angle Ω_i were to be $J_0 (1 + A_i R^\beta)$, and that from all other directions J_0, then the counting rate of an instrument would differ by an amount $\triangle N$ from the counting rate N given by (Rao et al, 1963; McCracken et al, 1965)

$$\frac{\triangle N}{N} = v (\Omega_i, \beta) . A_i \qquad .. 3.10$$

$J_0 A_i R^\beta$ is the anisotropic component of the radiation that arrives from all directions within the solid angle Ω_i. If $v (\Omega_i, \beta)$, the variational coefficients, are known for all possible Ω_i, the counting rate corresponding to any assumed anisotropy can be calculated. Without going into the details of the mathematical formulation of the variational coefficient, we illustrate the method of evaluating the variational coefficient.

The elementary solid angle Ω_i is defined by planes of geographic longitudes spaced five degrees apart and by surfaces of the constant geographic latitude every five degrees on either side of the equator. The estimate of $v (\Omega_i, \beta)$ is given by summation approximation

$$v (\Omega_i, \beta) = \sum_k W (R_k) . R_k^\beta . \frac{Y}{Y} \left(\frac{\Omega_i, R_k}{4\pi, R_k} \right) . \frac{R_{k+1} - R_{k-1}}{2}$$

$$.. 3.11$$

where summation extends from near cut-off-rigidity to a value R_{max}. $W (R_k)$ is the coupling coefficient (Dorman, 1957) or the

differential response function for rigidity R and interval k (Lockwood and Webber, 1967). The estimate of $Y(\Omega_i, R_k)$ is obtained for nine directions (θ_0, ϕ_0), for which the trajectory calculations have been made. For simplicity we assume the anisotropy to be a power law in rigidity of the type

$$\frac{\Delta J_i(R)}{J_0(R)} = A.R^\beta = f(\psi).Cos\Lambda.R^\beta \qquad .. 3.12$$

where A is the amplitude of anisotropy which can be represented as a separable function of the asymptotic latitude Λ and longitude ψ and varies as the nth power of the consine of declination. The fractional change in the total counting rate produced by the radiation from Ω_i can be written as

$$\frac{dN(\Omega_i)}{N} = f(\psi). v(\Omega_i, \beta). Cos\Lambda. \qquad .. 3.13$$

and summing over all Ω_i

$$\frac{dN(\psi_j)}{N} = f(\psi_j).\sum v(\Omega_i, \beta). Cos\Lambda_i$$
$$= f(\psi_j). V(\psi_j, \beta) \qquad .. 3.14$$

where $dN(\psi_j)$ is the solid angle defined by the two meridional planes 2.5 degrees on either side of the meridional plane at geographic longitude ψ_j. $V(\psi_j, \beta)$ which are defined as the modified variational coefficients, have been evaluated for a number of stations for ten values of β ($\beta \leq 0.6$) by McCracken et al (1965), and Shea et al (1968). It is interesting to note that the variational coefficients for $\beta = 0.0$ represent the

manner in which the cosmic ray particles from different asympto-
tic longitudes contribute to the total counting rate of a dete-
ctor. The author has extended the calculations for values of β
going upto +2.0 and for varying values of upper cut-off-rigidit-
ies (R_{max}), which have been extensively used for determining the
characteristics of the diurnal and semi-diurnal anisotropy.

3.32 Application to daily variation

From a knowledge of the variational coefficients and
observations at various stations, the amplitude and phase of any
anisotropy in space can be predicted. Consider an anisotropy
that is an arbitrary function of direction η and is expanded into
a Fourier series

$$f(\eta) = J_o(R). \sum_{m=1}^{\infty} \alpha_m . Cos\left[m(\eta - C_m) \right] \qquad .. \ 3.15$$

where α_m and C_m are arbitrary amplitude and phase constants,
and also C_m is the direction of viewing from which a maximum of
the mth harmonic is seen. According to Figure 3.4, $\eta = \psi + 15T$
$- 180^o$, and one can write the intensity from asymptotic longi-
tude ψ as

$$f(\psi) = J_o(R). \sum_{m=1}^{\infty} \alpha_m . Cos\left[m(\psi + 15T - 180^o - C_m) \right]$$

$$.. \ 3.16$$

where the asymptotic longitude $\psi = (5i + 2.5)^o$ is the mean
longitude of all the particles arriving from solid angles
lying between $\psi = 5i^o$ and $\psi = 5(i + 1)^o$.
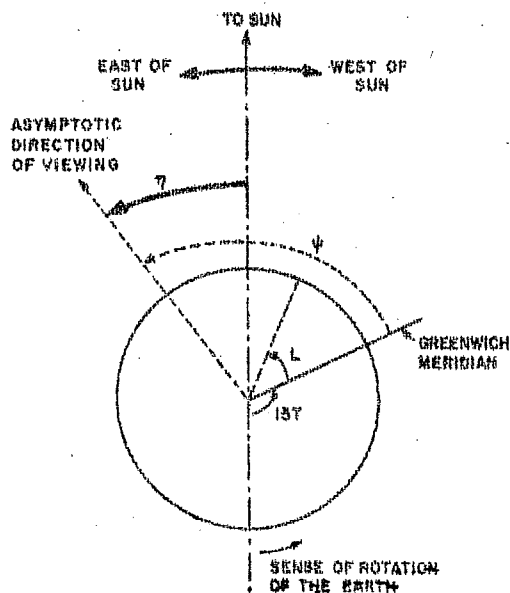
Fig. 3.4 – Define the angles employed to specify the asymptotic direction of viewing of an arbitrary station (after Rao et al, 1963).

One may substitute this value of $f(\psi)$ in equation 3.14 and sum over i. Then $\Delta N(T)$, the deviation of the counting rate of the detector at time T from the mean value N, becomes

$$\frac{\Delta N(T)}{N} = \sum_{i=0}^{71} V(\psi_j, \beta) \sum_{m=1}^{\infty} \alpha_m . \cos\left\{ m \left[51 + 2.5 + 15T - C_m - 180^\circ \right] \right\}$$

.. 3.17

$$= \sum_{m=1}^{\infty} \alpha_m B_m . \cos\left[m(15T - 180^\circ - C_m) + \gamma_m \right]$$

.. 3.18

where

$$B_m^2 = \left\{ \sum_{i=0}^{71} V(\psi_j, \beta) . \sin\left[m(51 + 2.5) \right] \right\}^2$$

.. 3.19

$$+ \left\{ \sum_{i=0}^{71} V(\psi_j, \beta) . \cos\left[m(51 + 2.5) \right] \right\}^2$$

and

$$\tan \gamma_m = \frac{\sum_{i=0}^{71} V(\psi_j, \beta) . \sin\left[m(51 + 2.5) \right]}{\sum_{i=0}^{71} V(\psi_j, \beta) . \cos\left[m(51 + 2.5) \right]}$$

.. 3.20

where α_m, B_m and $(-mC_m + \gamma_m)$ represent the amplitude and phase constants of the m-th harmonic. γ_m is the correction to be applied for deflection in the geomagnetic field. The universal time at which the maximum intensity is observed, is given by

$$T_m = \frac{180\,m + mC_m - \gamma_m}{15m} \quad \text{hours} \qquad \qquad ..\ 3.21$$

and the local time of maximum is $t_m = T_m + (L/15)$, where L is the geographic longitude of the station.

3.4   Estimation of rigidity exponent (β) and upper cut-off-rigidity (R_{max})

3.41   Neutron monitor observations

If the observed daily variation is due to a spatial aniso-tropy in interplanetary medium, the position and amplitude of the anisotropy as determined by different stations should agree, with each other within the limits of statistical error. Hence the best estimate of the value of β and the upper cut-off-rigi-dity (R_{max}) above which the daily variation is negligible can be estimated from a number of observations imposing the condition that there must be a minimum variance between observations as determined from X^2 statistics. The variance X^2 for both phase (X_ϕ^2) and amplitude (X_A^2) for each β and R_{max} is obtained by the relation

$$X_\phi^2 = \frac{\sum_{i=1}^{N} \left[\phi_i\,(\beta,\,R_{max}) - \phi_o\,(\beta,\,R_{max}) \right]^2}{N} \qquad ..\ 3.22$$

$$X_A^2 = \frac{\sum_{i=1}^{N} \left[A_i\,(\beta,\,R_{max}) - A_o\,(\beta,\,R_{max}) \right]^2}{N.\,A_o^2\,(\beta,\,R_{max})} \qquad ..\ 3.23$$

where $A_i(\beta, R_{max})$ and $\phi_i(\beta, R_{max})$ are the amplitudes and
phases in space obtained for the ith station after correction
for the geomagnetic effects and $A_o(\beta, R_{max})$ and $\phi_o(\beta, R_{max})$
are the corresponding mean values in space obtained for N stat-
ions. The most probable value of β, R_{max}, A_o and ϕ_o are the
ones that correspond to the minimum value of X_ϕ and X_A.

3.42 Meson and neutron monitor observations

The observations have indicated that both meson ($\bar{E} \sim 30$ GeV
at high latitude) as well as neutron ($\bar{E} \sim 8-10$ GeV) monitors show
significant daily variation due to primary cosmic rays. Since
the mean energy of response of the two monitors differ widely,
the use of high counting rate meson data would be very valuable
for estimating the energy spectrum of variation (β) and the
upper cut-off-rigidity (R_{max}). However, as meson intensity is
greatly affected by atmospheric temperature variations, any
uncertainty in the temperature correction makes the deductions
derived from meson data unreliable.

The correction for the temperature effects requires a
knowledge of the temperature distribution at different isobaric
levels (Maeda and Wada, 1954; Dorman and Feinberg, 1955).
Dorman (1957) and Maeda (1960) have computed the weighting
factors or 'density temperature coefficient', W_T^X, for different
isobaric levels from a detailed theoretical treatment of muon
production and propagation in the atmosphere which have been

critically re-examined by Carmichael et al (1967) and Bercovitch (1967). However, the practical application of these methods to daily variation has been greatly handicapped due to the non-availability of adequate radiosonde observations (which are seldom conducted more than twice a day) and the large radiation errors associated with these observations. Since the meteorological observations clearly show that the diurnal temperature variation becomes relatively insignificant at altitudes above 2-3 km and the temperature variation below this altitude, at least on an average, is well correlated with the ground temperature, many authors (Rao and Sarabhai, 1961; Bercovitch, 1966) have suggested the use of ground temperature observations to correct the diurnal variation of meson intensity.

We have evaluated the temperature effects on the diurnal variation of meson intensity for the MT-64 type cubical meson telescope for 1965-1969 by the method advocated by Bercovitch (1966). The equation connecting the diurnal vector $\underset{\sim}{M}$ for temperature uncorrected (pressure corrected) mesons and the diurnal vector $\underset{\sim}{N}$ for pressure corrected neutrons may be written as

$$\underset{\sim}{M} (\alpha_m, T_m) = R. \underset{\sim}{N} (\alpha_n, T_n + \phi) + \underset{\sim}{A} \qquad .. \ 3.24$$

Resolving the vectors into orthogonal components along 00 and 06 hour directions, we can write

$$\left. \begin{aligned} M_{oo} &= R \, Cos \, \phi . N_{oo} - R \, Sin \, \phi . N_{o6} + A_{oo} \\ M_{o6} &= R \, Cos \, \phi . N_{o6} + R \, Sin \, \phi . N_{oo} + A_{o6} \end{aligned} \right\} \qquad .. \ 3.25$$
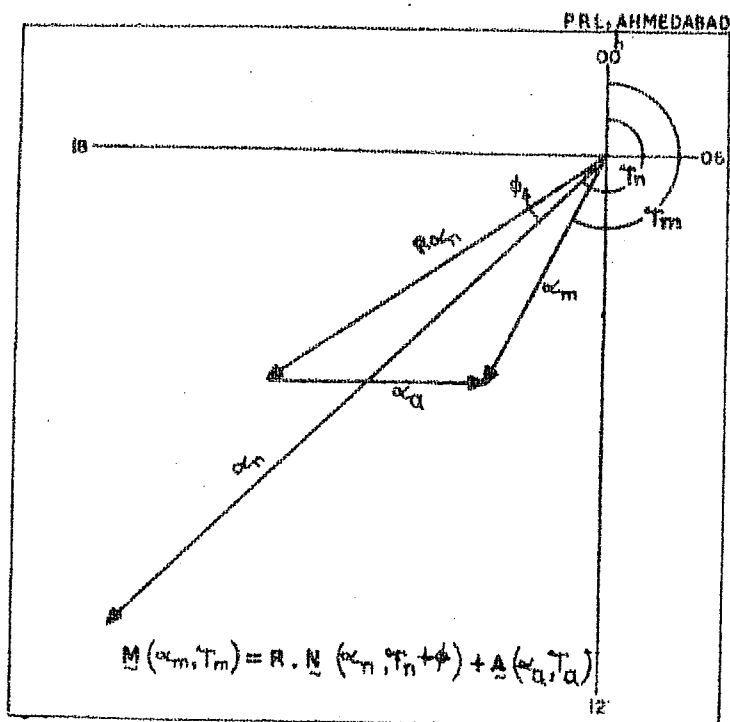
Fig. 3.5 - Showing the relationship between different vectors representing neutron, meson and atmospheric diurnal variation (see text for explanation).

and $\quad A = C_t \cdot T \left(\alpha_t, \quad T_t + \theta \right)$ $\qquad$ .. 3.26

where T, P, A are the vectors representing the observed ground temperature, pressure and atmospheric diurnal vectors respectively, while α and T are their amplitudes and phases. R is the ratio between meson and neutron diurnal amplitudes (α_m/α_n) due to the anisotropy in space and θ is the phase lag between A and T. The relationship between the various vectors is defined in Figure 3.5. Knowing the observed values of M and N vectors the values of R and ϕ can be computed using the least square fit method to the vector equation 3.25. The value of C_t and θ is further determined from equation 3.26 by dividing the data in

various temperature groups. The detailed evaluation of the
temperature coefficient using ground temperature data and its
usage are being presented in section 4.31.

3.5   Space - time diagram

The technique of examining the daily anisotropy in its
entirity by plotting the space-time diagram using a large number
of high latitude stations (cut-off-rigidity $\lesssim$ 2 GV and viewing
the equatorial region) well distributed in longitude, has been
very successful in separating time variations from space vari-
ations. With this method it is possible to clearly identify
the sources and sinks, and therefore are ideally suited to
study the characteristics of a rapidly evolving anisotropy
(Fenton et al, 1959; Ables et al, 1967; Mercer and Wilson, 1968;
Carmichael and Steljes, 1969). We describe in brief the method
used by us to study the characteristics of the large as well as
low amplitude wave trains in the diurnal variation of cosmic
ray intensity.

The data from a number of stations are selected such that
they satisfy the following conditions (1) have narrow asympto-
tic cone of acceptance, (2) essentially view the equatorial
plane of the celestial sphere, (3) are well distributed in lon-
gitude, and (4) have their daily mean intensity closely tracking
each other for long periods of time. The hourly count rates at
each station are then expressed as deviation from a normalised
mean level of intensity. After applying appropriate geomagnetic

bending correction, the percent hourly deviations for different stations (representing different directions in space at the same universal time) is plotted for each hour on a space time diagram. Such maps provide a good means of studying the characteristics of the time evolving anisotropies.

CHAPTER - IV

DIURNAL ANISOTROPY CHARACTERISTICS

In this chapter we first describe the results obtained from the Super Neutron Monitor at Ahmedabad. These are then compared with the data from the world-wide network of neutron monitors to establish the average properties of the diurnal variation of cosmic ray intensity and its long term changes. With the help of the data from various neutron monitoring stations including Ahmedabad (particulars of all the stations used in the thesis are given in Table 4.1), and the data from Deep River neutron and meson monitors we also derive the upper cut-off-rigidity (R_{max}) above which the cosmic ray particles do not undergo appreciable diurnal variation. The analysis is further extended to examine and understand the variability of the diurnal variation on a day to day basis, and from a comparison with low energy cosmic ray observations made on various spacecrafts, a new concept of diurnal variation is arrived at. By comparing the predicted behaviour of diffusion vector with the observed interplanetary magnetic field vector, we show that this new physical concept, which explains the diurnal variation simply in terms of radial convection and field aligned diffusion, is valid most of the time.

4.1   Results from Ahmedabad neutron monitor

4.11   Data processing

Before using the Ahmedabad neutron monitor data for deriving information on time variation, it is necessary to ensure

TABLE 4.1. - Geographic and asymptotic coordinates for a few selected neutron monitor stations, whose data have been utilised in this thesis.

Station No.	Station	Geographic coordinates		Altitude (meters)	Geomagnetic cut off* (in GV)	Mean Asymptotic Coordinates Lat. Long. (In degrees)	
		Latitude (degrees)	Longitude (degrees)				
1	Ahmedabad	23.01	72.61	S.L	15.94	19	125
2	Alma Ata	43.20	76.94	806	6.69	25	143
3	Calgary	51.08	245.91	1130	1.09	28	269
4	Churchill	58.75	265.91	39	0.21	40	286
5	Dallas	32.78	263.20	208	4.35	25	316
6	Deep River	46.10	282.50	145	1.02	27	319
7	Denver	39.75	255.00	1600	2.91	26	294
8	Durham	43.10	289.16	S.L	1.41	25	332
9	Goose Bay	53.33	299.58	46	0.52	35	339
10	Hermanus	-34.42	19.22	26	4.90	-24	70
11	Inuvik	68.35	226.27	21	<0.18	47	233
12	Jungfraujoch	46.55	7.98	3550	4.48	22	76
13	Port aux Francais	-49.35	70.22	S.L	1.19	-26	87
14	Kiel	54.33	10.13	54	2.29	30	60
15	Lindau	51.60	10.10	140	3.00	29	65
16	Mawson	-67.60	62.88	S.L	0.22	-42	55
17	Mt. Norikura	36.12	137.56	2770	11.39	26	195
18	Mt. Washington	44.30	288.70	1900	1.24	25	331
19	Mt. Wellington	-42.92	147.24	725	1.89	-25	193
20	Pic du Midi	42.93	0.25	2860	5.36	23	76
21	Sulphur Mountain	51.20	244.39	2283	1.14	27	270
22	Wilkes	-66.42	110.45	S.L	<0.05	-56	107
23	Alert	82.50	297.67	66	<0.05	77	331
24	Chacaltaya	-16.31	291.85	5220	13.10	-17	341
25	Kula, Hawaii	20.71	203.74	930	13.30	19	257

* Geomagnetic cut-off derived from McCracken et al (1965)

that the observed variations are not of instrumental origin but truly represent the anisotropy. The pressure corrected daily mean intensity of Ahmedabad 18-NM-64 monitor for the period July 1968 to December 1971 has been compared with both, the high latitude (Deep River) as well as low latitude (Kula) neutron monitoring stations. Figure 4.1 shows the normalised daily mean intensities of cosmic radiation for Ahmedabad, Kula and Deep River neutron monitoring stations for the year 1971 as a typical example. It is seen that, inspite of the monitors having different mean asymptotic latitudes and longitudes of response, they track with each other reasonably well with a correlation coefficient of ~ 0.9, even on an yearly basis. Most of the world-wide changes such as Forbush decreases are clearly reflected in Ahmedabad neutron monitor records, though usually with smaller amplitudes, which is consistent with their expected energy dependence of variation. As an additional check for the long term stability of the monitor, the constancy of the two monthly average ratios of the three individual tray count rates have also been checked (see Figure 4.2).

4.12 Long term isotropic variation

The normalised pressure corrected monthly mean intensity of neutrons as observed at Ahmedabad, Kula and Deep River stations are plotted for the period 1968-1971 in Figure 4.3. The monthly mean pressure for Ahmedabad is also plotted in the same figure to show that practically no correlation exists between
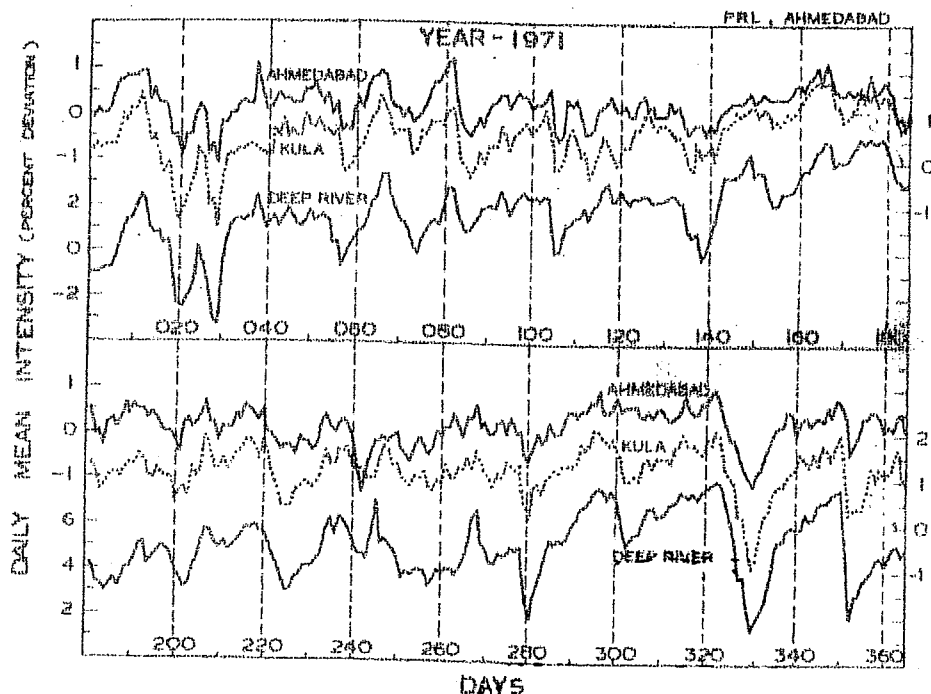
Fig. 4.1 – Plot showing the normalised daily mean intensity of cosmic radiation recorded by Ahmedabad, Kula and Deep River neutron monitor stations during 1971. Note that the intensity scale for Deep River is 2 times that for Ahmedabad and Kula. The scale for Kula is indicated on the right.
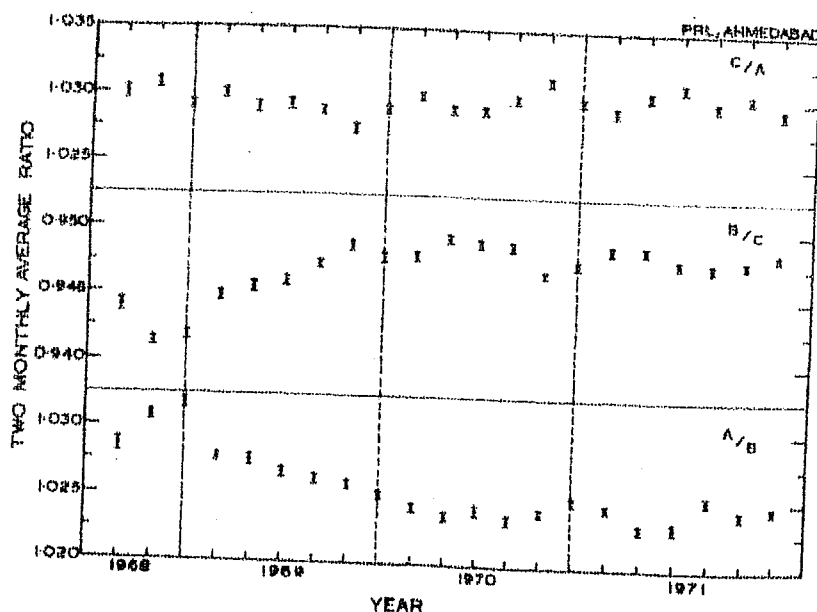

Fig. 4.2 – The two monthly average ratio of the individual tray rates for Ahmedabad 18-NM-64 monitor, for the entire period 1968-1971. The standard error of the mean (σ_m) shown with each point has been derived from the actual observed ratio on each day.

pressure corrected monthly mean intensity at Ahmedabad and the barometric pressure. The figure shows that the cosmic ray intensity attained a minimum in June 1969 (A secondary minima at equatorial stations is also seen in November 1968) after which it gradually recovered. The intensity recovery from June 1969 to December 1971 is observed to be $\sim$11% at middle and high latitude stations (cut-off-rigidity $\lesssim$ 2 GV) as compared to $\sim$ 3% at Ahmedabad. It may also be seen that even though the recovery is very fast, in the year 1971, at middle and high latitude stations ($\sim$ 5%), it is quite small at equatorial stations ($\sim$0.4% at Ahmedabad and $\sim$1% at Kula), showing that the high energy recovery takes place slowly in comparison with the recovery of low energy particles, during this period.

For a long time it has been believed that the form of the modulation function is independent of time. From a comparison of 3-monthly average neutron monitor intensity observed at Climax, Chicago and Huancayo during the period 1952 to 1969, Simpson and Wang (1970) showed that this was indeed the case. With the availability of data from super neutron monitors, in particular the super neutron monitor at low latitude stations like Kula, it has now been recently shown by Stoker and Carmichael (1971) and Carmichael and Katzman (1971) that there exist abrupt step like changes in the long term behaviour of the modulation function. Since Ahmedabad monitor has a cut-off-rigidity of the order of 16 GV, comparison of Deep River
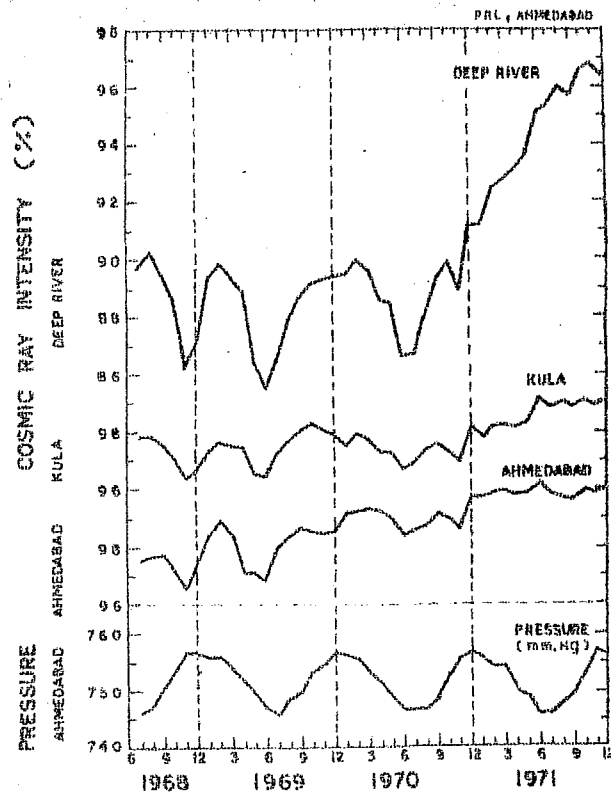
Fig. 4.3 - The normalised monthly mean intensity for three stations namely Ahmedabad, Kula and Deep River, during the period 1968-1971. The monthly mean pressure for Ahmedabad is shown at the bottom of the figure. The fast recovery observed at Deep River station in 1971 as compared to other two stations is clearly evident.

Fig. 4.4 - Monthly average cosmic ray intensity at 3 stations namely Ahmedabad, Kula and Deep River plotted against each other. The month of the year is indicated by the number next to the data point. The dashed lines represent the approximate fit to the data points and the arrows indicate excursion from one step to another.

and Ahmedabad neutron data should unambiguously confirm such step like changes in the modulation function.

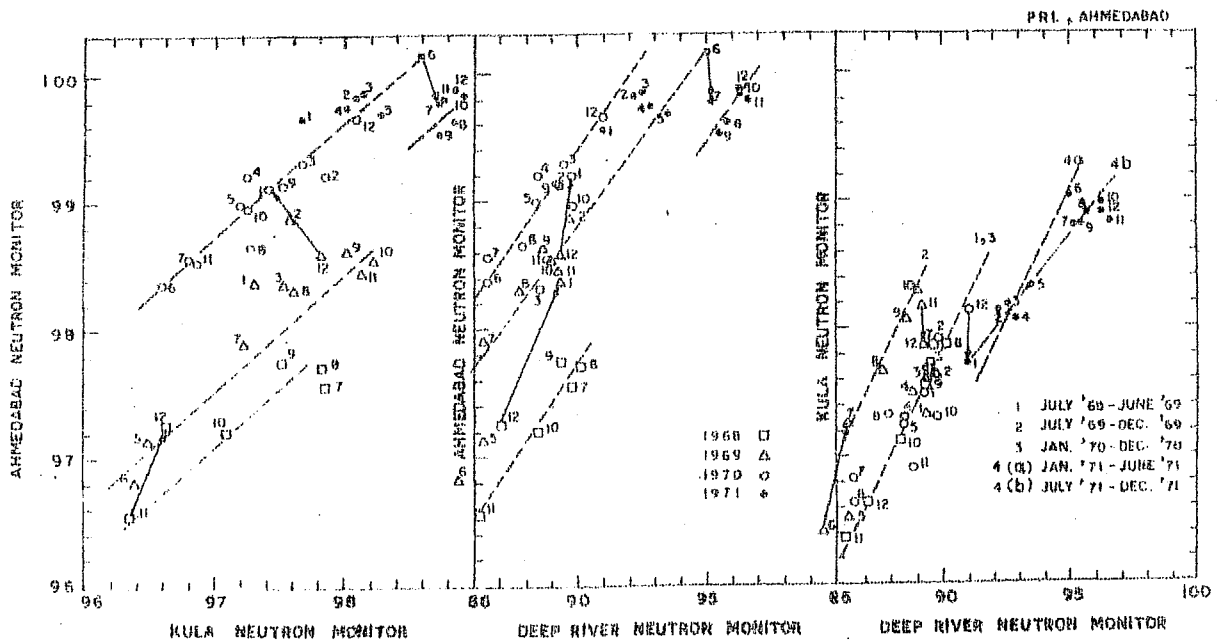Figure 4.4 shows the plot of Ahmedabad–Kula, Ahmedabad–Deep River and Kula–Ahmedabad neutron intensities for the period 1968–1971. Inspite of the small amplitude of the long term changes at Ahmedabad (due to high cut–off–rigidity) the step like excursions (indicated by arrows and noted in the figure) in the modulation function are prominently seen thus independently confirming the observations by Stoker and Carmichael (1971). The step like functions indicated in Figure 4.4 imply that at distinct times, t_1, t_2, etc., the regression lines instead of passing through origin make distinctly different intercepts. Thus particles with rigidities $\geqslant R$ GV do not seem to participate in the long term modulation, whereas particles below this rigidity obey the $\exp \left[- k(t)/R^m \right]$ dependence, m being roughly equal to 1. Such a behaviour can be physically understood by referring back to equation 1.7b and 1.13. Since both V and K_1 are independent of rigidity and there are indications of their being time invarient, only the systematic step like changes in K_2 and D, can probably provide an explanation for the step like changes in the long term modulation of cosmic ray intensity. Even though a number of authors have suggested the distinct possibility of a change in the form of $K_2(R,t)$ with time (Schmidt, 1972; Lockwood et al, 1972), the presently available results are not yet conclusive. The influence of the off–ecliptic phenomena on the observed long term modulation of cosmic ray intensity has also been recently suggested by Hedgecock et al, (1972).

4.13 Mean diurnal and semi-diurnal variation observed at
      Ahmedabad

The amplitude and phase of the observed diurnal and semi-
diurnal variation of cosmic ray intensity has been determined
for each day for a number of neutron monitoring stations includ-
ing Ahmedabad (Table 4.1), by harmonically analysing the pressure
corrected hourly data, which has already been corrected for long
term trend (sec 3.2). The yearly mean diurnal amplitude and
phase (time of maximum) for the year 1968-1971, derived from
these observations are listed in Table 4.2 and also pictorially
shown in Figure 4.5 a, b. The standard error of the mean (σ_m)
shown with the annual average vectors has been derived from the
actual scatter in the daily vectors. The size of the error
circle is slightly reduced if the Forbush decrease days are
removed. However, the change in the yearly mean vector thus
obtained is insignificant.

Examination of both the figures and the table shows that
the diurnal variation vector at each station for each year
during 1968 to 1970 is practically unchanged. However, a signi-
ficant phase shift to earlier hours in the time of maximum in
the year 1971 is noticeable at all the stations. The phase
shift is found to be larger at equatorial stations such as Kula
and Ahmedabad, as compared to other stations.

The same conclusion can be arrived even by examining the
diurnal variation on a day to day basis. Figure 4.6a, shows

TABLE 4.2 - The observed yearly average diurnal and semi-diurnal variation for 4-neutron monitoring stations namely Ahmedabad, Kula, Dallas and Deep River during the period 1968 to 1971. The vector average for the entire period along with the standard error of the mean is also listed.

DIURNAL VARIATION

YEAR	AHMEDABAD		KULA		DALLAS		DEEP RIVER	
	Amplitude (%)	Phase (Deg)	Amplitude (%)	Phase (Deg)	Amplitude (%)	Phase (Deg)	Amplitude (%)	Phase (Deg)
1968	0.287 ± 0.020	219	0.190 ± 0.014	204	0.296 ± 0.016	228	0.307 ± 0.018	228
1969	0.242 ± 0.015	216	0.197 ± 0.012	209	0.283 ± 0.015	229	0.294 ± 0.018	224
1970	0.188 ± 0.012	196	0.235 ± 0.013	198	0.274 ± 0.016	222	0.307 ± 0.016	222
1971	0.164 ± 0.010	172	0.195 ± 0.012	173	0.246 ± 0.014	207	0.337 ± 0.015	211
MEAN 1968-1971	0.210 ± 0.007	204	0.198 ± 0.006	196	0.272 ± 0.008	222	0.309 ± 0.008	221

SEMI-DIURNAL VARIATION

YEAR	AHMEDABAD		KULA		DALLAS		DEEP RIVER	
	Amplitude (%)	Phase (Deg)	Amplitude (%)	Phase (Deg)	Amplitude (%)	Phase (Deg)	Amplitude (%)	Phase (Deg)
1968	0.117 ± 0.015	56	0.035 ± 0.010	60	0.043 ± 0.010	62	0.058 ± 0.011	34
1969	0.104 ± 0.009	70	0.055 ± 0.009	59	0.039 ± 0.009	98	0.041 ± 0.010	35
1970	0.055 ± 0.009	64	0.069 ± 0.011	36	0.018 ± 0.010	60	0.047 ± 0.010	358
1971	0.050 ± 0.008	58	0.070 ± 0.008	23	0.043 ± 0.008	64	0.062 ± 0.010	29
MEAN 1968-1971	0.081 ± 0.005	61	0.055 ± 0.005	41	0.035 ± 0.005	72	0.051 ± 0.005	25
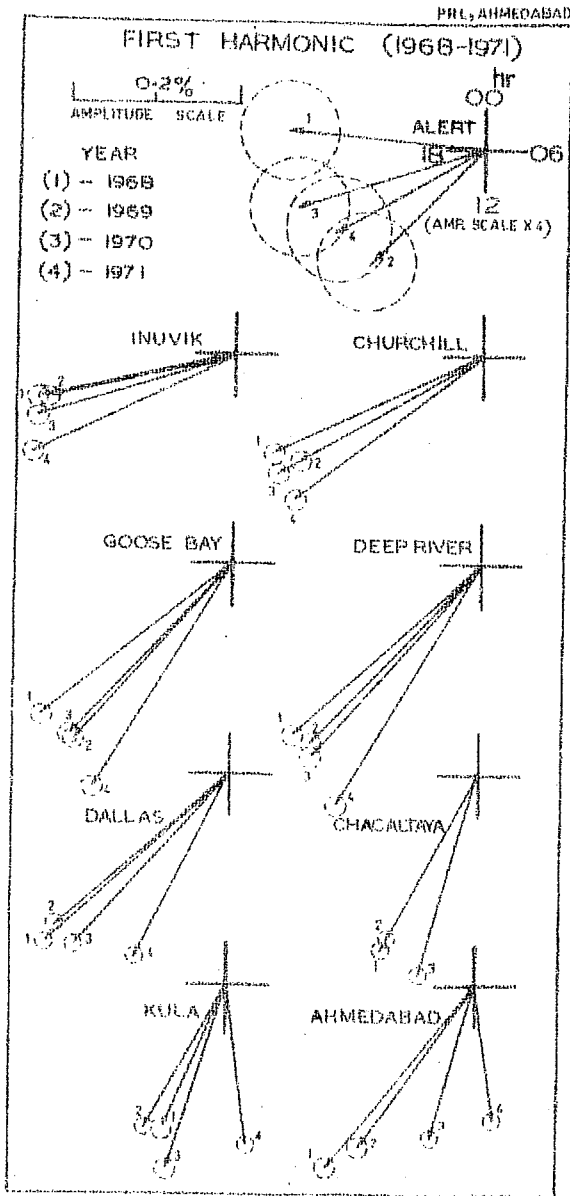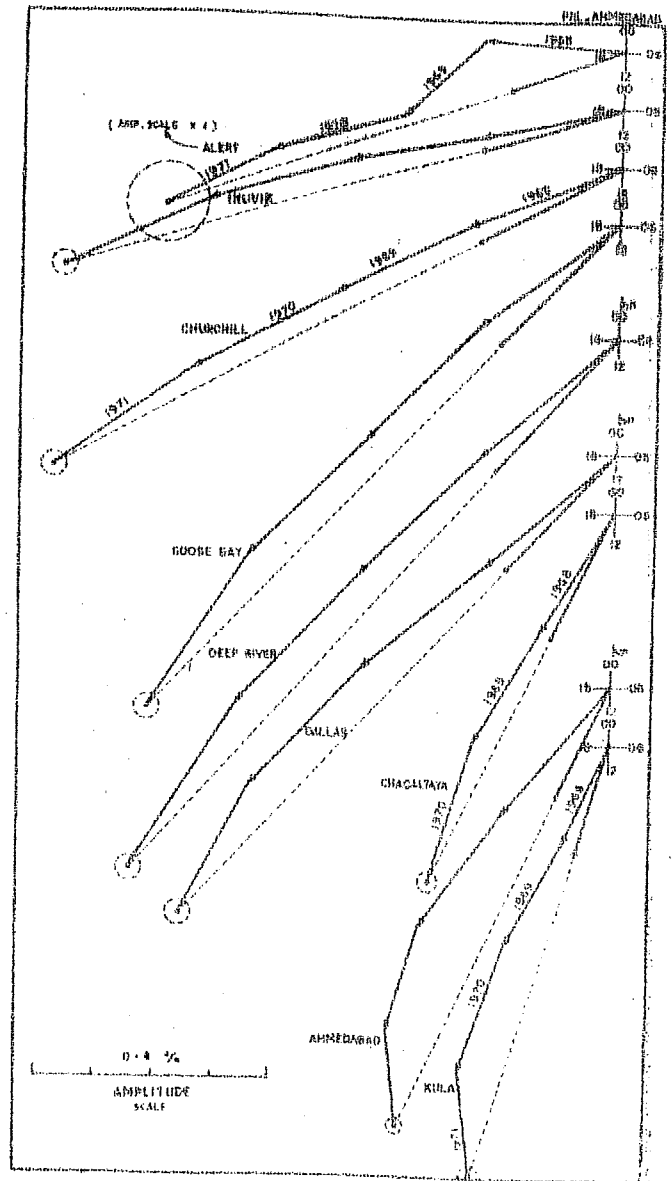
Fig. 4.5 - The observed yearly average diurnal variation for 9 stations during the period 1968 to 1971, plotted (a) on a harmonic dial and (b) as a vector addition diagram. Note, the phase shift to earlier hours in 1971, clearly evident in both the figures. The errors (σ_m) have been derived from the actual dispersion in the individual daily vectors.
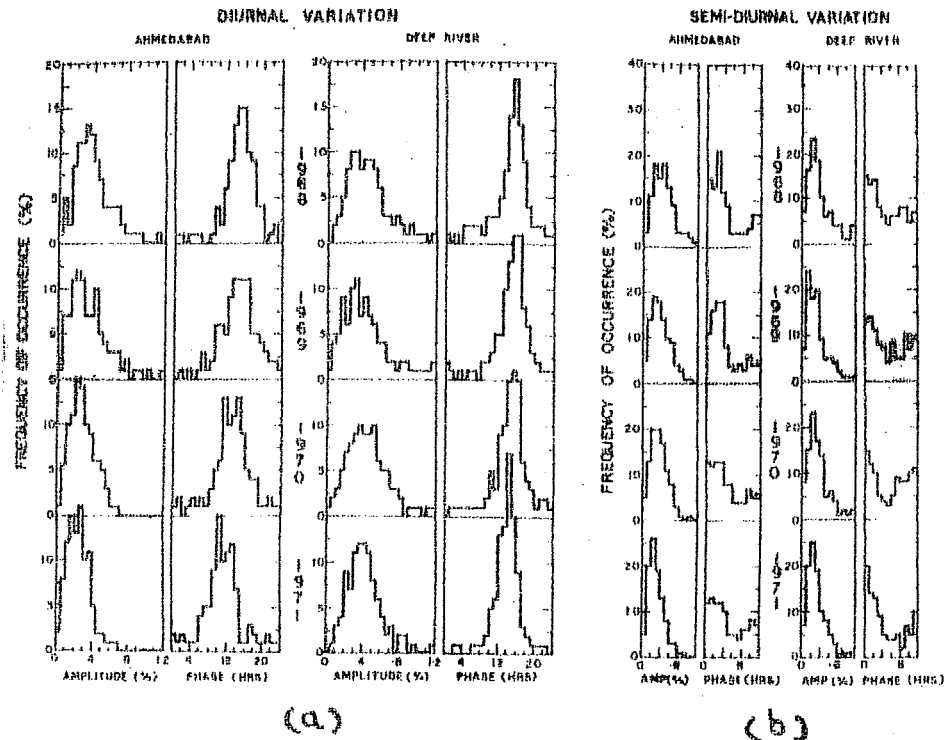
Fig. 4.6 - Histogram of the frequency of occurrence of the (a) diurnal and (b) semi-diurnal amplitude and time of maximum, observed at Ahmedabad and Deep River neutron monitoring station, during each year for the period 1968 to 1971.

Fig. 4.7 - The observed yearly average semi-diurnal variation for 9 stations during the period 1968 to 1971 plotted in a harmonic dial. The errors (σ_m) have been derived from the actual dispersion in the individual daily vectors.
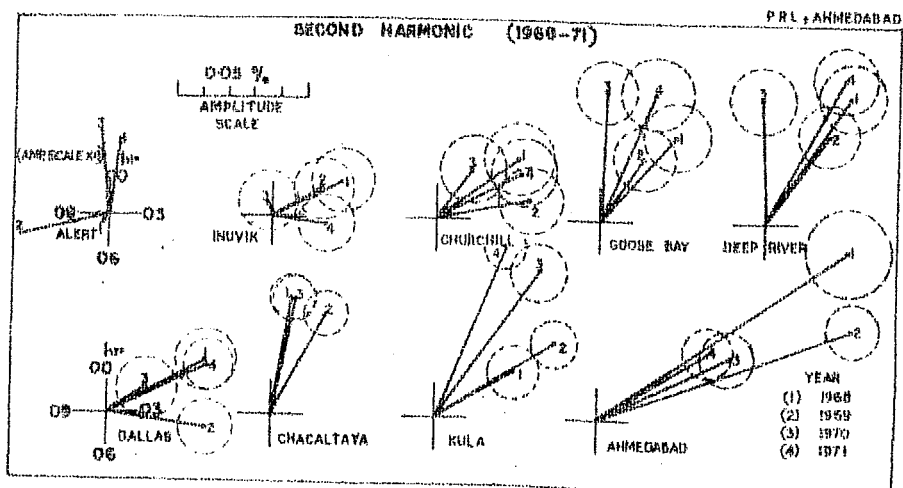
the histogram of frequency of occurrence of diurnal time of maximum and amplitude at Ahmedabad and Deep River for each day during the period 1968-1971. The general shift of the time of maximum to earlier hours in 1971 is very clearly seen from the figure. It is also interesting to note that the histogram of semi-diurnal time of maximum (Figure 4.6 b) shows a much larger scatter as compared to that of diurnal time of maximum, which is consistent with our previous observations. The observations for the yearly average semi-diurnal variation for the same period (Figure 4.7), however, are consistent with its being constant, both in amplitude and phase, during the entire period.

4.2 Average characteristics of the diurnal anisotropy

Using the variational coefficients provided by McCracken et al (1965), and further extended for a greater range of exponent of spectral variation (β) by the author the observed phases and amplitudes of diurnal and semi-diurnal variation at different stations have been corrected for the width of asymptotic cones of acceptance and geomagnetic bending to obtain the characteristics of these anisotropies in space. Figure 4.8-'a, b' show the correction necessary to obtain amplitudes and phases in space from the observed parameters for Ahmedabad and Deep River for various values of β and R_{max}. The ratio of the relative amplitude and phase difference between these two stations is also shown in the same figure, from an examination of which some useful general conclusions can be derived.
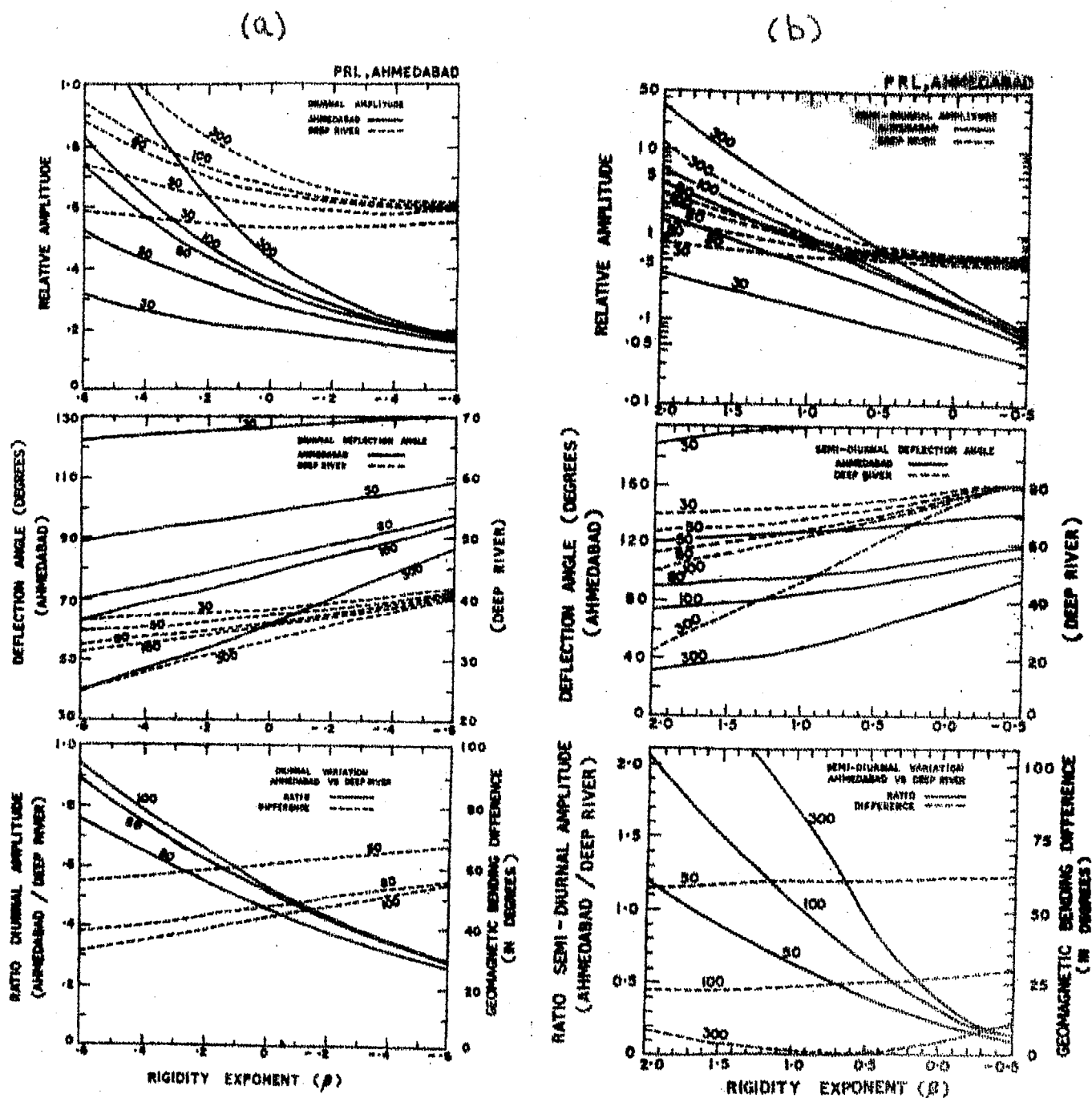
Fig. 4.8 - The relative amplitude and the deflection angle for Ahmedabad and Deep River neutron monitoring station for (a) diurnal and (b) semi-diurnal anisotropy, plotted against β, the spectral exponent, for various values of R_{max} indicated in the individual curves. The lower most portion of the plot shows the ratio and geomagnetic bending difference between these two stations.

(1)   The amplitude ratio is very sensitive to both β and R_{max}, for positive values of β.

(2)   The phase difference, though insensitive to changes in β, is observed to be very sensitive to R_{max}. This property can be used to accurately estimate the value of R_{max}.

The average diurnal anisotropy of cosmic radiation can be represented adequately by a spectrum of the type

$$\frac{\partial J\ (R)}{J\ (R)} = A.R^{\beta} . g\ (\Lambda) \text{ for } R < R_{max}$$
$$= 0 \quad \text{for } R > R_{max} \quad \Bigg\} \quad .. \ 4.1$$

where A is a constant, and $g\ (\Lambda)$ defines the dependence on declination Λ. Following the method of Rao et al (1963), the best fit value of β for each year during 1958 to 1968 has been obtained, using data from world-wide grid of neutron monitors. The best choice of β is the one for which the variance, between various values of anisotropy vectors estimated from observations at different stations is a minimum. The best value of β for the entire period 1958 to 1968 is observed to be $\approx 0.0 \pm 0.2$, which is in very good agreement with the results quoted by McCracken and Rao (1965)

Figure 4.9 and 4.10 show the yearly average diurnal anisotropy time of maximum and amplitude for the entire period 1958-1968. We observe from the figure, that the diurnal anisotropy phase has remained practically constant at $90^{\circ}E$ of the sun-earth line during the entire period, consistent with previous findings (McCracken and Rao, 1965). However, the yearly
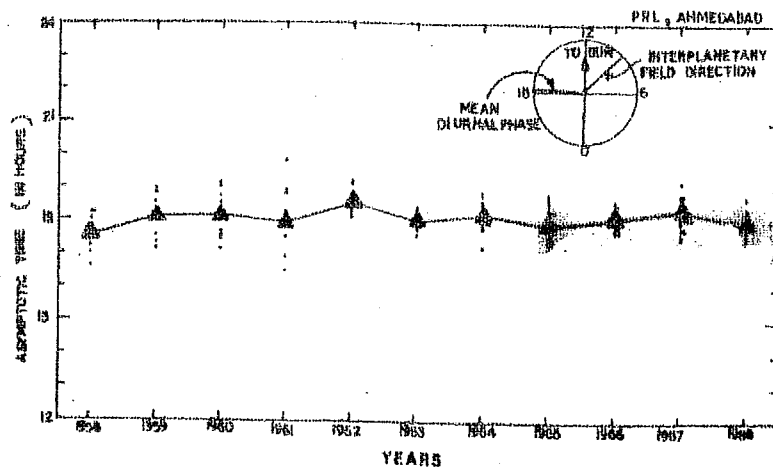
Fig. 4.9 — The yearly mean phase of the diurnal anisotropy during 1958-1968. The mean value for each year is indicated by a triangle and the value for individual stations are shown by dots.

Fig. 4.10 — The yearly average amplitude of diurnal anisotropy during 1958-1968. The mean value for each year is indicated by a triangle and the value for individual stations are shown by dots.
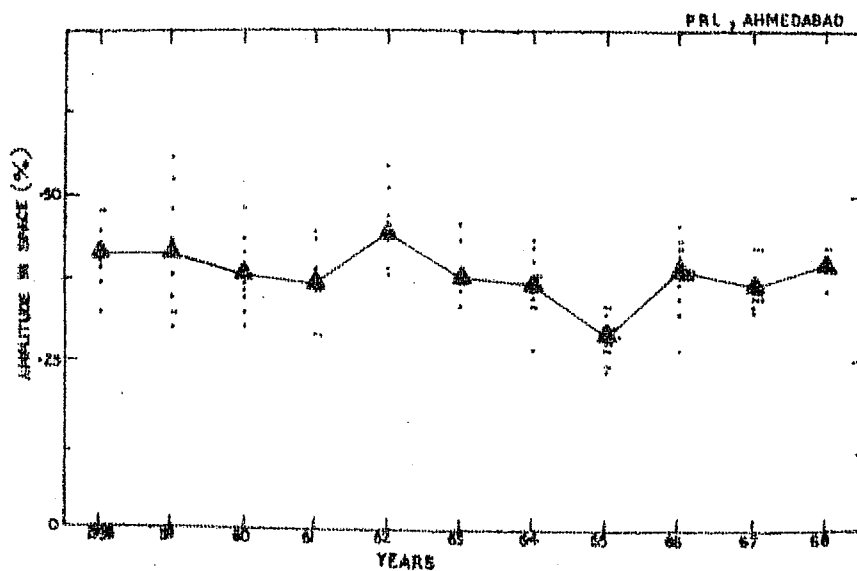
average amplitudes clearly show significant variations from year to year, the amplitude showing $\sim$ 20% decrease during the sunspot minimum year of 1965. The variations in the yearly average amplitudes have been generally attributed to the changing value of R_{max}.

Using data from underground monitors some estimates of R_{max} have been made (Ahluwalia and Ericksen, 1970, 1971). The value of R_{max} during 1968-1971 is generally observed to be around 80-100 GV. In Figure 4.11, the theoretically expected ratio of diurnal amplitude of Ahmedabad to that at Deep River for different values of R_{max} and β are plotted. The experimentally observed ratio of amplitudes for the period 1968-1971 clearly shows that the value of β, applicable to this period is $\approx$ 0.2 $\pm$ 0.2, even after taking extreme possible limits of R_{max} into consideration.

In summary we conclude that (1) the yearly average diurnal anisotropy is rigidity independent ($\beta \approx 0$) with a time of maximum corresponding to 18 hour in space and is time invariant during the period 1958 to 1970. (2) The amplitude, which is $\sim$ 0.4% in space, varies as cosine of the declination. In other words, the diurnal anisotropy is consistent, on an average, with cosmic ray particles undergoing corotation with the sun. The yearly average amplitude shows small but significant changes with solar cycle, due to the variation in upper cut-off-rigidity (R_{max}).

4.3   Long term variation of diurnal anisotropy and the change
       in upper cut-off-rigidity (R_{max})

R_{max}, the upper cut-off-rigidity upto which the diurnal

anisotropy exists, seems to be intimately associated with the

electromagnetic condition in interplanetary space, in particular

on the nature and size of the small scale irregularities in

interplanetary medium. Therefore, a reliable estimate of R_{max},

is of fundamental importance in understanding the electromagnet-

ic conditions of the interplanetary space. A reliable estimate

of R_{max} is possible by employing data from monitors having a

very high mean rigidity of response. This fact is borne out by

the data presented in Figure 4.12, wherein the yearly average

diurnal amplitude as observed at a typical low (A_E - (1)) and

middle latitude stations (A_M - (2)) are separately represented

for each year during the period 1958-1968. It is seen from the

figure that the range in the variation of mean diurnal amplitude

from year to year for low latitude stations having a higher

mean rigidity of response is much larger than that for middle

latitude stations. The value of R_{max} estimated by attributing

the entire variation of diurnal amplitude to the change in the

value of R_{max} is also plotted for each year for the same

period (4). The above calculation is performed using R_{max}

(1968) = 100 GV as the normalising point, for which there exist a

number of independent confirmatory evidences. It is seen that

the value of R_{max} changes approximately from 35 GV during 1965

to 100 GV during 1968, and is positively correlated with
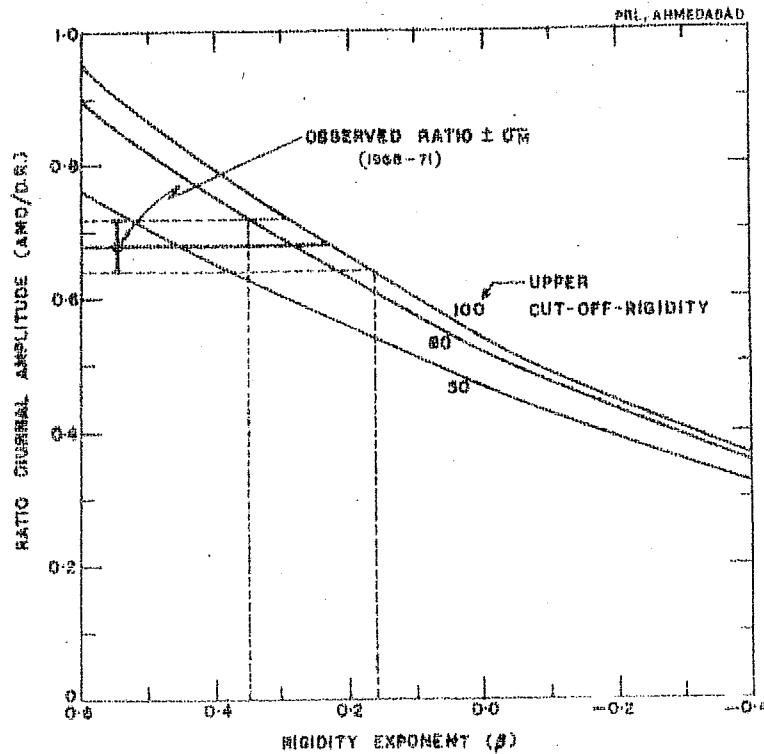
Fig. 4.11 - The ratio between the diurnal amplitude observed at Ahmedabad to that at Deep River during 1968-1971. The theoretically expected ratio for different values of β and for various values of R_{max} = 50, 80 and 100 GV, are also shown. The error has been derived from the actual dispersion of the daily vectors.
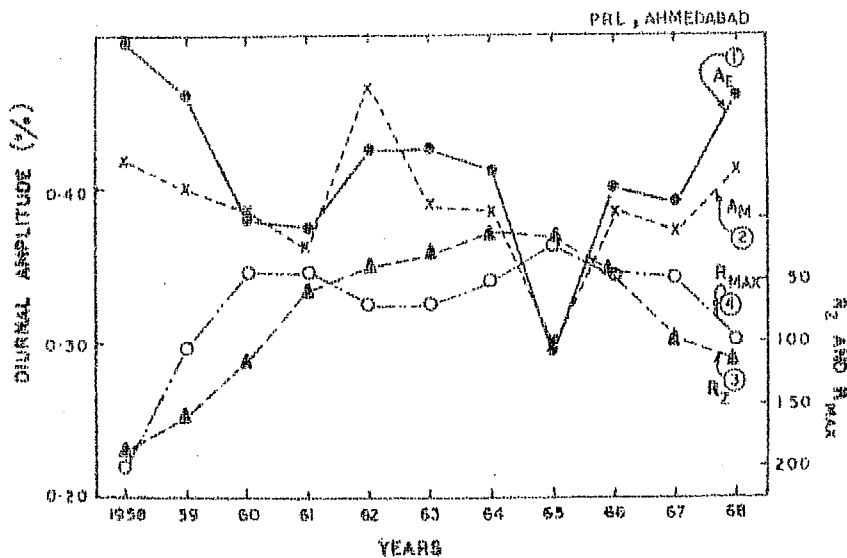
Fig. 4.12 - The variation of yearly average diurnal amplitude in space (1) for low latitude stations (A_E) and (2) for mid-latitude stations (A_M) along with the sun spot number R_z. The computed solar cycle variation of R_{max} for the period 1959 to 1968 is also shown (4). The scale of R_z and R_{max} increases from top to bottom.

sun-spot number R_Z and $\lambda 5303$ (Ahluwalia, 1971).

To obtain a better estimate of R_{max}, Rao et al (1963), Jacklyn et al (1970), and Ahluwalia and Ericksen (1970,1971), have used the data from underground meson monitoring stations having very high mean rigidity response. By comparing the observed diurnal variation amplitude in underground meson monitors with the diurnal variation amplitude as observed by surface neutron monitors, and knowing the spectral characteristics of the average diurnal variation, these authors have derived R_{max} for different periods of time. The results, in general, have shown that R_{max} varied from $\sim$40 GV during sun-spot minimum of 1965 to 80-100 GV during solar activity maximum of 1968. Inspite of the fact that the estimates are obtained using underground monitors with high mean rigidity of response, these results can at best be considered as rough estimates, due to the uncertainties introduced in the analysis arising from the lack of our knowledge of the coupling coefficients for underground monitors and the inaccuracy introduced in applying temperature correction to the underground meson data.

We have attempted to obtain independent reliable estimate of R_{max} for different years using neutron data from Ahmedabad which has a high rigidity of response and meson data from surface meson monitors such as Deep River meson monitor. Before proceeding with the determination of R_{max}, it is essential to apply adequate temperature correction to the surface

meson data. The author has therefore, first derived the appro-
priate temperature coefficient to be used for Deep River meson
monitor data. The data adequately corrected for temperature
variations in the atmosphere, along with Deep River and
Ahmedabad neutron monitor data, have been utilised to estimate
R_{max} for each year during the period 1965 to 1969.

4.31 Temperature correction factors for Deep River meson monitor

The diurnal anisotropy obtained from meson data corrected
for temperature (using the temperature correction factors
derived by Bercovitch (1966), see Table 4.5), have been used by
many authors to cast doubt on the 18-hour average corotational
anisotropy and to advocate the hypothesis of a two way energy
dependent diurnal anisotropy (Kodama and Nagashima, 1968;
Kitamura, 1968). In view of the fact that the diurnal anisotro-
py derived from neutron data show time invariance during 1958-
1970, with time of maximum $\sim$18 hr (Rao, 1972), the temperature
correction factors hitherto applied to the Deep River meson
data require to be re-examined. Since the temperature coeffic-
ient obtained by Bercovitch (1966) were for wide aperture muon
telescope which may not be applicable to the standard MT-64
cubical telescope, whose data have been used for all time
variation investigations, it is very important to derive the
appropriate temperature coefficients applicable to the standard
MT-64 cubical telescope. For this purpose we have used the

published data for 1965-1969 (Steljes, 1970) on diurnal variation derived from pressure corrected neutron and meson data (both temperature uncorrected and corrected using coefficients given by Bercovitch). The entire data, excepting Forbush decrease days, have been utilised and essentially the method of analysis suggested by Bercovitch (1966) described earlier in sec. 3.42 has been adopted for deriving the temperature effect on Deep River mesons.

4.311 Examination of presently used temperature coefficient

Figure 4.13 shows the histogram of the frequency of occurrence of the ratio R (α_m/α_n) of the diurnal amplitude observed by Deep River mesons to the corresponding amplitude observed by Deep River neutrons, and of ϕ ($T_m - T_n$) the phase difference between the two for each day during the period 1965-1969. It is clearly seen from the figure that for more than 70% of the days the ratio R is > 0.50. The theoretically expected ratio R and ϕ, for an energy independent anisotropy and for an upper cut-off-rigidity 100 GV are also shown by dotted lines in the figure. It is very clear from the figure that the computed amplitude ratio R and phase difference ϕ, between Deep River mesons and neutrons is far different from the theoretically expected value, indicating that the Bercovitch's(1966) temperature correction factor applied to Deep River meson is far from adequate. The normal variation in upper cut-off-rigidity will not affect the theoretically expected value to vary so
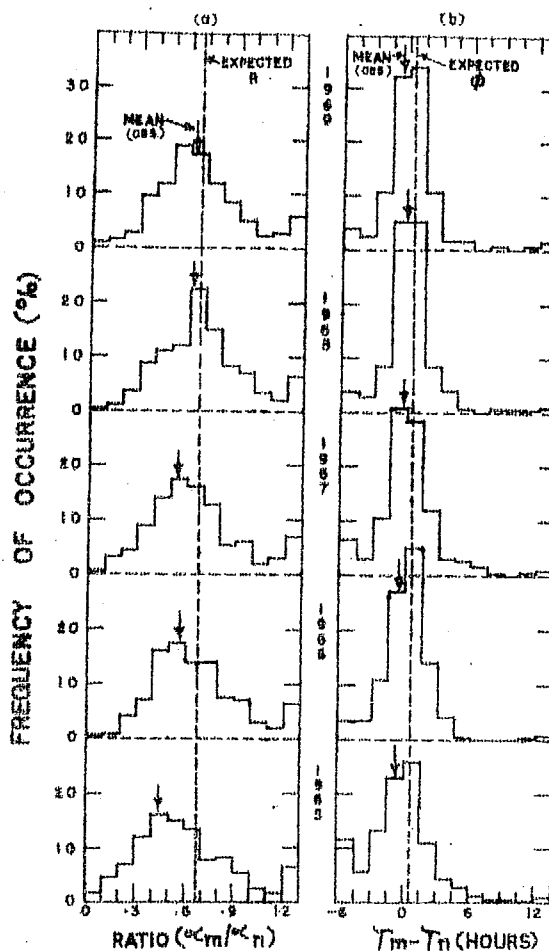
Fig. 4.13 - Histogram of the frequency of occurrence of (a) the ratio R between meson and neutron diurnal amplitude and (b) the phase difference between the two, for Deep River for each year during 1965-1969. Dashed lines show theoretically expected values for an assumed upper cut-off-rigidity of 100 GV (Mori, 1968 a, b), while arrows indicate the mean values for each year.

significantly as to affect our above generalised conclusion regarding the inaccuracy of the temperature correction factor. Therefore, instead of applying the temperature correction factor given by Bercovitch (1966), we proceed to derive the actual correction factors from the basic Deep River data for the period under consideration.

Following the method described in Sec. 3.42 and using the published values of $\underline{M}$ and $\underline{N}$ vectors (Steljes, 1970) the values of R and ϕ have been computed for each year using the least square fit method to the vector equation 3.25 for the period 1965-1969 (Table 4.3). In these calculations we have restricted our analysis to days on which the diurnal amplitude of neutrons at Deep River is $0.1 < \alpha_n < 0.7\%$. The low amplitude days have been neglected to avoid uncertainties due to statistical errors. Abnormally high amplitude days have been likewise neg-lected, as on such days the diurnal variation is likely to be influenced by contribution due to mechanisms other than corotat-ion and the energy spectrum on such days may not be energy independent. It is clear from Table 4.3 that the ratio R in each year is greater than 0.5, the best fit value for the entire period being 0.58 ± 0.04, with the phase difference between mesons and neutrons (ϕ) being 0.5 ± 0.1 hour, in good agreement with the theoretically expected values.

4.312 Evaluation of temperature coefficient

First order estimate of the temperature effect on meson data can be easily derived using days on which neutron monitors show negligible diurnal amplitude ($\alpha_n < 0.1\%$). For such days the observed variation of uncorrected meson data ($\underline{M}$) will be mainly due to the atmospheric temperature effects ($\underline{T}$), since the meson diurnal amplitude for such days is expected to be $< 0.05\%$. During the 5-year period under study, 63 such days

TABLE 4.3 - Showing the temperature correction factors for Deep River mesons in 1965-1969, obtained from the least square fit. The best fit values for the entire period is also listed

Year	R	ϕ (Deg)	Temp. Correction Vector (A)		Ground Temp. Vector (T)	
			Amp. (%)	Phase (deg)	Amp. (^{O}F)	Phase (deg)
1965	0.550	21.2	0.119	108	7.39	231
1966	0.605	8.4	0.085	85	7.27	226
1967	0.596	5.6	0.082	86	7.50	229
1968	0.575	6.3	0.063	122	7.69	230
1969	0.536	-2.2	0.026	88	7.33	232
1965-1969	0.582	7.0	0.075	95	7.43	230

were present for which a temperature coefficient of $-0.009\%/^O$F has been obtained. If appropriate correction for the small cosmic ray diurnal amplitude is also made, the average effective temperature coefficient for this period is found to be $C_t = -0.010\%/^O$F with $\theta = 3.2$ hour direction.

For a more rigorous evaluation of the temperature effect, we have examined the meson data on a day to day basis. We have divided the data for the entire period into five groups based on the diurnal amplitude of temperature. Table 4.4 gives the results obtained, employing the least squares fit criteria on individual daily values to equation 3.25 with the data grouped according to the diurnal amplitude of ground temperature α_t in the intervals of 3.6^OF. The mean value of α_t and T_t for each of the groups are also given in Table 4.4. It is seen from the

TABLE 4.4 - Variation of temperature correction vectors with the change in ground temperature variation. The best fit value of the temperature correction factor for groups 2 to 5 is also listed.

Temp. Groups	No.of days (1965-1969)	R	ϕ (deg.)	Temp.Correction Vector (A)		Ground Temp Vector(T)	
				Amp. (%)	Phase (deg)	Amp. (°F)	Phase (deg)
1	324	.592	8	.045	130	1.56	229
2	439	.614	9	.071	89	5.06	231
3	367	.547	5	.073	93	8.77	231
4	255	.577	6	.103	86	12.50	228
5	135	.623	-2	.126	78	16.08	227
(Gps. 2-5)	1196	.580	7	.085	90	9.03	229

Mean value C_t $(A/T) = -0.0095 \pm 0.0005\%/°F$

table that with the increase in the value of α_t, the contribution due to temperature effect (A) also increases linearly as expected. It is further seen that the value of R for each group is > 0.5. The best fit values have also been determined using equation 3.25 for the entire period excluding days of group 1. Group 1 days have been excluded from this particular analysis, since we believe that the systematic and random errors due to other factors could become quite significant compared to the small amplitude of diurnal temperature vectors on these days. The temperature effect obtained from the best fit value for all days can be represented by (Figure 4.14),

$$A = -0.0095 \ T \ (\alpha_t, \ T_t + 2.6h) \qquad .. \ 4.2$$

where $C_t = -0.0095\%/°F$ and $\Theta = 2.6$ hour.

It may however be noted that if we also include group 1 days, an alternative best fit shown in Figure 4.14 can be obtained which is given by

$$A = A_o \quad - \quad .0072 \ T \ (\alpha_t, \ T_t + 1.0h) \qquad \qquad .. \ 4.3$$

where A_o is a vector (indicated by the arrow) of amplitude 0.037% in a direction T = 0930 hr. A_o is essentially a constant and is independent of temperature, with its magnitude sensitive to the value of ϕ used. The above results are found to be essentially true even when the data is divided into a larger number of groups.

The physical significance of A_o in equation 4.3 is not immediately apparent. Further, for reasons given earlier, we believe that group 1 days on which the temperature variation is very small should be excluded from the analysis and hence we believe that equation 4.2 truly represents the temperature effect of mesons. Even though the choice of equation may matter on the individual days, we wish to emphasize that the results on an average basis derived here will not be altered if we were to use equation 4.3 instead of 4.2.

The value of ϕ = 0.5 hr. obtained from the least square fit method using data on individual days also agrees very well with the expected value derived, assuming that the mean cosmic ray diurnal anisotropy is independent of rigidity upto an upper cut-off-rigidity $\sim$ 50 to 100 GV.
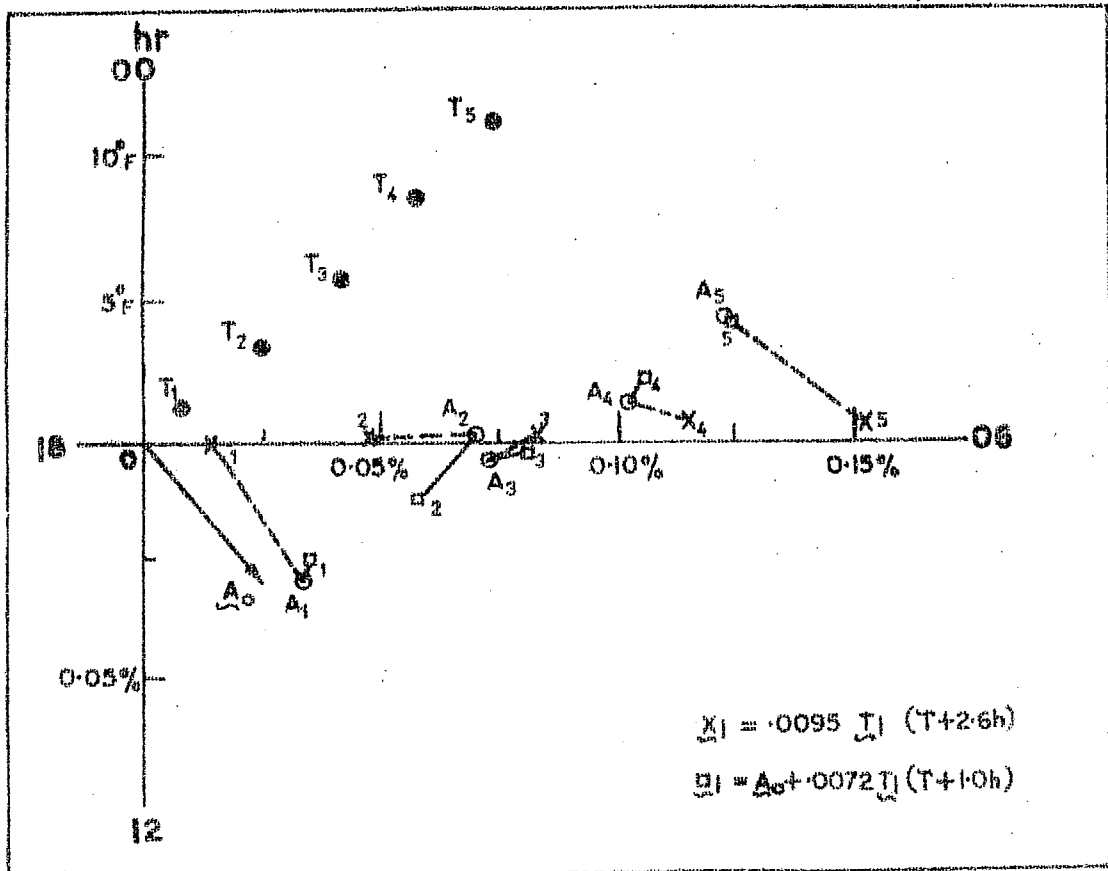
Fig. 4.14 - Harmonic dial representation of the end points of the A vectors (open circle, A₁ to A₅), and the T vectors shifted by 12 hours (solid points T₁ to T₅). The crosses (X) labelled 1 to 5 show the temperature correction vectors calculated from T using equation 4.2, while vector deviation of the fit is indicated by dashed lines. The open squares (□) show the temperature correction vectors calculated from T using equation 4.3, while the vector deviation of the fit is indicated by full lines.

Further confirmation of the correctness of the derived temperature coefficients can be obtained by comparing the temperature corrected diurnal vector from mesons (M) with the diurnal vector obtained from neutrons (N) on a day to day basis. We have calculated the vector variance σ² representing the difference between these two, for different combinations of

values for R, ranging from 0.46 to 0.70, ϕ from 0 to 1 hr, C_t from -0.006 to -0.013 and θ from 1 to 3 hrs., using the equations

$$\triangle_i = \underset{\sim}{M}_c - R.\underset{\sim}{N} (\propto_n, T_n + \phi) \qquad \text{.. 4.4a}$$

where $\underset{\sim}{M}_c = \underset{\sim}{M} (\propto_m, T_m) - \underset{\sim}{A} \qquad \text{.. 4.4b}$

and the variance σ^2 is given by $\frac{1}{N} \sum_{i=1}^{N} \left| \triangle_i \right|^2 \qquad \text{.. 4.4c}$

For the period 1965-1969, we observe that the values of R, C_t, θ and ϕ as derived by us and listed in Table 4.5, gives the minimum variance showing that the temperature coefficients derived by us are reliable even on a day to day basis.

It is probably possible to derive other sets of combinations of R, C_t, θ and ϕ, which are equally acceptable on a statistical basis. However, we wish to point out, that the temperature coefficient obtained by us even though not unique, are nevertheless, in our opinion, still the best choice amongst the different possible alternatives.

Figure 4.15 illustrates the good agreement between meson anisotropy vector obtained after correcting with the temperature coefficient (as given in equation 4.2) obtained from ground temperature data and neutron anisotropy vector. $\underset{\sim}{N}$, $\underset{\sim}{M}$ and $\underset{\sim}{M}_c$ represent the neutron, uncorrected meson and corrected meson diurnal vectors respectively. $\underset{\sim}{M}_c^*$ is the expected meson diurnal vector calculated from the neutron vectors using the best fit values of R = 0.58 and ϕ = 0.5 hr., which, in other

TABLE 4.5 - Comparison of temperature coefficients used earlier with the present results.

| Year | R | ϕ (HRS.) | Total Temperature coefficient | |
			c_t (%/$^{\circ}$F)	θ (HRS.)
1962-64 (Bercovitch, 1966)	0.473	0	-0.0061 $\pm$0.0004	1.9 $\pm$ 0.3
1965-69 (Present results)	0.580	0.5	-0.0095 $\pm$0.0005	2.65$\pm$ 0.20

words, represent the expected diurnal vector for corrected mesons to yield the value of diurnal anisotropy consistent with neutron observations. The good agreement between $\underset{\sim}{M}_c$ and $\underset{\sim}{M}_c^*$ clearly indicates the appropriateness of the temperature coefficient derived from ground temperature data. Table 4.5 summarises the temperature correction factors derived in the present investigation.

The temperature coefficient of -0.0095 $\pm$ 0.0005%/$^{\circ}$F derived here is substantially higher than the coefficient that have been used hitherto, but is in good agreement with those derived using direct radiosonde observations from Maniwaki, located $\sim$120 km from Deep River.
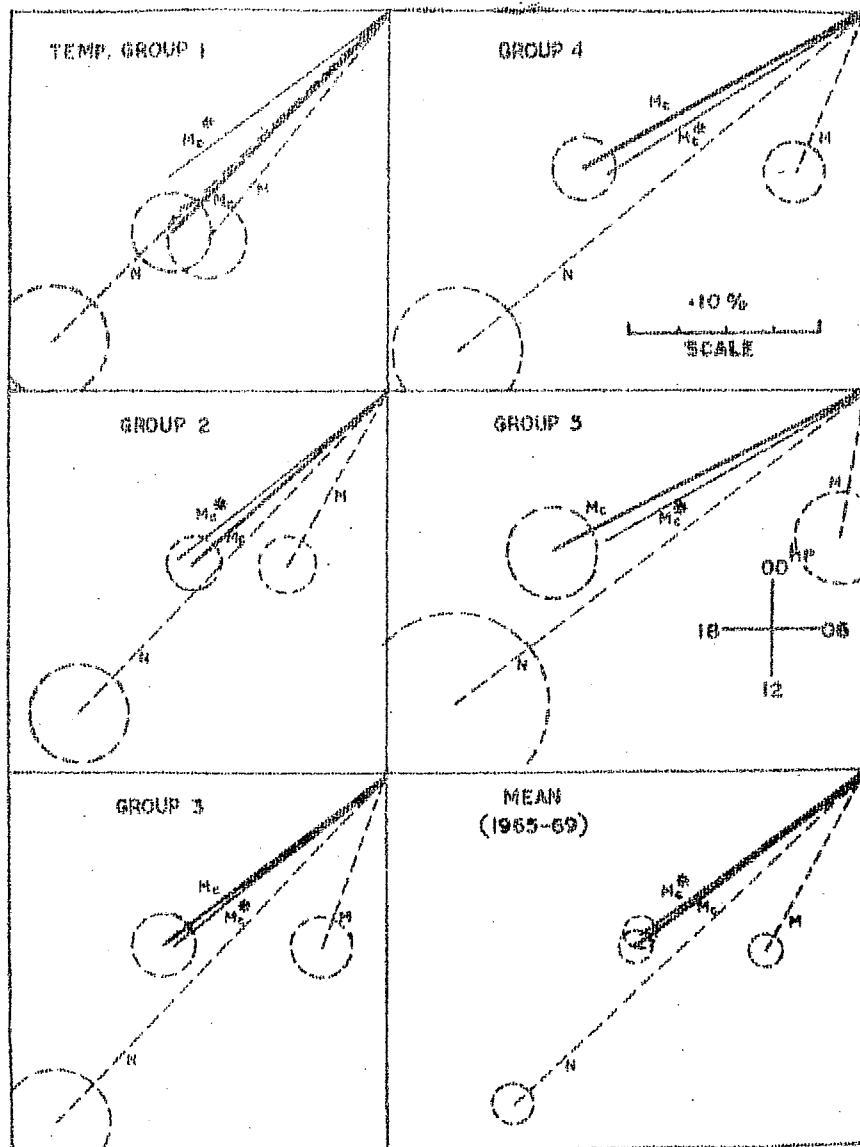
Fig. 4.15 - Illustrates the good agreement between the expected meson vector (M_c) using neutron data and the temperature corrected meson vector (M_c) using new temperature coefficients for different temperature groups as well as for all the days during 1965-1969.
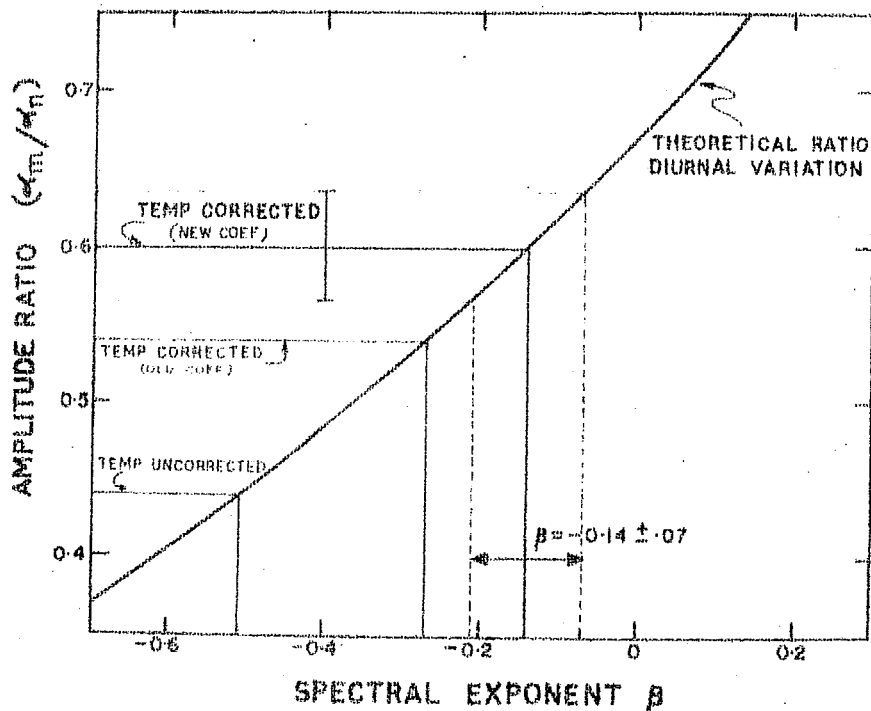
Fig. 4.16 — Theoretically calculated ratio R of the diurnal amplitude of mesons to neutrons for Deep River plotted against β, the spectral exponent of the rigidity spectrum of diurnal variation, calculated by assuming 100 GV for the upper cut-off-rigidity. The observed ratio obtained using temperature corrected and uncorrected mesons are also shown in the figure.

4.32 Rigidity spectrum of average daily variation:

The ratio of the amplitude of diurnal variation of mesons to neutrons (α_m/α_n) at Deep River has been calculated for different values of the rigidity spectral exponent β, assuming an upper cut-off-rigidity of 100 GV. Figure 4.16 shows the theoretically expected ratio plotted as a function of β, and the observed ratio for 1965-1969 obtained using the uncorrected meson data, temperature corrected meson data using the temperature coefficient given by Bercovitch and the temperature

corrected data using the temperature coefficient derived in the previous section. The figure clearly indicates that the ratio obtained using meson data corrected with our temperature coefficient gives the best values for the spectral exponent ($\beta = -0.14 \pm 0.007$) consistent with the spectral exponent derived for the average diurnal variation using neutron monitor data alone (sec 4.2). Similarly the energy spectrum of semi-diurnal variation obtained using neutron and meson data corrected using our temperature correction yields a value $\sim 0.8 \pm 0.2$, for the spectral exponent which again is consistent with the neutron monitor results, presented in the next chapter, thus providing an additional evidence for the correctness of the temperature coefficient derived earlier.

4.33 Change in upper cut-off-rigidity from year to year

Referring back to Table 4.3, it is seen that atmospheric temperature correction factor shows a significant progressive decrease from 1965 to 1969, even though the ground temperature vector is practically invariant. This clearly indicates that the derived variation in the correction factor is caused by other physical mechanisms, such as change in upper cut-off-rigidity.

Applying the new temperature correction factor obtained from using ground based temperature data, to the uncorrected meson intensity, the temperature corrected meson diurnal vector

TABLE 4.6 - Comparison of mean diurnal variation observed by mesons (corrected with appropriate temperature coefficient) with the mean variation observed by neutrons during the period 1965 to 1969.

Year	DIURNAL VARIATION				R	ϕ (deg)
	Neutrons		Mesons (Temp. corrected)			
	Amp. (%)	Phase (Deg)	Amp. (%)	Phase (Deg)		
1965	.226 ± .021	222	.113 ± .016	222	.50	0
1966	.291 ± .022	228	.179 ± .016	229	.61	+1
1967	.260 ± .027	224	.158 ± .020	232	.59	+8
1968	.307 ± .022	229	.209 ± .015	235	.68	+6
1969	.294 ± .020	225	.194 ± .014	234	.66	+9
Mean	.276 ± .010	226	.166 ± .007	232	.60	+6

has been derived for each year. Table 4.6 lists the neutron and temperature corrected meson diurnal vectors as well as the computed ratio R and phase difference ϕ between the diurnal vectors obtained for mesons and neutrons, for each year during 1965-1969. The values of R show a progressive increase with solar activity, the minimum coinciding with the minimum solar activity. Using Mori's (1968a, b) calculations, and assuming the rigidity spectrum of the diurnal variation to be rigidity independent, values of R for different assumed values of the

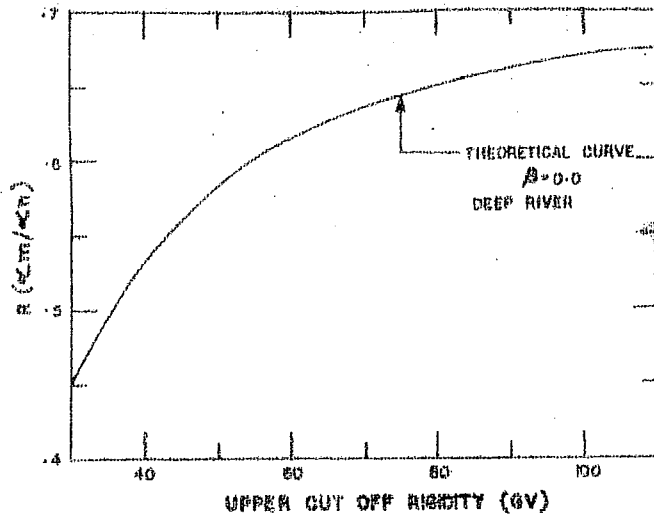Fig. 4.17 - Theoretically calculated value of the ratio R (for $\beta = 0$) plotted as a function of the assumed upper cut-off-rigidity.
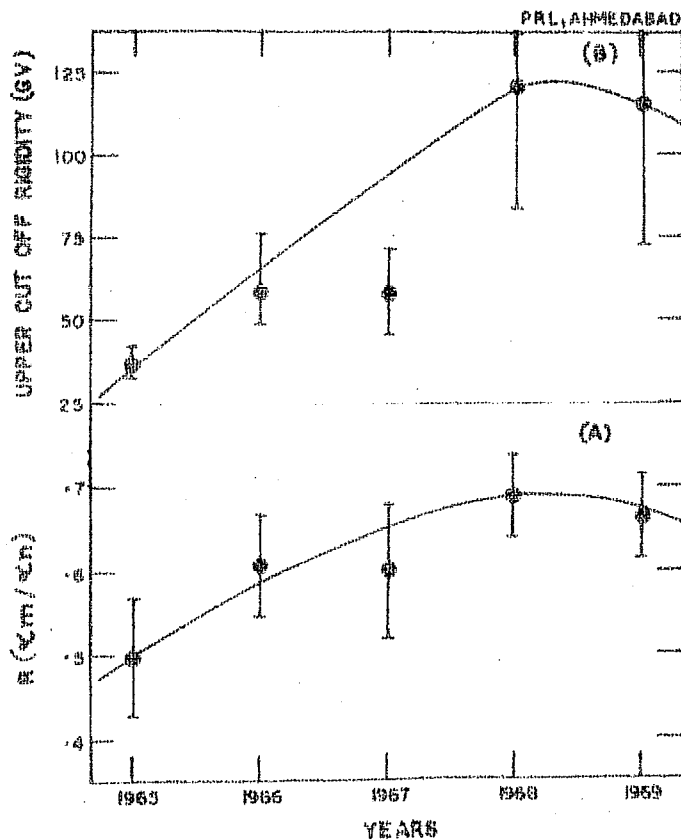

Fig. 4.18 - Showing the solar cycle variation of (a) the ratio R and (b) the upper cut-off-rigidity during 1965-1969. The meson data used have been corrected with newly derived coefficients. The errors have been derived from the dispersion of the observed daily vectors.

upper cut-off-rigidity have been calculated and plotted in
Figure 4.17. Using these calculations, the observed change in
R with solar cycle can be used to infer the change in the upper
cut-off-rigidity beyond which the diurnal variation ceases.
Figure 4.18 shows the solar cycle variation of R and the upper
cut-off-rigidity (R_{max}) during the period of 1965-1969. R_{max}
shows a minimum of about 35 GV during the quiet solar year of
1965 and a maximum of about $\sim$100 GV during 1968-1969. These
results are consistent with the results obtained by Ahluwalia
and Ericksen (1970), and Ahluwalia (1971) using data from
underground meson monitors.

4.34 Discussion:

The limiting rigidity R_{max} has been very often attributed
to the sector structure dimensions. The particles whose
gyroradius ($\sim$1 AU) is comparable to the dimension of the sector
structure will not partake in corotation. The change in R_{max}
can thus be attributed either to (a) variation of the number of
sectors during different phases of the solar cycle, (b) or due
to an increase in the effective size and/or number of I.M.F.
irregularities which can cause an appreciable variation of the
cosmic ray density gradient in and out of the ecliptic plane.

The former hypothesis is in qualitative agreement with
our findings on the variation of R_{max}, as Schatten's (1971)
result seems to indicate a much larger dimension for the sector

structure during the sun-spot maximum year of 1968. However, it is not possible, at the present time to make a clear cut choice between the two hypothesis presented above. Even though the direct field measurements (Ness, 1966; Schatten, 1971) as well as properties of cosmic ray semi-diurnal anisotropy (see next chapter) indicate that the average value of I.M.F. has not changed appreciably during the present solar cycle, there seems to be some evidence for a decrease in the scale size and number of the I.M.F. irregularities during 1965.

The interplanetary magnetic field measurements from Mariner-4 (November 29 to December 30, 1964) and from Heos-Al (December 11, 1968 to March 16, 1969) have shown significantly lower power spectral density in the B_z component of the magnetic field, during the period covered by Mariner-4 observations (low solar activity period), for resonant proton rigidity $\widetilde{\sim}$ 3 GV (Quenby and Sear, 1971). The reduction in power during minimum solar activity period, particularly in the B_z component can, in principle, produce the observed solar cycle variation in the upper cut-off-rigidity of diurnal variation.

4.4 Relationship between diurnal anisotropy and interplanetary magnetic field, and the cosmic ray density gradients

Even though the average characteristics of the cosmic ray diurnal anisotropy are well established and are explainable in terms of Parker-Axford model (see Sec 4.2), a number of discrepancies exist between the theoretical interpretation and the

actual observation. The observed average amplitude of 0.4% for diurnal variation in space (obtained using the correction factors as given in IQSY manual by McCracken et al., 1965) is only about two third of what is expected from theoretical considerations. Even though attempts have been made to explain the amplitude reduction, as due to presence of a significant perpendicular diffusion (K_1) on an average basis, the observed day to day variability both in the amplitude and in the time of maximum (Rao and Sarabhai, 1964; Patel et al., 1968), cannot be understood in terms of the simple theory. Consecutive days having abnormally large amplitude ($\geqslant 1\%$) have been reported by several workers (Mathews et al., 1969; Hashim and Thambyahpillai, 1969), who have concluded that the diurnal variation on such days is generally caused by a depletion of the cosmic ray intensity along the garden-hose direction. Likewise trains of days having abnormally low amplitudes are also evident in the data. Explanation of such abnormal amplitudes using the concept of corotation has not been satisfactory.

4.41 Anisotropy results at low energies and their extension
     to high energies

Recently McCracken et al. (1967, 1968) and McCracken and Rao (1970) in a series of papers, have shown that the low energy cosmic ray anisotropy during solar flares is large and field aligned initially, which then changes to an equilibrium type of anisotropy during the decay phase of the flare effect, directed

radially away from the sun. The equilibrium anisotropy has
been explained by them as due to the convection of the cosmic
ray particles by the radially blowing solar wind. The convect-
ive anisotropy of low energy solar flare particles is given by

$$\underset{\sim}{\xi}_C = 3C \frac{V}{v} \qquad\qquad .. 4.5$$

where C is the Compton-Getting factor, V is the solar plasma
velocity and v is the particle velocity. At energies of the
order of 10 MeV, the convective anisotropy is $\approx$ 10 to 15% while
at relativistic energies, the convective anisotropy is only
$\approx$ 0.6% (see Figure 1.3). At late times in the decay i.e. after
$T \geqslant 4$ days, McCracken et al. (1971) showed that the radial
convective anisotropy eventually evolves into an easterly equi-
librium type anisotropy along the direction 45° east of the
satellite - sun line. The easterly anisotropy has found a
fairly satisfactory explanation in terms of the establishment
of an equilibrium between the radially convective, and field
aligned diffusive anisotropy, the field aligned diffusion being
caused by the establishment of a positive density gradient by
the particles convected out of the solar system earlier. Based
on the anisotropy measurements of solar flare cosmic radiation
described above, it is apparent that at low energies ($\sim$ 10 MeV)
convection is the most dominant mechanism that determines the
escape of cosmic rays from the solar system and transverse
diffusion is negligible.

McCracken et al (1968) also suggested the extension of these physical ideas to explain the observed diurnal variations at relativistic energies, the theoretical formulation of which was subsequently provided by Forman and Gleeson (1970). Assuming K_1 to be negligible, the observed diurnal variation can be completely explained in terms of radial convection and field aligned diffusion. With the finding of Subramanian (1971 a) that if all correction factors are taken into account, the observed average diurnal anisotropy of 0.4% is consistent with the theoretical value, it is apparent that there is no need to invoke transverse diffusion causing amplitude reduction. In other words, it is possible to examine the observed diurnal variation in terms of the new physical concept proposed by McCracken et al. (1968) and Forman and Gleeson (1970). According to this new concept, the corotational diurnal vector observed, on an average basis, is merely a special case when equilibrium exists between convection and diffusion and there is no net flow of cosmic ray flux into or out of the solar system. On a day to day basis, the fluctuations in the interplanetary parameters such as solar wind properties and the I.M.F. must necessarily cause an imbalance between convection and diffusion through the introduction of varying density gradients resulting in abnormal amplitudes for diurnal variation. The enhanced field aligned inward diffusion at high energies caused simply by the establishment of a significant positive density gradient, can result from either or both the

processes, namely (a) through the establishment of regions of decreased density (Sink) in the garden-hose direction (b) through the establishment of regions of enhanced density (Source) in the anti-garden-hose direction, the physical processes responsible for the two mechanism being possibly different.

In order to prove the validity of the above concept on an experimental basis, we have resolved the observed cosmic ray average diurnal variation (δ) into two vectors, the convection vector along the 1200 hour direction (δ_c) which can be easily calculated from a knowledge of the solar wind velocity (V), and the diffusive vector (δ_d). The relationship can be expressed as

$$\delta = \delta_c + \delta_d \qquad \qquad .. \ 4.6$$

The amplitude of δ_c is $\approx 0.6\%$ when determined according to the relation 4.5, where C = 1.5 for V = 400 Km/Sec and for neutron monitors with mean rigidity of response $\geqslant 10$ GV. However, in all our treatment we shall deal only with a constant $\delta_c = 0.4\%$, which is equivalent to an amplitude of the diurnal anisotropy in space equal to 0.4% (using the correction factors of McCracken et al., 1965), since correction as suggested by Subramanian (1971 a) will only increase the true amplitude by a constant factor/and will not change any of our conclusions. The residual diffusion vector (δ_d) has been compared with the I.M.F. direction to verify the field aligned nature of the diffusion vector. The analysis has been performed to investi-

gate the field aligned nature of the diurnal variation both on an average basis as well as on a day to day basis, and in particular, for trains of days with enhanced diurnal variation.** For this purpose, the mean diurnal anisotropy vector ($\bar{\delta}$) has been obtained by using diurnal anisotropy vector of all those stations (from the list given in Table 4.1), which possess (a) cut-off-rigidity $\lesssim 2$ GV, (b) narrow asymptotic cone of acceptance and (c) essentially scan the equatorial region of the sky. For deriving the energy spectrum of the enhanced diurnal wave trains, however, all the stations listed in Table 4.1 are used.

Based on this model the necessary radial density gradients both on an average basis as well as on days associated with enhanced diurnal variation required to provide the observed field aligned diffusion have been calculated. The observations indicate that, at early times during trains of days having enhanced diurnal variation, the enhanced density gradient is caused by a sink in the garden-hose direction, which at late times ($\gtrsim 4$-5 days) changes to a source along the anti-garden-hose direction. The later change over to a source, is

_____

** Some of the concepts presented here have been independently verified by Hashim et al (1972), using selected data of days having enhanced diurnal variation. The present analysis, however is more comprehensive in that it also leads to definitive conclusions regarding the characteristics of sources and sinks in the interplanetary medium.

phenomenologically similar to the establishment of the positive

density gradient producing an easterly anisotropy at very late

times in the decay of low energy solar flare events.

4.42 Quiet day diurnal variation:

(a) 27 day average basis

The average diurnal anisotropy parameters (equation 4.6)

for each of the 27-day solar rotation periods, and the average

interplanetary magnetic field parameters for each of these

rotations during 1967-1968 (using the hourly values of the

interplanetary magnetic field measured by Explorer 33 or 35)

have been calculated separately, and are listed in Table 4.7.

Excepting the days on which Forbush decrease occur, all the

remaining days when concurrent I.M.F. data are available have

been utilised for this analysis. The phase difference, computed

between the diffusive vector and the magnetic field vector

$(\phi_d - \phi_B)$ for each rotation (Table 4.7), is shown by the

histogram in Figure 4.19. The figure clearly shows that in

nearly 80% of cases, the phase difference between the diffusive

vector and the I.M.F. vector on a 27 day average basis is $\leqslant 10^{o}$,

which is of the same order as the standard error of the obser-

vations thus indicating that the average quiet day diffusive

vector is field aligned.

The diffusive vector ($\underset{\sim}{S}_d$) can be resolved into two

components, one parallel to $\underline{B}$ vector and another perpendi -

cular to it, the amplitude of the perpendicular

TABLE 4.7 - The 27 day average cosmic ray diurnal vector, cosmic ray diffusive vector (see text) and interplanetary field vector for different solar rotations during 1967-1968. The computed phase difference between the diffusive vector and the field vector is also listed.

SOLAR ROTA-TION NO.	NO. OF DAYS USED	MEAN DIURNAL ANISOTROPY VECTOR (ξ) AMP (%)	PHASE ϕ(Deg)	MEAN DIFFUSION* VECTOR (ξ_d) AMP (%)	PHASE ϕ_d(Deg)	MEAN MAGNETIC FIELD VECTOR AMP (Gamma)	PHASE ϕ_B(Deg)	PHASE DIFF. $\phi_d - \phi_B$ (Deg)
1826	15	.43 $\pm$ .06	255 $\pm$ 7	.51	305	3.2	306	- 1 $\pm$ 7
1827	20	.63 $\pm$ .02	270 $\pm$ 5	.74	303	3.9	308	- 5 $\pm$ 5
1828	19	.30 $\pm$ .05	279 $\pm$ 5	.54	326	3.5	307	19 $\pm$ 5
1829	16	.81 $\pm$ .07	288 $\pm$ 6	1.00	310	2.9	321	-11 $\pm$ 6
1830	10	.51 $\pm$ .07	263 $\pm$ 5	.61	304	3.2	324	-20 $\pm$ 5
1833	13	.20 $\pm$ .06	266 $\pm$ 8	.45	333	3.3	325	8 $\pm$ 8
1834	16	.20 $\pm$ .03	239 $\pm$ 10	.34	330	3.5	321	9 $\pm$ 10
1835	21	.45 $\pm$ .07	254 $\pm$ 9	.51	303	3.7	308	- 5 $\pm$ 9
1836	19	.34 $\pm$ .02	274 $\pm$ 5	.54	321	3.7	312	9 $\pm$ 5
1837	16	.26 $\pm$ .06	313 $\pm$ 4	.60	342	3.6	312	30 $\pm$ 4
1838	24	.39 $\pm$ .04	270 $\pm$ 2	.56	315	4.2	311	4 $\pm$ 2
1839	20	.52 $\pm$ .07	263 $\pm$ 10	.62	303	4.1	301	2 $\pm$ 10
1840	17	.33 $\pm$ .05	274 $\pm$ 10	.53	322	3.7	312	10 $\pm$ 10
1841	13	.42 $\pm$ .06	267 $\pm$ 5	.56	312	4.2	309	3 $\pm$ 5
1842	19	.52 $\pm$ .09	268 $\pm$ 10	.65	306	3.5	314	- 8 $\pm$ 10

Contd...

1843	22	.64 ± .05	281 ± 6	.82	310	3.6	316	− 6 ± 6
1844	21	.49 ± .05	273 ± 8	.64	311	3.8	320	− 9 ± 8
1845	19	.35 ± .02	264 ± 8	.50	317	3.3	313	4 ± 8
1846	16	.40 ± .06	235 ± 10	.36	299	3.1	312	−13 ± 10
1847	17	.36 ± .02	278 ± 9	.57	322	3.4	313	9 ± 9
1848	16	.47 ± .05	267 ± 4	.60	309	4.0	304	5 ± 4
1849	18	.30 ± .07	268 ± 11	.49	322	3.0	318	4 ± 11
1850	18	.46 ± .05	280 ± 6	.66	317	3.9	312	5 ± 6
1851	13	.42 ± .04	294 ± 6	.69	326	4.1	321	5 ± 6
1852	23	.33 ± .03	250 ± 11	.42	313	3.6	311	2 ± 11

* The errors in the mean diffusive vector are of the same order as the errors in mean anisotropy vector.

component being a measure of the non-field aligned component.
Figure 4.20 shows the plot of parallel and perpendicular
components of the average diffusive vectors for different solar
rotations. It is evident from the figure that the parallel
component dominates and the perpendicular component is usually
less than a tenth of the parallel component, again indicating
that the average quiet day diffusive vector is field aligned.

(b) Annual average basis:

Resolving the observed yearly mean diurnal vector into
diffusive and convective vectors (using equation 4.6), the
annual mean diffusive vector ($\overset{\frown}{\underset{\sim}{D}}_d$) for each year during the
period 1964-1970 has been calculated. The yearly average I.M.F.
direction has been derived from the observed yearly average
solar wind velocity (Gosling et al., 1971), and assuming
Archimedean spiral structure for the field. Comparison of the
field azimuths for the period 1967-1968 computed from solar wind
observations with actual I.M.F. observations show that these
agree within 2-3°. Table 4.8 lists the yearly average diurnal
variation parameters along with the computed phase difference
between the average diffusive vector and the corresponding
field vector. The average diffusive vectors for each year
during 1964-1970, are also resolved parallel and perpendicular
to field direction and are plotted in Figure 4.20, along with
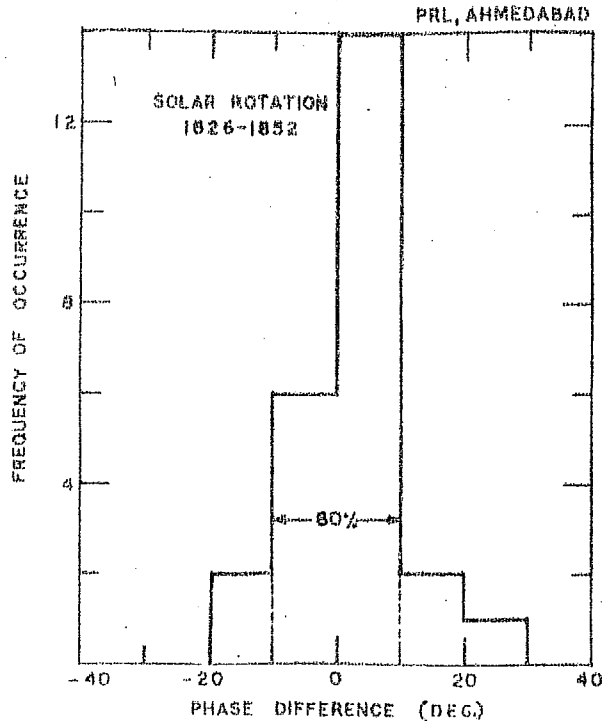the mean value for the entire period 1964 to 1970.

PRL, AHMEDABAD

Fig. 4.19 - Histogram showing the distribution of the phase difference between the average cosmic ray diffusive vector and the average magnetic field vector ($\phi_d - \phi_B$) for a number of solar rotations 1826-1852.
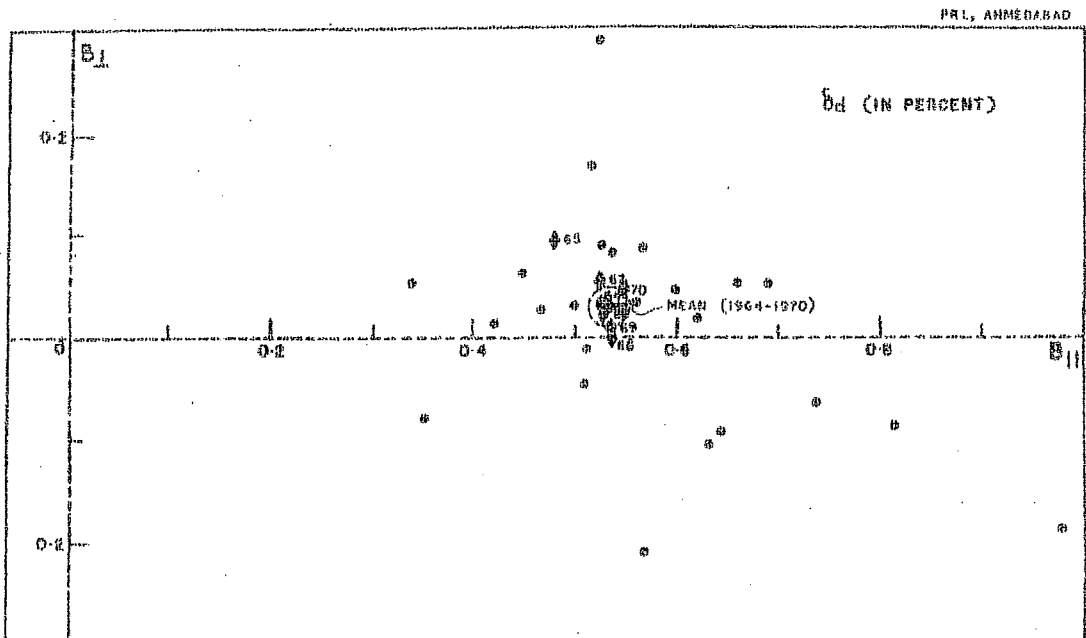
Fig. 4.20 - Showing the two components of the average diffusive vector, one parallel and the other perpendicular to the average I.M.F. vector for different solar rotations (1826-1852), during January 1967 - December 1968. The two components of the annual mean diffusive vector for the entire period during 1964-1970 are also shown in the figure.

TABLE 4.8 - Showing the phase difference between the yearly cosmic ray diffusive vector and the mean field vector. The field azimuth has been calculated from solar wind velocity assuming Archimedean spiral configuration. The cosmic ray diffusive vector is computed from the observed average diurnal vector using equation (4.6)

| YEAR | MEAN DIURNAL ANISOTROPY VECTOR (ξ) | | MEAN DIFFUSION VECTOR (ξ_d) | | MEAN SOLAR WIND VELOCITY (KM/Sec) | MEAN MAGNETIC FIELD DIRECTION ϕ_B (Deg) | PHASE DIFF. $\phi_d - \phi_B$ (Deg) |
	AMP (%)	PHASE ϕ (Deg)	AMP (%)	PHASE ϕ_d (Deg)			
1964	.35 ± .03	272 ± 3	.53	321	431	317	4 ± 3
1965	.28 ± .02	270 ± 4	.49	326	407	315	11 ± 4
1966	.36 ± .02	271 ± 3	.53	319	413	316	3 ± 3
1967	.35 ± .01	272 ± 5	.53	321	394	315	6 ± 5
1968	.37 ± .01	270 ± 3	.54	318	453	318	0 ± 3
1969	.36 ± .01	270 ± 2	.54	318	422	317	1 ± 2
1970	.37 ± .02	271 ± 2	.55	319	390	314	5 ± 2
Mean (1964-1970)	.35 ± .01	271 ± 2	.53	320	418	317	3 ± 2

The yearly mean diffusive vector for the entire period has an amplitude of $0.53 \pm 0.01\%$ and makes an angle of $3^\circ \pm 2^\circ$ with the I.M.F. vector (Table 4.8), the phase difference being of the same order as the observational error. In other words Figure-4.20 clearly indicates that within the observational errors, the yearly average diurnal variation is completely explainable in terms of summation of a normal convective vector and a field aligned diffusive vector, except during 1965, when the diffusive vector makes an angle of 11° with the I.M.F. direction.

Even though we deduce that the diffusive vectors obtained on 27 day and annual average basis are essentially field aligned, indicating no perpendicular diffusion, consistent with the low energy observations, there are occasions both on an average basis as well as on individual days, when it can be significant and which might result in a partial or complete cancellation of the diurnal anisotropy. The slight reduction in the observed average amplitude of diurnal variation in 1965 ($\phi_d - \phi_B = 11^\circ$) can be attributed to the increased value of $K_\perp$ during 1965 being $\sim 0.19 \pm 0.04$, almost a factor of 3 to 4 greater than the value observed during other periods.

4.43 Characteristics of days having enhanced diurnal variation

During the period 1966-1968, about 10 wave trains having enhanced diurnal amplitudes occurred. Out of these we have selected four prominent enhanced diurnal wave trains (shown in

Figure 4.21), which are not accompanied by any large changes in daily mean intensity. This is to ensure that the diurnal aniso-tropy vectors derived are free from effects due to universal time variations. Using the method of Rao et al. (1963) and described in Sec 3.41, the best fit rigidity spectral exponent (β) of diurnal anisotropy for each of the event (Table 4.9) has also been obtained. The results in each case are consistent with their being rigidity independent ($\beta = 0.0 \pm 0.2$). The enhanced diurnal anisotropy amplitude and phase in space, for each day and for each of the four events has been computed using data from a large number of neutron monitoring stations. Table 4.9 lists the average value of anisotropy for each event. It is observed that the diurnal anisotropy during these events shows a time of maximum at about 2000 hours, in contrast with the 1800 hour maximum observed for corotational anisotropy. The phase shift to later hours have also been reported by Tolba and Lindgren (1971) for days associated with the enhanced diurnal variation.

In order to establish the field aligned nature of the diffusive flow, we again resolve the observed diurnal vector ($\underset{\sim}{\delta}$) on each day into two components $\underset{\sim}{\delta}_c$ and $\underset{\sim}{\delta}_d$ (equation 4.6). Taking $\underset{\sim}{\delta}_c = 0.4\%$, with the same arguments as given earlier, we have calculated the magnitude and direction of the diffusive vector ($\underset{\sim}{\delta}_d$) for each day and for each of the events. Similar-ly the magnitude and direction of the I.M.F. vector for each day has also been calculated from the direct spacecraft obser-
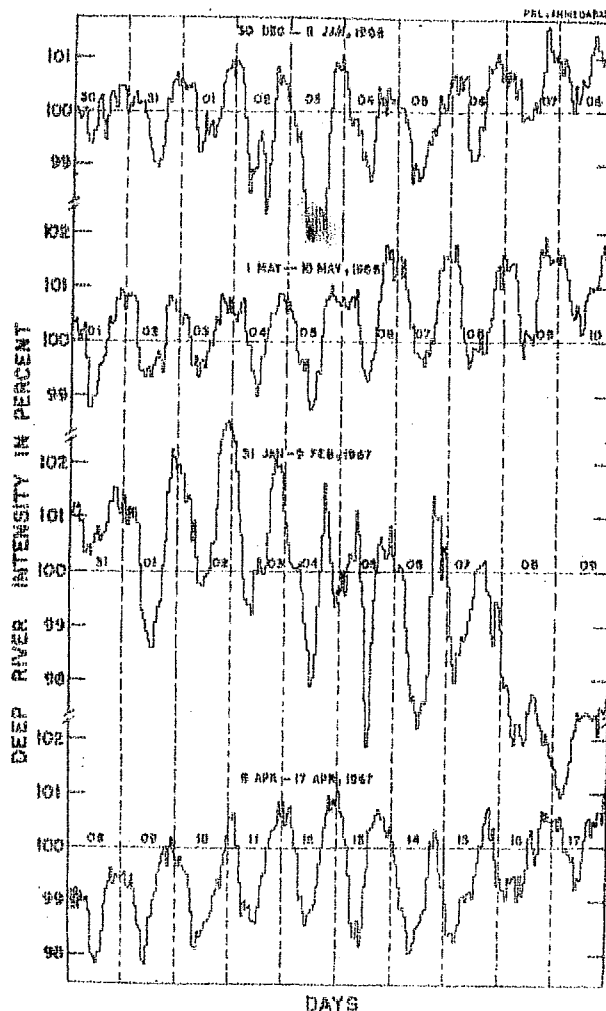
Fig. 4.21 - Showing typical enhanced diurnal wave trains, not associated with any large change in daily mean intensity, as observed by the Deep River neutron monitor.

vations (Pioneer 6, Explorer 33 or 35). In Figure 4.22, the diffusive flow vectors for each day is plotted end to end separately for each of the four events along with the I.M.F. vector to demonstrate the field aligned nature of the diffusive flow even on a day to day basis.

The mean diffusive vector and the corresponding mean I.M.F. vector are plotted for each of the four events in Figure 4.23

TABLE 4.9 — Mean diurnal anisotropy vector, mean diffusive vector and the mean interplanetary magnetic field vector during the selected enhanced diurnal variation events. The best fit spectral exponent (β) is also indicated for each event.

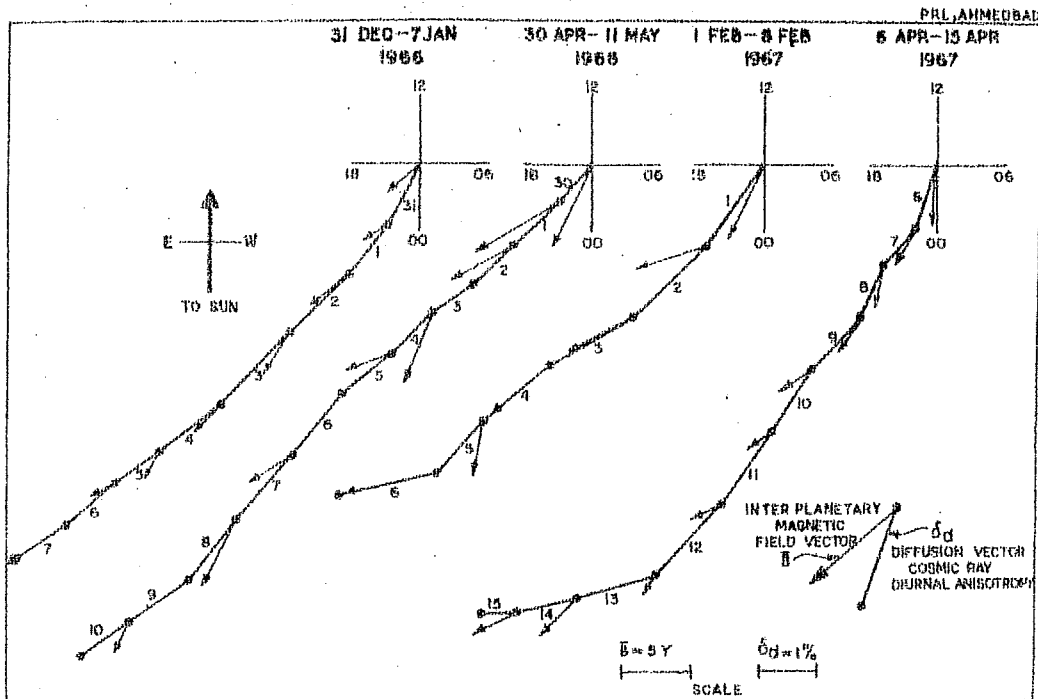| EVENTS	β	MEAN DIURNAL ANISOTROPY VECTOR(δ)		MEAN DIFFUSION VECTOR (δ_d)		MEAN MAGNETIC FIELD VECTOR		PHASE DIFF. $\phi_d - \phi_B$ (Deg)
		AMP (%)	PHASE ϕ (Deg)	AMP (%)	PHASE ϕ_d (Deg)	AMP (Gamma)	PHASE ϕ_B (Deg)	
31 DEC— 7 JAN, 1966	0.0	1.02+.12	298+ 5	1.26	314	3.0	314	0 ± 5
30 APR—11 MAY, 1966	0.0	0.91+.08	301+ 6	1.17	318	5.1	315	3 ± 6
1 FEB— 8 FEB, 1967	0.4	1.10+.10	289+ 7	1.29	306	4.9	308	-2 ± 7
6 APR—15 APR, 1967	-0.2	0.92+.07	299+ 4	1.17	316	2.8	322	-6 ± 4

Fig. 4.22 - Showing the cosmic ray anisotropy diffusion vector for each day plotted end to end for each of the four enhanced diurnal variation events. The I.M.F. vector for each day is also plotted along side the diffusive vector for each day. Note the good agreement between the field azimuth and the direction of the diffusive vector confirming the field aligned nature of the diffusive vector.
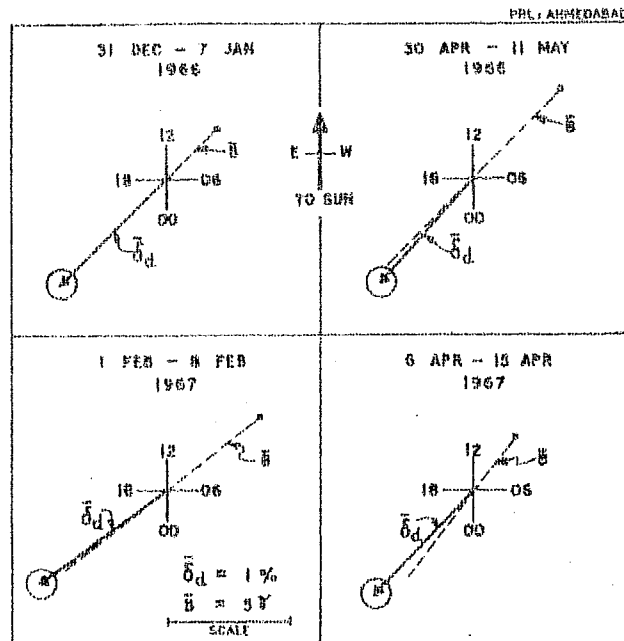

Fig. 4.23 - Showing that the average diffusive anisotropy vector for each event is aligned parallel or anti-parallel to the average I.M.F. vector during the events exhibiting enhanced diurnal variation.

and are given in Table 4.9. Both Figures 4.22 and 4.23 clearly demonstrate that enhanced diurnal variation is caused by a superposition of the enhanced field aligned diffusion current over the normal convective flow.

The observational results presented so far, both on an average basis as well as on days with enhanced diurnal variation, therefore suggests very strongly that the diffusive vector of the cosmic ray diurnal anisotropy, at most times is field aligned, and hence the diurnal variation is understandable simply in terms of radial convection and field aligned diffusion. In addition to the analysis presented here, we have also examined in great detail the diurnal variation on a day to day basis, where we observe that during 1967-1968 on more than 80% of the days, the diffusive vector is essentially field aligned and $K_{\perp}$ is negligible even on a day to day basis. The details of the result of the day to day analysis, however, are not included in the thesis, and are being presented elsewhere.

4.44 Unified convection - diffusion model

Figure 4.24 presents the new unified model to explain the anisotropy observations both at low and high energies. Figure 4.24a, explains the low energy cosmic ray anisotropy at different times during a solar flare. At early times in a flare event, the diffusive current driven by a negative cosmic ray density gradient due to solar produced particles dominates
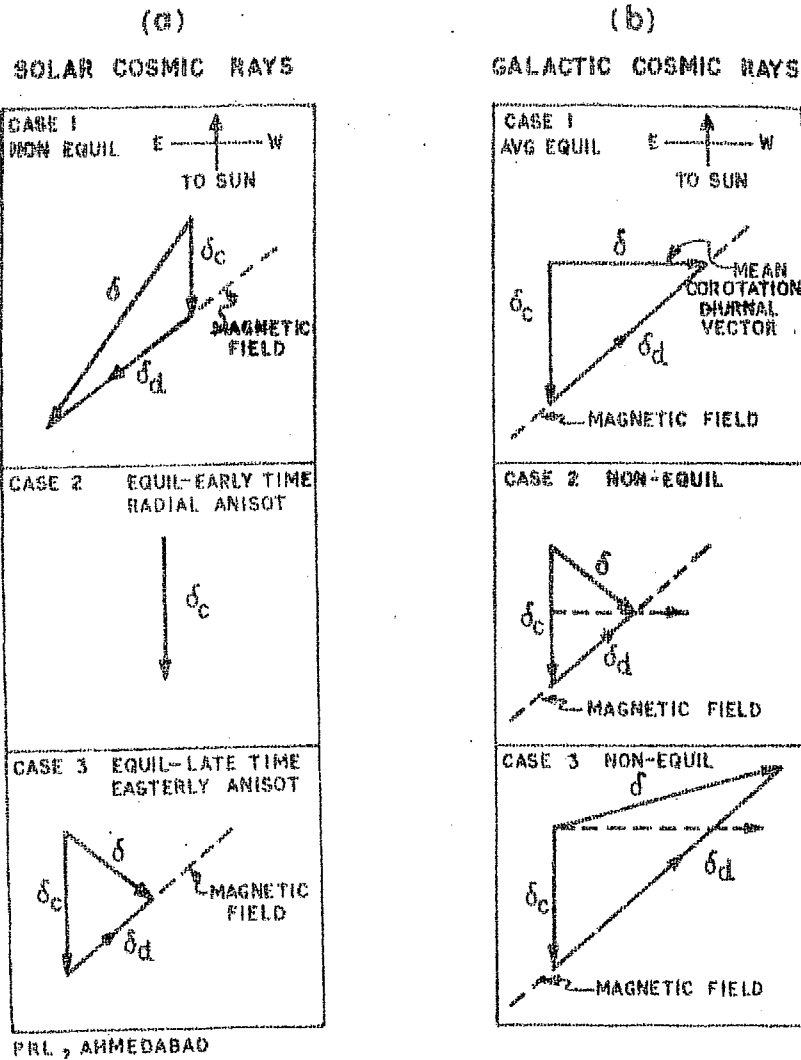
Fig. 4.24 - A unified model for explaining the anisotropy of low energy cosmic ray flare particles and also the diurnal anisotropy of high energy particles in terms of simple convection and field aligned diffusion (see text for explanation).

over the convective vector resulting in a predominantly field aligned anisotropic flux. During late times, the solar cosmic ray flow is in equilibrium and is consistent with it being simply convected out by the solar wind. At very late times, the positive density gradient created by the earlier convection provides a reverse diffusive current, which when superimposed

upon the convective vector results in an easterly anisotropy.
The model embodying the extension of these ideas to the galact-
ic anisotropy, is depicted in Figure 4.24b. Under equilibrium
condition, when there is no net flow of cosmic radiation either
into or from the solar system the radial convection current
$S_c = CU\underset{\sim}{V}$ is exactly balanced by the radial component of inward
diffusion $K_{\parallel} \left(\frac{\partial U}{\partial r}\right)_{\parallel}$ resulting in an average corotational aniso-
tropy of 0.4% along the 1800 hour direction. On a day to day
basis, the diffusion vector need not exactly balance the conve-
ctive vector. In the case when the diffusion vector is smaller,
the resulting observed anisotropy would show a maximum earlier
to 1800 hours and in the case of enhanced diurnal variation
when the diffusive vector is very much greater than the conve-
ctive vector, the time of maximum of the resulting diurnal
variation will shift towards 2100 hours, the mean direction of
the I.M.F. The diffusive vector, in all cases, is aligned
parallel or anti-parallel to the magnetic field.

The diffusion current (Gleeson, 1969; Forman and Gleeson,
1970) can be written

$$S_d = K_{\parallel} \left(\frac{\partial U}{\partial r}\right)_{\parallel} + K_{\perp} \left(\frac{\partial U}{\partial r}\right)_{\perp} \qquad .. \ 4.7$$

and since the average corotational anisotropy is obtained by
assuming the radial current $S_r = 0$ and $K_{\perp}$ to be negligible,
we may use this together with

$$\underset{\sim}{\xi}_d = 3S_d / VU \qquad .. \ 4.8$$

and the observed free space anisotropy, to calculate the

density gradient along the magnetic field $\frac{1}{U}\left|\frac{\partial U}{\partial r}\right|_{\parallel}$ from which

the radial density gradient (G) can be obtained.

$$G = \frac{1}{U}\left|\frac{\partial U}{\partial r}\right|_{\parallel} / \cos\psi \qquad\qquad .. \ 4.9$$

where ψ is the angle between the magnetic field and the radial

direction.

4.45 Radial density gradient of cosmic ray intensity

We have already shown that on an yearly or 27 day average

basis, the cosmic ray diurnal anisotropy is consistent with the

above theory with the average diffusive anisotropy vector having

a magnitude of 0.53 $\pm$ 0.01% which, in free-space corresponds to

0.8%. Using equation 4.7 to 4.9, we can calculate the radial

density gradient necessary to produce the diffusion vector, on

an average basis, provided the value of $K_{\parallel}$ is known. From the

observed I.M.F. power spectra, Jokipii and Coleman (1968) and

Bercovitch (1971 a) have shown that $K_{\parallel} \approx 5 \times 10^{21}. \ P.\beta \ cm^2. \ Sec^{-1}$

(P = rigidity, β = v/c). Using this value of $K_{\parallel}$, we find that

the average diffusive vector necessary to explain the observed

diurnal anisotropy requires a radial density gradient of

$\approx 4.5\%/AU$.

A number of both direct and indirect radial density

gradient (G) measurements, of the galactic cosmic ray flux,

have been made during the last ten years (Rao, 1972; O'Gallagher,

1972). The value of G $\approx$ 4.5%/AU obtained from the neutron

monitor anisotropy observations being essentially an integral

measurement (particle energy $\gtrsim$ 1 GeV), we have, for the purpose
of comparison, listed the values of G for particle energies
$\gtrsim$ 300 MeV in Table 4.10. Inspite of the dispersion existing
between different values, we can conclude that the radial density
gradient at relativistic energies is of the order of 4-5%/AU,
which is quite consistent with our values derived from quiet day
anisotropy measurements. Further, we believe that both the
radial density gradient values which show a large departure from
all other estimates (Table 4.10, Nos 8-9), being derived indire-
ctly from meteorite studies are not dependable.

The observed enhanced diurnal variation which is consis-
tent with a field aligned diffusive vector of 1.2 $\pm$ 0.1%,
requires an enhanced positive radial density gradient of $\approx$10%/AU.
From the results presented above, we believe that reliable
estimates of G, even on short term basis, can be inferred from
anisotropy measurements. Since by comparing the diffusive
vector with I.M.F. vector one can unambiguously show the absence
of transverse currents, the estimates derived from anisotropy
measurements can be taken to be accurate. We wish to point out,
that even the direct spacecraft measurements suffer from uncer-
tainties due to the difficulties in applying corrections for
proper normalisation and azimuthal gradients. Therefore, till
better detectors are available, the anisotropy measurements
are the most reliable observations to derive density gradients
at relativistic energies.

TABLE 4.10 - Observed heliocentric radial density gradient (Integral measurements) for galactic cosmic ray particles of energy ≥300 MeV, during various epochs

Sl No	Year	Spacecraft or method	Threshold kinetic energy of protons	Type of detector	Reference detector	Radial range(AU) r_{min}	r_{max}	Radial Gradient G %/AU	Reference
1	1965	Mariner-4	1.5 GeV	dE/dX range Telescope	Neutron monitor	1.0	1.57	9±1.5	O'Gallagher and Simpson(1967)
2	1965	Mariner-4	430 MeV	GM Counter	Neutron Monitor	1.0	1.57	< 3	Krimigis (1968)
3	1965	Neutron Monitor	1 GeV	N.A.	N.A	N.A	N.A	2±0.7	Bercovitch (1970)
4	1967-1968	Neutron Monitor	1 GeV	N.A	N.A	N.A	N.A	9±2.3	Bercovitch (1971 b)
5	1968	Pioneer-8	2 GeV	Multiple element Telescope	Neutron monitor	1.0	1.12	-1.5+6	Lezniak and Webber(1970)
6	1964-1970	Neutron monitor, average anisotropy	1 GeV	N.A	N.A	N.A	N.A	4.5	Present work
7	1967-1968	Neutron monitor, Enhanced anisotropy	1 GeV	N.A	N.A	N.A	N.A	10.0	Present work
8	1968	Alondroal meteorite	400 MeV	N.A	N.A	1.0	4.0	>15	Fireman and Geobel(1970)
9	1969	Lost city meteorite	1 GeV	N.A	N.A	1.0	2.6	60±15	Forman et al (1971)

4.46   Enhanced diurnal variation and location of 'sources'
        and 'sinks'

The enhanced radial density gradient $(G \approx 10\%/AU)$ during trains of days with enhanced diurnal variation can be caused either due to a 'sink' in the garden-hose direction or due to a 'source' of cosmic ray particles in the anti-garden-hose direction. Harmonic analysis of the data for both these types of mechanisms will yield essentially similar results (time of maximum ~ 21 hour), and therefore will not be able to identify the nature of particle distribution during such periods. To understand the detailed particle distribution in space, and to identify sources and sinks, three dimensional space-time diagrams (sec. 3.5) have been used by a number of workers (Fenton et al., 1959; Ables et al., 1967; Mercer and Wilson, 1968; Carmichael and Steljes, 1969). Such diagrams have been prepared for a number of interesting events, in particular for the four events studied above. Due to inadequate coverage of longitudes by the existing neutron monitoring stations, we have plotted the intensity in only eight directions in space for any given time, each directional belt covering a width of three hours in longitude.

Figure 4.25 shows the average intensity profile as a function of direction for the entire period 2 to 6 January 1966, derived from the detailed time intensity map for the event which occurred during the period 30 December 1965 - 07 January 1966. The intensity in each direction has been obtained by averaging the intensity for each 3-hourly interval during this
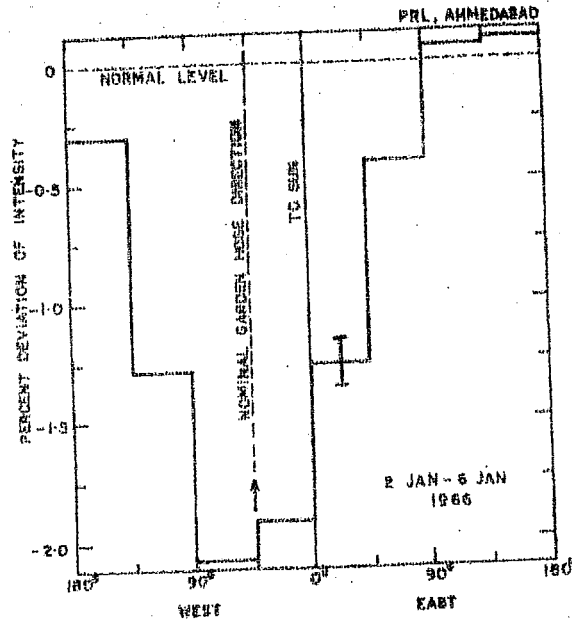
Fig. 4.25 - Mean cosmic ray intensity as a function of direction in space during 2-6 January 1966 (a corotating Forbush decrease event), when enhanced diurnal variation due to a predominent garden-hose depression was observed by neutron monitoring stations.
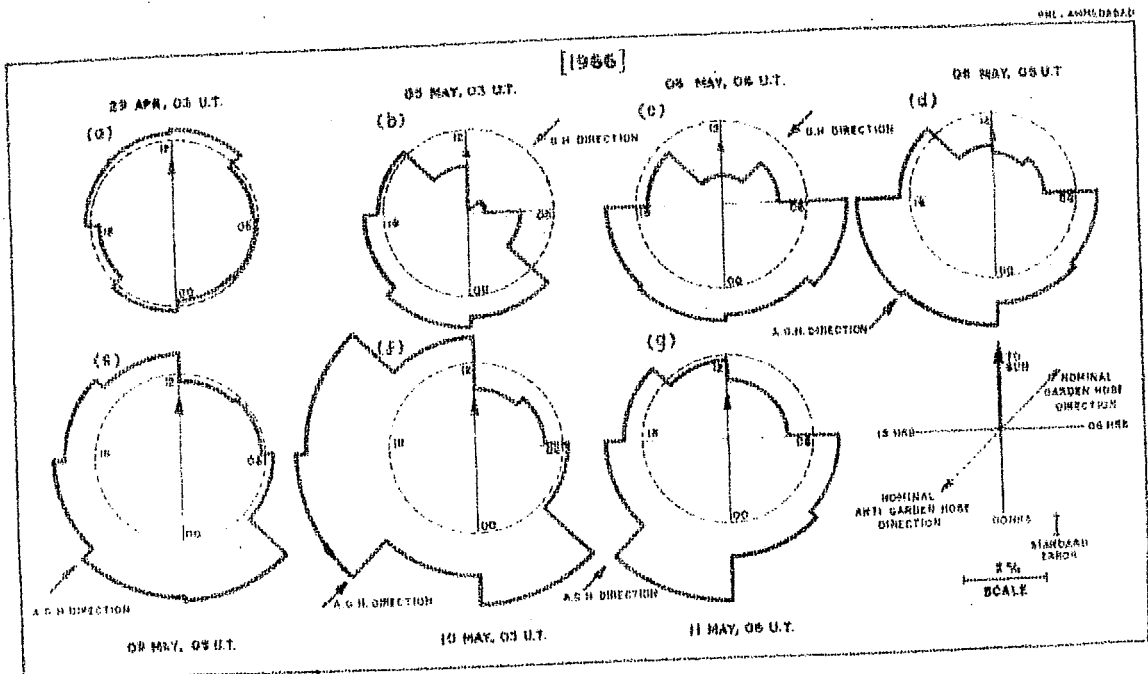

Fig. 4.26 - Showing the evolution of anisotropy during the enhanced diurnal variation event of 30 April - 11 May 1966. Note that during the early part of the event, the cosmic ray intensity is depressed along the garden-hose direction and during late in the event the cosmic ray flux in the garden-hose recovers to the normal value (shown by thin circle), where as the flux in the anti-garden-hose direction shows a large excess.

period. The figure very clearly shows a very significant depression below the normal along the garden-hose direction. The above event is typical of all the events particularly the short lived ones ($\leqslant$ 4-6 days), and shows clearly that the enhanced diurnal variation is caused by a sink in the garden-hose direction. Similar conclusion was arrived at by Mathews et al (1969) and Hashim and Thambyahpillai (1969), from an analysis of a number of events. It is interesting to note that this event coincides with the corotating Forbush decrease event observed at low energies ($\sim$ 10 MeV) by McCracken et al (1966 b), which lends further support to their conclusion that such corotating Forbush decreases observed at low energies often manifest themselves as enhanced diurnal variation at relativistic energies observed by ground based monitors.

In contrast to the above simple picture the long lived enhanced diurnal variation event of 30 April - 11 May 1966 shows a complex behaviour. Figure 4.26 shows the evolution of the cosmic ray flux distribution in space at various times during 30 April - 11 May 1966. On April 29, 1966, prior to the commencement of the enhanced wave train, the cosmic ray flux distribution in space was found to be practically isotropic (Figure 4.26a) showing a normal diurnal variation. During the early part of the enhanced diurnal variation event i.e. 1-7 May 1966, the cosmic ray intensity in the garden-hose direction is found to be well depressed below the normal level (Figure 4.26 b,c).

By 9 May 1966, the cosmic ray flux along the garden-hose direction seems to be just recovering to its normal value(Figure 4.26 e). However, the cosmic ray intensity in the anti-garden-hose direction is now found to show a large excess above the normal intensity (Figure 4.26 f, g). Thus during the later part of the event i.e. 8-11 May 1966, the enhanced diurnal amplitude seems to be caused by a source in the anti-garden-hose direction. Such a behaviour is expected in terms of the explanation offered by McCracken et al (1971) and Rao et al (1971) for the observed easterly anisotropy during late in the decay of low energy solar flare events. Using similar arguments, we can expect the enhanced convection by the high velocity solar wind associated with the initial shock wave which initially causes depressed intensity along the garden-hose-direction, to eventually establish a positive density gradient and thus a source along the anti-garden-hose direction during late in the event.

Referring to Figure 4.26 the change over from a sink in the garden-hose direction to a source in the anti-garden-hose direction occurs in a period of 4-5 days suggesting that the relaxation time of the interplanetary medium to follow the changes in the density gradient in the interplanetary modulating region is of the order of 4-5 days. Considering the magnitude of the solar wind velocity observed during such periods, this would indicate that the dimension of the modulating region is of the order of 2-3 AU, thus providing an independent experimental evidence for the location of a boundary, sometimes

assumed in dealing with the cosmic ray transport.

4.47 Low amplitude diurnal anisotropy

Recalling our previous arguments we note that even on a day to day basis on more than 80% of the days the diurnal vector can be considered as simple summation of convection and diffusion vector and that on such days $K_\perp$ is negligible. However on $\leqslant$ 20% of the days $K_\perp$ seems to be significant, often resulting in partial or complete cancellation of diurnal anisotropy. Even on an average basis, we note that in the year 1965, the amplitude reduction is explainable in terms of finite $K_\perp$, $K_\perp/K_{\parallel}$ being $\sim$ 0.19 $\pm$ 0.04. From an examination of diurnal variation on a day to day basis, it is found that very often trains of days of low amplitude diurnal variation occur. A catalogue of such low amplitude wave trains and their average diurnal anisotropy characteristics are listed in Table 4.11. A few typical low amplitude diurnal wave trains as observed at Deep River neutron monitoring station are also shown in Figure 4.27. For at least two of these events, which occurred during the period 27 August - 1 September 1967, and 27 July to 1 August 1968, concurrent I.M.F. data are available.

For both these events, the average diurnal amplitude is about 0.15%. Resolving as before the diurnal vector into diffusion ($\underset{\sim}{S}_d$) and convection ($\underset{\sim}{S}_c$) vector, and comparing the phase of the diffusion vector with that of the I.M.F. vector,

TABLE 4.11 - The characteristics of the daily variation derived from Deep River neutron data for a number of wave trains, with low diurnal amplitude.

| Sr. No. | EVENTS | Average Daily Variation (In space) | | | | Associated change in daily mean intensity | |
| | | I Harmonic | | II Harmonic | | | |
		Amp. (%)	Phase (Hrs.)	Amp. (%)	Phase (Hrs.)	Incr- eases	Decre- ases
1	26 Mar-31 Mar 1965	0.14**	20.1	0.09	3.5	No	No
2	8 Apr-14 Apr 1965	0.11	17.7	0.05	5.7	No	No
3	12 Sep-17 Sep 1965	0.04	13.5	0.11	2.2	No	No
4	9 Oct-14 Oct 1965	0.13	14.6	0.11	6.2	Yes	No
5	5 Feb-10 Feb 1966	0.03	13.5	0.05	1.7	No	No
6	12 Jun-16 Jun 1967	0.05	3.0	0.14	3.2	No	No
7	27 Aug- 1 Sep 1967	0.12	14.1	0.06	4.9	No	No
8	27 Jul- 1 Aug 1968	0.16	18.2	0.10	2.3	No	No
9	8 Aug-13 Aug 1968	0.08	19.1	0.06	5.3	Yes	No
10	14 Apr-20 Apr 1969	0.18	19.1	0.09	4.5	Yes	No

** Statistical error for daily harmonics $\sim 0.02\%$

we observe that $(\phi_d - \phi_B)$ is $\approx 30° \pm 8°$. This clearly indicates that during days of low amplitude wave trains, in addition to the normal convection and diffusion vector, there exists transverse diffusion. From the observed $(\phi_d - \phi_B)$ we find that $K_\perp/K_{||}$ is $\approx 0.5 \pm 0.2 \left[\tan(\phi_d - \phi_B)\right]$, which exceeds greatly the value of ≈ 0.05 observed during normal days. The increase in $K_\perp$ can probably be explained due to unusually large random walk by field lines.
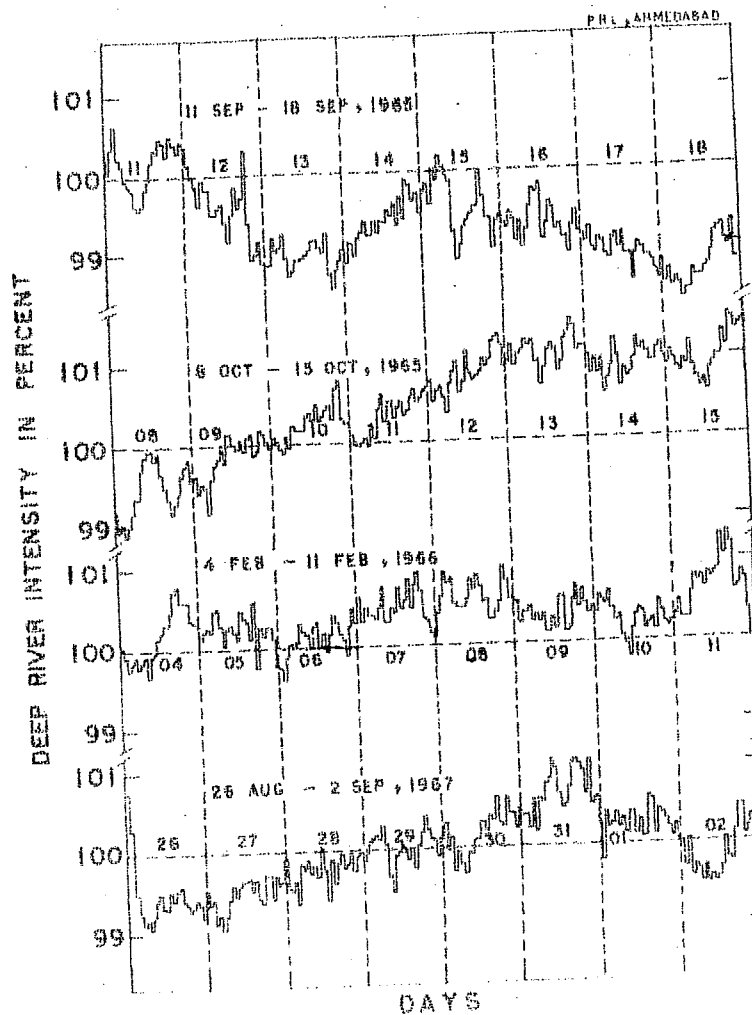
Fig. 4.27 - Typical examples showing the cosmic ray intensity at Deep River during abnormally low diurnal amplitude days.

The low amplitude observed during such days makes it difficult to perform a detailed analysis and study their different aspects of solar-terrestrial relationship associated with these events. Further understanding of the mechanism responsible for low diurnal variation can probably be accomplished if detailed I.M.F. data, in particular, the variance in the hourly values of B_z component is known. Such analysis is in progress and will be reported separately.

C H A P T E R - V

SEMI-DIURNAL ANISOTROPY CHARACTERISTICS

Even though the presence of a significant semi-diurnal component in the anisotropy of cosmic radiation has been suggested almost two decades ago (Elliot and Dolbear, 1950, 1951; Sarabhai and Nerurkar, 1956), the poor statistics and the observed low amplitude of the semi-diurnal variation had given rise to serious doubt about its existence. Subsequently Katzman and Venkatesan (1960) showed that the observed semi-diurnal variation in the neutron component of cosmic radiation, could be almost completely explained as due to the contribution from the semi-diurnal variation in pressure, except at equatorial latitudes. Since for a normal type of anisotropy having a negative or zero exponent one expects a smaller amplitude at equatorial stations, due to larger width of their asymptotic cone of acceptance, the observed higher amplitude at equatorial stations could not be explained.

The first positive confirmation for the existence of semi-diurnal anisotropy was provided by Rao and Sarabhai (1961), by using the crossed meson telescope. From a comparison of the observed variation in the east and west pointing telescope inclined at the same angle to zenith, where the atmospheric contribution to the observed daily variation can be cancelled to a first approximation (Elliot and Rothwell, 1956), the existence of the semi-diurnal component was strongly indicated.

With the availability of the data from super neutron monitors having high statistical significance and by using improved numerical filter techniques to obtain better signal to noise ratio, Ables et al. (1965) conclusively showed the existence of semi-diurnal component of world wide nature having a time of maximum aligned perpendicular to the interplanetary magnetic field direction. The authors, using power spectrum analysis technique clearly demonstrated the presence of a significant peak at two cycles/day. The analysis by Ables et al. (1965), Patel et al. (1968) and Lietti and Quenby (1968) have also indicated that the semi-diurnal component has a positive exponent, thus explaining its enhanced presence at equatorial latitudes.

With the availability of a large amount of data from various super neutron monitors including the data from equatorial super neutron monitors such as Ahmedabad, in the last 4-5 years, it has now been possible to investigate the semi-diurnal aniso-tropy characteristics in much greater detail. The author has conducted such detailed analysis to investigate the average characteristics of semi-diurnal anisotropy and their time varia-ion, the results of which are presented in the following sections.

5.1 Semi-diurnal pressure wave and the semi-diurnal variation of cosmic rays

The semi-diurnal component being essentially of the order of 0.1% or less, can be completely contaminated by pressure variations, if the pressure correction is incorrect. As for example, the observed semi-diurnal pressure wave of 0.3 mm of

TABLE 5.1 - The effect of variation of pressure coefficient on the amplitude and phase of the observed semi-diurnal component of cosmic ray intensity at Ahmedabad for a semi-diurnal pressure amplitude of 1.0 mm Hg

Pressure coefficient % per mm of Hg	Semi-diurnal amplitude (r_2)	Semi-diurnal phase (ϕ_2)
0.38	0.067%	34°
0.34	0.081%	61°
0.80	0.107%	78°

Hg, at middle latitudes, can constitute an error of $\approx 0.03\%$ in the semi-diurnal component, if the pressure coefficient is incorrect by 10%. At equatorial latitudes like Ahmedabad, where the semi-diurnal component of pressure wave is typically of the order of 1.0 mm Hg, the pressure contribution to the semi-diurnal variation arising from the application of incorrect pressure coefficient can be comparable, in magnitude, to the semi-diurnal component itself.

In Sec. 3.11, the pressure coefficient obtained for Ahmedabad neutron monitor for the years 1968-1971 namely 0.84% per mm Hg has been compared with other observations to demonstrate the excellent agreement between various recent estimates. From this comparison, we believe that the probability of the applied pressure coefficient being out by more than $\pm$ 0.04% per mm Hg, is negligible. Assuming the extreme case of the pressure coefficient used for Ahmedabad neutron monitor being out by $\pm$ 0.04%
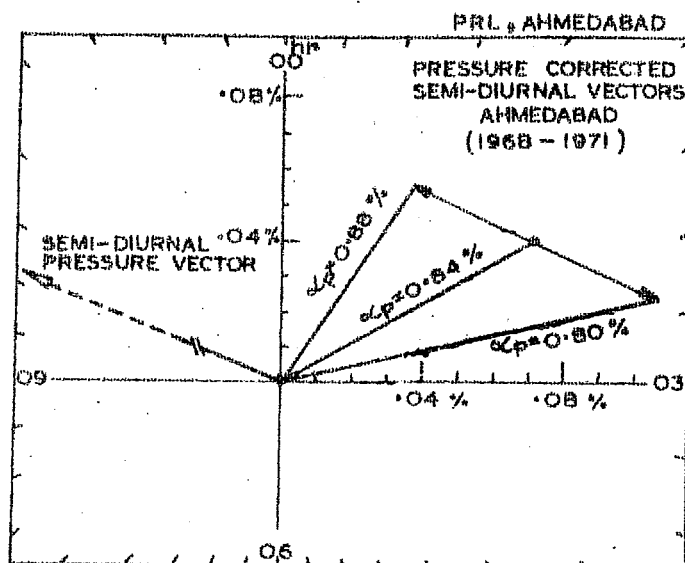
Fig. 5.1 - Vectorial representation of the pressure corrected semi-diurnal variation of cosmic ray intensity for 3 values of the pressure coefficient (α_p), for an observed semi-diurnal pressure vector of amplitude 1.0 mm Hg. The observed yearly average semi-diurnal pressure amplitude is $(r_{2p}) \approx 0.90$ mm Hg.

per mm Hg, the calculated maximum effect on the semi-diurnal component of cosmic radiation for a maximum expected semi-diurnal pressure wave of 1.0 mm Hg is shown in Figure 5.1 (see also Table 5.1). It is seen that even under the assumption of the extreme case, the error introduced in the semi-diurnal time of maximum is ~0.7 hour at equatorial latitudes and less than ~0.3 hour at mid-latitudes. The effect on the semi-diurnal amplitude will be relatively small, being only ≲ 20%.

5.2 Characteristics of average semi-diurnal anisotropy

For deriving the characteristics of average semi-diurnal anisotropy, we shall consider the simplest form of the anisotropy

(similar in form to the representation of diurnal anisotropy, equation 4.1), represented by

$$\frac{\partial J(R)}{J(R)} = A.g(\Lambda). R^{\beta} \quad \text{for } R < R_{max} \quad)$$
$$= 0 \quad \text{for } R > R_{max} \quad) \quad \quad .. \quad 5.1$$

where the function $g(\Lambda)$ describes the dependence of anisotropy on declination and R^{β} shows the dependence of anisotropy on rigidity. In the following section we shall obtain the best fit spectrum for the semi-diurnal anisotropy (β) for each year. In all our calculations, we assume that maximum rigidity (R_{max}) beyond which the anisotropy ceases is equal to 200 GV, the reasons for which will be presented in section 5.24.

Using the results of the theoretical calculation showing the relative amplitude and phase of the semi-diurnal variation (Figure 4.8b) for an assumed anisotropy in space, and the observations from a number of neutron monitoring stations given in Table 4.1, the author has attempted for the first time, to derive the detailed characteristics of the semi-diurnal anisotropy of cosmic radiation. In the following sections, we first derive the characteristics of the average semi-diurnal anisotropy and then compare the results with the theoretical predictions.

5.21 Spectral exponent of semi-diurnal anisotropy

Figure 5.2 shows the histogram of the frequency of occurrence of the semi-diurnal time of maxima in space observed at various stations for the year 1965 and 1966. The histograms
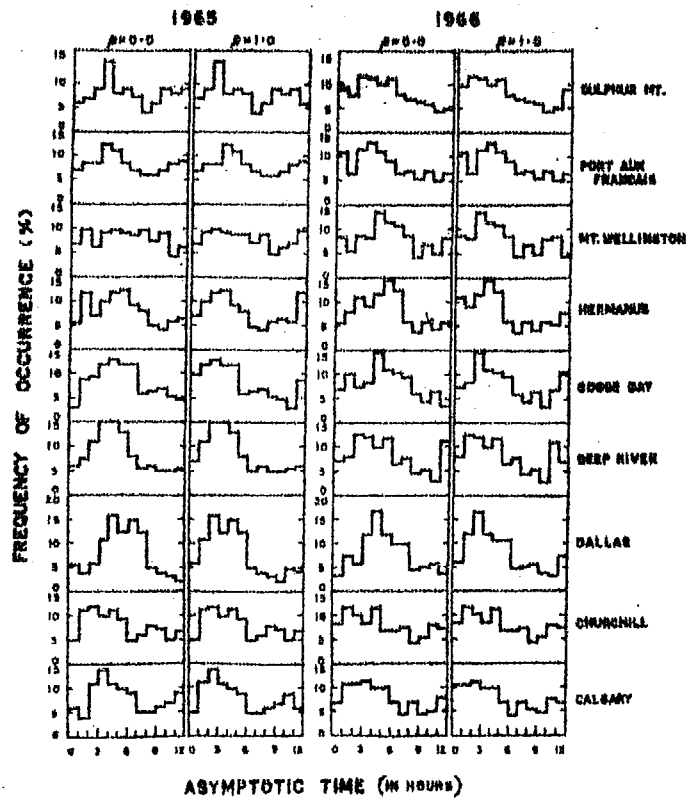
Fig. 5.2 - Histogram of the frequency of occurrence of
the semi-diurnal time of maximum in space for different stations
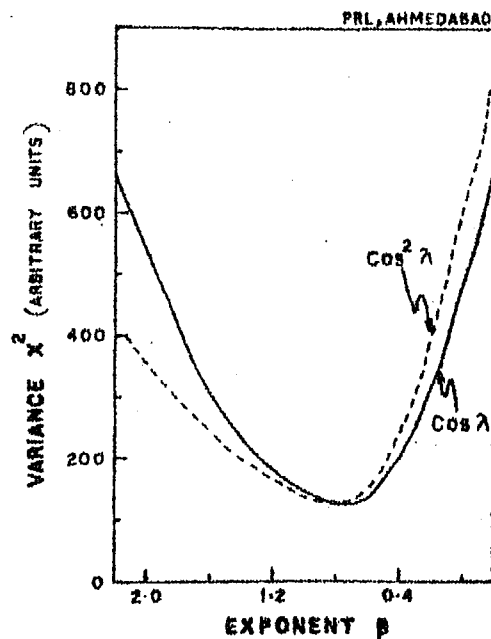during 1965 and 1966 calculated using $\beta = 0.0$ and $\beta = 1.0$.

Fig. 5.3 - Observed variance in the values of semi-diurnal
phase as a function of the exponent of variation for the year
1966, for $g(\Lambda) = Cos\Lambda$ and $g(\Lambda) = Cos^2\Lambda$.

are plotted against the asymptotic time for $\beta = 0$ and $\beta = 1.0$
obtained after correcting the observed time of maximum at each
station for the geomagnetic bending and the width of asymptotic
cone of acceptance, using the method of Rao et al. (1963) as
described in Chapter III. In the above calculation g (Λ) is
assumed to vary as $\cos\Lambda$. The figure shows a very good inter-
station agreement with $\beta = 1.0$, indicating that the semi-diurnal
maxima observed at all the cosmic ray recording stations is due
to an anisotropy, which has a positive spectral exponent with
the maximum flux incident from the direction $\approx 45°$ East ($135°-$
West) of the earth-sun line, a direction that is essentially
perpendicular to the direction of average interplanetary magnetic
field (I.M.F.).

A more **exact** determination of the spectral index, can be
obtained through a comparison of either the semi-diurnal time of
maxima in space (ϕ_2) or the semi-diurnal amplitude (r_2) as
observed at different stations. The value of (ϕ_2) has been deri-
ved for each station and each year for different values of β
ranging from + 2.0 to -1.0. The variance (x^2) in the value of
ϕ_2 determined for different stations are evaluated for diffe-
rent values of β for each year during 1958-1968. The best fit
value of β is obtained by imposing the condition that the vari-
ance at that value should be a minimum (Rao et al., 1963).

Figure 5.3 shows the plot of variance as a function of
β for 1966 obtained under the assumption namely g(Λ) = $\cos\Lambda$

and $g(\Lambda) = \cos^2 \Lambda$. It is seen that the minimum variance is obtained for $\beta = +1.0$ for both $g(\Lambda) = \cos \Lambda$ and $g(\Lambda) = \cos^2 \Lambda$. In other words, the assumption of the form of $g(\Lambda)$ does not seem to produce a significant difference in the derivation of β and the best fit value of β is $+1.0$. This is understandable since the change in time of maximum in space between the two assumptions is less than $< 3°$ even for $\beta = 1.0$. The analysis has been extended to the entire period to derive the best fit values of β for each year during 1958 to 1968, using both time of maximum as well as the semi-diurnal amplitude.

Figure 5.4 shows the plot of variance of the time of maximum against β for each year during 1953-1968. The standard deviation in the variation of phase even for an average IGY type of station is $\sim 5°$, thus the statistical error in variance can be considered to be ~ 25 square degrees. From the figure it is seen that the minimum variance for each year is obtained for $\beta = 1.0 \pm 0.2$, showing that the rigidity spectrum of the semi-diurnal component has an exponent 1.0 ± 0.2. However the minimum variance observed during each year is larger than can be expected from statistical uncertainties alone.

The ratio of the expected amplitude of the semi-diurnal component at Ahmedabad, to the amplitude at Deep River has been evaluated for each β and for various values of R_{max}. Figure 5.5 shows the theoretically expected ratio plotted as a function of β, for values of β ranging from $+2.0$ to 0.0 and for various
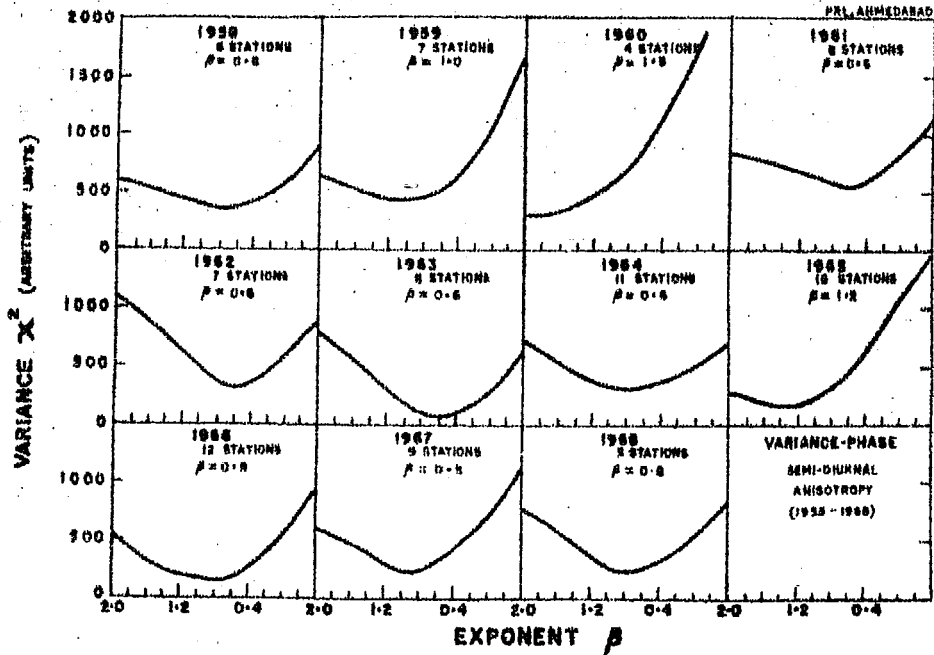
Fig. 5.4 - The observed variance between the asymptotic
time of semi-diurnal maxima calculated for each station as a
function of β, the exponent of variation for each year during
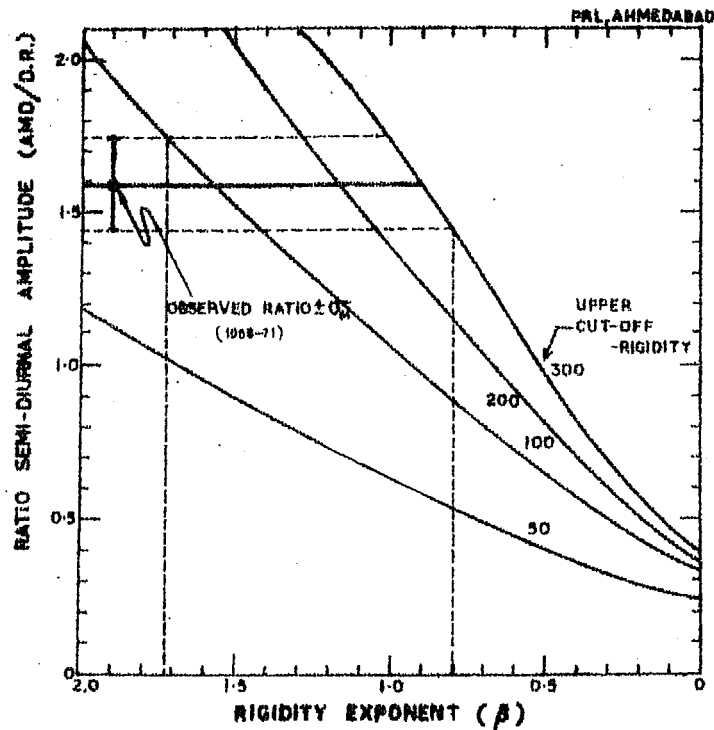1958-1968.

Fig. 5.5 - The ratio between the semi-diurnal amplitude
observed at Ahmedabad to that at Deep River during 1968-1971.
The theoretically expected ratio for different values of β,
and for various values of R_{max} = 50, 100, 200 and 300 GV are
also shown. The error (σ_m) has been derived from the actual
dispersion of the daily vectors.

values of R_{max} = 50, 100, 200 and 300 GV. The observed ratio of the average amplitude during the years 1968 to 1971 is also shown in the same figure. The observed ratio is consistent with $\beta \approx 1.0$, for values of R_{max} lying between 200 to 300 GV. The error indicated with the observed ratio is the actual dispersion error obtained considering the daily semi-diurnal vectors at each station, and does not include the uncertainty in the value of pressure coefficient. However, an uncertainty of 0.01% per mm Hg in the pressure coefficient at Ahmedabad will introduce an error of $\sim$ 10% in the observed ratio, which is of the same order as is shown in the figure. Even though unique values for both R_{max} and β cannot be obtained from the above figure, we note that the observed relative magnitude of semi-diurnal amplitude at Deep River and Ahmedabad is consistent with $R_{max} \approx$ 200 GV and $\beta \approx 1.0 \pm 0.2$.

A more accurate value of β can be determined by an inter-comparison of semi-diurnal amplitude at a number of stations. Figure 5.6 shows the plot of variance in the values of amplitudes of the semi-diurnal component as observed at different stations calculated for each value of β (equation 3.23) during 1958 to 1968. The curves again clearly show that the minimum variance is observed for values of β = 1.0 $\pm$ 0.2 consistent with our previous conclusions derived from an examination of the phase of the semi-diurnal anisotropy.
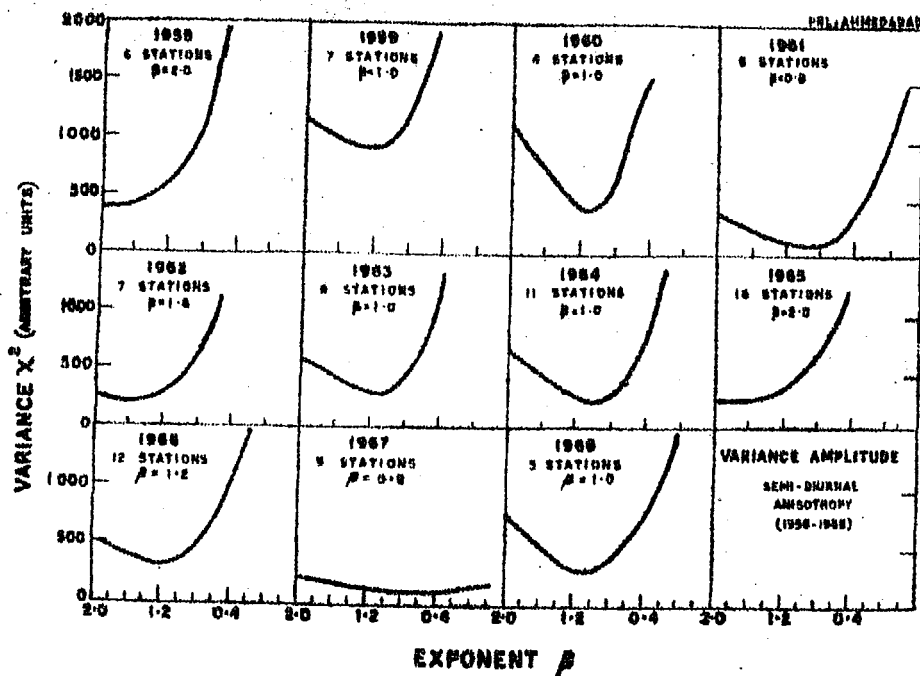
Fig. 5.6 - The observed variance between the semi-diurnal amplitude in space calculated for each station as a function of β, the exponent of variation, for each year during 1958-1968.
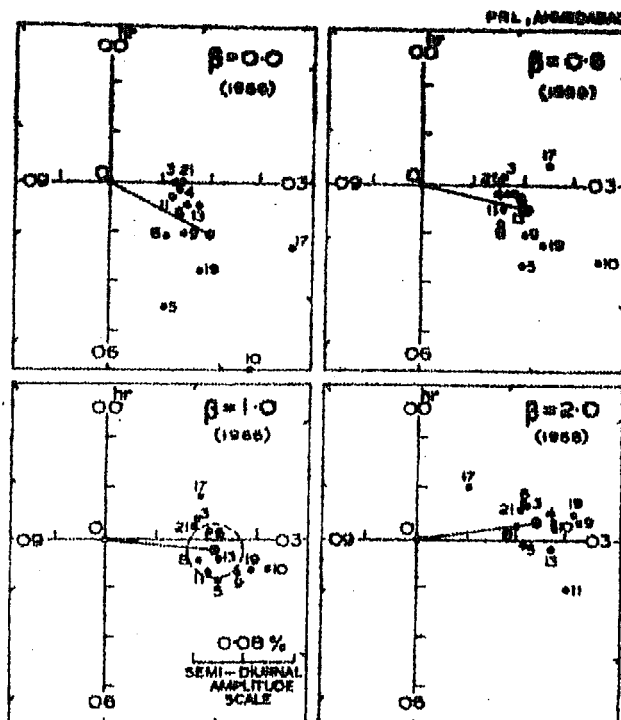

Fig. 5.7 - The phase and amplitude of the semi-diurnal anisotropy in space as observed at different stations during 1966 plotted on a harmonic dial. The plots show the scatter for four different values of β, namely 0.0, 0.6, 1.0 and 2.0. The mean semi-diurnal anisotropy vector in space is also shown along with 3σ error circle (for $\beta = 1.0$).

The phase and amplitude of the semi-diurnal anisotropy in space, as observed at different stations, are plotted on a harmonic dial in Figure 5.7, for different values of β namely 0.0, 0.6, 1.0 and 2.0 for the year 1966. The average vector derived from the individual observation for each value of β is also plotted in the same figure. It is evident from the figure that the minimum scatter between different vectors occurs for $\beta = +1.0$. Most of the observations are seen to be within 3 standard deviation (3σ) error circle of the mean vector for $\beta = 1.0$, and practically all the observational points lie within 5σ error circle. This is consistent with the fact that the minimum variance is slightly larger than can be expected from statistical uncertainties alone.

In Figure 5.8 the harmonic dial representation of the semi-diurnal anisotropy vector in space as observed at different stations for each year during 1964 to 1967, along with their vectorial mean for each year is plotted for $\beta = 1.0$. The larger scatter in the observations during earlier years may be attributed to the fact that most of the monitors operating during these years were of the IGY type.

5.22 Dependence of the semi-diurnal anisotropy on declination

To investigate the dependence of amplitude of the semi-diurnal anisotropy on declination, the yearly mean semi-diurnal amplitude observed at different stations, after correction for attenuation due to the finite width of asymptotic cone of
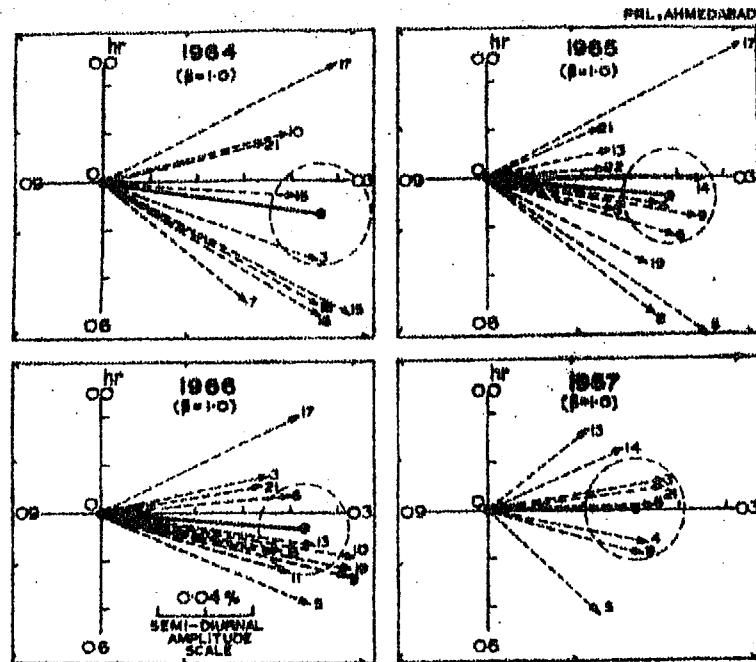
Fig. 5.8 - The phase and amplitude of the semi-diurnal anisotropy in space as observed at different stations calculated for $\beta = 1.0$, are shown for each year on a harmonic dial. The mean anisotropy vector along with 3σ error circle for each year is also indicated in the same figure.
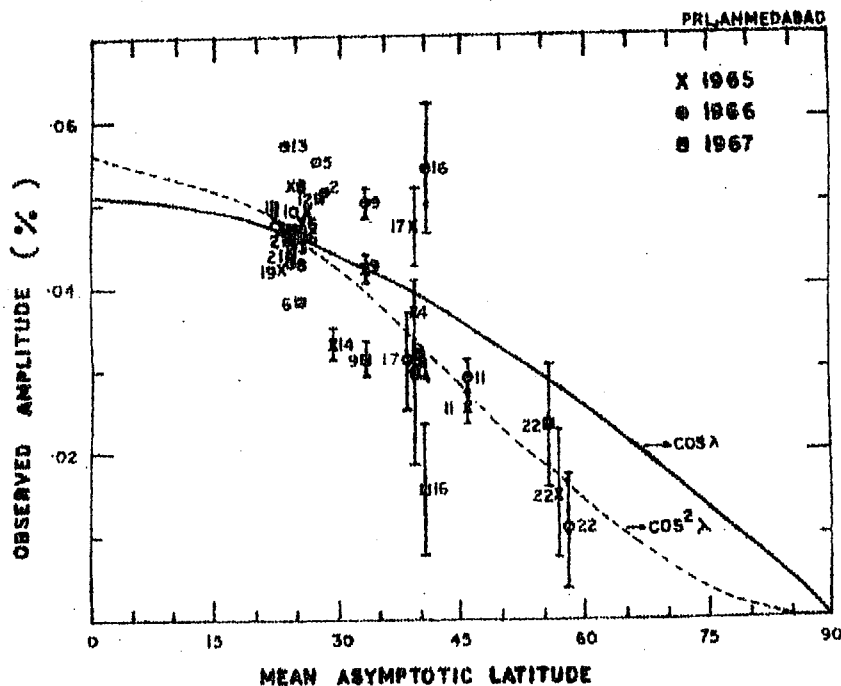

Fig. 5.9 - The amplitude of semi-diurnal anisotropy calculated for each station corrected only for the width of asymptotic cone of acceptance plotted against the mean asymptotic latitude. The theoretically expected behaviour for $\cos \lambda$ and $\cos^2 \lambda$ dependence are also shown.

acceptance, is plotted against the mean asymptotic latitude λ of the stations in Figure 5.9. The data for the years 1965, 1966 and 1967 are used in the figure. The theoretical curves defining $\cos\lambda$ and $\cos^2\lambda$ relationship are also shown in the same figure. Even though large statistical errors do not permit an unambiguous conclusion, it is clear that the distribution of points strongly favours a $\cos^2\lambda$ dependence.

From all the observational analysis presented above, we conclude that the semi-diurnal anisotropy in space has a positive spectral exponent of 1.0 ± 0.2, a mean amplitude of about 0.10% and the maximum flux arriving from 0300 hours, which is perpendicular to the direction of mean I.M.F. vector. Further the semi-diurnal anisotropy amplitude varies as $\cos^2\lambda$, where λ is declination. It is very satisfying to note that subsequent to this work a number of other authors, who have also investigated the nature of the semi-diurnal anisotropy using both surface as well as underground observations (Cini Castagnoli et al, 1968 and reference therein; Hashim et al, 1969; Krivoshapkin et al, 1970; Subramanian, 1971b; Thomson and Sumner, 1971; Mori et al, 1971; Nagashima et al, 1972 a, b; and sec. 4.32), have essentially confirmed these observations.

5.23 Long term variation of semi-diurnal anisotropy

Figures 5.10 and 5.11 show the yearly mean phase and amplitude in space of the semi-diurnal vector for each year during 1958-1968. The points plotted in the figure indicate
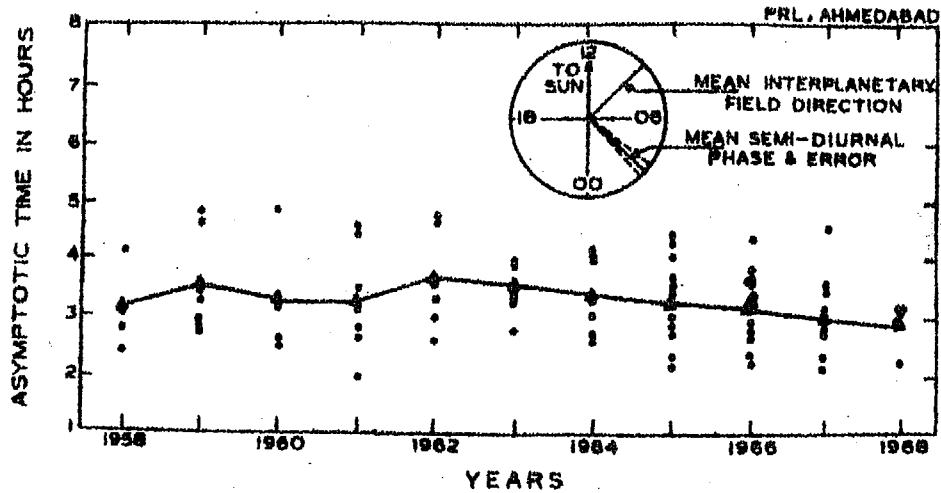
Fig. 5.10 - The phase of the semi-diurnal anisotropy in space for each year during 1958-1968. The mean value for each year is represented by triangle, while the dots represent the value as obtained from the observations at individual stations. The mean semi-diurnal phase for the entire period with its associated standard error and the direction of the mean I.M.F. are also shown.
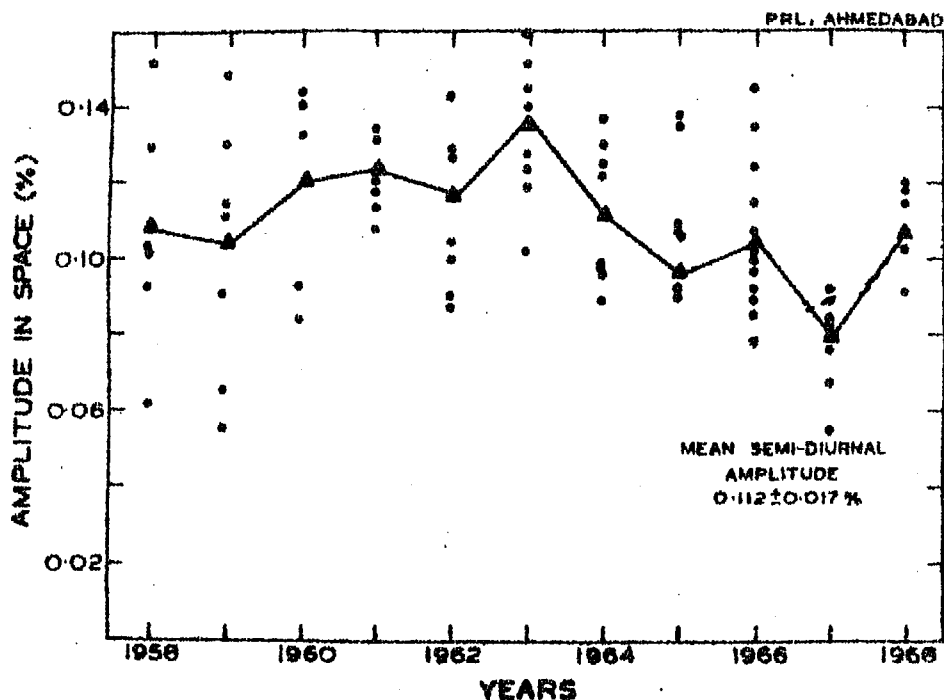

Fig. 5.11 - The amplitude of the semi-diurnal aniso-tropy in space for each year during 1958-1968. The representation is similar to Figure 5.10.

the observations at different stations. It is seen from the figure 5.10, that the mean semi-diurnal phase for the entire period 1953-1968 is almost constant, the maximum flux coming from the direction $132 \pm 6°$ West (3.2 ± 0.4 hours) of the earth-sun line. The mean semi-diurnal amplitude (Figure 5.11), however, shows a slight random variation during the same period, varying between 0.13 ± 0.03 in 1963 to 0.08 ± 0.03 in 1967, the observed variation being within the statistical uncertainty. The observations are therefore, consistent with a time invariant semi-diurnal amplitude. The mean amplitude in space for the entire period 1953-1968 is 0.112 ± 0.017.

5.24 Upper cut-off-rigidity of semi-diurnal anisotropy (R_{max})

Since the existence of both diurnal as well as semi-diurnal anisotropies in the interplanetary medium are the direct consequence of the solar modulation effects, which essentially depend on the electromagnetic conditions in space, it is expected that there must exist an upper cut-off-rigidity (R_{max}) above which the particles are not affected.

Figure 5.12 shows the variance of the amplitude and phase of the semi-diurnal anisotropy as a function of R_{max}, for $\beta = + 1.0$ and for the year 1966. It is seen from the figure that both the amplitude and phase of the semi-diurnal anisotropy show a minimum variance for $R_{max} \approx 200$ GV. However, we note that even at $R_{max} = 200 \pm 100$ GV the variance is not significantly higher than for $R_{max} = 200$ GV, showing that the present
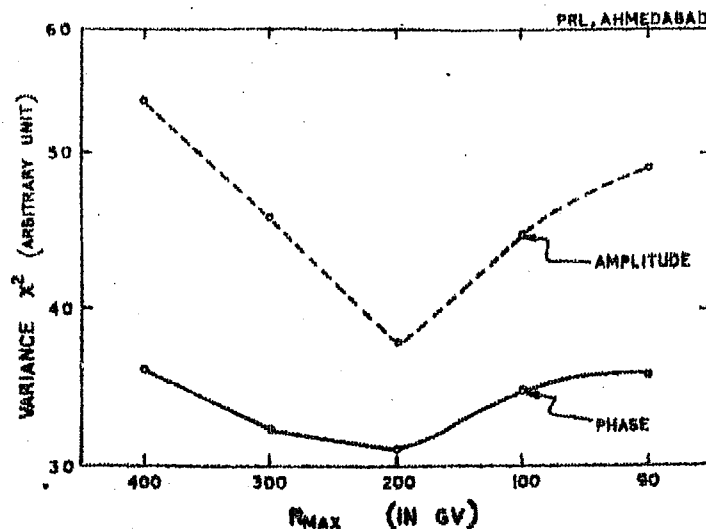
Fig. 5.12 - The variance in phase and amplitude of semi-diurnal anisotropy plotted as a function of R_{max} for $\beta = 1.0$ and for the year 1966.
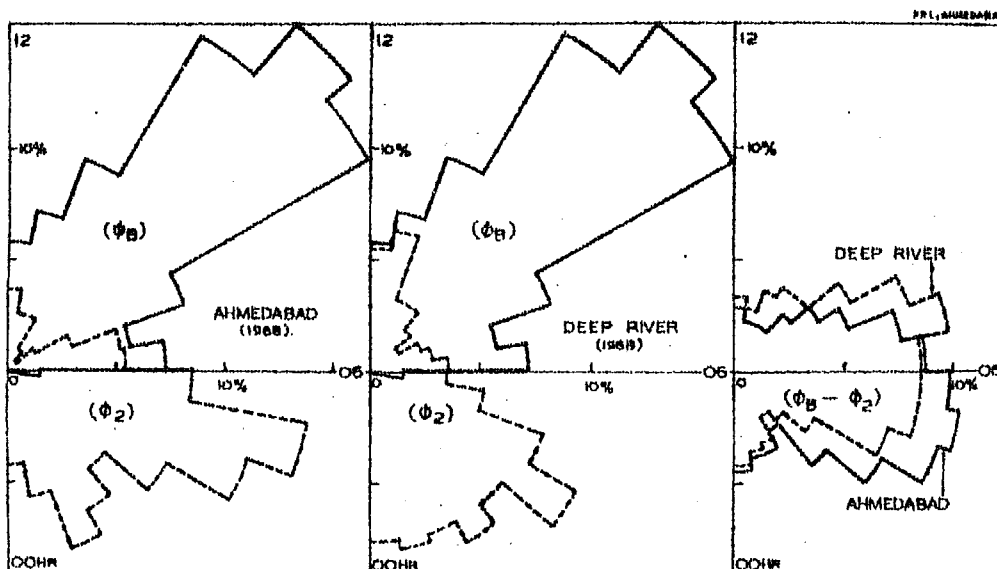

Fig. 5.13 - Polar histogram of the frequency of occurrence of the time of maximum of the semi-diurnal aniso- tropy (ϕ_2) for Ahmedabad and Deep River neutron monitoring stations, and the I.M.F. direction (ϕ_B) during 1968. The difference ($\phi_B - \phi_2$) for both the stations is also shown, which indicates a distribution with its maximum along 90^0.

set of data are not sufficient for an unambiguous fixation of the value of R_{max}, though R_{max} = 200 GV is the best choice. A similar analysis for all the years during 1958 to 1968 shows no systematic long term change in the value of R_{max}, unlike that observed in the diurnal anisotropy.

Referring again to Figure 5.5, it is seen that under the assumption β = 1.0, the observed ratio of Semi-diurnal amplitude at Ahmedabad to that at Deep River is consistent with an upper cut-off-rigidity of 200 GV even during the period 1968-1971. In other words, the presently available data is consistent with a time invariant R_{max} of 200 $\pm$ 100 GV for the entire period 1968-1971. For a more accurate estimate of R_{max} and its secular change, it is obvious that we need data from more equatorial stations.

5.25 Summary of the results

In summary, on the basis of the detailed observational evidence presented above, we conclude that (a) the semi-diurnal variation is consistent with an anisotropy which could be expressed by

$$\frac{\partial J(R)}{J(R)} = K.R.\ Cos^2\Lambda\ .\ Cos\ 2.\left[\theta - (48 \pm 6)\right]\ \%$$

$$\text{for } R < R_{max}$$

$$= 0 \qquad \text{for } R > R_{max} \qquad \qquad ..\ 5.2$$

where R is rigidity, Λ is declination, and $K \approx 0.004$.

(b) the average semi-diurnal amplitude in space for cosmic ray particles in the range 1-200 GV, is 0.11 ± 0.02% during the period 1953-1971. The time of maximum of the average semi-diurnal anisotropy is along ~0300 hours direction, which is essentially perpendicular to the direction of the average I.M.F. (c) the phase of the semi-diurnal anisotropy is time invariant and perpendicular to the direction of the average I.M.F. during the period 1958-1968 (d) the amplitude of the average semi-diurnal anisotropy shows no appreciable change between 1958-1968.

The analysis has been further extended on a day to day basis to show the perpendicular alignment of the time of maximum of the semi-diurnal component with the I.M.F. Figure 5.13 shows the histogram of frequency of occurrence of the semi-diurnal time of maximum in space (ϕ_2) obtained for Ahmedabad and Deep River neutron data and the observed I.M.F. direction for the year 1968. The difference between the two ($\phi_B - \phi_2$) is also plotted. An examination of the figure shows that on a statistical scale the semi-diurnal anisotropy even on a day to day basis is aligned perpendicular to the I.M.F. direction. The poor statistics and the non-availability of a large number of equatorial neutron monitor stations prevent a more critical examination of the day to day variability of the semi-diurnal anisotropy of cosmic radiation.

5.3 Theoretical interpretation of semi-diurnal anisotropy and conclusion

In seeking to find an explanation for the observed semi-diurnal anisotropy, both Subramanian and Sarabhai (1967) and Quenby and Lietti (1968) have independently proposed that the second harmonic component of the cosmic ray daily variation can arise due to the particle density gradient in the plane perpendicular to the plane of ecliptic (sec. 1.55). The basic difference between the two mechanisms however, is in the assumption of the nature of the perpendicular density gradient profile. As already discussed in Sec. 1.55, both the theories derive the average properties of the semi-diurnal anisotropy which are in essential agreement with the experimental observations discussed above.

The essential requirement of both the models is the existence of the increasing density of cosmic ray particles, both above and below the equatorial plane of the sun. The presence of such a gradient can be indirectly inferred from the observations of the cosmic ray intensity variation during the course of one year, when the earth's position changes by $\pm 7.25^\circ$ in heliographic latitude. Comparison of cosmic ray intensities, after proper normalization, observed when the earth is in different heliolatitude position with respect to sun, should provide a direct measure of the perpendicular density gradient. Even though the results from such an analysis are not conclusive, Subramanian (1971b) has shown that observed cosmic ray

intensity variation does not provide necessary density gradients to explain the observed semi-diurnal anisotropy of cosmic rays.

Nagashima et al. (1972a, b) and Barnden (1972) have recently attempted to refine the convection-diffusion theory by invoking the hypothesis of 'pitch angle distribution' in the I.M.F. irregularities. In particular, the model presented by Barnden (1972), makes use of the 'origin of scatter coefficients' technique, which involves the theoretical computation of the trajectories of the particle in the realistic configuration of the I.M.F., to obtain the hour by hour profile of the daily variation as observed at the earth, associated with any arbitrary radial cosmic ray density gradient when the mean-free-paths are specified. The approach, in many respects is similar to the trajectory tracing of the cosmic ray particle in the simulated geomagnetic field (McCracken et al., 1962, 1965). With this refinement the semi-diurnal component comes out as a natural consequence of pitch angle scattering.

Occurrence of the semi-diurnal variation can be attributed to mainly two reasons. First, to the fact that the number density decreases more sharply towards the sun from a given point than it increases away from the sun as a result of radial dependence of the density gradient. Second, the two mean sampling points parallel to the I.M.F., are not equispaced relative to the perpendicular viewing points. In essence, the density variation along the field line due to density gradients is the

same as the 'sink' proposed earlier by Rao and Sarabhai (1964), with the result that such a profile contains both diurnal and semi-diurnal variation components (Sarabhai and Subramanian, 1966).

Considering the most acceptable values of scattering mean-free-path and the radial density gradient, the resulting diurnal and semi-diurnal variations for cosmic ray particles have been calculated. The diurnal variation derived with these best fit parameters shows a $R^{+0.2}$ dependence below 25 GV and $R^{-1.0}$ dependence above 25 GV. These calculations also predict a semi-diurnal variation with $R^{+1.2}$ dependence upto 30 GV above which the value of the exponent should decrease. The agreement of the theory with experimental results is not very satisfactory. However, since the theoretical prediction are sensitive to the initial assumptions concerning the mean-free-paths and radial density gradient profile, a more rigorous analysis with a better understanding of the mean-free-path is necessary before accepting the expectation.

...

R E F E R E N C E S

Ables, J.G.,
McCracken, K.G. and
Rao, U.R.   1965   Proc.Int.Conf.Cosmic rays
                                      (London) 1, 208.

Ables, J.G.,
Barouch, E. and   1967   Planet.Space Sci., 15, 547.
McCracken, K.G.

Ahluwalia, H.S.   1962   Proc.Phys.Soc., 80, 472.

Ahluwalia, H.S.   1971   Proc.Int.Conf.Cosmic rays
                                      (Hobart), 2, 641.

Ahluwalia, H.S. and   1962   Planet.Space Sci., 9, 195.
Dessler, A.J.

Ahluwalia, H.S. and   1970   Acta Physica Hung., 29, Supp.2,
Ericksen, J.H.   139.

Ahluwalia, H.S. and   1971   J. Geophys.Res., 76, 6613.
Ericksen, J.H.

Alfven, H.   1950   Cosmical Electrodynamics,
                                      Oxford press, (London).

Axford, W.I.   1965a   Planet.Space Sci., 13, 115.

Axford, W.I.   1965b   Planet.Space Sci., 13, 1301.

Axford, W.I.   1968   Space Sci.Rev., 8, 331.

Bachelet, F.,
Balata, P.,   1965   Nuovo Cimento, 35, 23.
Dyring, E. and
Iucci, N.

Bachelet, F.,
Dyring, E.,   1967   Nuovo Cimento, 52B, 106.
Iucci, N. and
Villoresi, G.

Bachelet, F.,
Iucci, N.,   1972a   Nuovo Cimento, 7B, 17.
Villoresi, G. and
Sporre, B.

Bachelet, F.,
Iucci, N.,   1972b   Nuovo Cimento, 11B, 1.
Villoresi, G. and
Zongrilli, N.

Bame, S.J.,
Asbridge, J.R.,   1967   Trans.Amer.Geophys.Union
Hundhausen, A.J. and   abstract, 48, 190.
Strong, I.B.

Barker, M.C. and Hatton, C.J.	1970	Acta.Physica.Hung., 29, Supp.2, 177.
Barker, M.C. and Hatton, C.J.	1971	Planet.Space Sci., 19, 549.
Barnden, L.R.	1972	Preprint, Rome - LPS-72-8.
Bercovitch, M.	1963	Proc.Int.Conf.Cosmic rays (Jaipur), 332.
Bercovitch, M.	1966	Can .J. Phys., 44, 1329.
Bercovitch, M.	1967	Proc.Int.Conf.Cosmic rays (Calgary), Part A, 269.
Bercovitch, M.	1970	Acta Physica Hung., 29, Supp.2, 169.
Bercovitch, M.	1971a	Proc.Int.Conf.Cosmic rays (Hobart), Rapporteur report.
Bercovitch, M.	1971b	Proc.Int.Conf.Cosmic rays (Hobart), 2, 579.
Bercovitch, M. and Robertson, B.C.	1965	Proc.Int.Conf.Cosmic rays (London), 1, 489.
Biermann, L.	1951	Z. Astrophys., 29, 274.
Biermann, L.	1957	Observatory, 77, 109.
Burlaga, L.F.	1971	Space Sci.Rev., 12, 600.
Burlaga, L.F. and Ness, N.F.	1968	Can.J.Phys., 46, S962.
Carmichael, H.	1964	Cosmic rays, IQSY Instruction Manual No.7 (London).
Carmichael, H. and Bercovitch, M.	1969	Can . J.Phys., 47, 2073.
Carmichael, H. and Steljes, J.F.	1969	World data Centre A, Rep., UAG-5.
Carmichael, H. and Katzman, J.	1971	Proc.Int.Conf.Cosmic rays (Hobart), 2, 744.
Carmichael, H. and Peterson, R.W.	1971	Proc.Int.Conf.Cosmic rays (Hobart), 3, 887.

Carmichael, H., Bercovitch, M. and Steljes, J.F.   1967   Tellus, 19, 143.

Carmichael, H., Bercovitch, M., Shea, M.A., Magidin, M. and Peterson, R.W.   1968   Can.J.Phys., 46, S1006.

Carmichael, H., Shea, M.A. and Peterson, R.W.   1969   Can.J.Phys., 47, 2057

Chapman, S. and Bartels, J.   1940   Geomagnetism, II, Oxford University press.

Cini-Castognoli, G., Dodero, M.A. and Andreis, L.   1968   Can.J.Phys., 46, S839.

Coleman, Jr. P.J.   1966   J. Geophys.Res., 71, 5509.

Compton, A.H. and Getting, I.A.   1935   Phys.Rev., 47, 817.

Debrunner, H. and Fluckiger, E.   1971   Proc.Int.Conf. Cosmic rays (Hobart), 3, 911.

Dessler, A.J.   1967   Rev.Geophys., 5, 1.

Dorman, L.I.   1957   Cosmic ray variations, State Pub. house, Moscow.

Dorman, L.I.   1963   Prog.Elemetary Particle and Cosmic ray Physics, VII, North-Holland Pub.Co., Amsterdam.

Dorman, L.I. and Feinberg, E.L.   1955   Proc.Int.Conf. Cosmic rays (Guanajuato), 393.

Duggal, S.P. and Pomerantz, M.A.   1962   Phys.Rev. letters, 8, 215

Duggal, S.P., Forbush, S.E. and Pomerantz, M.A.   1967   Nature, 214, 154.

Duggal, S.P., Forbush, S.E. and Pomerantz, M.A.   1970a   Acta.Physica Hung., 29, Supp. 2, 55.

Duggal, S.P.,
Forbush, S.E. and
Pomerantz, M.A.

1970b   J. Geophys.Res., 75, 1150.

Dyring, E. and
Sporre, B.

1970   Acta.Physica Hung., 29, Supp.2,
95.

Elliot, H.

1952   Prog. in Cosmic ray Phys., I,
455.

Elliot, H. and
Dolbear, D.W.N.

1950   Proc.Phys.Soc., 63, 137.

Elliot, H. and
Dolbear, D.W.N.

1951   J.Atmo.Terr.Phys., 1, 205.

Elliot, H. and
Rothwell, P.

1956   Phil.Mag., 1, 699.

Faller, A.M. and
Marsden, P.L.

1965   Proc.Int.Conf. Cosmic rays
(London), 1, 231.

Fenton, A.G.,
McCracken, K.G.,
Rose, D.C. and
Wilson, B.G.

1959   Can.J.Phys. 37, 970.

Fireman, E.L. and
Goebel, R.

1970   J.Geophys.Res., 75, 2115.

Fisk, L.A. and
Axford, W.I.

1968   J. Geophys.Res., 73, 4396.

Fisk, L.A. and
Axford, W.I.

1969   J. Geophys.Res., 74, 4973.

Fisk, L.A. and
Axford, W.I.

1970   Solar Phys., 12, 304.

Forbush, S.E.

1958   J. Geophys. Res., 63, 651.

Forbush, S.E.

1967   J. Geophys. Res., 72, 4937.

Forbush, S.E.

1969   J. Geophys. Res., 74, 3451.

Forbush, S.E. and
Venkatesan, D.

1960   J. Geophys. Res., 65, 2213.

Forman, M.A.

1968   Can.J.Phys., 46, S 1087.

Forman, M.A. and
Gleeson, L.J.

1970   Preprint, Manash University.

Forman, M.A., Stoenner, R.W. and Davis, Jr. R.	1971	Proc.Int.Conf. Cosmic rays (Hobart), 2, 575.
Fowler, I.L.	1963	Rev.Sci.Instr., 34, 731.
Gleeson, L.J.	1969	Planet.Space Sci., 17, 31.
Gleeson, L.J.	1971a	Proc.Int.Conf. Cosmic rays (Hobart), Rapporteur report.
Gleeson, L.J.	1971b	Astrophys.Space Sci., 10, 471.
Gleeson, L.J. and Axford, W.I.	1967	Astrophys.J., 149, L.115.
Gleeson, L.J. and Axford, W.I.	1968a	Astrophys.Space.Sci., 2, 431.
Gleeson, L.J. and Axford, W.I.	1968b	Astrophys. J., 154, 1011.
Gosling, J.T., Hansen, R.T. and Bame, S.J.	1971	J. Geophys.Res., 76, 1811.
Harman, C.V. and Hatton, C.J.	1968	Can.J.Phys., 46, S1052.
Hashim, A. and Thambyahpillai, T.	1969	Planet.Space Sci., 17, 1879.
Hashim, A. and Bercovitch, M.	1972	Planet. Space Sci., 20, 791.
Hashim, A., Peacock, D.S., Quenby, J.J. and Thambyahpillai, T.	1969	Planet. Space Sci., 17, 1749.
Hashim, A., Bercovitch, M. and Steljes, J.F.	1972	Solar Phys., 22, 220.
Hasselmann, K. and Wibberentz, G.	1968	Z.Geophys., 34, 353.
Hatton, C.J.	1971	Prog.Elementary particle and Cosmic ray physics, X, North-Holland Pub.Co., Amsterdam, 1.

Hatton, C.J. and Carmichael, H.   1964   Can.J.Phys., 42, 2443.

Hatton, C.J. and Barker, M.C.   1971   Proc.Int.Conf. Cosmic rays (Hobart), 2, 603.

Hatton, C.J., Marsden, P.L. and Willetts, A.C.   1968   Can.J.Phys., 46, S915.

Hedgecock, P.C., Quenby, J.J. and Webb, S.   1972   Nature, 240, 173.

Hughes, E.B. and Marsden, P.L.   1966   J.Geophys.Res., 71, 1435.

Hughes, E.B., Marsden, P.L., Brooke, G., Meyer, M.A. and Wolfendale, A.W.   1964   Proc.Phys.Soc.London, A83, 239.

Hundhausen, A.J.   1968   Space Sci.Rev., 8, 690.

Hundhausen, A.J.   1970   Rev.Geophys.Space Phys., 8, 729.

Jacklyn, R.M., Duggal, S.P. and Pomerantz, M.A.   1970   Acta Phys. Hung., 29, Supp.2, 47.

Jokipii, J.R.   1966   Astrophys.J., 146, 480.

Jokipii, J.R.   1967   Astrophys.J., 149, 405.

Jokipii, J.R.   1971   Rev.Geophys.Space Phys., 9, 27.

Jokipii, J.R. and Coleman, Jr. P.J.   1968   J.Geophys.Res., 73, 5495.

Jokipii, J.R. and Parker, E.N.   1967   Planet. Space Sci., 15, 1375.

Jokipii, J.R. and Parker, E.N.   1968   Phys.Rev. letters, 21, 44.

Jokipii, J.R. and Parker, E.N.   1969   Astrophys. J., 155, 777.

Jokipii, J.R. and Parker, E.N.	1970	Astrophys. J., 160, 735.
Kane, R.P.	1960	Proc.Ind.Acad.Sci., 52, 69.
Kane, R.P.	1962	J.Phys.Soc.Japan, 17, 468.
Kane, R.P.	1964	Nuovo Cimento, 32, 273.
Kane, R.P.	1966	Nuovo Cimento, 45, 8.
Kane, R.P.	1968	Nuovo Cimento, B57, 36.
Kane, R.P.	1972	J.Geophys.Res., 77, 5573.
Katzman, J. and Venkatesan, D.	1960	Can.J.Phys., 38, 1011.
Kitamura, M.	1968	Can.J.Phys., 46, S828.
Kodama, M.	1967	Can.J.Phys., 45, 2733.
Kodama, M. and Inoue, A.	1970	JARE, Scientific Reports Series A, No.9, 1.
Kodama, M. and Nagashima, K.	1968	Can.J.Phys., 46, S825.
Krimigis, S.M.	1968	Can.J.Phys., 46, S976.
Krymskiy, G.F.	1964	Geomag. and Aeronomy, 4, 763.
Krivoshapkin, P.A., Krymskiy, G.F., Kuzmin, A.I., Skripin, G.V. and Metlyaeva, E.A.	1970	Acta Physics Hung., 29, Supp.2, 147.
Lapointe, S.M. and Rose, D.C.	1962	Can.J.Phys., 40, 687.
Lezniak, J.A. and Webber, W.R.	1970	Acta Physica Hung., 29, Supp.2, 111.
Lietti, B. and Quenby, J.J.	1968	Can.J.Phys., 46, S942.
Lindgren, S.	1970	Acta Physica Hung., 29, Supp.2, 345.
Lockwood, J.A.	1971	Space Sci.Rev., 12, 658.

Lockwood, J.A. and Webber, W.R.	1967	J. Geophys. Res., 72, 3395.
Lockwood, J.A., Lezniak, J.A. and Webber, W.R.	1972	J. Geophys. Res., 77, 4839
Maeda, K.	1960	J. Atm. Terr.Phys., 19, 184.
Maeda, K. and Wada, M.	1954	J. Sci.Res.Inst.Tokyo, 48, 71.
Mathews, T., Mercer, J.B. and Venkatesan, D.	1968	Can.J.Phys., 46, S854.
Mathews, T., Venkatesan, D. and Wilson, B.G.	1969	J.Geophys. Res., 74, 1218.
Mathews, T., Quenby, J.J. and Sear, J.	1971	Nature, 229, 246.
McCracken, K.G.	1962	J. Geophys. Res., 67, 447.
McCracken, K.G. and Rao, U.R.	1965	Proc.Int.Conf.Cosmic rays (London), 1, 213.
McCracken, K.G. and Rao, U.R.	1966	Planet Space Sci., 14, 649.
McCracken, K.G. and Rao, U.R.	1970	Space Sci.Rev., 11, 155.
McCracken, K.G., Rao, U.R. and Shea, M.A.	1962	M.I.T.Tech.Rep.No.77.
McCracken, K.G., Rao, U.R. and LeFan, B.W.	1966a	Preprint, Southwest Centre for advanced studies, Dallas, Texas No. DASS-66-1.
McCracken, K.G., Rao, U.R. and Bukata, R.P.	1966b	Phys.Rev. letters, 17, 928.
McCracken, K.G., Rao, U.R. and Bukata, R.P.	1967	J.Geophys.Res., 72, 4293.

McCracken, K.G.,
Rao, U.R. and
Ness, N.F.
1968   J. Geophys. Res., 73, 4159.

McCracken, K.G.,
Rao, U.R.,
Bukata, R.P. and
Keath, E.P.
1971   Solar Phys., 18, 100

McCracken, K.G.,
Rao, U.R.,
Fowler, B.C.,
Shea, M.A. and
Smart, D.F.
1965   IQSY Instruction Manual No. 10.

Mercer, J.B. and
Wilson, B.G.
1968   Can.J.Phys., 46, 5849.

Michel, F.C.
1967   J.Geophys.Res., 72, 1917.

Mori, S.
1966   J.Geomag.Geoelec., 18, 417.

Mori, S.
1968a   Nuovo Cimento, B58, 1.

Mori, S.
1968b   Nuovo Cimento, B58, 58.

Mori, S.,
Yasue, S. and
Ichinose, M.
1971   Rep.Ionosphere Space Res.,
        25, 271.

Nagashima, K.,
Ueno, H.,
Fujimoto, K.,
Fujii, Z. and
Kondo, I.
1972a   Rep.Ionosphere Space Res.,
        26, 1.

Nagashima, K.,
Fujimoto, K.,
Fujii, Z.,
Ueno, H. and
Kondo, I.
1972b   Rep.Ionosphere Space Res.,
        26, 31.

Ness, N.F.
1966   J.Geophys.Res., 71, 3319.

Neher, H.V.
1952   Prog.in Cosmic ray Physics,
        I, Interscience Pub.

Ng, C.K. and
Gleeson, L.J.
1971   Solar Phys., 20, 166.

O'Gallagher, J.J.
1967   Astrophys.J., 150, 675.

O'Gallagher, J.J.   1972   Rev.Geophys.Space Phys., 10, 821.

O'Gallagher, J.J. and   1967   Astrophys.J., 147, 819.
Simpson, J.A.

Ostman, Bo. and   1970   Preprint, Cosmic ray group,
Awadalla, E.   Inst.of Phys., Uppsala.

Pai, G.L.,   1967   Trans.Amer.Geophys.Union,
Bridge, H.S.,   48, 176.
Lyon, E.F. and
Egidi, A.

Parker, E.N.   1958a Astrophys.J., 128, 664.

Parker, E.N.   1958b Phys.Rev., 110, 1445.

Parker, E.N.   1960   Astrophys.J., 132, 175.

Parker, E.N.   1963   Interplanetary Dynamical
                                          Processes, Interscience,
                                          New York.

Parker, E.N.   1964   Planet.Space Sci., 12, 735.

Parker, E.N.   1965   Planet.Space Sci., 13, 9.

Parker, E.N.   1967   Planet.Space Sci., 15, 1723.

Parker, E.N.   1969   Space Sci.Rev., 9, 325.

Patel, D.,   1968   Planet.Space Sci., 16, 1131.
Sarabhai, V. and
Subramanian, G.

Pathak, P.N. and   1970   Planet.Space Sci., 18, 81.
Sarabhai, V.

Phillips, J. and   1962   J.Phys.Soc.Japan (Supp.AII),
Parsons, N.R.   17, 519.

Pomerantz, M.A. and   1971   Space.Sci.Rev., 12, 75.
Duggal, S.P.

Pomerantz, M.A.,   1962   J.Phys.Soc.Japan (Supp.AII),
Duggal, S.P. and   17, 464.
Nagashima, K.

Quenby, J.J.   1965   Proc.Int.Conf.Cosmic rays
                                          (London), 1, 3.

Quenby, J.J.   1967   Handbuch der Physik, 46, 2, 310.

Quenby, J.J. and   1969   Planet.Space Sci., 17, 1121.
Hashim, A.

Quenby, J.J. and   1968   Planet.Space Sci., 16, 1209.
Lietti, B.

Quenby, J.J. and   1971   Proc.Int.Conf.Cosmic rays
Sear, J.F.   (Hobart), 2, 771.

Rao, U.R.   1972   Space Sci.Rev., 12, 719.

Rao, U.R. and   1961   Proc.Roy.Soc., A263, 101.
Sarabhai, V.

Rao, U.R. and   1964   Planet.Space Sci., 12, 1055.
Sarabhai, V.

Rao, U.R.,   1963   J.Geophys.Res., 68, 345.
McCracken, K.G. and
Venkatesan, D.

Rao, U.R.,   1967   J.Geophys.Res., 72, 4343.
McCracken, K.G. and
Bartley, W.C.

Rao, U.R.,   1971   Solar Phys., 19, 209.
McCracken, K.G.,
Allum, F.R.,
Palmeira, R.A.R.,
Bartley, W.C. and
Palmer, I.

Rau, W.   1939   Z.Phys., 114, 482.

Razdan, H. and   1971   Proc.Int.Conf.Cosmic rays
Bemalkhedkar, M.M.   (Hobart), 2, 697.

Richard, K.F.,   1963   Rev.Scientific Inst., 34, 504.
Rao, U.R. and
Smith, W.B.

Roelof, E.C.   1968   Can.J.Phys., 46, S990.

Ryder, P. and   1968   Can.J.Phys., 46, S999.
Hatton, C.J.

Sandstrom, A.E.   1968   Can.J.Phys., 46, S862.

Sarabhai, V. and Nerurkar, N.W.   1956   Ann.Rev.Nucl.Sci., 6, 1.

Sarabhai, V. and Subramanian, G.   1965   Proc.Int.Conf.Cosmic rays (London), 1, 204.

Sarabhai, V. and Subramanian, G.   1966   Astrophys.J., 145, 206.

Sarabhai, V., Pai, G.L. and Wada, M.   1965   Nature, 206, 703.

Sari, J.W. and Ness, N.F.   1969   Solar Phys., 8, 155.

Schatten, K.H.   1971   Rev.Geophys. and Space Phys., 9, 773.

Schmidt, P.J.   1972   J.Geophys.Res., 77, 3295.

Severney, A., Wilcox, J.M., Scherrer, P.H. and Colburn, D.S.   1970   Solar Phys., 15, 3.

Shea, M.A.   1972   Ground-based Cosmic ray instrumentation Catalogue, AFCRL-72-0411.

Shea, M.A., Smart, D.F., McCracken, K.G. and Rao, U.R.   1968   Supp.IQSY Instruction Manual No.10, Cosmic ray tables, AFCRL-68-0030.

Shen, M.L.   1968   Supp.Nuovo Cimento., 4, 1177.

Simpson, J.A.   1948   Phys.Rev., 73, 1389.

Simpson, J.A.   1949   Echo lake.Conf.on Cosmic rays p.175 and 252.

Simpson, J.A.   1957   Ann.I.G.Y. (London Pergamon Press) Part VII.

Simpson, J.A. and Wang, J.R.   1967   Astrophys.J.letters, 149, 73.

Simpson, J.A. and Wang, J.R.   1970   Astrophys.J., 161, 265.

Simpson, J.A., Fonger, W. and Treiman, S.B.	1953	Phys.Rev., 90, 934.
Skadron, G.	1967	Preprint.Tech.Report No.678, Univ.of Maryland.
Singer, S.F., Laster, H. and Lencheck, A.M.	1962	J.Phys.Soc.Japan (Supp.AII), 17, 583.
Siscoe, G.L., Davis, Jr. L., Coleman, Jr. P.J., Smith, E.J. and Jones, D.E.	1968	J.Geophys.Res., 73, 61.
Snyder, C.W., Neugebauer, M. and Rao, U.R.	1963	J.Geophys.Res., 68, 6361.
Stern, D.	1964	Planet.Space Sci., 12, 973.
Steljes, J.F.	1970	AECL. Reports, 3479, 3561, 3608, 3651, 3658.
Stoker, P.H. and Carmichael, H.	1971	Astrophys. J., 169, 357.
Stoker, P.H., Raubenheimer, B.C. and Vander Walt, A.J.	1972	J.Geophys.Res., 77, 3575.
Subramanian, G.	1971a	J.Geophys.Res., 76, 1093.
Subramanian, G.	1971b	Can.J.Phys., 49, 34.
Subramanian, G. and Sarabhai, V.	1967	Astrophys.J., 149, 417.
Swinson, D.B.	1971	Proc.Int.Conf.Cosmic rays (Hobart), 2, 588.
Tanskanen, P.J.	1968	Can.J.Phys., 46, S819.
Thomson, D.M. and Sumner, D.J.	1971	Proc.Int.Conf.Cosmic rays (Hobart), 2, 635.
Tolba, M.F. and Lindgren, S.T.	1971	Proc.Int.Conf.Cosmic rays (Hobart), 2, 690.

Treiman, S.B.   1952   Phys.Rev., 86, 917.

Wainio, K.M.,   1968   Can.J.Phys., 46, S1048.
Colvin, T.H.,
More, K.A. and
Tiffany, O.L.

Webber, W.R.   1967   Proc.Int.Conf.Cosmic rays
                                         (Calgary), Part A, 146.

Webber, W.R. and   1959   Phil.Mag., 4, 654.
Quenby, J.J.

Wilcox, J.M. and   1965   J. Geophys.Res., 70, 5793.
Ness, N.F.

Wilcox, J.M. and   1972   J. Geophys.Res., 77, 751.
Colburn, D.S.

Willets, A.C.,   1970   Acta.Physica.Hung., 29,
Griffiths, W.K.,   Supp.2, 61.
Hatton, C.J. and
Marsden, P.L.

. . . .

MULTIPLICITY MEASUREMENTS AT AHMEDABAD

S. P. AGRAWAL, S. K. RAY, U. R. RAO

Physical Research Laboratory, Ahmedabad, India

MULTIPLICITY MEASUREMENTS AT AHMEDABAD

S. P. Agrawal, S. K. Ray, U. R. Rao

Physical Research Laboratory, Ahmedabad, India

An 18 NM-64 Super Neutron Monitor at Ahmedabad (cut-off rigidity 16 GV) having a count rate of about 0.2 million per hour, commenced operation from August 1968. A neutron multiplicity meter has been attached to the monitor to investigate the energy spectrum of the time variation of cosmic radiation in great detail. The results indicate a much larger percentage of high multiplicity neutrons as compared with the high multiplicity events at middle and high latitude stations. The barometric coefficient of the neutrons of different multiplicities are evaluated and compared with earlier results.

Introduction

The multiple production of evaporation neutrons produced by cosmic radiation in neutron monitors of different types has been studied by a number of workers. It is well known that nearly 80% of neutrons detected by the monitor are due to neutron interactions, about 11% are due to proton interactions and the remaining 9% are due to muons and pions. Fieldhouse et al. [1] and Hughes and Marsden [2] have clearly shown that higher multiplicities are due to higher energy primary cosmic radiation and hence a study of the multiplicity of neutrons can yield very profitable information on the energy spectrum of primary cosmic radiation and its changes. The multiplicity distribution depends very much on the geometry and location of the monitor. In this paper, we present some preliminary results of the multiplicity measurements made with an 18 NM-64 super neutron monitor at sea level at Ahmedabad, India (Geogr. Latitude 23.01° N, Geographic Longitude 72.61° E, Geomagnetic cut-off 16.0 GV).

The intensity of neutrons of different multiplicities up to 10 and the intensity of all neutrons of multiplicity more than 10 are measured by a conventional type of multiplicity meter. The choice of gate width was determined by examining the ratio of the total events of multiplicity $N \geq 2$ to the total count rate in the neutron monitor (Fig. 1). The ratio after correcting for chance coincidence, overlapping of two events and for dead time losses using the method suggested by Debrunner and Walther [3] is also plotted in the same figure. Since the corrected ratio is found to be almost constant from 1300 μsec onwards, a gate width of 1350 μsec is taken as the most appropriate gate width.

The attenuation coefficient of the detected neutrons of different multiplicity was determined for all the quiet days. Days on which Forbush decreases occurred and two days preceding and following these were removed from the total data.

Fig. 2 shows the pressure coefficient for different multiplicities obtained for the super neutron monitor at Ahmedabad. The results of KODAMA and OHUCHI [4] for the latitude survey and the results from Itabashi neutron monitor [5], both using a 3 NM-64 monitor, are also shown in the same figure. The attenuation coefficients we obtain at Ahmedabad are found to be slightly lower than those quoted by KODAMA and
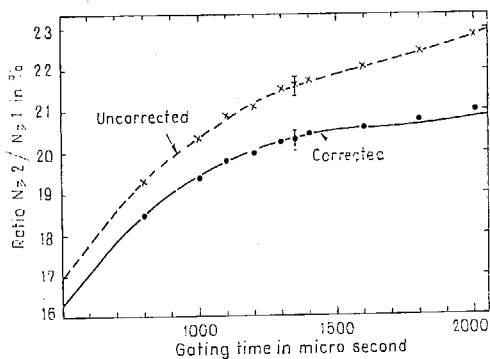

Fig. 1. The ratio of events with $N \geq 2$ to the counting rate of a neutron monitor as a function of gate width. The ratio after correction for chance coincidence, overlapping of events and dead time losses is also shown in the figure
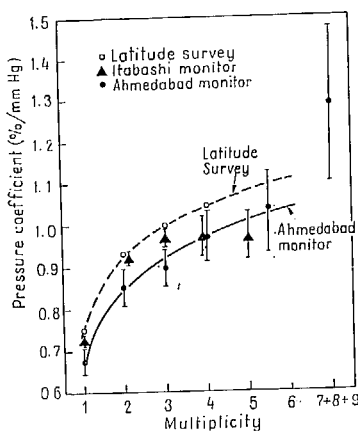
Fig. 2. Attenuation coefficient for different multiplicities for the 18 NM-64 monitor at Ahmedabad. The results for the Latitude Survey [4] and for the Itabashi 3 NM-64 monitor [5] are also shown

OHUCHI [4] even though the statistical uncertainties do not permit us to draw any definitive conclusion. It is, however, very clear that the pressure coefficient for all multiplicities is lowest at the equator, which has been explained as due to the increasing contribution from captured μ mesons (press. coeff. 0.25%/mm Hg) to the single multiple event with the increase in cut-off rigidity. An exactly opposite effect is seen when one examines the relationship between the pressure coefficient and

multiplicity. The higher multiplicity events which are due to higher energy cosmic ray primaries have a higher pressure coefficient; a result consistent with the results obtained by HATTON and GRIFFITHS [6]. HATTON and GRIFFITHS have given a simple model to explain the decrease of the pressure coefficient with cut-off rigidity and increase of the coefficient with multiplicity in terms of the statistics of interactions in the atmospheric cascade processes.

Fig. 3 shows the multiplicity spectrum for Ahmedabad. When compared with multiplicity spectra for other super neutron monitors, it is evident that the percentage of higher multiplicity events at Ahmedabad is much larger owing to the higher geomagnetic cut-off rigidity. The mean multiplicity at Ahmedabad during 1968 − 69 is 1.331 ± 0.008. KODAMA and OHUCHI [4] have shown that the mean
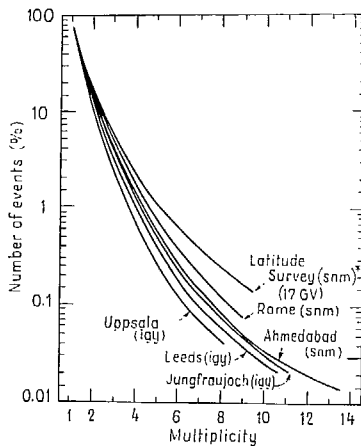

Fig. 3. Mean multiplicity spectrum for various neutron monitors

multiplicity increases almost linearly with the threshold rigidity. For a threshold rigidity of 16 GV, the mean multiplicity expected from their latitude survey results is 1.442 ± 0.005. The mean multiplicity for a 3 NM-64 monitor is approximately 3% less than that for a 6 NM-64 monitor whereas the effect of the removal of the square lead blocks is to increase the multiplicity by approximately 6%. The net result is that a 3 NM-64 monitor of the type used by KODAMA and OHUCHI will show a 3% increase in mean multiplicity compared with that of a standard 6 NM-64 super monitor. Correcting our result for this effect for comparison purposes, the mean multiplicity at Ahmedabad for a monitor of the specification by KODAMA and OHUCHI, would be 1.36 ± 0.008. The slight discrepancy between the values expected from their curve and those obtained by us may be due to the copper counters used in our monitor for which the multiplicity seems to be between those of stainless-steel counters of IQSY type and the IGY counters.

References

1. P. FIELDHOUSE, E. B. HUGHES, P. L. MARSDEN, J. Phys. Soc. Japan, 17, Suppl. A II, 518, 1962.
2. E. B. HUGHES, P. L. MARSDEN, J. Geophys. Res., 71, 1435, 1966.
3. DEBRUNER, WALTHER, Canad. J. Phys., 46, S1140, 1968.
4. M. KODAMA, T. OHUCHI, Canad. J. Phys., 46, S1090, 1968.
5. M. KODAMA, Y. ISHIDA, Rep. Ion. Space Res. Japan, 21, 55, 1967.
6. C. J. HATTON, W. K. GRIFFITHS, J. Geophys. Res., 72, 7503, 1968.

ALBANIA
Ndermarja Shtetnore e Botimeve
Tirana

AUSTRALIA
A. Keesing
Box 4886, GPO
Sydney
Cosmos Bookshop
145 Acland St.
ST. KILDA,
Vic. 3182

AUSTRIA
Globus (VAZ)
Höchstädtplatz 3
A—1200 Wien I

BELGIUM
Office International
de Librairie
30 Avenue Marnix
Bruxelles 5

BULGARIA
Directia R.E.P. Pl. Slaveikov 11
Sofia

CANADA
Pannonia Books
2 Spadina Road
Toronto 4. Ont.

CHINA
Beijing Waiwen Shudian,
P.O.B. 50
Peking

CZECHOSLOVAKIA
P.N.S. Dovoz tlače,
Leningradska 14
Bratislava
P.N.S. Dovoz tisku,
Vinohradska 46
Praha 2
Mad'arská Kultura
Vaclavské Nám. 2
Praha I

DENMARK
Ejnar Munksgaard,
Prags Boulevard 47
Copenhagen/S

FINLAND
Akateeminen Kirjakauppa
Keskuskatu 2
Helsinki

FRANCE
Office International de
Documentation et Librairie
48, rue Gay Lussac
Paris 5

**GERMAN DEMOCRATIC
REPUBLIC**
Zeitungsvertriebsamt
Fruchtstrasse 3—4
1004 Berlin

GERMAN FEDERAL REPUBLIC
Kunst und Wissen
Erich Bieber, Postfach 46
Wilhelmstrasse 4
7 Stuttgart Ie

GREAT BRITAIN
Collet's Holdings Ltd.
Dennington Estate
London Rd.
Welingborough, Northants
Blackwell's Oxenford House,
Magdalen Street
Oxford
Robert Maxwell & Co. Ltd.,
4—5 Fitzroy Square
London W. I
Wm Dawson and Sons Ltd.
Cannon House,
Macklin Street,
London W. C. 2

HOLLAND
Swets & Zeitlinger,
Keizersgracht 487
Amsterdam C
Martinus Nijhoff
Lange Voorhout 9
The Hague

ITALY
Santo Vanasia
Via M. Macchi 71
20104 Milano
LICOSA
Via Lamarmora 45
Firenze

JAPAN
Nauka Ltd. 30—19 Minami-
Ikebukuro 2-chome
Toshima-ku
Tokyo
Maruzen & Co. Ltd.
P.O. Box 605
Tokyo-Central
Far Eastern Booksellers
Kanda P.O. Box 72
Tokyo

KOREA
Chulmanpul
Phenjan

NORWAY
Tidsskrift-Sentralen
Tanum-Cammermeyer
Karl Johansgátan 41/43
Oslo I

POLAND
B.K.W.Z. RUCH
ul. Wronia 23
Warszawa

ROUMANIA
OSEP
Bucureşti
OSEP
Oradea

SOVIET UNION
Pochtamt-Import
Moscow
Pochtamt-Import
Leningrad

SWEDEN
Almqvist and Wiksell
Gamla Brogatan 26
Stockholm
Wennergren-Williams A.B.
Nordenflychtsvägen 70
S—10120 Stockholm 30

SWITZERLAND
Karger Libri
Arnold-Böcklin-Strasse 25
4000 Basel II

USA
Stechert Hafner Inc.
31 East 10th Street
New York N. Y. 10003
Fam Book Service
69 Fifth Avenue
New York N. Y. 10003
Lippincott Company
East Washington Square
Philadelphia Pa 19105

YUGOSLAVIA
Forum
Vojvode Misića 1
Novi Sad
Jugoslovenska Knjiga
Terazije 27
Beograd

(1) Semi-diurnal anisotropy of Cosmic radiation.....
       J. Geophys. Res., Space Phys., 75, 2391 (1970)

(2) Effect of non-uniform solar wind .....
       Ind.J.Pure & Applied Phys., 9, 498 (1971)

(3) Characteristics of cosmic ray diurnal variation ...
       Can.J.Phys., 50, 1323 (1972)

(4) Characteristics of quiet as well as enhanced .....
       Planet. Space Sci., 20, 1799 (1972)

. . . . .

CHARACTERISTICS OF QUIET AS WELL AS ENHANCED DIURNAL ANISOTROPY OF COSMIC RADIATION

U. R. RAO, A. G. ANANTH and S. P. AGRAWAL

Physical Research Laboratory, Ahmedabad, India

Abstract—It is shown that the model which has been successful in explaining the anisotropy of low energy cosmic radiation of solar origin in terms of simple convection and field aligned diffusion can also be extended to explain both the quiet and enhanced diurnal variation of cosmic radiation at higher energies. The enhanced diurnal variation which shows a maximum around ~ 2000 hr is shown to be caused by the superposition of normal convection and enhanced field aligned diffusion due to an enhanced positive density gradient of approximately ~ 10 per cent/AU. The enhanced gradient in the early part of the event is caused by a depletion of cosmic ray intensity along the garden-hose direction and later in the event ($T \geqslant 4$ days) is caused by an excess flux from the anti-garden-hose direction. The quiet day average diurnal anisotropy of cosmic radiation can be understood as due to an equilibrium between the convective and diffusive flow, resulting in a corotation vector along the 1800 hr direction.

CHARACTERISTICS OF QUIET AS WELL AS ENHANCED DIURNAL ANISOTROPY OF COSMIC RADIATION

U. R. RAO, A. G. ANANTH and S. P. AGRAWAL

Physical Research Laboratory, Ahmedabad, India

Abstract—It is shown that the model which has been successful in explaining the anisotropy of low energy cosmic radiation of solar origin in terms of simple convection and field aligned diffusion can also be extended to explain both the quiet and enhanced diurnal variation of cosmic radiation at higher energies. The enhanced diurnal variation which shows a maximum around ~2000 hr is shown to be caused by the superposition of normal convection and enhanced field aligned diffusion due to an enhanced positive density gradient of approximately ~10 per cent/AU. The enhanced gradient in the early part of the event is caused by a depletion of cosmic ray intensity along the garden-hose direction and later in the event ($T \geqslant 4$ days) is caused by an excess flux from the anti-garden-hose direction. The quiet day average diurnal anisotropy of cosmic radiation can be understood as due to an equilibrium between the convective and diffusive flow, resulting in a corotation vector along the 1800 hr direction. The observed amplitude of the annual mean diffusive vector is consistent with a positive radial density gradient of ~4·5 per cent/AU, which agrees with other radial gradient measurements. The diffusive vector during both quiet and enhanced anisotropy periods is shown to be along the interplanetary field direction. The ratio of perpendicular to parallel diffusion coefficient under normal conditions is derived to be $\leqslant 0\cdot05$ indicating that the transverse gradients, in general, are negligible.

1. INTRODUCTION

The diurnal anisotropy of cosmic radiation has generally been explained in terms of azimuthal corotation (Parker, 1964; Axford, 1965), the magnitude of the corotation itself being subject to modification by transverse diffusion and transverse gradient currents. The experimental observation of 0·4 per cent mean diurnal amplitude along the 1800 hr direction (Rao *et al.*, 1963; McCracken and Rao, 1965; Rao, 1972) using the world wide neutron monitor data has been considered as supporting this concept. The reduction in the observed average amplitude from the expected full corotation vector of ~0·6 per cent has been generally attributed to the transverse diffusion. Recently, however, Subramanian (1971), has made a careful estimation of the various cumulative errors that should be considered, from which he concludes that the observed amplitude during most of the period is in reasonably good agreement with the expected amplitude indicating that the transverse diffusion, on an average basis, is negligible even at relativistic energies. Such an inference is essentially in agreement with the solar flare particle data.

Even though the explanation of the average daily variation in terms of corotation has been considered generally satisfactory, considerable deviations from the above average picture (Rao and Sarabhai, 1964; Patel *et al.*, 1968) exist, on a day to day basis. The existence of consecutive days having abnormally large amplitudes ($\geqslant 1$ per cent) has been reported by several workers (Mathews *et al.*, 1969; Hashim and Thambyahpillai, 1969), who have concluded that the diurnal variation on such days is generally caused by a depletion of the cosmic ray intensity along the garden-hose direction. Likewise trains of days having abnormally low amplitudes have also been observed in the data (Ananth *et al.*, 1971). Explanation of such abnormal amplitudes using the concept of corotation has not been satisfactory.

In this communication we present detailed data in support of a new concept for the interpretation of the diurnal variation. This concept is that the diurnal variation is completely

explainable in terms of radial convection together with diffusion which is principally along the magnetic field line. The notion that these components might be relevant to the diurnal variation was first mentioned by McCracken et al. (1968) as an extension of their studies of the anisotropies of solar cosmic rays. As specific formulation for both solar cosmic-ray events and the diurnal variation, together with a full theoretical basis, was given by Forman and Gleeson (1970), following earlier work on solar event anisotropies by Forman (1970). The important steps taken in this paper are the application of this convection–diffusion concept to explain diurnal variation at high energies and the demonstration that the diffusion component is mainly field aligned. According to this concept the corotational diurnal vector observed, on an average basis, is merely a special case when equilibrium exists between convection and diffusion and there is no net flow of cosmic ray flux into or out of the solar system. On a day-to-day basis, however, the fluctuation in the interplanetary parameters such as solar wind properties and the interplanetary field must necessarily cause an imbalance between convection and diffusion through the introduction of density gradients resulting in abnormal amplitudes for diurnal variation. Brief preliminary reports of observational data, at neutron monitor energies, which support this concept were presented at the 12th International Conference on Cosmic Rays at Hobart, in August 1971 by us (Ananth et al., 1971); Tolba and Lindgren (1971) and Hashim et al. (1972) have also reported on this topic. The concept is particularly attractive because the same ideas have been used to explain anisotropy changes throughout solar cosmic-ray burst events (McCracken et al., 1971) and in models which reproduce these (Ng and Gleeson, 1971).

Study of the anisotropy of low energy cosmic radiation of solar origin has clearly indicated that convection is the most important mechanism during the decay of the flare events. During the initial phase of the decay, the observed equilibrium anisotropy is from the sunward direction (McCracken et al., 1967, 1968; McCracken and Rao, 1970; Rao et al., 1971) suggestive of the convective removal of these particles by the solar wind. The equilibrium anisotropy during this period is given by the expression

$$\delta_c = 3C \frac{V_p}{V} \tag{1}$$

where C is the Compton–Getting factor, V_p the solar plasma velocity and V is the particle velocity.

At low energies ($\sim$10 MeV), the convective anisotropy is $\sim$10–15 per cent while at relativistic energies, the convective anisotropy is only $\sim$0·6 per cent. During late times in the decay, the anisotropy of low energy solar flare particles is observed to be from 45°E direction (McCracken et al., 1971; Rao et al., 1971) which has been interpreted as due to an equilibrium between the outward convective flow and the inward diffusion, the latter being caused by a positive density gradient set up in the interplanetary medium by the earlier enhanced convection. We believe that similar mechanism must also operate on galactic particles over short periods of time when equilibrium conditions are not established.

Separating the anisotropy vector into its two components, namely the convective and the diffusive vectors, Hashim et al. (1972) have recently shown that the diffusive vector is aligned along the interplanetary field direction. The field aligned inward diffusion caused by the establishment of a significant positive density gradient can result from either or both the processes (a) through the establishment of regions of decreased density (sink) in the garden-hose direction (b) through the establishment of regions of enhanced density

(source) in the anti-garden-hose direction, the physical processes responsible for the two mechanisms being possibly different.

In this communication, we show that the enhanced diurnal variation can be simply understood as due to a resultant between convection and enhanced field aligned diffusion by comparing the cosmic ray diurnal variation data with the interplanetary field data. We further show that the field aligned diffusion at early times during enhanced wave trains is caused by a sink in the garden-hose direction and at late times due to a source in the anti-garden-hose direction as a result of the establishment of a strong positive density gradient. Finally we show that even the average quiet day diurnal variation is explainable in terms of this new concept.

2. DATA MANIPULATION

The cosmic ray anisotropy characteristics have been determined from the data from a number of high and middle latitude neutron monitor stations well distributed in longitude and having narrow asymptotic cones of acceptance (See Table 1). As the Earth spins on

TABLE 1. PARTICULARS OF NEUTRON MONITORING STATIONS WHOSE DATA HAVE BEEN
USED IN THE ANALYSIS

| No. | Stations | Geographic co-ordinates | | Cut-off rigidity (GV) | Mean asymptotic co-ordinates | |
		Latitude (Deg)	Longitude (Deg)		Latitude (Deg)	Longitude (Deg)
1.	Ahmedabad	23·0	72·6	15·94	19	125
2.	Alert	82·5	297·7	<0·05	77	331
3.	Alma-Ata	43·2	76·9	6·69	25	143
4.	Calgary	51·1	245·9	1·09	28	269
5.	Churchill	58·8	265·9	0·21	40	286
6.	Dallas	32·8	263·2	4·35	25	316
7.	Deep River	46·1	282·5	1·02	27	319
8.	Durham	43·1	289·2	1·41	25	332
9.	Goose Bay	53·3	299·6	0·52	35	339
10.	Hermanus	−34·4	19·2	4·90	24	67
11.	Inuvik	68·4	226·3	<0·18	47	233
12.	Kiel	54·3	10·1	2·29	31	63
13.	Lindau	51·6	10·1	3·00	29	67
14.	Mawson	−67·6	62·9	0·22	−42	55
15.	Mt. Norikura	36·1	137·6	11·39	26	195
16.	Mt. Washington	44·3	288·7	1·14	25	331
17.	Mt. Wellington	−42·9	147·2	1·89	−25	193
18.	Pic-du-Midi	42·9	0·3	5·36	26	73
19.	Sulphur Mt.	51·2	244·4	1·14	27	270
20.	Wilkes	−66·4	110·5	<0·05	−56	107

its axis, each of these monitors scan a narrow region of the celestial sky. Combining the data from all the stations, three dimensional space time maps of cosmic ray intensity time profile in the interplanetary medium have been constructed using the method developed by Fenton et al. (1959), Ables et al. (1967), Mercer and Wilson (1968) and Carmichael and Steljes (1969). Such maps define the cosmic ray flux as a function of direction at any given time and thus provide an integrated view of the cosmic ray demography in space and therefore are ideally suited to study the characteristics of a rapidly evolving anisotropy and to identify the sources and sinks. During the period 1965–1969, there are about 25 such wave trains having enhanced diurnal amplitudes. For an unambiguous identification of sinks and sources, we have selected only four of these which are not accompanied by

large changes in the daily mean intensity. Figure 1 shows the selected abnormally high amplitude wave trains as observed at the Deep River neutron monitoring station.

The mean intensity three days prior to the commencement of the enhanced diurnal wave train, when not accompanied by large changes in flux, has been used for normalization purposes. Due to the inadequate coverage of certain longitudes because of the non-availability of neutron monitoring stations, we have been able to represent the intensity in only eight directions in space at any time, each directional belt covering a width of 3 hr in longitude. The mean of the observed amplitude in different directions have been obtained taking care to normalize the amplitude at each station to the width and declination of its asymptotic cone of acceptance. Three dimensional space–time diagrams are drawn for each three hourly interval on each day.

Besides the use of three dimensional space–time intensity profile maps, the data at various stations have also been utilised to derive the diurnal and semi-diurnal anisotropy
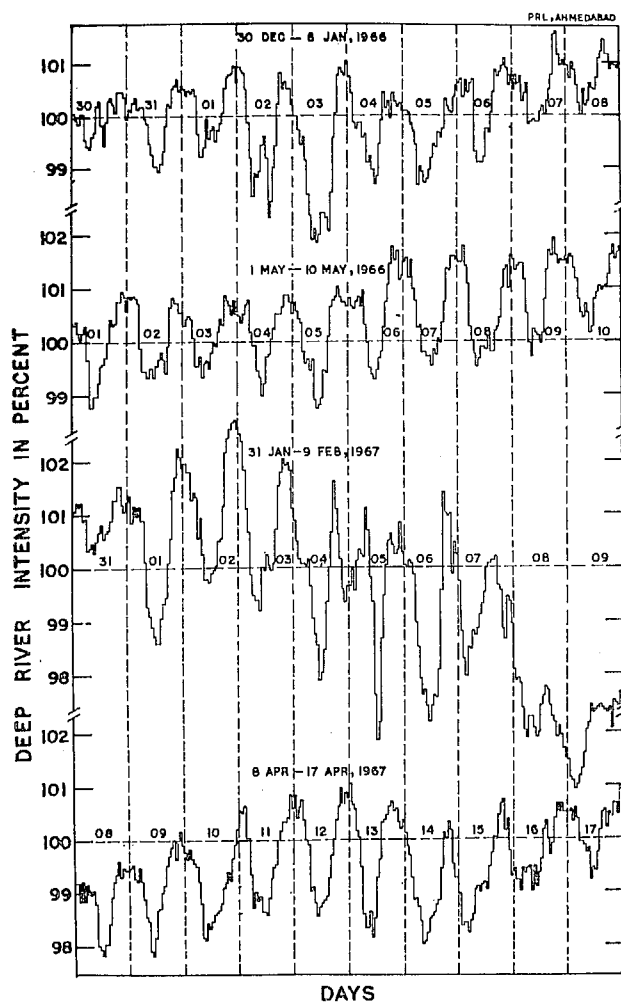
FIG. 1. SHOWING TYPICAL ENHANCED DIURNAL WAVE TRAINS AS OBSERVED BY THE DEEP RIVER NEUTRON MONITOR.

amplitudes and phases in space along with their energy spectral characteristics using the variational coefficient techniques developed by Rao *et al.* (1963) and McCracken *et al.* (1965). The interplanetary field parameters for each of these days have also been obtained from Pioneer 6, Explorer 33 and 35 measurements for comparison with the diurnal anisotropy vectors.

3. LOCATION OF SOURCES AND SINKS DURING DAYS OF ENHANCED DIURNAL VARIATION

McCracken *et al.* (1966) have suggested that the corotating Forbush decreases often observed in the low energy cosmic radiation ($\sim$10 Mev) will essentially manifest themselves as enhanced diurnal variation at relativistic energies, the depressed intensity along the garden-hose direction causing the diurnal maxima to occur along the anti-garden-hose direction. The enhanced diurnal wave train which occurred during 30 December, 1965–7 January, 1966 coincides with the corotating Forbush decrease event identified by McCracken *et al.* (1966) and we use it to test the above suggestion. Figure 2 presents the intensity profile in different directions (1200 corresponding to sunward direction)
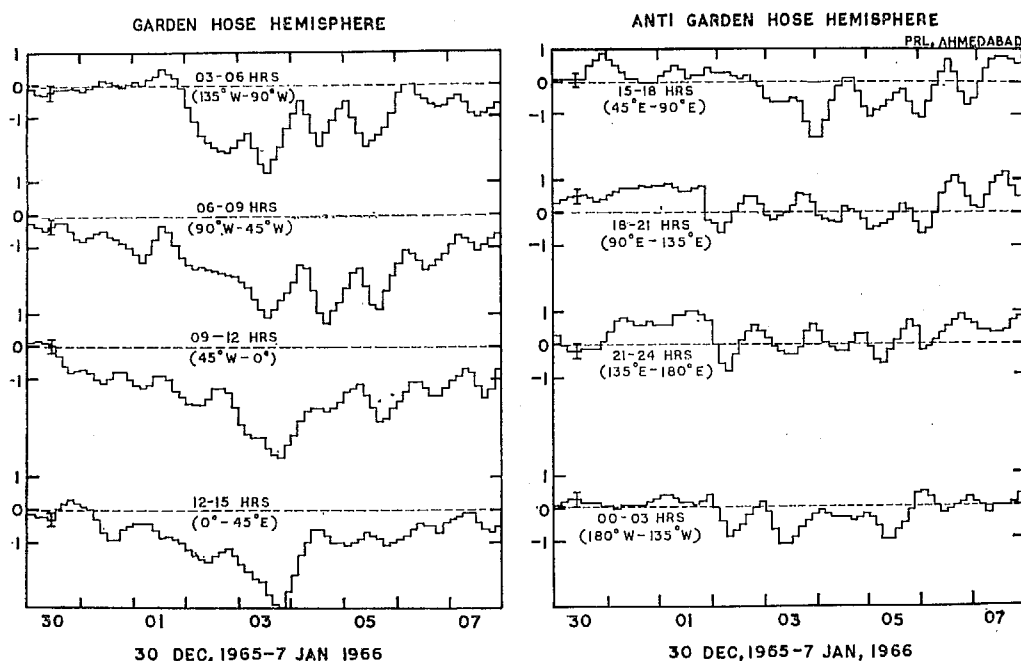
FIG. 2. COSMIC RAY SPACE TIME INTENSITY DIAGRAM DURING THE PERIOD 30 DECEMBER, 1965–7 JANUARY, 1966, DURING WHICH THE COSMIC RAY NEUTRON MONITORING STATIONS RECORDED ENHANCED DIURNAL ANISOTROPY.

during 30 December, 1965–7 January, 1966 in which period enhanced diurnal amplitude was recorded by various neutron monitors. During this period, a large depression of intensity ($\sim$2 per cent) is observed in the garden-hose hemisphere, whereas the intensity in the anti-garden-hose hemisphere is practically unaffected. In Fig. 3 the average intensity for five days (2 January–6 January, 1966) during which the garden-hose depression was predominant, is plotted as a function of direction which dramatically brings out the large depression centred around the garden-hose direction. Earlier analysis of Mathews *et al.*
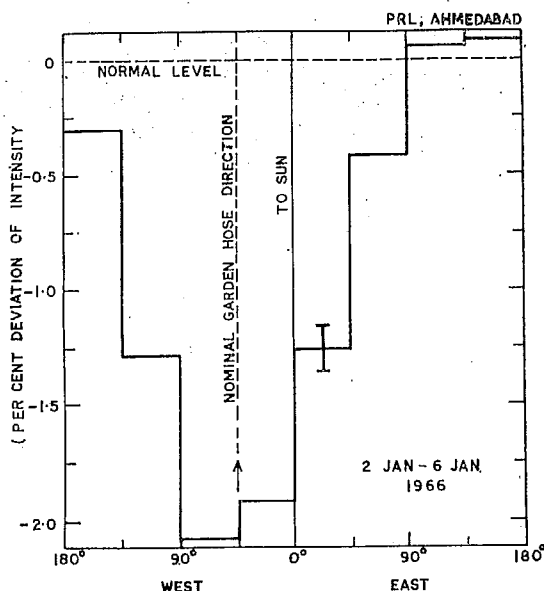
FIG. 3. MEAN COSMIC RAY INTENSITY AS A FUNCTION OF DIRECTION IN SPACE DURING 2–6 JANUARY, 1966, WHEN ENHANCED DIURNAL VARIATION DUE TO A PREDOMINANT GARDEN-HOSE DEPRESSION WAS OBSERVED BY THE NEUTRON MONITORING STATIONS.

(1969) and of Hashim and Thambyahpillai (1969) of a few events also confirm the presence of such an enhanced depression along the garden-hose direction causing enhanced diurnal variation.

In contrast to the above simple picture the long lived enhanced diurnal variation event of 30 April–11 May, 1966 shows a complex behaviour. Figure 4 shows the evolution of the cosmic ray flux distribution in space at various times during 30 April–11 May, 1966. On 29 April, 1966, prior to the commencement of the enhanced wave train, the cosmic ray flux distribution in space was found to be practically isotropic (Fig. 4a) showing a normal diurnal variation. During the early part of the enhanced diurnal variation event, i.e. 1–7 May, 1966, the cosmic ray intensity in the garden-hose direction is found to be well depressed below the normal level (Fig. 4b, 4c). By 9 May, the cosmic ray flux along the garden-hose direction seems to be just recovering to its normal value (Fig. 4e). However, the cosmic ray intensity in the anti-garden-hose direction is now found to show a large excess above the normal intensity (Fig. 4f, 4g). Thus during the later part of the event, i.e. 8–11 May, 1966, the enhanced diurnal amplitude seems to be caused by a source in the anti-garden-hose direction. We note that such a behaviour is to be expected in terms of the explanation offered by McCracken et al. (1971) and Rao et al. (1971) for the observed easterly anisotropy late in the decay of low energy solar flare events. Using similar arguments, we can expect during such times the enhanced convection by the high velocity solar wind associated with the initial shock wave which causes depressed intensity along the garden-hose-direction, to eventually establish a positive density gradient and thus a source along the anti-garden-hose direction during the later part of such enhanced diurnal wave train events.

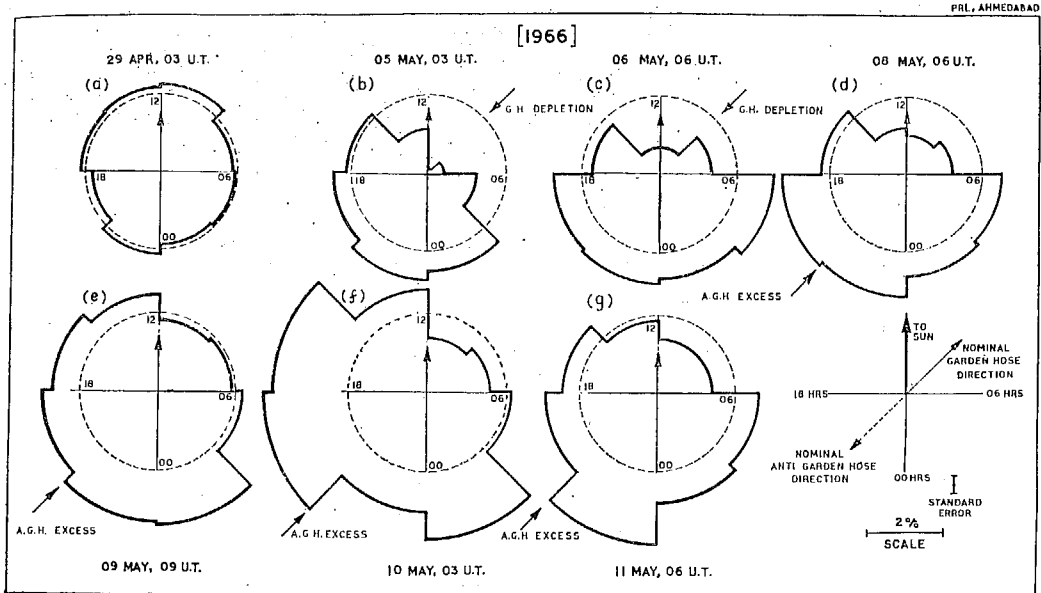We wish to emphasise that the simple harmonic analysis of the data would not have

FIG. 4. SHOWING THE EVOLUTION OF ANISOTROPY DURING THE ENHANCED DIURNAL VARI-
ATION EVENT OF 30 APRIL–11 MAY, 1966.

Note that during the early part of the event, the cosmic ray intensity is depleted along the
garden-hose direction and during late in the event the cosmic ray flux in the garden-hose
recovers to the normal value (shown by thin circle) whereas the flux in the anti-garden-
hose direction shows a large excess.

revealed the complete physical nature of the mechanism. Both a source in the anti-garden-
hose and a sink in the garden-hose directions essentially give the same time of maxima,
i.e. around ~2000 hr. It is only through the type of analysis presented in this paper
that the existence of sources and sinks in space can be identified. In the next section, we
show that the enhanced diurnal variation whether caused by a sink in the garden-hose or a
source in the anti-garden-hose direction can be explained as a resultant of normal convection
and enhanced field aligned diffusion.

Referring to Fig. 4, we see that the change over from a sink in the garden-hose direction
to a source in the anti-garden-hose direction occurs in a period of 4–5 days suggesting that
the relaxation time of the interplanetary medium to follow the changes in the density
gradient in the entire modulating region is of the order of 4–5 days. For the normal solar
wind velocity observed during such periods, this would indicate that the dimension of the
modulating region is of the order of 2 AU thus providing an independent experimental
evidence for the location of a boundary sometimes assumed in dealing with the cosmic ray
transport.

4. CHARACTERISTICS OF ENHANCED DIURNAL VARIATION

The enhanced diurnal variation amplitude and phase on each day has been obtained for
each of these events. The diurnal variation during such events is observed to show a maximum
at about 2000 hr during the entire period of enhanced diurnal variation in contrast with
the 1800 hr maximum observed for corotational anisotropy. Figure 5 shows the diurnal
anisotropy amplitude and the time of maximum for each day for two of the events along
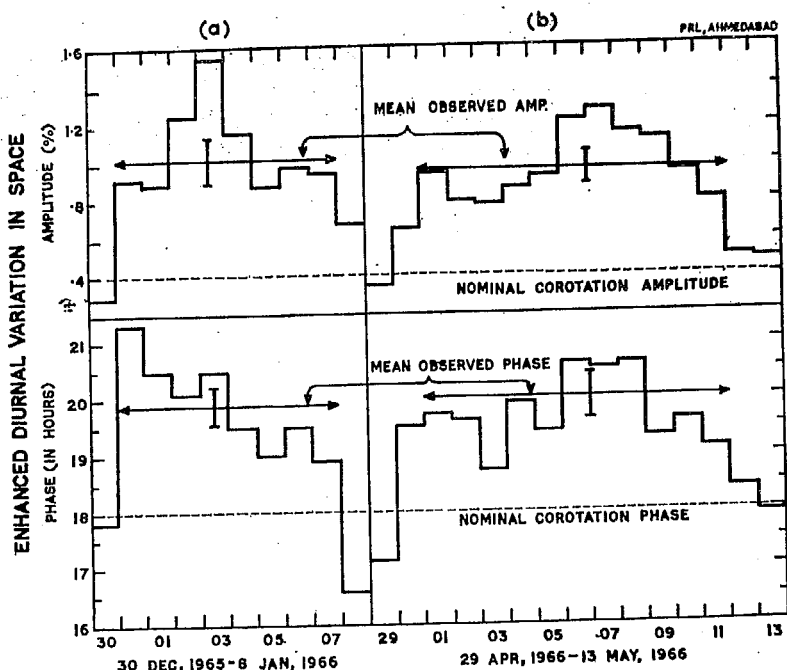with the average value of these parameters for each of the events.

FIG. 5. THE AMPLITUDE AND PHASE OF THE DIURNAL ANISOTROPY IN SPACE ON EACH DAY DURING (a) 30 DECEMBER 1965–8 JANUARY, 1966 AND (b) 29 APRIL–13 MAY, 1966 DERIVED FROM THE DATA FROM A NUMBER OF NEUTRON MONITOR STATIONS.

The figure includes some observations both prior and later to the actual enhanced diurnal event. The mean phase and amplitude during the event is marked by an arrow.

The energy spectrum of variation for each of the enhanced diurnal variation events has been calculated using the well known method given by Rao *et al.* (1963). Computing the direction of anisotropy in space as observed by different stations for different values of the spectral exponent, the variance between the different values has been calculated. The spectral exponent corresponding to the minimum variance represents the true spectral exponent of the diurnal anisotropy. Figure 6 shows the plot of the variance in the diurnal time of maximum as a function of the spectral exponent along with the number of neutron monitoring stations whose data have been utilised for the spectral determination. The figure clearly shows that the spectral exponent in each case is consistent with it being energy independent (0 ± 0.2).

The mean amplitude and phase of the semi-diurnal component during the periods of enhanced diurnal variation generally do not exhibit any significant departure from the average picture of the semi-diurnal component given by Rao and Agrawal (1970). We, therefore, have neglected the semi-diurnal component from our discussion.

5. ENHANCED FIELD ALIGNED DIFFUSION DURING DAYS OF ENHANCED DIURNAL VARIATION

In order to establish the field aligned nature of the diffusive flow due to either a sink in the garden-hose or a source in the anti-garden-hose direction, we resolve the observed diurnal vector into two components.

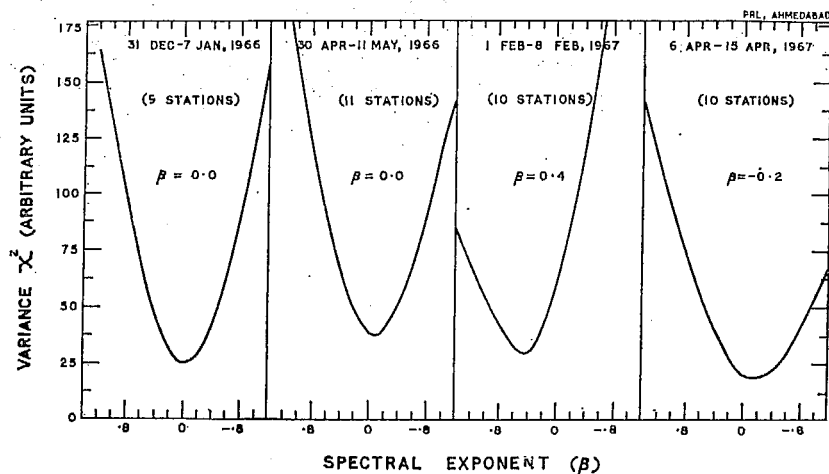$$\delta = \delta_c + \delta_d \qquad (2)$$

FIG. 6. VARIANCE IN THE OBSERVATIONAL VALUES OF THE DIURNAL TIME OF MAXIMUM AS A FUNCTION OF THE SPECTRAL EXPONENT FOR EACH EVENT. THE MINIMUM VARIANCE IN ALL CASES IS CONSISTENT WITH AN ENERGY INDEPENDENT SPECTRAL EXPONENT ($\beta = 0 \pm 0.2$).

where δ_c is the anisotropy vector due to convective flow, and δ_d is the anisotropy vector due to diffusive flow. The amplitude of δ_c is ≈ 0.6 per cent when determined according to Equation (1) with a solar wind speed ≈ 400 km/sec and $C = 1.5$, which is appropriate to the mean energy of response (~ 8 GeV). The space anisotropy amplitude obtained from neutron monitor observations, using the correction factors for the geomagnetic bending and width of the asymptotic cones of acceptances as given in IQSY manual (McCracken *et al.*, 1965) is ~ 0.4 per cent. When this is corrected for the changes in C with energy, the upper cut off rigidity and the detector response (Subramanian, 1971), the free space amplitude would be ~ 0.6 per cent. In all our treatment however, we shall deal only with the uncorrected space amplitude of 0.4 per cent, since the correction as suggested by Subramanian will only increase the true amplitude by a constant factor and will not change any of our conclusions. Using a value of 0.4 per cent in the 1200 hr direction for the convective vector, the magnitude and direction of the diffusive vector δ_d for each day for each of the four events has been calculated. Similarly the magnitude and the direction of the inter-planetary field vector for each day has also been calculated from the direct spacecraft observations (Pioneer 6, Explorer 33 or Explorer 35). In Fig. 7, the diffusive flow vectors for each day is plotted end to end separately for each of the four events along with the interplanetary field vector to demonstrate the field aligned nature of the diffusive flow even on a day to day basis.

The mean diffusive vector and the corresponding mean interplanetary field vector are plotted for each of the four events in Fig. 8 (see also Table 2). Both Figs. 7 and 8 clearly demonstrate that the enhanced diurnal variation is caused by a superposition of the enhanced field aligned diffusion over the normal convective flow.

6. QUIET DAY DIURNAL VARIATION

In this section we extend the analysis of the role of convection and diffusion to the quiet day diurnal variation to show that the present concept of diurnal variation being due to convection and parallel diffusion applies most of the time. For this purpose, we have
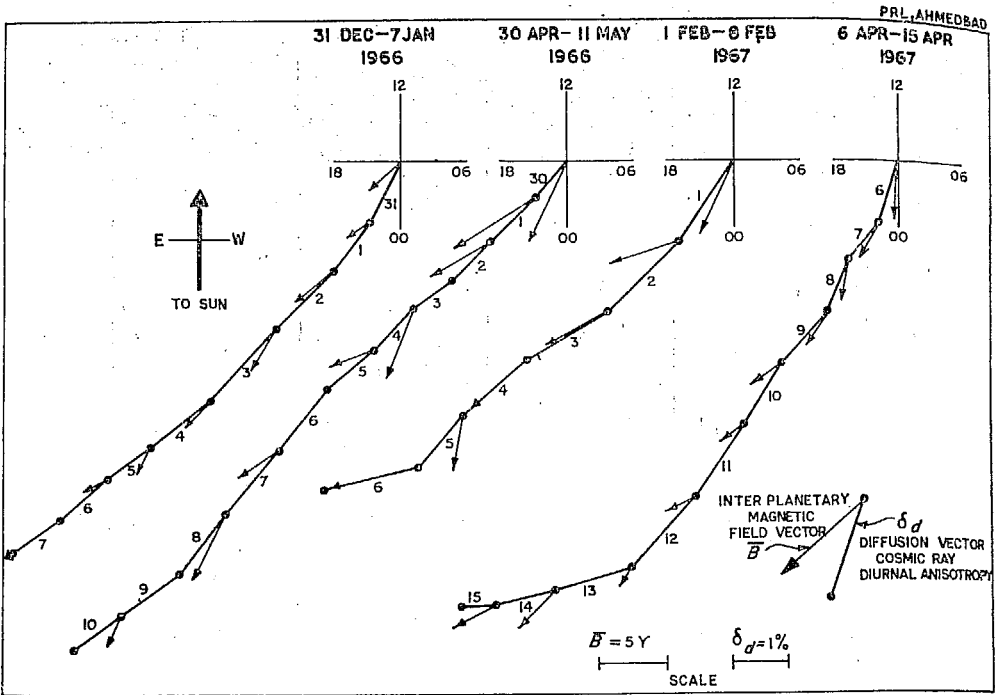
FIG. 7. SHOWING THE COSMIC RAY ANISOTROPY DIFFUSION VECTOR FOR EACH DAY PLOTTED END TO END FOR EACH OF THE FOUR ENHANCED DIURNAL VARIATION EVENTS.

The interplanetary magnetic field vector for each day is also plotted alongside the diffusive vector for each day. Note the good agreement between the field azimuth and the direction of the diffusive vector confirming the field aligned nature of the diffusive vector.
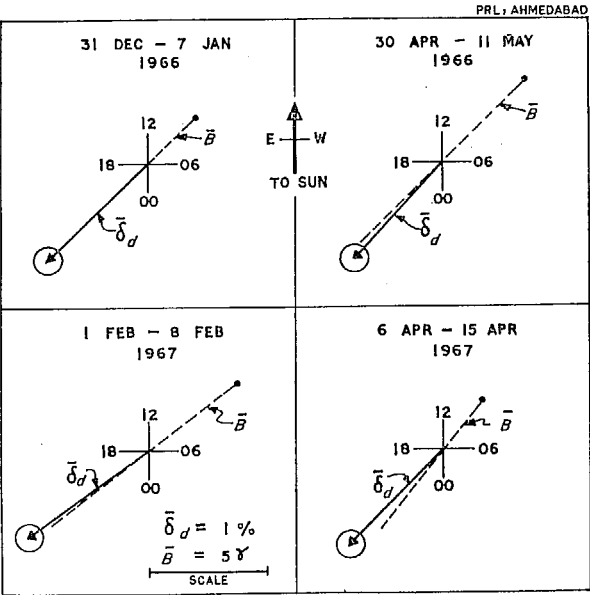

FIG. 8. SHOWING THAT THE AVERAGE DIFFUSIVE ANISOTROPY VECTOR FOR EACH EVENT IS ALIGNED PARALLEL OR ANTI-PARALLEL TO THE AVERAGE INTERPLANETARY MAGNETIC FIELD VECTOR DURING THE EVENTS EXHIBITING ENHANCED DIURNAL VARIATION.

TABLE 2. MEAN DIURNAL ANISOTROPY VECTOR, MEAN DIFFUSIVE VECTOR AND THE MEAN INTERPLANETARY MAGNETIC FIELD VECTOR DURING THE SELECTED ENHANCED DIURNAL VARIATION EVENTS

No.	Events	Mean diurnal anisotropy vector		Mean diffusion vector		Mean magnetic field vector		Phase diff.
		amp (%)	phase ϕ (Deg)	amp (%)	phase ϕ_d (Deg)	amp (γ)	phase ϕ_B (Deg)	$\phi_d - \phi_B$ (Deg)
1.	31 *Dec.*– 7 *Jan.* 1966	1·02 ± 0·12	298 ± 5	1·26	314	3·0	314	0 ± 5
2.	30 *Apr.*–11 *May* 1966	0·91 ± 0·08	301 ± 6	1·17	318	5·1	315	3 ± 6
3.	1 *Feb.*– 8 *Feb.* 1967	1·10 ± 0·10	289 ± 7	1·29	306	4·9	308	−2 ± 7
4.	6 *Apr.*–15 *Apr.* 1967	0·92 ± 0·07	299 ± 4	1·17	316	2·8	322	−6 ± 4

(Derived using correction factors given in IQSY manual)

utilised the neutron monitor data for the entire period of January 1967–December, 1968, for which the interplanetary field data is available. We have utilised the data on all days excepting the days of Forbush decrease onset when large intensity gradients are observed. The average diurnal variation parameters for each of the 27 day solar rotation periods, and the average interplanetary field parameters for each of these rotations have been calculated separately. Table 3 lists the parameters along with the average diffusion vectors derived from the cosmic ray diurnal vectors using Equation (2) and the computed difference

TABLE 3. THE 27 DAY AVERAGE COSMIC RAY DIURNAL VECTOR, COSMIC RAY DIFFUSIVE VECTOR (SEE TEXT) AND INTERPLANETARY FIELD VECTOR FOR DIFFERENT SOLAR ROTATIONS DURING 1967–1968. THE COMPUTED PHASE DIFFERENCE BETWEEN THE DIFFUSIVE VECTOR AND THE FIELD VECTOR IS ALSO LISTED

No.	Solar rotation no.	No. of days used	Mean diurnal anisotropy vector		Mean diffusion* vector		Mean magnetic field vector		Phase diff.
			amp (%)	phase ϕ (Deg)	amp (%)	phase ϕ_d (Deg)	amp (γ)	phase ϕ_B (Deg)	$\phi_d - \phi_B$ (Deg)
1.	1826	15	0·43 ± 0·06	255 ± 7	0·51	305	3·2	306	−1 ± 7
2.	1827	20	0·63 ± 0·02	270 ± 5	0·74	303	3·9	308	−5 ± 5
3.	1828	19	0·30 ± 0·05	279 ± 5	0·54	326	3·5	307	19 ± 5
4.	1829	16	0·81 ± 0·07	288 ± 6	1·00	310	2·9	321	−11 ± 6
5.	1830	10	0·51 ± 0·07	263 ± 5	0·61	304	3·2	324	−20 ± 5
6.	1833	13	0·20 ± 0·06	266 ± 8	0·45	333	3·3	325	8 ± 8
7.	1834	16	0·20 ± 0·03	239 ± 10	0·34	330	3·5	321	9 ± 10
8.	1835	21	0·45 ± 0·07	254 ± 9	0·51	303	3·7	308	−5 ± 9
9.	1836	19	0·34 ± 0·02	274 ± 5	0·54	321	3·7	312	9 ± 5
10.	1837	16	0·26 ± 0·06	313 ± 4	0·60	342	3·6	312	30 ± 4
11.	1838	24	0·39 ± 0·04	270 ± 2	0·56	315	4·2	311	4 ± 2
12.	1939	20	0·52 ± 0·07	263 ± 10	0·62	303	4·1	301	2 ± 10
13.	1840	17	0·33 ± 0·05	274 ± 10	0·53	322	3·7	312	10 ± 10
14.	1841	13	0·42 ± 0·06	267 ± 5	0·56	312	4·2	309	3 ± 5
15.	1842	19	0·52 ± 0·09	268 ± 10	0·65	306	3·5	314	−8 ± 10
16.	1843	22	0·64 ± 0·05	281 ± 6	0·82	310	3·6	316	−6 ± 6
17.	1844	21	0·49 ± 0·05	272 ± 8	0·64	311	3·8	320	−9 ± 8
18.	1845	19	0·35 ± 0·02	264 ± 8	0·50	317	3·3	313	4 ± 8
19.	1846	16	0·40 ± 0·06	235 ± 10	0·36	299	3·1	312	−13 ± 10
20.	1847	17	0·36 ± 0·02	278 ± 9	0·57	322	3·4	313	9 ± 9
21.	1848	16	0·47 ± 0·05	267 ± 4	0·60	309	4·0	304	5 ± 4
22.	1849	18	0·30 ± 0·07	268 ± 11	0·49	322	3·0	318	4 ± 11
23.	1850	18	0·46 ± 0·05	280 ± 6	0·66	317	3·9	312	5 ± 6
24.	1851	13	0·42 ± 0·04	294 ± 6	0·69	326	4·1	321	5 ± 6
25.	1852	23	0·33 ± 0·03	250 ± 11	0·42	313	3·6	311	2 ± 11

(Derived using correction factors given IQSY manual)

* The errors in the mean diffusive vector are of the same order as the errors in mean anisotropy vector.

between the diffusive vector and the field vector. Figure 9 shows the histogram of the phase difference between the average diffusive vector and the average interplanetary field vector. Both Table 3 and Fig. 9 show that in nearly 80 per cent of the cases, the phase difference between the diffusive vector and interplanetary field vector even on a 27 day average basis is $\leqslant 10°$, which is of the same order as the standard error of the observations thus indicating that the average quiet day diffusive vector is also field aligned.

The diffusive vector can be resolved into two components, one parallel to **B** vector and another perpendicular to it, the amplitude of the perpendicular component being a measure of the non-field aligned component. From Fig. 10 which shows the plot of the parallel and perpendicular components of the average diffusive vectors for different solar rotations, it is evident that the parallel component corresponding to the field aligned component dominates and the perpendicular component is usually less than a tenth of the parallel component.

The annual mean diurnal anisotropy has an amplitude of ≈ 0.35 per cent and a direction of maximum around 1800 hr (Rao, 1972) during the period 1964–1970. The annual mean diffusive vector for each year during this period has been calculated using Equation (2). The yearly average interplanetary field direction has been derived from the observed yearly average solar wind velocity (Gosling *et al.*, 1971) and assuming Archimedean spiral structure for the field. Comparison of the field azimuths for the period 1967–1968 computed from solar wind observations with actual interplanetary magnetic field observations show that these agree within 2–3°. Table 4 lists the yearly average diurnal variation parameters and the deduced interplanetary field parameters along with the computed phase difference between the yearly average diffusive vector and the corresponding field vector. The average diffusive vectors calculated for each year during 1964–1970 is also plotted in Fig. 10 along with the mean diffusive vector for the entire period 1964–1970.

The yearly mean diffusive vector for the entire period has an amplitude of 0.53 ± 0.01 per cent and makes an angle of $3 \pm 2°$ with the interplanetary field vector, the phase difference being of the same order as the observational error. In other words, the figure clearly indicates that within the observational errors, the yearly average diurnal variation is also completely explainable in terms of summation of a normal convective vector and a field aligned diffusive vector. Except during 1965 when the diffusive vector makes an angle of 11°, the diffusive vector during other years is practically aligned with the field direction. In addition to the average picture, we have also examined, in great detail, the diurnal variation on a day-to-day basis and we observe that during 1967–1968, on more than ~ 60 per cent of the days, the diffusive vector is essentially field aligned and $k_\perp$ is negligible even on a day-to-day basis. The detailed results of the analysis on a day-to-day basis will be published later.

7. DISCUSSION AND CONCLUSIONS

We now examine whether an unified model can be proposed to explain the diurnal variation, both quiet and enhanced as well as anisotropy of low energy solar flare cosmic radiation. Figure 11 depicts such a model. Referring to Fig. 11 (a), we observe that at early times in a flare event, the diffusive current driven by a negative cosmic ray density gradient due to solar produced particles dominates over the small convective vector resulting in a predominantly field aligned anisotropic flux. During late times the solar cosmic ray flow is in equilibrium and is consistent with it being simply convected out by the solar wind. At very late times, the positive density gradient created by the earlier convection provides a
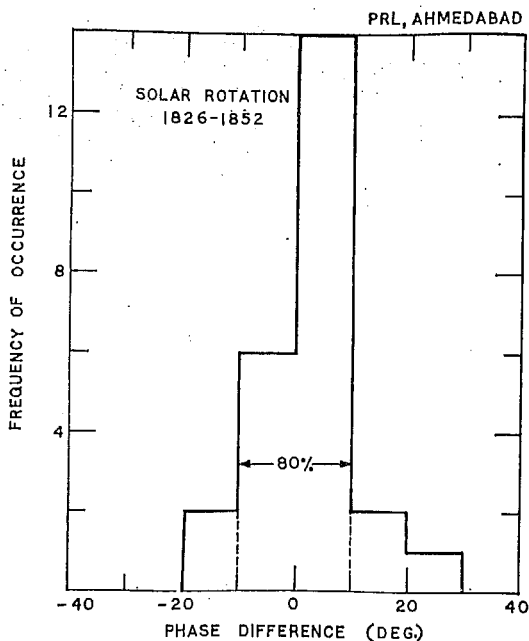
FIG. 9. HISTOGRAM SHOWING THE DISTRIBUTION OF PHASE DIFFERENCE BETWEEN THE AVERAGE COSMIC RAY DIFFUSIVE VECTOR AND THE AVERAGE MAGNETIC FIELD VECTOR FOR A NUMBER OF SOLAR ROTATIONS 1826–1852.
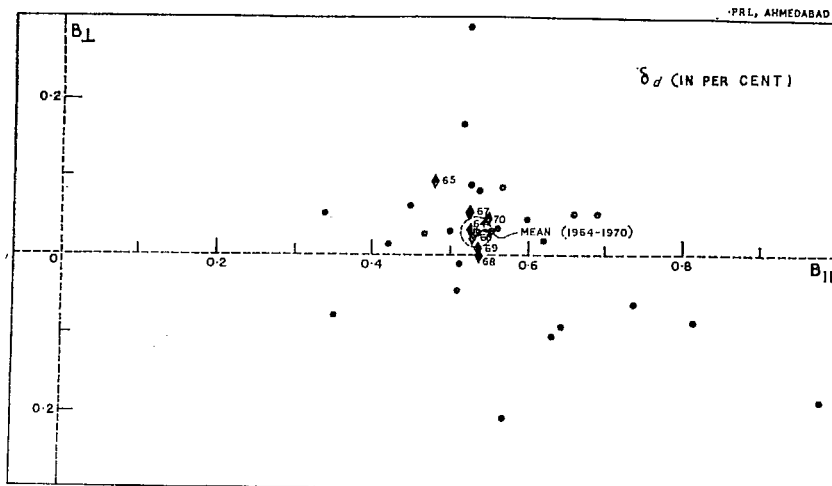

FIG. 10. SHOWING THE TWO COMPONENTS OF THE AVERAGE DIFFUSIVE VECTOR, ONE PARALLEL AND THE OTHER PERPENDICULAR TO THE AVERAGE INTERPLANETARY FIELD VECTOR FOR DIFFERENT SOLAR ROTATIONS (1826–1852) DURING JANUARY, 1967–DECEMBER, 1968.

The two components of the annual mean diffusive vector for the entire period during 1964–1970 are also shown in the figure.

TABLE 4. SHOWING THE PHASE DIFFERENCE BETWEEN THE YEARLY COSMIC RAY DIFFUSIVE VECTOR AND THE MEAN FIELD VECTOR. THE FIELD AZIMUTH HAS BEEN CALCULATED FROM SOLAR WIND VELOCITY ASSUMING ARCHIMEDEAN SPIRAL CONFIGURATION. THE COSMIC RAY DIFFUSIVE VECTOR IS COMPUTED FROM THE OBSERVED AVERAGE DIURNAL VECTOR USING EQUATION (2)

Year	Mean diurnal anisotropy vector		Mean diffusion vector		Mean solar wind velocity (km/sec)	Mean magnetic field direction ϕ_B (Deg)	Phase diff. $\phi_d - \phi_B$ (Deg)
	amp (%)	phase ϕ (Deg)	amp (%)	phase ϕ_d (Deg)			
1964	0.35 ± 0.03	272 ± 3	0.53	321	431	317	4 ± 3
1965	0.28 ± 0.02	270 ± 4	0.49	326	407	315	11 ± 4
1966	0.36 ± 0.02	271 ± 3	0.53	319	413	316	3 ± 3
1967	0.35 ± 0.01	272 ± 5	0.53	321	394	315	6 ± 5
1968	0.37 ± 0.01	270 ± 3	0.54	318	453	318	0 ± 3
1969	0.36 ± 0.01	270 ± 2	0.54	318	422	317	1 ± 2
1970	0.37 ± 0.02	271 ± 2	0.55	319	390	314	5 ± 2
Mean (1964–1970)	0.35 ± 0.01	271 ± 2	0.53	320	418	317	3 ± 2
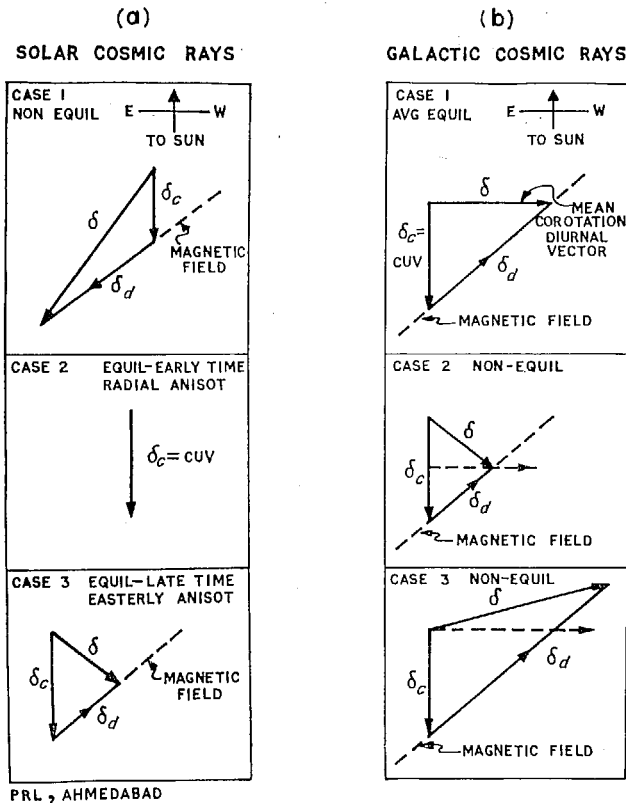
FIG. 11. A UNIFIED MODEL FOR EXPLAINING THE ANISOTROPY OF LOW ENERGY COSMIC RAY FLARE PARTICLES AND ALSO THE DIURNAL ANISOTROPY OF HIGH ENERGY PARTICLES IN TERMS OF SIMPLE CONVECTION AND FIELD ALIGNED DIFFUSION (SEE TEXT FOR EXPLANATION).

diffusive current which when superposed upon the convective vector results in an easterly anisotropy. The model embodying the extension of the same ideas to the galactic anisotropy is depicted in Fig. 11(b). Under equilibrium condition, when there is no net flow of cosmic radiation either into or from the solar system, the radial convection current $S_c = CUV$ is exactly balanced by the radial component of inward diffusion $k_\parallel (\partial U/\partial r)_\parallel$ resulting in an average observed corotation anisotropy of ≈ 0.4 per cent along 1800 hr direction. On a day-to-day basis, the diffusion vector need not exactly balance the convective vector. In the case when the diffusion vector is smaller, the resulting observed anisotropy would show a maximum earlier than 1800 hr and in the case of enhanced diurnal variation when the diffusive vector is very much greater than the convective vector, the time of maximum of the resulting diurnal variation will shift towards ~ 2100 hr, the mean direction of the inter-planetary magnetic field. The diffusive vector, in all cases, is aligned parallel or anti-parallel to the magnetic field.

The diffusion current (Gleeson, 1969; Forman and Gleeson, 1970) can be written

$$S_d = k_\parallel \left(\frac{\partial U}{\partial \mathbf{r}}\right)_\parallel + k_\perp \left(\frac{\partial U}{\partial \mathbf{r}}\right)_\perp \tag{3}$$

and since the average co-rotational anisotropy is obtained assuming the radial current $S_r = 0$ and $k_\perp$ to be negligible we may use this together with

$$\delta_d = 3S_d/VU \tag{4}$$

and the observed free space anisotropy to calculate first the density gradient along the magnetic field $(1/U) | (\partial U/\partial r)_\parallel|$ and from this the radial gradient

$$G = \frac{1}{U} \left|\left(\frac{\partial U}{\partial \mathbf{r}}\right)_\parallel\right| \Big/ \cos \psi \tag{5}$$

with ψ the angle between the magnetic field and the radial direction.

The magnetic power spectra of Jokipii and Coleman (1968) and Bercovitch (1971a) indicate that at neutron monitor energies $k_\parallel \approx 5 \times 10^{21} p \beta$ cm^2 sec^{-1} ($p =$ rigidity, $\beta = V/c$) and, from the observed mean diffusive anisotropy of 0.53 ± 0.01 per cent the corresponding free space anisotropy is ≈ 0.8 per cent. These values lead to a radial gradient ≈ 4.5 per cent AU which is in good agreement with those from many other independent observations and summarised by Bercovitch (1971b). During the period of enhanced diurnal variation the observed average diffusive vector (Table 2) is seen to be about 1.2 ± 0.1 per cent which corresponds to an enhanced positive radial density gradient of ≈ 10 per cent/A.U. These gradients are sensitive to the value assumed for the diffusion coefficient.

From Figs. 9 and 10, we observe that the mean diffusive vectors obtained on 27 day and annual average basis are essentially field aligned, the phase difference between the diffusive vector and the field vector being, on an average, $3° \pm 2°$. This indicates that on an average, the ratio $k_\perp/k_\parallel \leqslant 0.05$ (from Equation 3) which is consistent with the low energy observations.

It must be emphasised that even though $k_\perp$ is negligible on an average basis, there are occasions when it can be significant and which might result in a partial or complete cancellation of the diurnal anisotropy. Figure 12 shows some representative examples of trains of days when the observed diurnal variation at Deep River was negligible over a period of days. We have examined the average diurnal as well as the diffusive vectors for two such events which occurred on 27 August–1 September, 1967 and 27 July–1 August, 1968 for
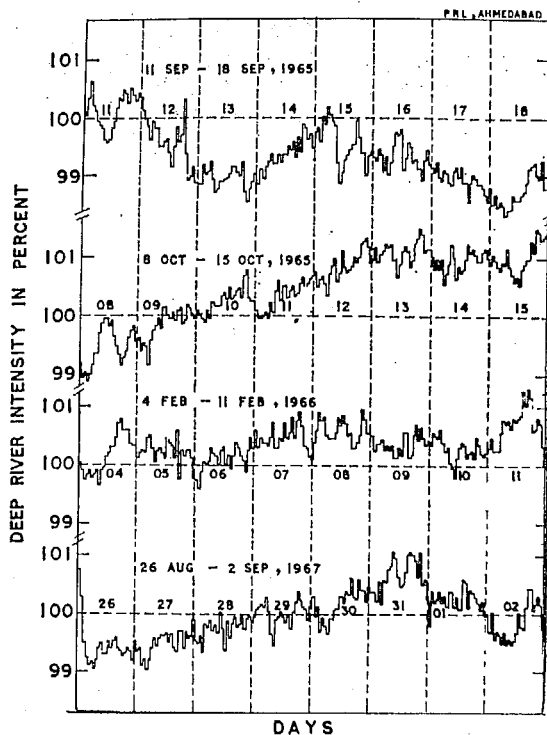
FIG. 12. TYPICAL EXAMPLES SHOWING THE COSMIC RAY INTENSITY AT DEEP RIVER DURING ABNORMALLY LOW DIURNAL AMPLITUDE DAYS.

which concurrent magnetic field data are available. For both these events, we find that the average diurnal amplitude is about 0·15 per cent and the phase difference between the average diffusive vector and the field vector is $\sim 25° \pm 8°$ indicating that for such periods $k_\perp/k_\parallel \approx 0·5 \pm 0·2$, which exceeds greatly the normal value of $\sim 0·05$ observed during other days. Similarly the slight reduction in the observed average amplitude of diurnal variation in 1965 can be attributed (Fig. 11) to the increased value of $k_\perp$, $k_\perp/k_\parallel$ for 1965 being about $0·19 \pm 0·04$ almost a factor of three greater than the values observed during other periods.

From the data presented earlier and the discussion, we draw the following conclusions:

(1) The diurnal variation during both quiet and disturbed periods can be understood in terms of convection and field aligned diffusion. On an average basis, the net radial convection current is zero, i.e. the convection and diffusion vectors balance each other resulting in corotational anisotropy. On a day-to-day basis, the two vectors do not balance each other resulting in varying amplitudes and times of maxima for the observed diurnal anisotropy. The proposed mechanism can also explain the observed anisotropies of low energy cosmic ray flux during solar flare events. In other words, the changes in the diurnal anisotropy of cosmic radiation is explainable in terms of redistribution of cosmic ray flux following transient changes in the interplanetary medium.

(2) The diffusion vector, at most times is field aligned.

(3) On an annual or 27 day average basis, the phase difference between the diffusion vector and the interplanetary field vector is $\approx 3° \pm 2°$ which indicates that the ratio of

the perpendicular diffusion coefficient to parallel diffusion coefficient is $\leqslant 0.05$. In other words, the transverse gradients, on an average basis, are negligible.

(4) The quiet day diffusion vector has an amplitude of 0.53 ± 0.01 per cent on an average basis, which corresponds to a positive radial density gradient of ≈ 4.5 per cent/AU.

(5) The spectral characteristics and observed time of maxima during periods of enhanced diurnal variation are consistent with their being caused by a superposition of convective flow with enhanced field aligned diffusive flow.

(6) During the early part of the enhanced diurnal wave train, the abnormal variation is caused by a depletion (sink) of cosmic ray particle population from the garden-hose direction. At late times, the earlier enhanced convection eventually sets up a source along the anti-garden-hose direction. Thus during the later part of the enhanced diurnal wave train, the abnormal variation is caused by a source along the anti-garden-hose direction. In both cases, the density gradient is positive.

(7) The change over from garden-hose sink to anti-garden-hose source requires about 4–5 days which represents a relaxation time of the modulation region having a dimension of about 2–3 AU.

(8) The enhanced field aligned diffusion vector during periods of enhanced diurnal variation causes the observed time of maximum of the resultant diurnal anisotropy to shift to later hours (around 2000 hr).

(9) The enhanced diffusion vector, on an average basis, has an amplitude of 1.2 ± 0.1 per cent which corresponds to an enhanced positive radial density gradient of ≈ 10 per cent/AU.

(10) Even though the ratio $k_\perp/k_\parallel$ is, on an average, negligible, there are days on which it could be significant which causes a drastic reduction in the diurnal variation. The small reduction in the average diurnal amplitude in 1965 can be attributed to an increase in the ratio of $k_\perp/k_\parallel$ by a factor of ~ 3 as compared to other periods.

REFERENCES

ABLES, J. G., BAROUCH, E. and MCCRACKEN, K. G. (1967). *Planet. Space Sci.* **15**, 547.
ANANTH, A. G., AGRAWAL, S. P. and RAO, U. R. (1971). *Proc. 12th Int. Conf. on Cosmic Rays* (Hobart) **2**, 651.
AXFORD, W. I. (1965). *Planet. Space Sci.* **13**, 115.
BERCOVITCH, M. (1971a). *Proc. 12th Int. Conf. on Cosmic-rays* (Hobart) **2**, 579.
BERCOVITCH, M. (1971b). *Rapporteur Report, Intensity Gradients in the Solar System* (Hobart).
CARMICHAEL, H. and STELJES, J. F. (1969). *World Data Centre A, Rep.* UAG-5, Feb.
FENTON, A. G., MCCRACKEN, K. G., ROSE, D. C. and WILSON, B. G. (1959). *Can J. Phys.* **37**, 970.
FORMAN, M. A. (1970). *J. geophys. Res.* **75**, 3147.
FORMAN, M. A. and GLEESON, L. J. (1970). Unpublished.
GLEESON, L. J. (1969). *Planet. Space Sci.* **17**, 31.
GOSLING, J. T., HANSEN, R. T. and BAME, S. J. (1971). *J. geophys. Res.* **76**, 1811.
HASHIM, A., BERCOVITCH, M. and STELJES, J. F. (1972). *Solar Physics.* **22**, 220.
HASHIM, A. and THAMBYAPILLAI, T. (1969). *Planet. Space Sci.* **17**, 1879.
JOKIPII, J. R. and COLEMAN, P. J., JR. (1968). *J. geophys. Res.* **73**, 5495.
MATHEWS, T., VENKATESAN, D. and WILSON, B. G. (1969). *J. geophys. Res.* **74**, 1218.
MCCRACKEN, K. G. and RAO, U. R. (1965). *Proc. Cosmic Ray Conf.* (London) **1**, 213.
MCCRACKEN, K. G. and RAO, U. R. (1970). *Space Sci. Rev.* **11**, 155.
MCCRACKEN, K. G., RAO, U. R., FOWLER, B. C., SHEA, M. A. and SMART, D. C. (1965). IQSY Instruction Manual No.10.

MCCRACKEN, K. G., RAO, U. R. and BUKATA, R. P. (1966). *Phys. Rev. Letters* **17**, 928.
MCCRACKEN, K. G., RAO, U. R. and BUKATA, R. P. (1967). *J. geophys. Res.* **72**, 4293.
MCCRACKEN, K. G., RAO, U. R. and NESS, N. F. (1968). *J. geophys. Res.* **73**, 4159.
MCCRACKEN, K. G., RAO, U. R., BUKATA, R. P. and KEATH, E. P. (1971). *Solar Phys.* **18**, 100.
MERCER, J. B. and WILSON, B. G. (1968). *Can. J. Phys.* **46**, S849.
NG, C. K. and GLEESON, L. J. (1971). *Proc. 12th Int. Conf. on Cosmic-rays* (Hobart) **2**, 498.
PARKER, E. N. (1964). *Planet. Space Sci.* **12**, 735.
PATEL, D., SARABHAI, V. and SUBRAMANIAN, G. (1968). *Planet. Space Sci.* **16**, 1131.
RAO, U. R. (1972). *Space Sci. Rev.* **12**, 719.
RAO, U. R. and SARABHAI, V. (1964). *Planet. Space Sci.* **12**, 1055.
RAO, U. R., MCCRACKEN, K. G. and VENKATESAN, D. (1963). *J. geophys. Res.* **68**, 345.
RAO, U. R., MCCRACKEN, K. G., ALLUM, F. R., PALMEIRA, R. A. R., BARTLEY, W. C. and PALMER, I. (1971). *Solar Phys.* **19**, 209.
RAO, U. R. and AGRAWAL, S. P. (1970). *J. geophys. Res.* **75**, 2391.
SUBRAMANIAN, G. (1971). *J. geophys. Res.* **76**, 1093.
TOLBA, M. F. and LINDGREN, S. T. (1971). *Proc. 12th Int. Conf. on Cosmic Rays* (Hobart) **2**, 690.

Canadian Journal of Physics

Characteristics of Cosmic Ray Diurnal Variation from Deep River Neutron and Meson Data and Temperature Effects

S. P. AGRAWAL, A. G. ANANTH, AND U. R. RAO

Characteristics of Cosmic Ray Diurnal Variation from Deep River Neutron and Meson Data and Temperature Effects

S. P. Agrawal, A. G. Ananth, and U. R. Rao

Physical Research Laboratory, Ahmedabad, India

Received August 16, 1971[1]

From an extensive analysis of Deep River meson data for over 5 years, new temperature coefficients have been derived for correcting the meson data. It is shown that meson data corrected using new coefficients yield values of diurnal and semidiurnal anisotropy consistent with those obtained from neutron monitors. Using the temperature-corrected meson and neutron data, the upper cutoff rigidity beyond which the diurnal variation ceases is shown to vary with solar cycle showing a minimum of about 35 GV during the Quiet Solar Year of 1965, and a maximum of ≈ 125 GV during 1968–1969.

Une analyse approfondie des données sur les mesons recueillies à Deep River durant plus de 5 ans a permis de déterminer de nouveaux coefficients de variation en fonction de la température. On montre qu'en corrigeant les données sur les mesons avec ces coefficients, on obtient des valeurs de l'anisotropie diurne et semi-diurne compatibles avec celles que fournissent les moniteurs de neutrons. En utilisant les données sur les mesons, corrigées pour la température, et les données sur les neutrons, on établit que la rigidité de coupure au-delà de laquelle la variation diurne disparaît varie avec le cycle solaire. Elle a présenté un minimum d'environ 35 GV durant l'année solaire calme de 1965 et un maximum de 125 GV durant 1968–1969.

1. Introduction

Study of data from the worldwide network of neutron monitoring stations has clearly demonstrated that the properties of the average diurnal variation of cosmic ray intensity is in good agreement with the Parker–Axford theory of partial corotation, while the average semidiurnal variation with a positive spectral exponent can be explained in terms of latitudinal gradients. The experimental observations over the period 1957–1970 have further indicated that both the mean diurnal (McCracken and Rao 1965; Rao 1972) and the semidiurnal (Rao and Agrawal 1970) anisotropies are practically time invariant contradicting the earlier results obtained using meson monitor data alone, which clearly showed a 22 year cycle of activity in the time of maximum of the diurnal variation (Thambyahpillai and Elliot 1953; Sarabhai *et al.* 1955). The recent analysis of Duggal *et al.* (1970) using both neutron and temperature-corrected meson data reveals the presence of a small component with a 22 year periodicity superimposed upon the normal corotation vector, which if confirmed must show a significant energy dependence, having a larger contribution at higher energies detected by meson monitors

($\bar{E} \approx 30$ GeV) and practically negligible contribution at lower particle energies to which neutron monitors ($\bar{E} \approx 10$ GeV) mainly respond. However, any uncertainty in correcting the meson intensity for atmospheric temperature variations makes the deductions derived from meson data unreliable. Besides, due to the large differences in the mean energy responses of meson and neutron monitors, use of high counting rate meson data would be valuable for estimating the energy spectrum of variation, and therefore a proper understanding of the temperature effects of meson intensity recorded at ground is very important.

In spite of the availability of a large number of both experimental and theoretical (Dorman 1957; Bercovitch 1966; Wada 1960; Olbert 1954) studies of the effect of atmospheric temperature on meson intensity, practical application of these methods to daily variation has been greatly handicapped due to the nonavailability of adequate radiosonde observations (which are seldom conducted more than twice a day) and the large radiation errors associated with these observations. Since the meteorological observations clearly show that the diurnal temperature variation becomes relatively insignificant at altitudes above 2–3 km and the temperature variation below this altitude, at least on an
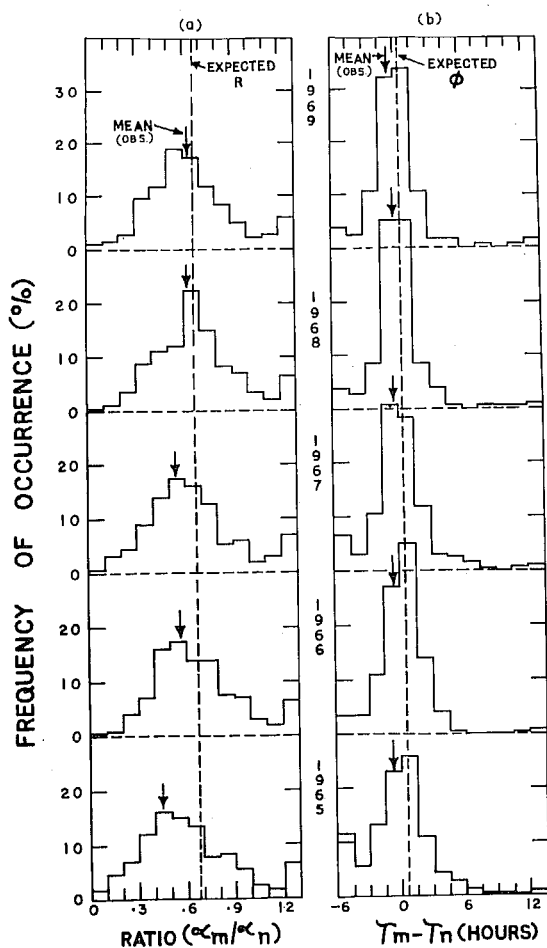
FIG. 1. Histogram of the occurrence of (a) the ratio R between meson and neutron diurnal amplitude and (b) the phase difference between the two for Deep River for each year during 1965–1969. Dashed line shows theoretically expected values for an assumed upper cutoff rigidity of 100 GV (Mori 1968a, b), while arrows indicate the mean values for each year.

average, is well related to the ground temperature, many authors (Rao and Sarabhai 1961; Bercovitch 1966) have suggested the use of ground temperature observations to correct the diurnal variation of meson intensity.

Meson data corrected for temperature using the temperature correction factors derived by Bercovitch (see Table 3) have been used by many authors to cast doubt on the 18 h average corotational anisotropy, and to advocate the hypothesis of a two way energy dependent diurnal anisotropy (Kodama and Nagashima

1968; Kitamura 1968). We wish to point out, however, that the temperature coefficients obtained by Bercovitch (1966) were for wide aperture muon telescope and hence may not be applicable to the standard MT-64 cubical telescope whose data have been used extensively for time variation investigations. In view of the fact that the diurnal anisotropy derived from neutron data shows time invariance during 1957–1970 (Rao 1972), we believe that it is very important to derive the appropriate temperature coefficients applicable to the standard MT-64 cubical meson telescope. For this purpose we have used the published data (Steljes 1970) on diurnal anisotropy, derived from pressure-corrected neutron and meson data (both temperature uncorrected and corrected using coefficients given by Bercovitch). The entire data, excepting Forbush decrease days, have been utilized and essentially the method of analysis suggested by Bercovitch (1966) has been adopted for evaluating the temperature effect on mesons.

2. Examination of the Temperature Coefficient Presently Used

In Fig. 1 are shown the histograms of the frequency of occurrence of the distribution of the ratio R of the diurnal amplitude of meson to neutron (α_m/α_n) and the phase difference ϕ between the two ($\tau_m - \tau_n$) for each day during the period 1965–1969, computed from the temperature-corrected meson data published by Steljes (1970). The theoretically expected ratio and the phase difference, using Mori's (1968a, b) calculations for an upper cutoff rigidity = 100 GV are also shown in the same figure. In spite of the wide distribution due to the inherent large statistical errors on a day-to-day basis, the figure clearly demonstrates that on more than 70% of the days the ratio $R > 0.50$, which is different from the corresponding values obtained by Bercovitch (1966) for the period 1962–1964.

Following Bercovitch (1966) we evaluate the temperature coefficients applicable to MT-64 cubical meson data using the vector equation given below which connects the diurnal vector M for temperature-uncorrected (pressure-corrected) mesons and the diurnal vector N for pressure-corrected neutrons.

TABLE 1. Temperature correction factors for Deep River mesons in 1965–69

Year	R	ϕ (deg)	Atmospheric vector (A)		Ground temperature vector (T)	
			Amplitude (%)	Phase (deg)	Amplitude (°F)	Phase (deg)
1965	0.550	21.2	0.119	108	7.39	231
1966	0.605	8.4	0.085	85	7.27	226
1967	0.596	5.6	0.082	86	7.50	229
1968	0.575	6.3	0.063	122	7.69	230
1969	0.536	−2.2	0.026	88	7.33	232
1965–69	0.582	7.0	0.075	95	7.43	230

[1] $\quad M(\alpha_m, \tau_m) = R \times N(\alpha_n, \tau_n + \phi) + A$

Resolving the vectors into orthogonal components along 00 and 06 h directions, we can write

[2]
$$M_{00} = R \cos \phi \times N_{00} - R \sin \phi \times N_{06} + A_{00}$$
$$M_{06} = R \cos \phi \times N_{06} + R \sin \phi \times N_{00} + A_{06}$$

[3] $\quad\quad A = C_t T(\alpha_t, \tau_t + \theta)$

where T, P, A are the vectors representing the observed ground temperature, pressure, and atmospheric diurnal vectors respectively, and α and τ are their amplitudes and phases. R is the ratio between meson and neutron diurnal amplitudes (α_m/α_n) due to the anisotropy in space and θ is the phase lag between T and A. The relationship between the various vectors is defined in Fig. 2.

Using the published values of M and N vectors (Steljes 1970) the values of R and ϕ have been computed for each year using the least-squares fit method to the vector eq. 2 for the period 1965–1969 (Table 1). In these calculations, we have restricted our analysis to days on which the diurnal amplitude of neutrons at Deep River is $0.1\% < \alpha_n < 0.7\%$. The low amplitude days have been neglected to avoid uncertainties due to statistical errors. Abnormally high amplitude days have been likewise neglected, as on such days the diurnal variation is likely to be caused by mechanisms other than corotation and the energy spectrum on such days may not be energy independent. It is clear from Table 1 that the ratio R in each year is greater than 0.5, the best-fit value for the entire period being 0.58 ± 0.04, with the phase difference between mesons and neutrons (ϕ) being 0.5 ± 0.1 h.

For $\phi = 0$, eq. 2 represents two straight lines each having a slope equal to R, and intercepts equal to A_{00} and A_{06}. Grouping the entire data, according to neutron diurnal amplitude α_n in intervals of 0.1%, the mean of the resolved components M_{00}, M_{06}, and N_{00}, N_{06} for each group for the year 1965–1969 have been calculated. Figure 3 shows the slope and intercept of the best-fit lines through the observational points. The slope of the best-fit line M_{00}/N_{00} would be slightly reduced if appropriate weight to the statistical significance of individual observational points were to be considered. Nevertheless, we observe that the slope of the

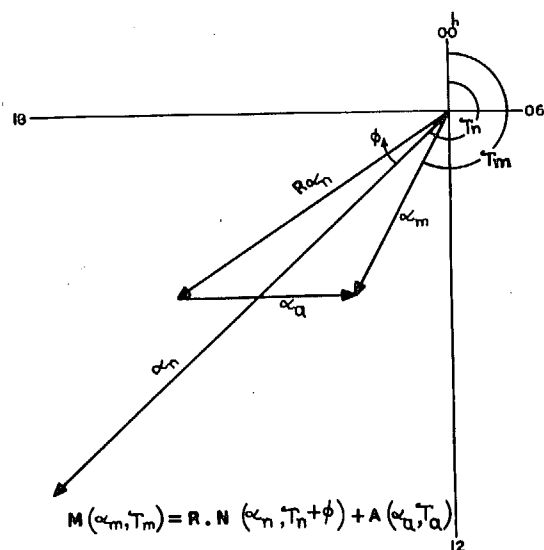$$M(\alpha_m, T_m) = R \cdot N (\alpha_n, T_n + \phi) + A (\alpha_a, T_a)$$

FIG. 2. Showing the relationship between different vectors representing neutron, meson, and atmospheric diurnal variation (see text for explanation).
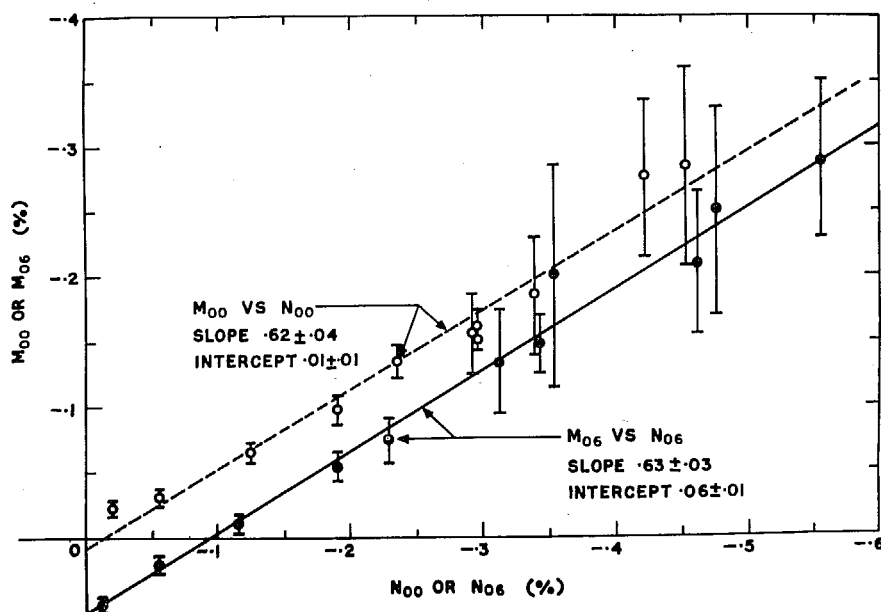
FIG. 3. The components of N resolved in 00 and 06 h axis are plotted against the corresponding components of M for Deep River for 1965–1969. The intercept on the M axis gives the component of mean atmospheric diurnal vector.

appropriately weighted best-fit lines through the observational points yields $A_{00} \approx 0$ and $A_{06} = 0.06 \pm 0.01\%$.

From all the observations cited above it is clear that the ratio of diurnal amplitude of meson to neutron is $= 0.58 \pm 0.04$ and the phase difference between meson and neutron is 0.5 ± 0.1 h during the period 1965–1969 and the temperature corrections obtained by Bercovitch (1966) for wide angle meson telescopes are not applicable to the standard MT-64 cubical meson telescope.

3. Evaluation of the Temperature Coefficient

A first-order estimate of the temperature effect on meson data can be easily derived using only days on which neutron monitors show negligible diurnal amplitude ($\alpha_n < 0.1\%$). For such days, the observed variation of uncorrected meson data (M) will be mainly due to the atmospheric temperature effects (T), since the meson diurnal amplitude for such days is expected to be $< 0.05\%$. During the 5 year period under study, 63 such days were present for which a temperature coefficient of $-0.009\%/°F$ has been obtained. If appropriate corrections for the small

cosmic ray diurnal amplitude is also made, the average effective temperature coefficient for this period is found to be $C_t = -0.010\%/°F$ with $\theta = 3.2$ h.

Part of the year-to-year variations could be attributed to the change in the upper cutoff rigidity. In order to obtain a reliable estimate of the temperature effect we have examined the meson data on a day-to-day basis. We have divided the data for the entire period into five groups based on the diurnal amplitude of temperature. Table 2 gives the results obtained employing the least-squares fit criteria on individual daily values to eq. 2 with the data grouped according to the diurnal amplitude of ground temperature α_t in the intervals of 3.6 °F. The mean values of α_t and τ_t for each of the groups are also given in Table 2. It is seen from the table that with the increase in the value of α_t, the contribution due to temperature effect (A) also increases linearly as expected. It is further seen that the value of R for each group is > 0.5. The best-fit values have also been determined using eq. 2 for the entire period excluding days of group 1. Group 1 days have been excluded from this particular analysis since we believe that the systematic and random

TABLE 2. Variation of temperature correction vectors with the change in ground temperature variation

Temperature groups	Number of days (1965–69)	R	ϕ (deg)	Atmospheric vector (A)		Ground temperature vector (T)	
				Amplitude (%)	Phase (deg)	Amplitude (%)	Phase (deg)
1	324	0.592	8	0.045	130	1.56	229
2	439	0.614	9	0.071	89	5.06	231
3	367	0.547	5	0.073	93	8.77	231
4	255	0.577	6	0.103	86	12.50	228
5	135	0.623	−2	0.126	78	16.08	227
Groups 2–5	1196	0.580	7	0.085	90	9.03	229

NOTE: Mean value C_t $(A/T) = -0.0095 \pm 0.0005\%/°F$.

errors due to other factors could become quite significant compared with the small amplitude of diurnal temperature vectors on these days. The temperature effect obtained from the best-fit value for all days can be represented by

[4] $\quad A = -0.0095T(\alpha_t, \tau_t + 2.6 \text{ h})$

where $C_t = -0.0095\%/°F$ and $\theta = 2.6$ h.

It may be noted, however, that if we also include group 1 days, an alternative best fit can be obtained which is given by

[5] $\quad A = A_0 - 0.0072T(\alpha_t, \tau_t + 1.0 \text{ h})$

where A_0 is a vector of amplitude 0.037% in a direction $\tau = 0930$ h. A_0 is essentially a constant and is independent of temperature, with its magnitude sensitive to the value of ϕ used. The above results are found to be essentially true even when the data is divided into a larger number of groups.

The physical significance of A_0 in eq. 5 is not immediately apparent. Further, for reasons given earlier, we believe that the group 1 days on which the temperature variation is very small should be excluded from the analysis and hence we believe that eq. 4 truly represents the temperature effect of mesons. Even though the choice of the equation may matter on the individual days, we wish to emphasize that the results on an average basis derived in this paper will not be altered if we were to use eq. 5 instead of eq. 4.

The value of $\phi = 0.5$ h obtained from the least-squares fit method using data on individual days also agrees very well with the expected value derived assuming that the mean cosmic ray diurnal anisotropy is independent of rigidity up to an upper cutoff rigidity ≈ 50 to 100 GV.

Further confirmation of the correctness of the derived temperature coefficients can be obtained by comparing the temperature-corrected diurnal vector from mesons (M_c) with the diurnal vector obtained from neutrons on a day-to-day basis. We have calculated the vector variance σ^2 representing the difference between these two for different combinations of values for R ranging from 0.46 to 0.70, ϕ from 0 to 1 h, C_t from -0.006 to -0.013, and θ from 1 to 3 h, using the equations

[6a] $\quad \Delta_i = M_c - RN(\alpha_n, \tau_n + \phi)$

where

[6b] $\quad M_c = M(\alpha_m, \tau_m) - A$

and the variance σ^2 is given by

[6c] $\quad \dfrac{1}{N} \sum_{i=1}^{N} |\Delta_i|^2$

For the period 1965–1969, we observe that the values of R, C_t, θ, and ϕ as derived by us (Table 3) gives the minimum variance showing that the temperature coefficients derived by us are reliable even on a day-to-day basis.

We wish to point out, however, that there also exist other combinations of R, C_t, θ, and ϕ for which the variance is not significantly higher than that obtained for the combinations mentioned above. In other words, the temperature coefficients obtained by us, though not unique, are in our opinion still the best choice among the different possible alternatives.

Figure 4 illustrates the good agreement between the meson anisotropy vector obtained after correcting with the temperature coefficient (as given in eq. 4) obtained from ground tem-

TABLE 3. Comparison of temperature coefficients used earlier with the present results

Year	R	ϕ (h)	Total temperature coefficient	
			C_t (%/°F)	θ (h)
1962–64 (Bercovitch 1966)	0.473	0	-0.0061 ± 0.0004	1.9 ± 0.3
1965–69 (present results)	0.580	0.5	-0.0095 ± 0.0005	2.6 ± 0.2
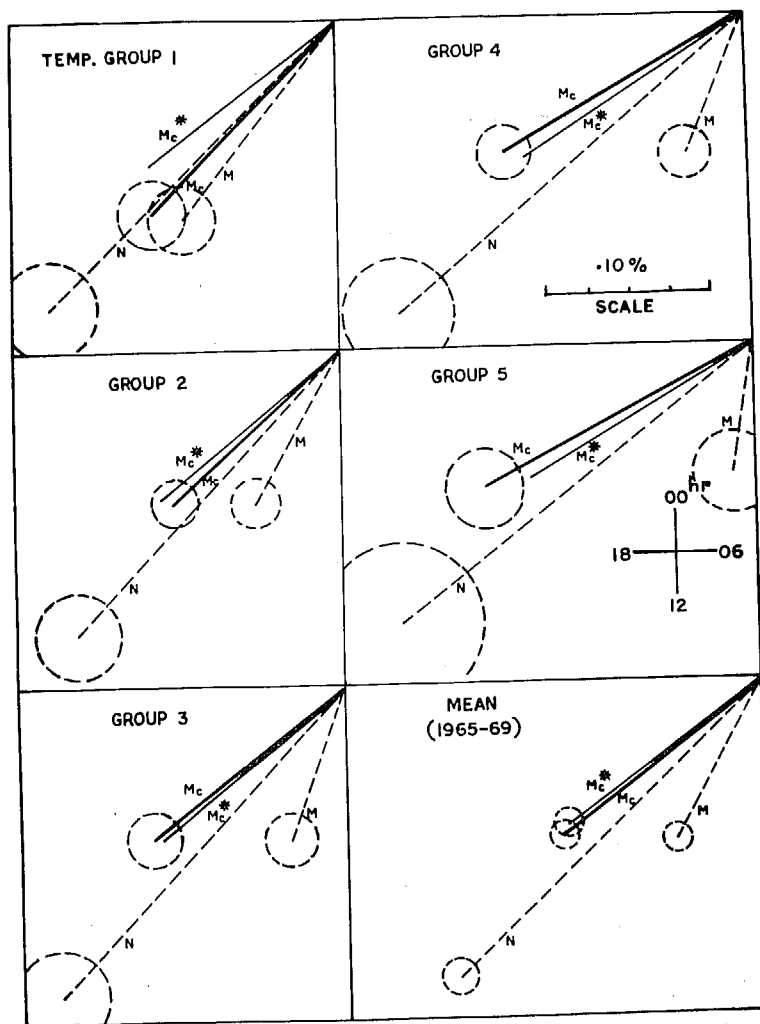
FIG. 4. Illustrates the good agreement between the expected meson vector (M_c^*) using neutron data and the temperature-corrected meson vector (M_c) using new temperature coefficients for different temperature groups as well as for all the days during 1965–1969.

perature data and the neutron anisotropy vector. N, M, and M_c represent the neutron, uncorrected meson, and corrected meson diurnal vectors respectively. M_c^* is the expected meson diurnal vector calculated from the neutron vectors using the best-fit values of $R = 0.58$ and
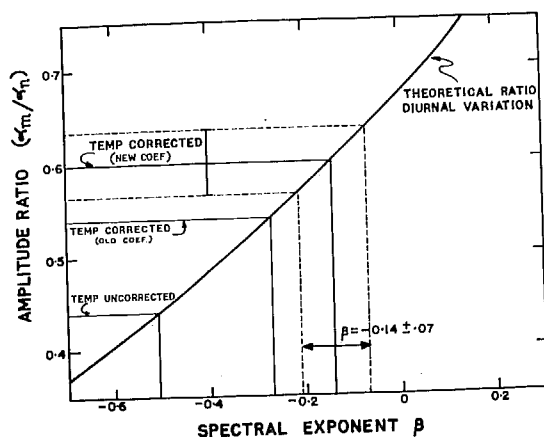
FIG. 5. Theoretically calculated ratio R of the diurnal amplitude of mesons to neutrons for Deep River plotted against β, the spectral exponent of the energy spectrum of diurnal variation, calculated assuming 100 GV for the upper cutoff rigidity. The observed ratio obtained using temperature-corrected and uncorrected mesons are also shown in the figure.

$\phi = 0.5$ h, which in other words represent the expected diurnal vector for corrected mesons to yield the value of diurnal anisotropy consistent with neutron observations. The good agreement between M_c and M_c^* clearly indicates the appropriateness of the temperature coefficient derived from ground temperature data. Table 3 summarizes the temperature correction factors derived in the present investigation.

4. Energy Spectrum of Average Daily Variation Using Meson and Neutron Data

The ratio of the amplitude of diurnal variation of mesons to neutrons (α_m/α_n) at Deep River

has been calculated for different values of the energy spectral exponent β, assuming an upper cutoff rigidity of 100 GV. Figure 5 shows the theoretically expected ratio plotted as a function of β, and the observed ratio for 1965–1969 obtained using the uncorrected meson data, temperature-corrected meson data using the temperature coefficient given by Bercovitch, and the temperature-corrected data using the temperature coefficient derived in this paper. The figure clearly indicates that the ratio obtained using meson data corrected with our temperature coefficient gives the best values for the spectral exponent ($\beta = -0.14 \pm 0.07$) consistent with the spectral exponent derived for the average diurnal variation using neutron monitor data alone. Similarly the energy spectrum of semidiurnal variation obtained using neutron and meson data corrected using our temperature correction yields a value 0.8 ± 0.2, for the spectral exponent which again is consistent with the results of Rao and Agrawal (1970), thus providing additional evidence for the correctness of the temperature coefficient derived in this paper.

5. Change in Upper Cutoff Rigidity from Year to Year

Since meson monitors respond to much higher particle energies, meson data can be very useful in deriving the upper cutoff rigidity beyond which the diurnal variation is ineffective, provided an appropriate temperature correction is applied to the data. From Table 1 it is clear that the amplitude of the calculated atmospheric temperature correction vector (A)

TABLE 4. Comparison of mean diurnal variation observed by mesons (corrected with appropriate temperature coefficient) with the mean variation observed by neutrons

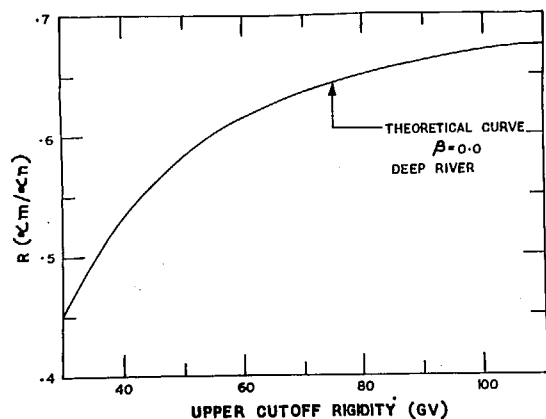| | Diurnal variation | | | | | |
| | Neutrons | | Mesons (temperature-corrected) | | | |
Year	Amplitude (%)	Phase (deg)	Amplitude (%)	Phase (deg)	R	ϕ (deg)
1965	0.226 ± 0.021	222	0.113 ± 0.016	222	0.50	0
1966	0.291 ± 0.022	228	0.179 ± 0.016	229	0.61	+1
1967	0.260 ± 0.027	224	0.153 ± 0.020	232	0.59	+8
1968	0.307 ± 0.022	229	0.209 ± 0.015	235	0.68	+6
1969	0.294 ± 0.020	225	0.194 ± 0.014	234	0.66	+9
Mean	0.276 ± 0.010	226	0.166 ± 0.007	232	0.60	+6

FIG. 6. Theoretically calculated value of the ratio R (for $\beta = 0$) plotted as a function of the assumed upper cutoff rigidity.
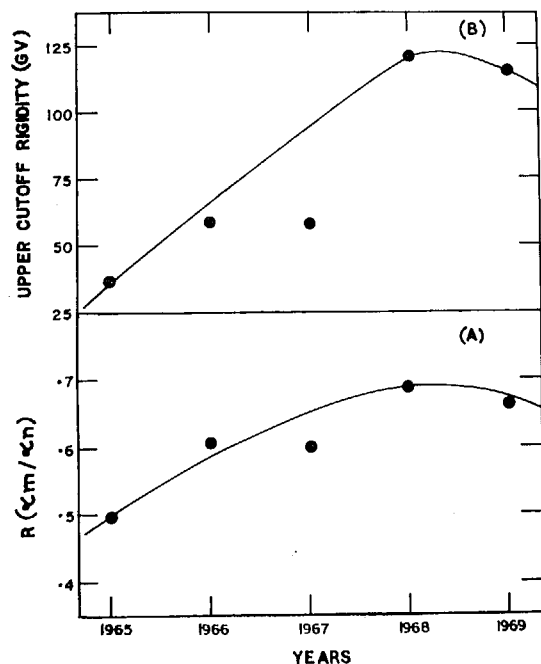

FIG. 7. Showing the solar cycle variation of the (a) ratio R and (b) the upper cutoff rigidity during 1965–1969. The meson data used have been corrected with newly derived coefficients.

is different from year to year, even though the mean diurnal amplitude of temperature (α_t) itself does not show significant variation. The variation of A is quite systematic, being maxi-

mum in 1965 and then progressively decreasing with solar activity and reaching a minimum in 1968–1969.

Applying the new temperature correction factor obtained from using ground-based temperature data to the uncorrected meson intensity, the temperature-corrected meson diurnal vector has been derived for each year. Table 4 lists the neutron and temperature-corrected meson diurnal vectors as well as the calculated ratio R and phase difference ϕ between the diurnal vectors obtained from mesons and neutrons for each year during 1965–1969. The values of R show a progressive increase with solar activity, the minimum coinciding with the minimum solar activity. Using Mori's (1968a, b) calculations, and assuming the energy spectrum of the diurnal variation to be energy independent, values of R for different assumed values of the upper cutoff rigidity have been calculated and plotted in Fig. 6. Using these calculations, the observed change in R with solar cycle can be used to infer the change in the upper cutoff rigidity beyond which the diurnal variation ceases. Figure 7 shows the solar cycle variation of R and the upper cutoff rigidity (R_{max}) during the period 1965–1969.

6. Discussions and Conclusions

The temperature coefficient of $-0.0095 \pm 0.0005\%/°F$ derived in this paper, when used to correct Deep River mesons, yields diurnal and semidiurnal anisotropies for cosmic rays that are consistent with the neutron observations. The temperature coefficient derived in this paper is substantially higher than the coefficients that have been used hitherto, but are in good agreement with those derived using direct radiosonde observations from Maniwaki, located ≈ 120 km from Deep River. Using the temperature-corrected meson data, along with neutron observations, the upper cutoff rigidity is found to vary with solar cycle, showing a minimum during the quiet solar year of 1965 and a maximum in 1968–1969. These results are in substantial agreement with the solar cycle variation of the upper cutoff rigidity inferred by Agrawal and Rao (1969) using neutron data and Ahluwalia and Erickson (1970) using underground meson data.
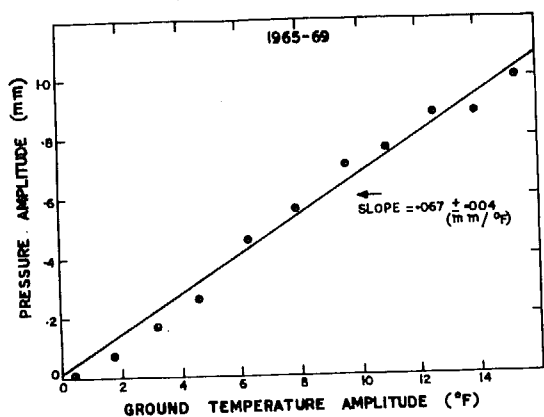
FIG. 8. Correlation between the diurnal amplitudes of Deep River ground temperature and barometric pressure.

Appendix: Temperature-Induced Pressure Effects

Bercovitch (1966) has shown that the total atmospheric effects are partly due to the temperature variations and partly to the temperature-correlated pressure changes. Figure 8 shows the relationship between the diurnal amplitude of ground temperature and the diurnal amplitude of pressure. The straight line relationship between the two with a correlation coefficient of 0.95 demonstrates that the temperature and pressure variations are closely correlated. In other words, eq. 3 can be rewritten as

$$[7] \quad A = C_t^* \times T(\alpha_t, \tau_t + \theta) + C_p^* \times P(\alpha_p, \tau_p)$$

where C_t^* is the new partial temperature coefficient to be used in combination with the partial pressure coefficient C_p^* and $\delta C_t^* / \delta C_p^* = 0.067$ mm/°F (Fig. 8).

Since A can be evaluated independently using eq. 7 and $R = 0.58$, $\phi = 0.5$ h, the best values of C_t^* and C_p^* on a day-to-day basis can be computed, demanding the variance σ^2 given by eq. 6 to be a minimum. The results show that

whereas $C_p^* = 0.050\%$/mm, the same as that obtained by Bercovitch, the partial temperature coefficient $C_t^* = -0.0061\%$/°F is almost a factor of two higher than the value quoted by Bercovitch for the wide angle muon telescope.

AGRAWAL, S. P. and RAO, U. R. 1969. Proc. 11th Symp. Cosmic Rays, Delhi, India, Vol. II (Government of India, Bombay), p. 332.
AHLUWALIA, H. S. and ERICKSON, J. H. 1970. Acta Phys. Hung. 29, Suppl. 2, 139.
BERCOVITCH, M. 1966. Can. J. Phys. 44, 1329.
DORMAN, L. I. 1957. Cosmic ray variations (State Pub. House, Moscow), p. 145.
DUGGAL, S. P., FORBUSH, S. E., and POMERANTZ, M. A. 1970. J. Geophys. Res. 75, 1150.
KITAMURA, M. 1968. Can. J. Phys. 46, S828.
KODAMA, M. and NAGASHIMA, K. 1968. Can. J. Phys. 46, S825.
McCRACKEN, K. G. and RAO, U. R. 1965. Proc. Int. Conf. Cosmic Rays, London, 1, 213.
MORI, S. 1968a. Nuovo Cimento, B, 58, 1.
——— 1968b. Nuovo Cimento, B, 58, 58.
OLBERT, S. 1954. Phys. Rev. 96, 1400.
RAO, U. R. 1972. Space Sci. Rev. 12, 719.
RAO, U. R. and AGRAWAL, S. P. 1970. J. Geophys. Res. 75, 2391.
RAO, U. R. and SARABHAI, V. 1961. Proc. Roy. Soc. (London), A, 263, 101.
SARABHAI, V., DESAI, U. D., and VENKATESAN, D. 1955. Phys. Rev. 99, 1490.
STELJES, J. F. 1970. AECL Reports 3479, 3561, 3608, 3651, 3658.
THAMBYAHPILLAI, T. and ELLIOT, H. 1953. Nature, 171, 918.
WADA, M. 1960. Sci. Papers I.P.C.R. Jap. 54, 335.

Effect of Non-uniform Solar Wind Velocity on Interplanetary Medium & on Cosmic Radiation

A. G. ANANTH & S. P. AGRAWAL

Physical Research Laboratory, Ahmedabad 9

The consequences of solar wind streaming with non-uniform velocity on the interplanetary medium are discussed. It is shown that the co-rotating shock fronts which produce the co-rotating Forbush decreases in the low energy cosmic ray intensity, cause enhanced diurnal wave trains in the cosmic radiation at high energies. The enhanced diurnal variation in the initial stage is shown to be primarily due to a sink along the garden hose direction which, after 3-4 days, results from an excess flux of cosmic rays from the anti-garden hose direction. The latter finding is interpreted as a result of the positive density gradient in the cosmic ray ion density set-up initially by the enhanced solar wind through convection process.

UNDER equilibrium conditions between outward convection and inward diffusion of cosmic ray particles in the interplanetary space, the partial co-rotation of high energy cosmic rays is known to produce a diurnal variation as seen from a ground-based cosmic ray detector[1,2]. The diurnal anisotropy is found to have an average amplitude of 0·4% and a direction of maximum of 1800 hrs in space. However, even though the observed variation on a day-to-day basis is consistent with the general picture on most days, the existence of a number of days having enhanced as well as low amplitude diurnal waves has been noticed by a number of workers[3,4]. These workers conclude that the enhanced diurnal variation which often occurs on groups of days is usually caused by a decrease in cosmic ray intensity from the garden hose direction.

The study of low energy cosmic ray propagation in the interplanetary space has clearly shown the importance of the part played by the solar wind in providing an effective convection mechanism. During the initial phase of the decay of a solar flare event, the anisotropy is observed to be always from the sunward direction, suggestive of the convective removal of flare particles by the solar wind[5,6]. However, McCracken et al.[7] have argued that such a convection should eventually produce a positive density gradient and result in an easterly anisotropy during the late phase of the flare decay. We believe that such a mechanism must also operate on galactic particles for short periods of time when equilibrium conditions will not necessarily be established. During such periods the sun can be either a source or a sink. In this paper we attempt to show that the significant departures from the co-rotation theory occur in the diurnal variation on a day-to-day basis and that such departures can be completely explained in terms of re-distribution of cosmic ray intensity in the interplanetary medium following transient changes in the cosmic ray flux.

Analysis

Two particular events, one occurring during 1-7 Jan. 1966 and the second during 1-11 May 1966, have been analysed in great detail to examine the role played by convection and the density gradient in the interplanetary medium. We have selected high latitude super neutron monitor stations well distributed in longitude and having narrow asymptotic cones of acceptance $\leqslant 30°$ (Rao et al.[8]). As the earth spins on its axis, each of these monitors scan a narrow region of the celestial sky. Utilizing the data from a number of stations, well distributed in longitude, three-dimensional space-time maps of cosmic ray intensity profile in space can be constructed. Such maps define the cosmic ray flux as a function of direction at any given time and thus provide an integrated view of the cosmic ray demography in space from which the sources and sinks in space can be easily identified. The mean intensity three days prior to the commencement of the enhanced diurnal wave train, when not accompanied by large changes in flux, has been used for normalization purposes. Due to the inadequate coverage of certain longitudes because of the non-availability of neutron monitoring stations, we have been able to represent the intensity in only eight directions in space at any time, each directional belt covering a width of 3 hr in longitude. The mean of the observed amplitude in different directions has been obtained, taking care to normalize the amplitude at each station to the width and declination of its asymptotic cone of acceptance. Three-dimensional space-time diagrams are drawn for each three hourly interval on each day. Fig. 1 shows the amplitude deviation from the normal in each direction as a function of time during the period 29 April to 12 May 1966. The event of 1-7 Jan. 1966 has also been analysed similarly.

From Fig. 1, it is clear that the enhanced diurnal variation during 1-7 May 1966 was caused by a
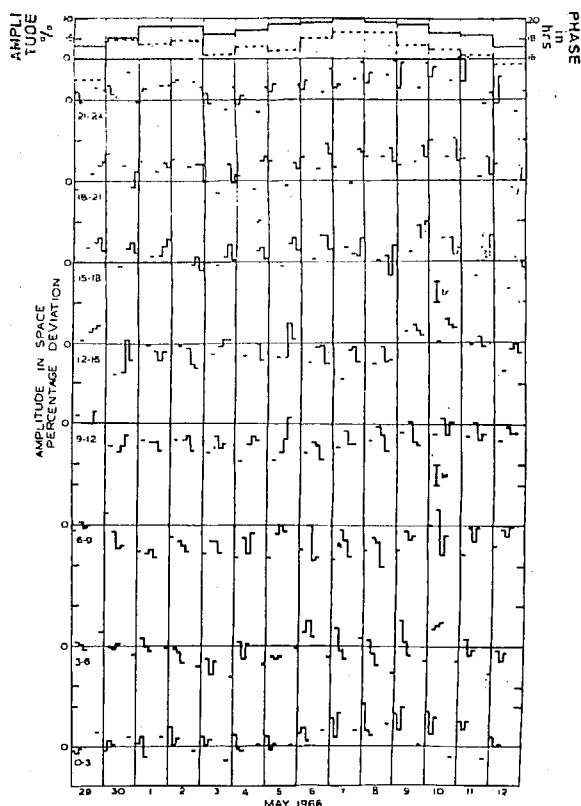
Fig. 1 — Plot of the observed amplitude deviation (in per cent) of cosmic ray intensity at each station (corrected for the width and declination of its asymptotic cone of acceptance) in different directions with respect to universal time at intervals of 3 hr [The histogram shows the amplitude deviation in eight directions in space at any instant of universal time. At the top of the figure the diurnal amplitude in per cent (continuous lines) and phase in hours (broken lines) observed at Deep River is also shown]

depression of cosmic ray intensity from the garden hose direction, the amplitude of the depression being of the order of 1-1·5%. During this period, no significant change in the cosmic ray flux from the anti-garden hose direction is observed clearly indicating that the observed enhanced diurnal amplitude is caused predominantly by a sink developing from the garden hose direction. Subsequent to the establishment of a sink and during 8-11 May 1966, an excess flux is observed from the anti-garden hose direction, while the garden hose direction is still recovering. This excess flux can be clearly seen from the directions 18-21 and 21-24 hrs having an amplitude of the order of ≈ 1·5%. We interpret the excess flux from the anti-garden hose direction late in the event as caused by a positive density gradient set up by enhanced convection during the earlier phase of the event.

Discussion

McCracken et al.[9] were able to convincingly prove the existence of co-rotating Forbush decreases from the data from Pioneer 6 and 7 spacecrafts. These co-rotating Forbush decreases result from the exclusion of galactic particles by the enhanced magnetic fields at the co-rotating shock fronts which are themselves produced at the interface where the fast moving plasma interacts with the slow plasma ahead of it. The magnitude of such co-rotating Forbush decreases, being usually about 5% at 10 MeV, will produce a corresponding variation of ≈ 1% at relativistic energies which will be completely masked by the diurnal variation effects. They[9] predicted that co-rotating Forbush decreases will manifest themselves as enhanced diurnal variation in high energy cosmic rays as seen by ground-based detectors. The enhanced wave train during 1-7 Jan. 1966 coincides with the co-rotating Forbush decreases identified by McCracken et al.[9], confirming their hypothesis.

Fig. 2 shows the plot of the amplitude of diurnal variation and the solar wind velocities measured by Pioneer 6. The enhanced diurnal wave train starting on 31 Dec. 1965 and on 30 April 1966 are found to follow the enhanced wind velocity after 3-5 days.. The enhanced convection from the garden hose direction will produce a sink along this direction causing an increase in the observed diurnal variation. Late in the event, the enhanced convection will set up a positive density gradient and produce enhanced diurnal variation as a consequence of a source along the anti-garden hose direction. The experimental observations depicted in Figs. 1 and 2 are in good agreement with the above hypothesis. It is important to
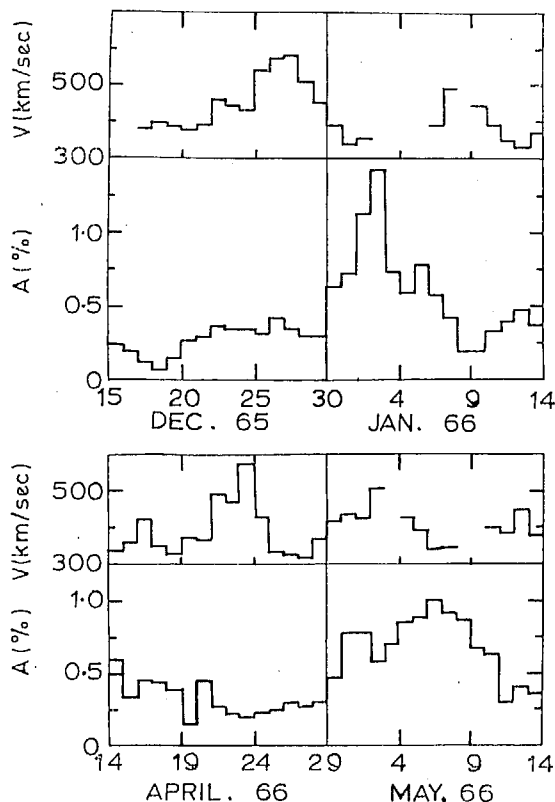

Fig. 2 — Diurnal amplitude (Deep River) and solar wind velocity (Pioneer 6) during the 15 days preceding and 15 days following the start of enhanced wave trains observed during 1-8 Jan. 1966 and 1-11 May 1966 (The epoch day is taken as the beginning of the enhanced wave train)

note that the conventional harmonic analysis shows a time of maximum around 20 hrs in space for both cases and thus would not reveal the exact mechanism for the production of enhanced diurnal variation.

Conclusion

We conclude, from the data presented above, that even though the average diurnal variation is consistent with partial co-rotation, on a day-to-day basis, equilibrium conditions between the outward convection of cosmic ray particles by the solar wind and the inward diffusion will not be balanced resulting in the production of trains of days with enhanced or negligible diurnal variation. Co-rotating shock fronts which cause co-rotating Forbush decreases at low energies can also cause enhanced diurnal variation at high energies. The enhanced diurnal variation is caused initially by the presence of regions with depleted cosmic ray intensity along the garden hose direction. The increased wind velocity causing increased convection sets up a positive density gradient resulting in the enhanced diurnal variation being caused by excess flux from the anti-garden hose direction, during the later phase of the event. In the diurnal wave trains analysed by us, the setting up of a positive density gradient and switch over from the garden hose sink to the anti-garden hose source takes place in about 3-5 days, suggesting that the relaxation time of the interplanetary medium to follow the changes in density gradient within the entire modulating region is of the order of 3-5 days.

References

1. PARKER, E. N., *Planet. Space Sci.*, **12** (1964), 735.
2. AXFORD, W. I., *Planet. Space Sci.*, **13** (1965), 115.
3. MATHEWS, T., VENKATESAN, D. & WILSON, B. G., *J. geophys. Res.*, **74** (1969), 1218.
4. HASHIM, A. & THAMBYAHPILLAI, T., *Planet. Space Sci.*, **17** (1969), 1879.
5. McCRACKEN, K. G. & RAO, U. R., *Space Sci. Rev.*, **11** (1970), 155.
6. RAO, U. R., McCRACKEN, K. G., ALLUM, F. R., PALMEIRA, R. A. R., BARTLEY, W. C. & PALMER, I., *Solar Phys.*, (1971), (in press).
7. McCRACKEN, K. G., RAO, U. R., BUKATA, R. P. & KEATH, E. P., *Solar Phys.*, (1971), (in press).
8. RAO, U. R., McCRACKEN, K. G. & VENKATESAN, D., *J. geophys. Res.*, **68** (1963), 345.
9. McCRACKEN, K. G., RAO, U. R. & BUKATA, R. P., *Phys. Rev. Lett.*, **17** (1966), 928.

DISCUSSION

Comment

H. RAZDAN: We also observe occasionally increases from the garden hose direction.

Semi–Diurnal Anisotropy of Cosmic Radiation in the Energy Range 1 to 200 Gev

U. R. Rao and S. P. Agrawal

Physical Research Laboratory, Navrangpura, Ahmedabad, India

From an analysis of the data from the worldwide network of neutron monitor stations, the general characteristics of the yearly mean semi–diurnal component of cosmic radiation are derived. The mean semi–diurnal component in the energy range 1–200 Gev can be represented as $[\Delta J(R)/J(R)] = 4 \times 10^{-5} R \cos^2 \Lambda$, for $R < 200$ Gv, and $[\Delta J(R)/J(R)] = 0$, for $R > 200$ Gv. The semi–diurnal component has a maximum along a direction perpendicular to the direction of the mean interplanetary field vector, varies as the first power of rigidity, and varies as $\cos^2 \Lambda$ where Λ is declination. The phase and the amplitudes of the semi–diurnal component also seem to be practically invariant with time during the period 1958–1968. The mean properties of the semi–diurnal anisotropy are consistent with the hypothesis of a positive density gradient of cosmic ray intensity in a direction perpendicular to the plane of ecliptic.

It has been known for some time that the cosmic radiation in the energy range 1–200 Gev exhibits a diurnal variation. The average diurnal variation has been found to be energy independent, with an amplitude of about 0.4% and a time of maximum of 1800 hours in space (*Rao et al.*, 1963; *McCracken and Rao*, 1965). The diurnal anisotropy can be understood as a result of the partial corotation of particles with the sun, with an azimuthal velocity V of about 300 km/sec at the orbit of the earth (*Parker*, 1964; *Axford*, 1965).

Although the existence of semi–diurnal anisotropy was inferred by *Rao and Sarabhai* (1961) long ago, *Ables et al,* (1965) conclusively showed the existence of a semi–diurnal component by means of numerical filter techniques, which consisted of numerical hetrodyne filtration followed by phase and amplitude demodulation, which improve the detection of small signals in the presence of statistical fluctuations or noise. Ables et al. showed that the semi–diurnal component of the cosmic radiation had a positive spectral exponent and an amplitude of about 0.1%, with maximum flux incident from a direction perpendicular to the direction of the interplanetary magnetic field. *Patel et al.* (1968) and *Lietti and Quenby* (1968) have also noted that the energy spectrum of the semi–diurnal component has a positive spectral exponent unlike the diurnal component of cosmic radiation.

In order to study any transient anisotropy in cosmic radiation, it is necessary to obtain data from a number of neutron monitoring stations whose 'asymptotic cones of acceptance' (*Rao et al.*, 1963) successively scan the celestial sky, one after the other, as the earth spins on its axis. Most of the monitors used by *Ables et al.* were of the IGY type with large statistical errors, and they could not study the semi–diurnal component in all its detail. In this paper we have utilized the data from all the super neutron monitors (including the Super neutron monitor at Ahmedabad, India), which are located near the geomagnetic equator and scan the equatorial region of the sky, to make a detailed study of the general properties of the semi–diurnal anisotropy of cosmic radiation.

DATA ANALYSIS

Data from a worldwide network of neutron monitoring stations were selected on the basis of the self–consistency criterion described by *Rao et al.* (1963), namely that the month to month changes in mean counting rate should be similar at various stations. As far as possible, data from mountain stations have not been utilized, to prevent any ambiguity in the results creeping in, due to the uncertanity in the value of coupling coefficients for such stations. Table 1 gives the list of stations and the coordinates that are used in the present analysis. The numerical filtraton techniques and the complex demodulation methods described by *Ables et al.* (1965) have been used, for most of the data, to derive the amplitude and phase of the first and second harmonic components.

Because the second harmonic component of the cosmic radiation is of the order of 0.1%, it is very important to ascertain that the results obtained are not contaminated by atmospheric effects. Incorrect pressure corrrection can give rise to spurious daily variation. The long–term variation of barometric coefficient is a main source of error for high latitude stations. From the known amplitude of the semi–diurnal pressure wave, which is about 0.3 mm of Hg at middle latitudes, we find that the error in the semi–diurnal component due to 10% error in the pressure coefficient is about 0.02%. At equatorial latitudes like Ahmedabad, India, where the semi–diurnal component of pressure wave is about 1.0 mm Hg, the pressure contribution to the semi–diurnal variation arising from the application of incorrect pressure co–efficient can be quite large. The pressure coefficient at various places, derived from the analysis of latitude survey conducted by *Carmichael et al.* (1968) and *Kodama and Ohuchi* (1968), also indicates that the pressure coefficients derived for equatorial latitudes have the largest statistical error. Because the semi–diurnal time of maximum of pressure wave is about 1000 hour LT, however, its effect on the cosmic ray semi–diurnal vector, which is roughly perpendicular to the pressure wave, is not appreciable. We have used the latitude survey of Carmichael et al. and Kodama and Ohuchi to derive the pressure coefficient at Ahmedabad, India. The value so obtained, namely 0.84 %/mm Hg, is in close agreement with the pressure coefficient derived for the Ahmedabad neutron monitor data by conventional multiple correlation analysis techniques. Even if we assume that the pressure coefficient used by us for Ahmedabad is out by 0.04%/mm Hg, Table 2 shows the maximum effect on the semi–diurnal component of cosmic radiation that can be expected for a maximum expected semi–diurnal pressure wave of 1.0 mm Hg. Even an error of 0.04%/mm Hg in pressure coefficient will introduce an error of only about 0.7 hours in the semi–diurnal time of maximum at equatorial latitudes and less than 0.3 hours at mid–latitudes. Thus, it may be seen that the effect on the amplitude and the time of maximum is not appreciable even at equatorial stations, and because we have used only one equatorial station, namely Ahmedabad, in our analysis, the general properties of the mean semi–diurnal variation of cosmic radiation derived in this paper are quite valid.

CHARACTERISTICS OF AVERAGE SEMI–DIURNAL VARIATION

By using the concept of the asymptotc cone of acceptance of a detector, *McCracken et al.* (1962, 1965) have published tables of variational coefficients which provide a quantitative technique for computing the observed variations due to cosmic ray anisotropy in space. These tables give the relative amplitudes $\alpha_m B_m$ and phases ϕ_m of both the first and second harmonic components for different values of β, ranging from 0.6 to —1.5, where β is the exponent of the spectrum of variation. We have extended the calculation of the variational coefficients from $\beta = 0.6$ to 2.0 for different values of R_{max} and for all the stations used in the present analysis. In this paper we shall consider the simplest form of semi–diurnal anisotropy of the type

2

TABLE 1

| Station No. | Station | Geographic coordinates | | Altitude (meters) | Geomagnetic cutoff* (in Gv) |
		Latitude (degrees)	Longitude (degrees)		
1	Ahmedabad	23.01	72.61	S.L.	15.94
2	Alma Ata	43.20	76.94	806	6.69
3	Calgary	51.08	245.91	1110	1.09
4	Churchill	58.75	265.91	39	0.21
5	Dallas	32.78	263.20	208	4.35
6	Deep River	46.10	282.50	145	1.02
7	Denver	39.75	255.00	1600	2.91
8	Durham	43.10	289.16	S.L.	1.41
9	Goose Bay	53.33	299.58	46	0.52
10	Hermanus	—34.42	19.22	26	4.99
11	Inuvik	68.35	226.27	21	0.18
12	Jungfraujoch	46.55	7.98	3450	4.48
13	Port Aux Francais	—49.35	70.22	S.L.	1.19
14	Kiel	54.33	10.13	54	2.29
15	Lindau	51.60	10.10	140	3.00
16	Mawson	—67.60	62.88	S.L.	0.22
17	Mt. Norikura	36.12	137.56	2770	11.39
18	Mt. Washington	44.30	288.70	1917	1.24
19	Mt. Wellington	—42.92	147.24	725	1.89
20	Pic du Midi	42.93	0.25	2860	5.36
21	Sulphur Mountain	51.20	244.39	2283	1.14
22	Wilkes	—66.42	110.45	S.L.	0.01

*Geomagnetic cutoff derived from *McCracken et al.* (1965).

$$\frac{\Delta J(R)}{J(R)} = A \; g(\Lambda) R_r^{\beta} \quad \text{for} \; R \leqslant R_{max}$$

$$\frac{\Delta J(R)}{J(R)} = 0 \quad \text{for} \; R > R_{max}$$

where the function $g(\Lambda)$ describes the dependence of anisotropy on declination and R^{β} shows the dependence of anisotropy on rigidity. Results are obtained for $g(\Lambda) = \cos \Lambda$ as well as for $g(\Lambda) = \cos^2 \Lambda$. R_{max} is taken to be 200 Gv for all our calculations; the reasons for this will be presented in the later section.

TABLE 2

The effect of variation of pressure coefficient on the amplitude and phase of the observed semi–diurnal component at Ahmedabad for a semi–diurnal pressure amplitude of 1.0 mm Hg.

Pressure coefficient %per mm of Hg	Semi–diurnal amplitude	Semi–diurnal phase
0.88	0.09%	18°
0.84	0.10%	41°
0.80	0.12%	58°

Figure 1 shows the histograms of the frequency of occurrence of the semi–diur–nal time of maxima in space observed at various stations for the years 1965 and 1966. The histograms are plotted against the asymptotic time for $\beta=0$ and $\beta=1.0$ obtained after correcting the observed time of maximum at each station for the geomagnetic bending and the width of the asymptotic cone of acceptance using the method described by *Rao et al.* (1963). In the above calculations, $g(\Lambda)$ is assumed to vary as $\cos \Lambda$. The figure shows a very good interstation agreement, thus indicating that the semi–diurnal maxima observed at all the cosmic ray recording stations is due to an anisotropy, with the maximum flux coming from the direction 45° east (135° West) of the earth–sun line, a direction that is essentially perpendicular to the direction of the general interplanetary magnetic field.
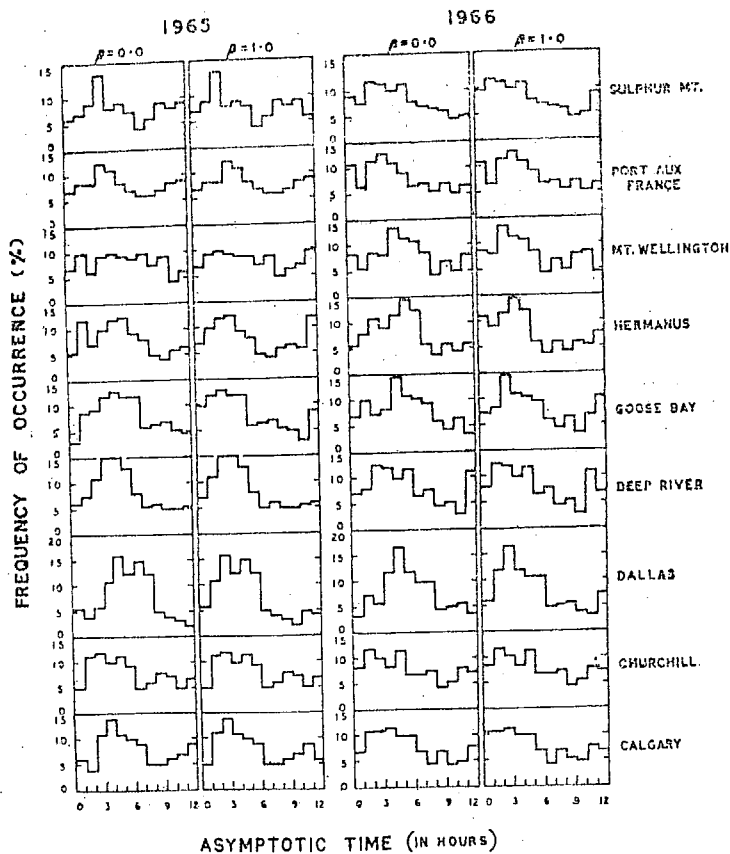
Fig. 1. Histogram of occurrence of the semi–diurnal maximum in space for different stations during 1965 and 1966. The histograms are plotted for semi–diurnal maxima calculated using $\beta=1.0$ and $\beta=0.0$

Because the effect of incorrect pressure correction on the determination of the semi–diurnal time of maximum ϕ_2 is not appreciable even at equatorial latitudes, we have used observations of ϕ_2 in space for evaluating β, the exponent of variation. ϕ_2 in space is derived for each station and each year for different values of β ranging from $+2.0$ to -1.0. The true value of β is the one for which there is a good interstation agreement in the observed value of ϕ_2 in space. In other words, there should be a minimum dispersion between the values of ϕ_2 determined for different stations for the same period of time. The

4

variance (X^2) in the value of ϕ_2 determined for different stations are evaluated for different values of β, for each year during 1958–1968. Figure 2 shows the plot of variance as a function of β for 1966, obtained for $g(\Lambda) = \cos\Lambda$ and $g(\Lambda) = \cos^2\Lambda$. The minimum variance is obtained for $\beta = 1.0$ for both the cases. Figure 3 shows the plot of variance against β for each year during 1958–1968. The standard deviation of variation of phase for an average station is 5°; thus the statistical error in variance can be considered to be 25 square degrees. From the figure it is seen that the minimum variance for each year is obtained for $\beta = 1.0 \pm 0.2$, thus showing that the energy spectrum of the semi–diurnal component has an exponent of 1.0 ± 0.2. We note, however, that the minimum variance observed during each year is larger than can be expected from statistical uncertainties alone.
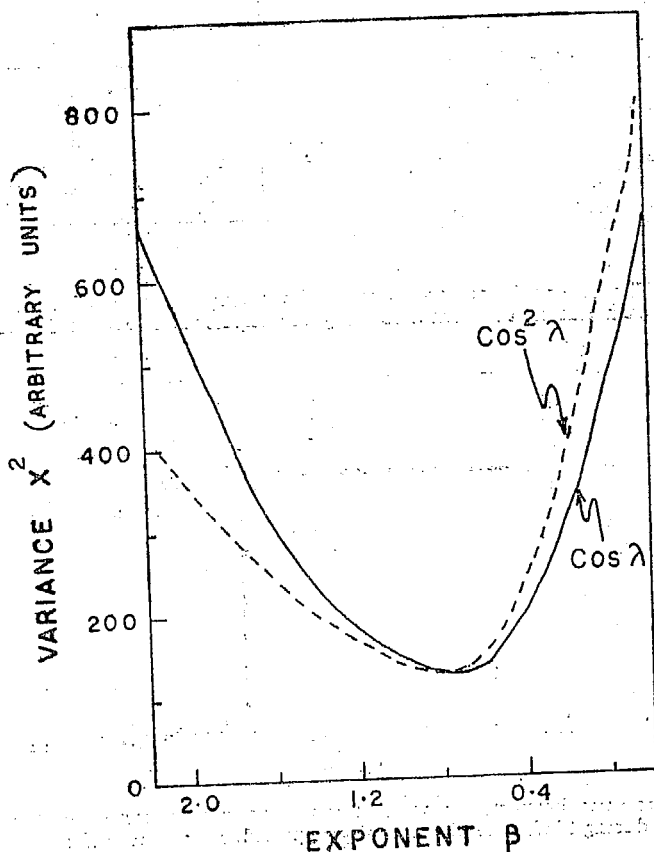
Fig. 2. Observed variance in the values of semi–diurnal phase as a function of the exponent of variation for the year 1966. The variance for both $g(\Lambda) = \cos\Lambda$ and $g(\Lambda) = \cos^2\Lambda$ are shown in the curve.

The ratio of the observed amplitude of the semi–diurnal component at Ahmedabad, India, to the amplitude at Deep River can be evaluated for each β. Figure 4 shows the theoretically expected ratio plotted as a function of β, for values of β ranging from -0.2 to 2.0. The observed ratio of amplitudes during 1968 is also plotted in the same figure. The observed ratio of amplitudes is consistent with an exponent of $\beta = 1.1 \pm 0.01$ for the energy spectrum of the semi–diurnal anisotropy of cosmic radiation. The above error includes only the statistical error. If, on the
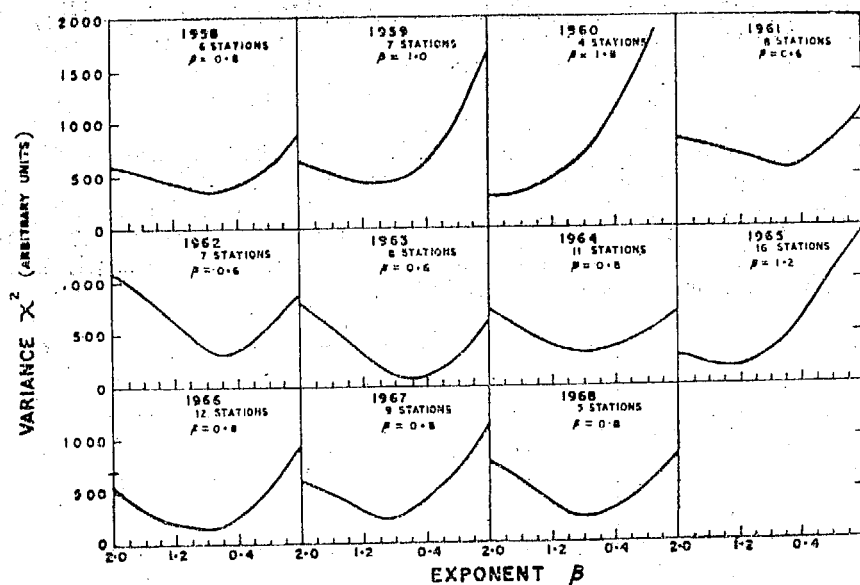
5

Fig. 3. The observed variance between the asymptotic time of semi–diurnal maxima calculated for each station as a function of β, the exponent of varation for each year during 1958–1968.
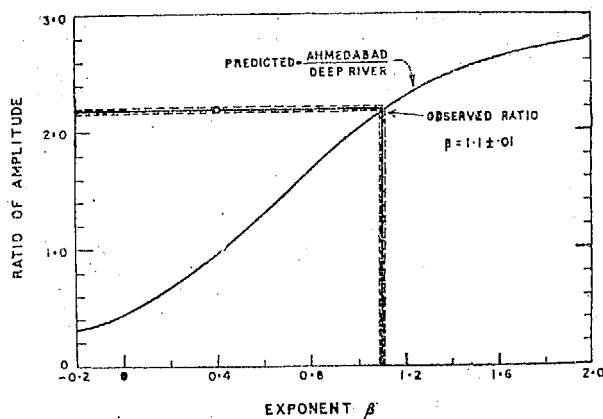

Fig. 4. The ratio between the semi–diurnal amplitude observed at Ahmedabad to that at Deep River during 1968. The theoretically expected ratios for different values of β are also shown.

other hand, an uncertainty of 0.01%/mm Hg in the pressure coefficient at Ahmedabad is taken into account, the error in the exponent β will be about 0.04.

Figure 5 shows the plot of the variance in the values of the amplitudes of the semi–diurnal component for different stations calculated for each value of β during 1958–1968. The normalized variance in amplitude is calculated using the formula

$$ x = \left\{ \frac{\sum\limits_{i=1}^{N} [A_i(\beta) - A_0(\beta)]^2}{N} \right\}^{1/2} \Big/ A_0(\beta) \qquad (2) $$

6
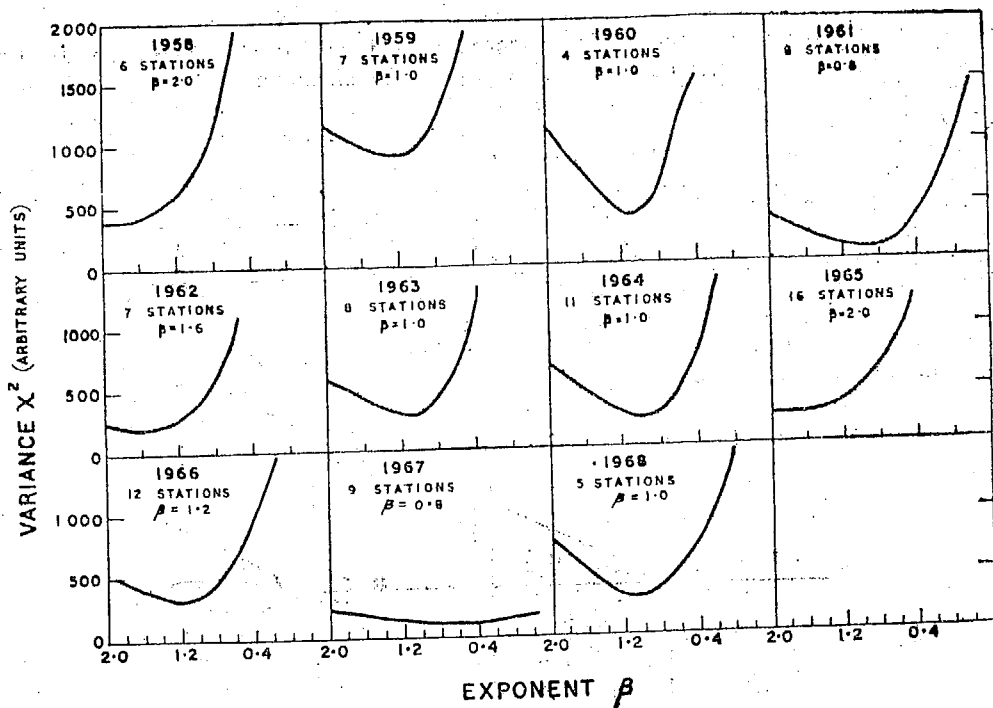
Fig. 5. The observed variance between the semi–diurnal amplitude in space calculated for each station as a function of β, the exponent of variation. The curves show the plots for each year during 1958–1968.
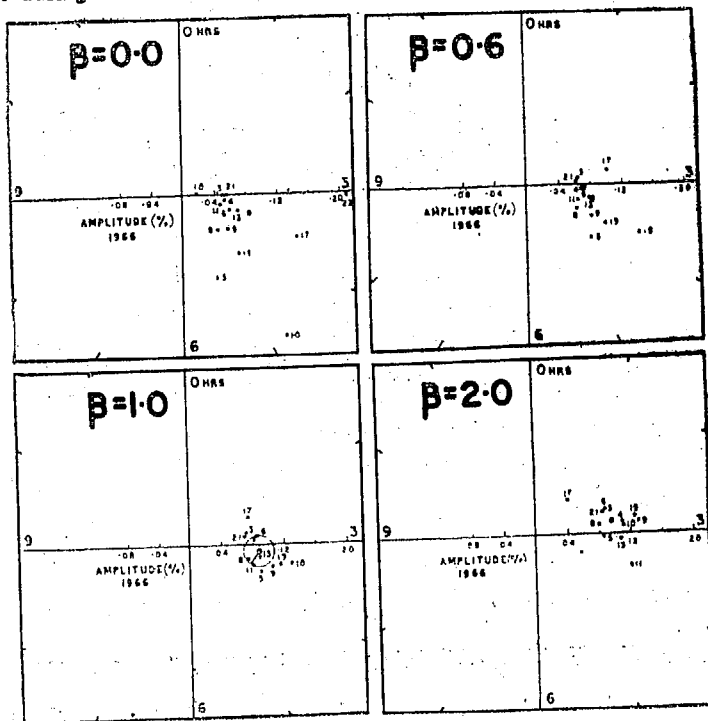

Fig. 6. The phase and amplitude of the semi–diurnal anisotropy in space as observed at different stations during 1966 plotted on a harmonic dial. The plots show the scatter for four different values of β, namey 0.0, 0.6, 1.0, and 2.0. The mean semi–diurnal anisotropy vector in space is also shown along with the 3σ circle.

where $A_i(\beta)$ is the percent amplitude in space obtained for for the ith station after correction for the geomagnetic bending and $A_0(\beta)$ is the mean amplitude of semi–diurnal varation in space obtained from the values for N stations. The curves again clearly show that the minimum variance is observed for values of $\beta = 1.0 \pm 0.2$ consistent with our observations of the phase of the semi–diurnal anisotropy. The phase and amplitude of the semi–diurnal anisotropy in space, as observed at different stations, are plotted on a harmonic dial in Figure 6, for four values of β, namely 0.0, 0.6, 1.0, and 2.0, for the year 1966. It is evident from the figure that the minimum variance occurs for $\beta \pm 1.0$. The mean semi–diurnal vector along with the three standard deviation error circle is also shown in the figure for $\beta = 1.0$. Practically all the observational points lie within 5σ error circle, which is consistent with the fact that the minimum variance is slightly larger than can be expected form statistical uncertainties alone. Figure 7 shows the harmonic dial representation of the semi–diur–
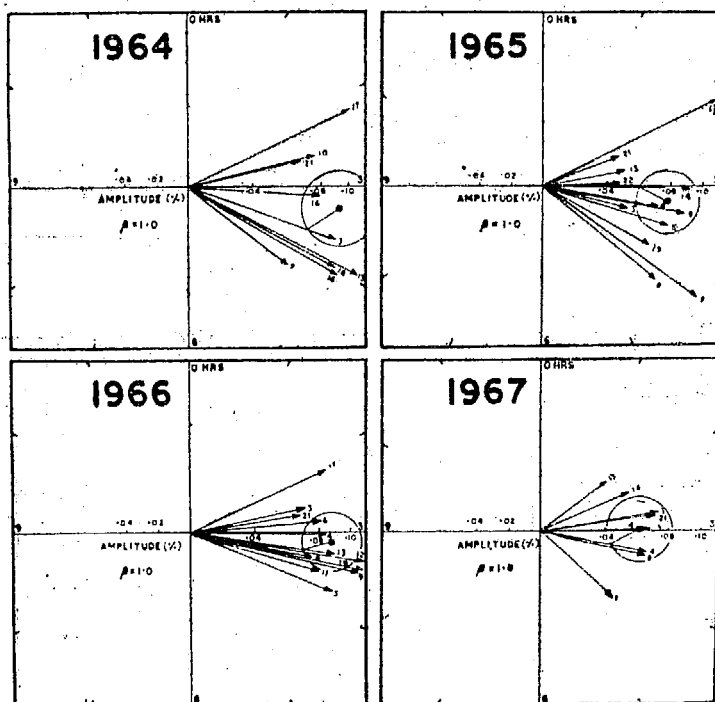

Fig. 7. The phase and amplitude of the semi–diurnal anisotropy in space as observed at different stations calculated for $\beta = 1.0$ are shown for each year on a harmonic dial. The mean anisotropy vector for each year is also shown in the same figure.

nal anisotropy vector in space for each year during 1964–1967, with the mean semi–diurnal vector for each year calculated for $\beta = 1.0$. The larger scatter in the observations during earlier years may be attributed to the fact that most of the monitors operating during these years were of the IGY type. We conclude that the semi–diurnal anisotropy in space has a positive exponent of $\beta = 1.0 \pm 0.2$, a mean amplitude of about 0.1%, and the maximum flux arriving from 0300 hours, which is perpendicular to the direction of the mean interplanetary field vector.

DEPENDENCE OF SEMI–DIURNAL ANISOTROPY ON DECLINATION

To investigate the dependence of the amplitude of the semi–diurnal anisotropy on declination, the yearly mean amplitude, after correction for attenuation due to the

finite width of the asymptotic cone of acceptance, is plotted against the mean asymptotic latitude λ of the station in Figure 8. The data for the years 1965, 1966, and 1967 are used in the figure. The theoretical curves defining $\cos \lambda$ and $\cos^2 \lambda$ function are also shown in the same figure. Even though the large statistical errors do not permit an unambiguous conclusion, it is clear that the distribution of points strongly favors a $\cos^2 \lambda$ dependence.
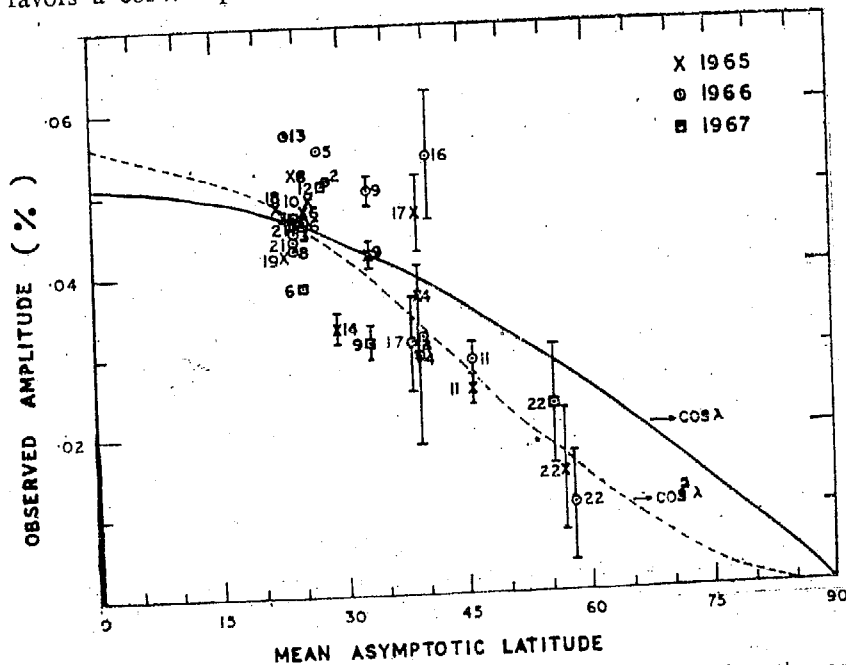

Fig. 8. The amplitude of semi–diurnal anisotropy calculated for each station corrected only for the width of the asymptotic cone of acceptance plotted against the mean asymptotic latitude. The theoretically expected behaviors for $\cos \lambda$ and $\cos^2 \lambda$ dependence are also shown in the same figure.

TIME VARIATION OF SEMI–DIURNAL ANISOTROPY

Figures 9 and 10 show the yearly mean phase and amplitude of the semi–diurnal vector for each year during 1958–1968. The points plotted in the figures indicate the observations at different stations. The mean semi–diurnal phase for the period 1958–1968 is almost constant; the maximum flux comes from the direction 132 $\pm$ 6° west (3.2 $\pm$ 0.4 hours) of the earth sun line. The mean phase does not differ by more than 3° for $g(\Lambda) = \cos \Lambda$ and $g(\Lambda) = \cos^2 \Lambda$. The mean semi–diurnal amplitude, however, shows a slight random variation during the same period, varying between 0.13% in 1963 to 0.08% in 1967 (for $g(\Lambda)=\cos^2\Lambda$). Figure 10 shows the yearly mean amplitude of semi–duirnal anisotropy calculated by assuming both $g(\Lambda) = \cos \Lambda$ and $g(\Lambda) = \cos^2\Lambda$. The year to year changes for both functions show identical behaviour; the mean amplitude in space for the period 1958–1968 is 0.112 $\pm$ 0.017%, for $g(\Lambda) = \cos^2\Lambda$.

DISCUSSION AND CONCLUSIONS

Both *Subramanian and Sarabhai* (1967) and *Lietti and Quenby* (1968) have suggested that the second harmonic component of the cosmic ray daily variation can
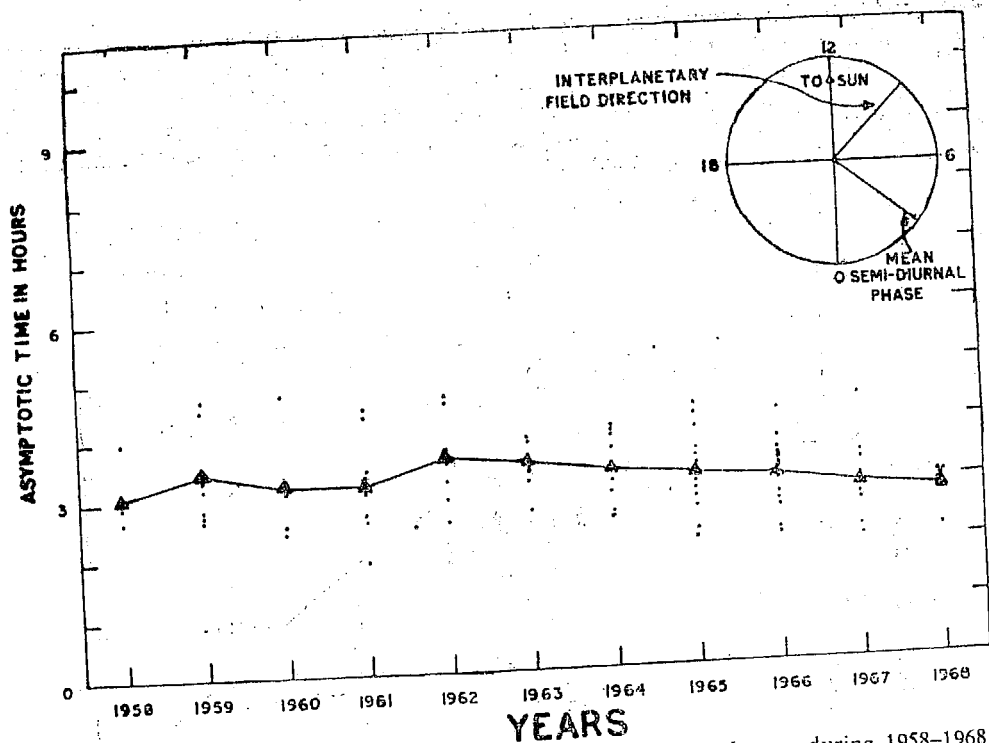
9

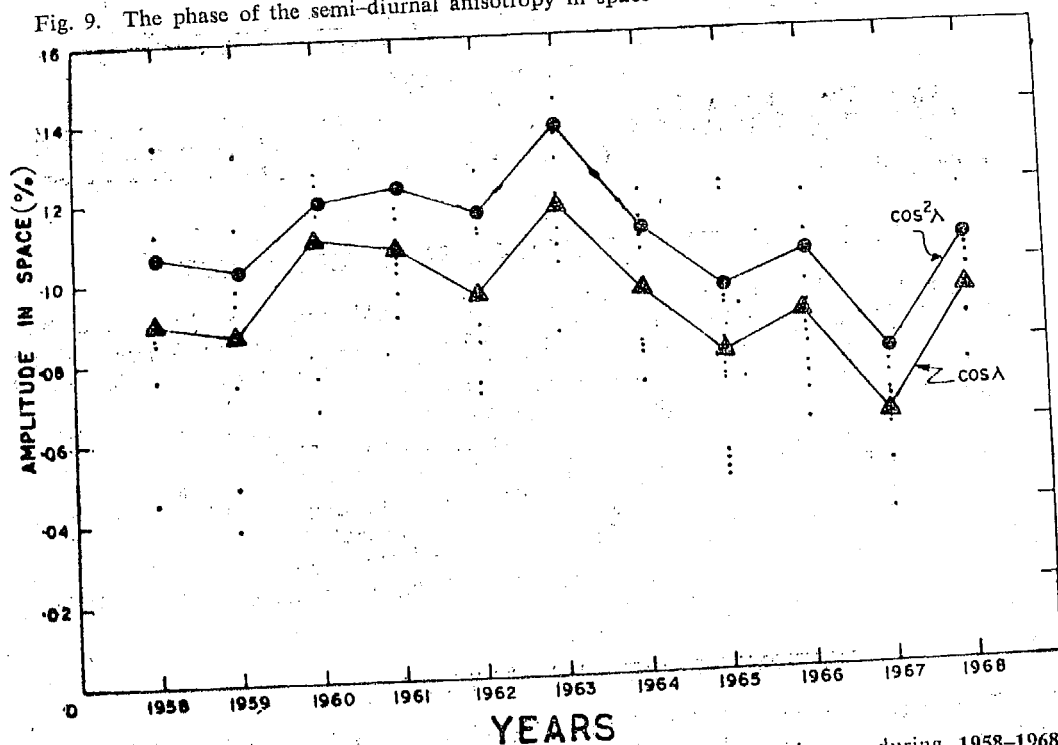Fig. 9. The phase of the semi–diurnal anisotropy in space for each year during 1958–1968.

Fif 10. The amplitude of the semi–diurnal anisotropy in space for each year during 1958–1968.

10

be due to the particle density gradient in the plane perpendicular to the plane of ecliptic. If we assume an Archemides spiral configuration for the interplanetary field, it is evident that the particles arriving along the sun's polar field lines suffer much less modulation when compared with those arriving in the ecliptic plane, thus giving rise to a cosmic ray density gradient, with the intensity increasing away from the plane of ecliptic. Viewing along the interplanetary magnetic field lines of force (i.e. along the garden hose direction), a neutron monitor on earth measures cosmic ray flux characteristic of the equatorial plane. Viewing in a direction perpendicular to the magnetic field, the detector samples particles arriving from higher heliolatitudes; the heliolatitude corresponds to the gyroradius of the particle under consideration. Thus the higher the energy, the higher is the heliolatitude of sampling by the monitor. Consequently, the positive gradient of cosmic ray density with the increase in heliolatitude gives rise to a semi–diurnal maximum aligned in a direction perpendicular to the direction of the interplanetary magnetic field, because the earth, as it spins, measures cosmic ray intensity twice along and twice perpendicular to the field direction in the course of a day.

The basic difference between Subramanian and Sarabhai's and Lietti and Quenby's mechanism is the assumption of the nature of the density gradient profile in the direction perpendicular to the plane of ecliptic. Whereas Lietti and Quenby's theory is based on the geometry of the interplanetary field, Subramanian and Sarabhai's treatment involves assumptions as to the form of the perpendicular density gradient that are based on the coronal observations. Both theories predict that the semi–diurnal anisotropy as observed in space (1) has an exponent of $R^{+1.0}$ where R is rigidity; (2) varies as $\cos^2 \lambda$, where λ is the mean asympotic latitude of response; (3) has a maximum flux in a direction perpendicular to the interplanetary magnetic field. This immediately gives rise to a much larger semi–diurnal variation at equatorial latitudes, as compared with that at middle latitudes. The experimental observations we have presented in this paper are essentially in agreement with the theoretical predictions.
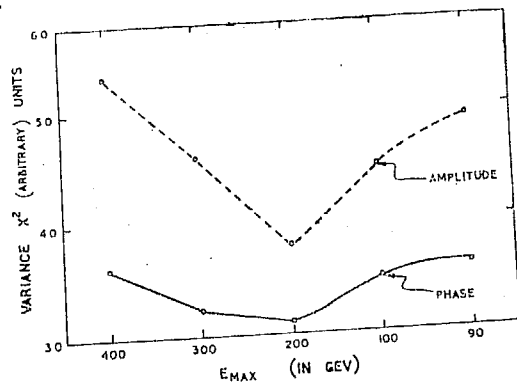

Fig. 11. The variance in the phase and amplitude of semi–diurnal anisotropy plotted as a function of E_{max}.

Because the semi–diurnal variation is a direct consequence of the density gradient of cosmic radiation in the plane perpendicular to the plane of ecliptic, we can set an approximate upper limit on the maximum energy that will exhibit the semi–diurnal anisotropy as it corresponds to particles of rigidity, $R_{max} \approx 200$ Gv, whose gyroradius is about 1 AU. The influence of the solar magnetic field that is responsible for this density gradient is not likely to extend beyond 1 AU in the plane perpendicular to the plane of ecliptic. Figure 11 shows the variance of the amplitude

11

and phase of the semi–diurnal anisotropy as a function of R_{max} for $\beta = 1.0$ and for the year 1966. It is seen from the figure that both the amplitude and phase of the semi–diurnal anisotropy show a minimum variance for $R_{max} \approx 200$ Gv, even though the statistical uncertainty does not permit an unambiguous determination of R_{max}. We find that the value of 200 Gv for R_{max} is in agreement with the data for all the years within the large statistical uncertainties. We wish to note that all the conclusions regarding the energy spectrum, time of maximum and dependence on declination of the semi–diurnal anisotropy are valid even if R_{max} is different from 200 Gv.

On the basis of the evidence presented here, we advance the following conclusions on the properties of the average semi–diurnal variation of cosmic radiation in the energy range 1–200 Gev.

(a) The semi–diurnal variation is consistent with an anisotropy which could be expressed by

$$\frac{\Delta J(R)}{J(R)} = KR \cos^2 \Lambda \cos 2 \left[\theta - (48 \pm 6)\right] \% \text{ for } R < 200 \text{ Gv}$$

$$\frac{\Delta J(R)}{J(R)} = 0 \text{ for } R > 200 \text{ Gv}$$

where R is the rigidity, Λ is the declination, and K ≈ 0.004, which is highly dependent on the choice of R_{max}. The average semi–diurnal amplitude in space for cosmic ray particles in the range 1–200 Gv, however, is a more fundamental quantity and has a value of 0.11 $\pm$ 0.02% during the period 1958–1968. The time of maximum of the average semi–diurnal anisotropy is along ~0300 hours direction, which is essentially perpendicular to the direction of the average interplanetary magnetic field.

(b) The phase of the average semi–diurnal anisotropy is time invariant and perpendicular to the direction of the average interplanetary magnetic field during the entire period 1958–1968.

(c) The amplitude of the average semidiurnal anisotropy shows no appreciable change between 1958–1968.

References

Ables, J. G., K. G. McCracken, and U. R. Rao, The semi–diurnal anisotropy of the cosmic radiation, *Proc. Cosmic Ray Conf. (London)*, 208, 1965.

Axford, W. I., The modulation of galactic cosmic rays in the interplanetary medium, *Planet. Space Sci., 13,* 115, 1965.

Carmichael, H., M. Bercovitch, M. A. Shea, M. Magidin, and R. W. Peterson, Attenuation of neutron monitor radiation in the atmosphere, *Can. J. Phys.,* 46, S1006, 1968.

Kodama, M., and J. Ohuchi, Latitude survey of neutron multiplicity using a shipborne NM–64 neutron monitor, *Can. J. Phys.,* 46, S1090, 1968.

Lietti, B., and J. J. Quenby, The daily variation second harmonic and a cosmic ray intensity gradient perpendicular to the ecliptic, *Can. J. Phys., 46*, S942, 1968.

McCrackean, K. G., U. R. Rao, and M. A. Shea, The trajectories of cosmic rays in a high degree simulation of the geomagnetic field, *M.I.T. Tech. Rep. No. 77*, 1962.

McCracken, K. G., and U. R. Rao, A survey of the diurnal anisotropy, *Proc. Cosmic Ray Conf. (London), 213*, 1965.

McCracken, K. G., U. R. Rao, B. C. Fowler, M. A. Shea, and D. F. Smart, Cosmic ray variational coefficients for different stations, *I.Q.S.Y. Instruction Manual No. 10*, 1965.

Parker, E. N., Theory of streaming of cosmic rays and the diurnal variation, *Planet. Space Sci., 12*, 735, 1964.

Patel, D., V. Sarabhai, and G. Subramanian, Anisotropies of galactic cosmic rays in solar system, *Planet. Space Sci., 16*, 1131, 1968.

Rao, U. R. and V. Sarabhai, Time variations of directional cosmic ray intensity at low latitudes, 2, Time variations of east–west asymmetry, *Proc. Roy. Soc. (London), 263A*, 118, 1961.

Rao, U. R., K. G. McCracken, and D. Venkatesan, Asymptotic cones of acceptance and their use in the study of the daily variation of cosmic radiation, *J. Geophys., Res., 68*, 345, 1963.

Subramanian, G., and V. Sarabhai, Consequences of the distribution of galactic cosmic ray intensity in the solar system, *Astrophys. J., 149, 417, 1967*.